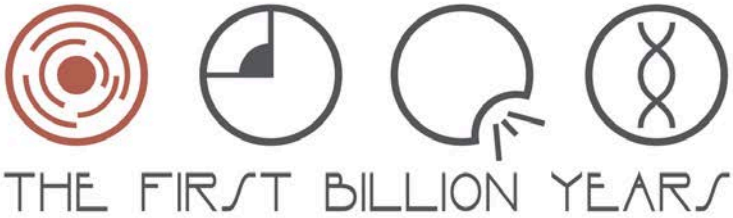

THE FIRST BILLION YEARS

#1st1e9

ACCRETION

Houston, Texas August 15–18, 2017

Program

LUNAR AND PLANETARY INSTITUTE

USRA

Accretion:
Building New Worlds Conference

August 15–18, 2017 • Houston, Texas

Institutional Support

Lunar and Planetary Institute

Universities Space Research Association

Conveners

Jeff Cuzzi
NASA Ames Research Center

Christine Floss
Washington University

Harold Levison
Southwest Research Institute

Justin Simon
NASA Johnson Space Center

Allan Treiman
Lunar and Planetary Institute

Science Organizing Committee

Hans-Peter Gail
University of Heidelberg

Levke Kööp
University of Chicago

Sebastiaan Krijt
University of Chicago

Ryan Ogliore
Washington University, Saint Louis

Cristina Thomas
Planetary Science Institute

Lunar and Planetary Institute 3600 Bay Area Boulevard Houston TX 77058-1113

Abstracts for this conference are available via the conference website at

www.hou.usra.edu/meetings/accretion2017/

Abstracts can be cited as

Author A. B. and Author C. D. (2017) Title of abstract. In *Accretion: Building New Worlds Conference,* Abstract #XXXX. LPI Contribution No. 2043, Lunar and Planetary Institute, Houston.

Guide to Sessions

Tuesday, August 15, 2017

8:30 a.m.	Great Room	Registration
9:00 a.m.	Lecture Hall	Early Protoplanetary Disks: Gas and Dust
2:00 p.m.	Lecture Hall	Growth and Motion of Larger Particles: CAIs and Chondrules

Wednesday, August 16, 2017

9:00 a.m.	Lecture Hall	Environment and Timing of Planetesimal Formation: Isotopic Constraints
2:00 p.m.	Lecture Hall	Asteroidal Constraints on Planetesimal Formation
5:00 p.m.	Great Room	Poster Session

Thursday, August 17, 2017

9:00 a.m.	Lecture Hall	Mechanisms of Planetesimal Formation
2:00 p.m.	Lecture Hall	Dynamics of Planetesimals: Mixing and Segregation

Friday, August 18, 2017

9:00 a.m.	Lecture Hall	Accretion of Terrestrial Planets

Program

Tuesday, August 15, 2017
EARLY PROTOPLANETARY DISKS: GAS AND DUST
9:00 a.m. Lecture Hall

Chair: Jeff Cuzzi

9:00 a.m. Treiman A. Kiefer W. *
Welcome and Introduction

9:15 a.m. Cleeves L. I. *
Zooming in on the Physics and Chemistry of Protoplanetary Disks with ALMA **[#2052]**
During the protoplanetary disk phase, the physical environment and spatial composition of the disk play a direct role in the outcome of planet formation, both in the types of planets formed and their composition.

9:45 a.m. Banzatti A. * Pontoppidan K. M. Salyk C. van Dishoeck E. F. Herczeg G. J. Blake G. A. Garufi A. Kama M. Pascucci I. Edwards S.
Revealing the Physical and Thermo-Chemical Evolution of Planet-Forming Disk Regions **[#2016]**
We report results of a large campaign to reveal the evolving structure of planet-forming disks at 0.05–20 au: cavities are formed in the terrestrial-planet zone, inner disks dry out within the snow line, while dust accretes and winds disperse.

10:05 a.m. Umurhan O. M. * Estrada P. R. Cuzzi J. N.
Turbulence in Protoplanetary Disk Dead Zones — Recent Advances **[#2044]**
In this talk I will review recent developments in our understanding of turbulence in planet forming accretion disks.

10:25 a.m. Hu Z. W. * Winarski R. P.
Insights into Aggregation of Submicron Grains from 3-D Structure of a Primitive Fine-Grained Cosmic Dust Particle **[#2042]**
We present new findings of the pristine structure and morphologies of an intact fine-grained cosmic dust particle in 3-D ~ 10 nm detail, which yield new insights into grain accretion in the outer protoplanetary disk.

10:40 a.m. *Coffee Break*

10:55 a.m. Garcia A. J. L. * Gonzalez J.-F.
Growing Porous Grains in 3D SPH Simulations **[#2003]**
In protoplanetary discs, grains grow through 13 orders of magnitude from submicrons to kilometers. In this work, we investigate growth and drift of grains with a changing porosity model in order to overcome the radial-drift barrier.

11:10 a.m. Brisset J. * Colwell J. E. Dove A. Maukonen D.
Using Orbital Platforms to Study Planet Formation **[#2002]**
We will present results from the ISS NanoRocks experiment as well as the design of the Q-PACE CubeSat to demonstrate how orbital miniaturized payloads can be used to collect unprecedented amounts of data on the collision behavior of PPD dust grains.

11:25 a.m. Wetteland C. J. * Crespillo M. Keffer D. J. Sickafus K. E. Taylor L. A. McSween H. Y. Jr.
Experimental and Theoretical Considerations for Proton Processing of Early Solar System Solids **[#2018]**
Developing stars variably discharge energetic particles over the course of their evolution. Experimental and theoretical approaches have been examined to explore how energetic particles may process early solar materials in the first billion years.

11:40 a.m. Ogliore R. C. *
Cometary Dust and the Young Solar System **[#2041]**
Precise microanalyses of cometary dust have yielded insight into the early history and far outer reaches of our solar system.

12:10 p.m. GENERAL DISCUSSION

12:30 p.m. *Lunch*

Tuesday, August 15, 2017
GROWTH AND MOTION OF LARGER PARTICLES: CAIs AND CHONDRULES
2:00 p.m. Lecture Hall

Chair: Levke Kööp

2:00 p.m. Estrada P. R. * Cuzzi J. N.
Growth and Drift of Solids in Protoplanetary Nebulae **[#2047]**
The earliest stages of planetary formation are still poorly understood. The growth from dust-to-planetesimals remains the roadblock in our interpretation of how planetary systems form and their architecture. We discuss the current state of the field.

2:30 p.m. Krijt S. * Schwarz K. Ciesla F. J. Bergin E. A.
Connecting CO Abundances Before, During, and After Pebble Migration **[#2043]**
Pebbles form, sink, drift / Moving ices back and forth / Where does CO go?

3:00 p.m. Desch S. J. *
How Chondrules and Calcium-Rich, Aluminum-Rich Inclusions Constrain Disk Processes and Planet Formation **[#2046]**
I review how chondrules and CAIs constrain the disk processes and planet formation.

3:30 p.m. *Coffee Break*

3:45 p.m. Perez A. M. * Desch S. J. Schrader D. L. Till C. B.
Determining the Relative Timing of Formation of Chondrules vs. Planetary Embryos Through Experiments **[#2037]**
We have conducted vertical furnace experiments to investigate cooling rates consistent with the planetary embryo bow shock model to determine the relative timing of formation of chondrules versus planetary embryos.

4:00 p.m. Hanna R. D. * Ketcham R. A.
Evidence for Accretion of Fine-Grained Rims in a Turbulent Nebula for CM Murchison **[#2012]**
The 3D morphology of FGRs and enclosed chondrules indicate that FGRs formed in a weakly turbulent nebula and that chondrule surface morphology influenced the amount of dust accreted to the chondrule.

4:15 p.m. Xiang C. * Matthews L. S. Carballido A. Morris M. A. Hyde T. W.
Modeling the Growth of Chondrule Dust Rims with Molecular Dynamics **[#2048]**
We present a method to investigate the structure of dust rims formed around chondrules as the latter sweep up dust in the nebula gas, by using an N-body code to model the collision processes of micron sized aggregates with a mm-sized spherical body.

4:30 p.m. Simon J. I. * McCain K. A. Cato M. J. Christoffersen P. A. Fisher K. R. Srinivasan P. Tait A. W. Cuzzi J. N.
Broad Size-Dependent Particle Populations in Chondritic Meteorites: Implications for Planetary Accretion **[#2009]**
Instead of the relatively narrow size-frequency distributions often used in astrophysical models to simulate the dynamics of protoplanetary disks, we observe broad size-frequency distributions across all particle types in primitive meteorites.

4:45 p.m. GENERAL DISCUSSION

Wednesday, August 16, 2017
ENVIRONMENT AND TIMING OF PLANETESIMAL FORMATION: ISOTOPIC CONSTRAINTS
9:00 a.m. Lecture Hall

Chair: Allan Treiman

9:00 a.m. Dwarkadas V. V. * Dauphas N. Meyer B. S. Boyajian P. H. Bojazi M.
Abundances of Short-Lived Radionuclides and the Implications for the Formation of the Solar System **[#2004]**
Analysis of primordial meteorites shows a high abundance of ^{26}Al, accompanied by low ^{60}Fe. This indicates that our solar system originated within a Wolf-Rayet bubble formed by stellar mass-loss from a massive star that was the main source of ^{26}Al.

9:15 a.m. Wadhwa M. *
Meteoritic Constraints on Timescales of Planetesimal Accretion in the Early Solar System **[#2053]**
The details of the physical processes involved in the accretion of planetesimals in the early solar system are not well understood, and have been the focus of several recent theoretical modeling investigations.

9:45 a.m. Simon J. I. *
Utilizing Stable Isotopes and Isotopic Anomalies to Study Early Solar System Formation Processes **[#2023]**
Invited talk on stable isotope record of early formed planetary materials.

10:15 a.m. Kita N. T. * Tenner T. J. Ushikubo T. Nakashima D. Defouilloy C. Hertwig A. T. Chaumard N. Rudraswami N. G. Weisberg M. K. Kimura M. Nagahara H. Bischoff A.
Oxygen Isotope Systematics in Chondrules from Multiple Chondrite Groups: Implication to the Isotope Reservoirs in the Protoplanetary Disk **[#2020]**
SIMS O-isotope analyses of ~600 chondrules show systematics variability among chondrite groups that are related to Fe redox states. Inner disk might be homogenized in O-isotopes, while outer disk might have ^{16}O-rich dry dust and ^{16}O-poor water ice.

10:35 a.m. *Coffee Break*

10:50 a.m. Kööp L. * Davis A. M.
Accretion and Processing of Presolar Components as Recorded by Nebular Materials **[#2035]**
We review the ^{26}Al-^{26}Mg, Ca, Ti, and O isotopic systematics of different generations of nebular materials in order to trace the arrival, processing, and origin of different stellar components in the solar nebula.

11:10 a.m. Goodrich C. A. *
The Carbonaceous - Non-Carbonaceous Chondrite Reservoir Dichotomy and the Challenge of Ureilites **[#2013]**
Solar system materials are strongly divided into CC (carbonaceous chondrite) and NCC (non-CC) groups in terms of nucleosynthetic isotope anomalies. Ureilites are in the NCC group but seem to have had volatile-rich precursors. How could this be?

11:25 a.m. Keller L. P. * Snead C. McKeegan K. D.
Clustering of Inner Solar System Oxygen Isotopic Compositions: A Result of Gap Formation in the Protoplanetary Disk? **[#2040]**
Gap formation provides a mechanism to explain the clustering of oxygen isotopic compositions for inner solar system materials, including the terrestrial planets and meteorites, relative to the Sun.

11:40 a.m. GENERAL DISCUSSION

12:10 p.m. *Lunch*

Wednesday, August 16, 2017
ASTEROIDAL CONSTRAINTS ON PLANETESIMAL FORMATION
2:00 p.m. Lecture Hall

Chair: Sebastiaan Krijt

2:00 p.m. Thomas C. A. *
The Current Solar System and Clues to Its Past **[#2051]**
The current physical characteristics of the small body populations enable investigations of the evolution of our solar system. As we continue to characterize physical properties, we further our understanding of the solar system as a whole.

2:30 p.m. Delbo M. * Morbidelli A. Walsh K. J. Tsirvoulis G. Avdellidou C. Bolin B. T. Tsiganis K.
Hunting the Planetesimals Size Distribution Hidden in the Main Asteroid Belt **[#2028]**
The size distribution of the planetesimals is one of the most fundamental constraints for theories and models of planetary formation. Here we report new findings about the size distribution of the planetesimals in the Main Asteroid Belt.

2:50 p.m. Weiss B. P. * Fu R. R. Wang H. Bai X.-N. Gattacceca J. Harrison R. J. Schrader D. L.
History of the Solar Nebula from Meteorite Paleomagnetism **[#2054]**
Here we review recent advances in our understanding of the magnetism of the solar nebula as inferred from meteorites.

3:20 p.m. Vaci Z. * Agee C. B. Ziegler K. Asmerom Y. Polyak V. J. Humayun M.
Northwest Africa 11042: A Primitive Achondritic Melt from the L Chondrite Parent Body **[#2005]**
NWA 11042 is a primitive achondrite with L chondritic oxygen isotopes. It is an igneous rock which has undergone differentiation and might represent a melt from the L chondrite parent body.

3:35 p.m. *Coffee Break*

3:50 p.m. Downes H. * Rai N.
A New Model for Planetesimal Formation **[#2011]**
Mixing of two types of chondrules produces trends in bulk chemistry and oxygen isotopes which match those of the reconstructed planetesimal source of ureilites. Before heating up, the original body was zoned from Mg-rich centre to Fe-rich exterior.

4:05 p.m. Castillo-Rogez J. C. * McSween H. Y. McCord T. B. De Sanctis M. C. Raymond C. A. Marchi S. Russell C. T.
Constraints on Vesta's and Ceres' Origins from Dawn's Observations **[#2026]**
Vesta and Ceres are the best studied leftover planetary building blocks. In the context of the First Billion Years conference series, these bodies offer remarkable examples where differentiation state can help constrain accretion environments.

4:20 p.m. GENERAL DISCUSSION

Wednesday, August 16, 2017
POSTER SESSION
5:00 p.m. Great Room

Ashrafi K. S. Esparza S. Xiang C. Matthews L. Carballido A. Hyde T. Shotorban B.
Effects of Stochastic Charging on Micron Sized Grains in Protoplanetary Disks **[#2045]**
We use a model of discrete stochastic charging to calculate time-dependent electric charging of dust aggregates. We compare the electron and ion currents to micron and submicron grains.

Bravenec A. D. Bromiley G. D. Kohn S. C.
Water in the Early Solar System and Mantle Melting in Terrestrial Planets **[#2008]**
A hydrous lunar interior implies water was inherited from accretionary processes. Experiments will determine the partitioning of H_2O in the reduced conditions of early planetary interiors to investigate the source and compare water contents.

Castillo-Rogez J. C. Walsh K. J. Vernazza P. Takir D.
Constraints on the Time of Formation of Ceres and Ceres-Like Asteroids — A Joint Reservoir with C-Type Irregular Satellites? **[#2025]**
Comparisons between the geophysical properties of planetesimals in the 100–300 km range can help infer times of formation and genetic relationships between planetesimal reservoirs.

Heinze W. D.
A Terrestrial Conjecture on Convection, Magnetic Fields, and Water **[#2031]**
Enough knowledge of the terrestrial planets and accretion modeling is now available to form a conceptual, if speculative, framework describing a continuum of accretionary outcomes and their consequences for long-term habitability.

Jackson A. P. Perera V. Elkins-Tanton L. T. Asphaug E.
Impact Generation of Holes in the Early Lunar Crust **[#2017]**
Debris that escaped the Earth-Moon system after the Moon-forming impact would return and re-impact the newly formed Moon. We model these debris re-impacts into the flotation crust overlying the early lunar magma ocean, generating holes.

Kochemasov G. G.
Some Examples of Cosmic Bodies Accretion from Solid Particles Preliminary Density Sorted in Rotating Gas-Dust Cloud: Sulfur Behavior **[#2007]**
Minerals in some meteorites and larger bodies are collected by density rather then temperature factor. Accretion started with already sorted by density minerals and intergrowths. Examples: the whole planetary system, asteroid belt, Mercury, Io.

Miura Y.
Active Processes in Asteroids and Planets Developed to Water Planet and Life **[#2050]**
Active processes are formed by amorphous and crystalline solids. Water droplets formed from meteorite heating are obtained to be evidences of volatiles ions. Life is produced at large water-planet system as sedimentary deposits with carbon elements.

Perov N. I.
A Role of Jupiter in the Process of the Terrestrial Type Planets Bombarding by the Solar System Peripheral Small Bodies **[#2006]**
The space-time position of Jupiter for the effective mixing of the peripheral and internal matter of the solar system is under consideration. In the frame of the three body problem the corresponding "key hole" for Jupiter equals 0.004 rad.

Petö M. K. Lugaro M.
On the Need of Constraining the ^{244}Pu Content of the Early Solar System **[#2038]**
We present our comprehensive approach to estimate the initial ^{244}Pu abundance of the solar system and to apply the Pu-Xe system to both pre-solar and terrestrial chronometry.

Thursday, August 17, 2017
MECHANISMS OF PLANETESIMAL FORMATION
9:00 a.m. Lecture Hall

Chair: Ilsedora Cleeves

9:00 a.m. Blum J. *
Planetesimal Formation and Collisional Evolution **[#2001]**
I will present the latest laboratory and modeling results on the formation of planetesimals and will compare them with findings from the Rosetta mission to comet 67P. On top of that, the collisional evolution of planetesimals will be discussed.

9:30 a.m. Carrera D. *
Formation of Planetesimals Through the Streaming Instability **[#2032]**
The streaming instability is a candidate mechanism for the formation of planetesimals in a protoplanetary disk. In this talk I will give a general overview of how the streaming instability works, and under what conditions.

10:00 a.m. Simon J. B. * Armitage P. J. Youdin A. N. Li R.
Planetesimal Formation in Protoplanetary Disks **[#2022]**
In this work, we present a series of numerical calculations of planetesimal formation via the streaming instability. We find evidence that the size distribution of planetesimals is robust to different parameters, such as initial particle size.

10:30 a.m. *Coffee Break*

10:45 a.m. Shannon A. * Wu Y. Lithwick Y. Dawson R.
Forming the Cold Classical Kuiper Belt by Collisional Pebble Accretion, Considering the Hot **[#2021]**
We model of Kuiper belt object (KBO) growth by collisional pebble accretion. The model produces KBOs with high efficiency, allowing the *in-situ* formation of the Cold Classicals. It can also explain the orbital properties of ultra-wide KBO binaries.

11:15 a.m. Cuzzi J. N. * Hartlep T. Simon J. I. Estrada P. R.
Planetesimals Born Big by Clustering Instability? **[#2039]**
Problems with the formation of "primary" planetesimals will be presented, and relevant observations summarized. A small amount more growth by sticking due to new physics, followed by a combination of two current scenarios, looks encouraging.

11:45 a.m. Hartlep T. * Cuzzi C. N.
A Path to Chondrule Aggregates **[#2049]**
We discuss recent advances in the understanding and modeling of gas-particle dynamics in turbulence which we hypothesize may be able to overcome the currently accepted mm-sized bouncing barrier in the accretion of primitive asteroids.

12:00 p.m. GENERAL DISCUSSION

12:30 p.m. *Lunch*

Thursday, August 17, 2017
DYNAMICS OF PLANETESIMALS: MIXING AND SEGREGATION
2:00 p.m. Lecture Hall

Chair: Paul Estrada

2:00 p.m. Walsh K. J. *
Planet Formation Constrained by the Early Asteroid Belt **[#2010]**
The collisional history of the asteroid belt, as represented by CB chondrites and ancient asteroid families, can thus help constrain our understanding of the planet formation processes.

2:30 p.m. Kretke K. A. * Bottke W. F. Levison H. F. Kring D. A.
Mixing of the Asteroid Belt due to the Formation of the Giant Planets **[#2027]**
Using ``pebble accretion'' we model how the process of giant planet formation naturally scatters outer solar system material in to the asteroid belt, providing a source for the C-type asteroids without dramatic migrations of the giant planets.

2:50 p.m. Kring D. A. *
Planetary Accretion as Informed by Meteoritic Samples of Early Solar System Planetesimals **[#2034]**
Meteoritic impact melts and impact breccias contain information about the timing and sizes of collisions, which, when augmented with hints about impactor compositions, provide clues about mixing and the dynamical situation in the early solar system.

3:10 p.m. Alexander C. M. O'D. *
Sources of Terrestrial Volatiles: Primordial Atmospheres and Planetesimals from the Outer Solar System **[#2019]**
CI-CM-like objects were the major sources of terrestrial volatiles, but comets may have contributed to noble gas inventories. The carbonaceous chondrites formed beyond the orbit of Jupiter and were scattered into the terrestrial planet region >4 Ma.

3:30 p.m. *Coffee Break*

3:45 p.m. GENERAL DISCUSSION

4:00 p.m. POP-UP TALKS

4:30 p.m. *Poster Viewing*

Friday, August 18, 2017
ACCRETION OF TERRESTRIAL PLANETS
9:00 a.m. Lecture Hall

Chair: Steve Desch

9:00 a.m. Burbine T. H. * Greenwood R. C. Franchi I. A.
What Material Accreted to Form the Earth? **[#2014]**
One unsolved question in planetary science is what was the dominant material that accreted to form the Earth. Could the Earth be composed primarily of chondritic material not currently found in our meteorite collections?

9:20 a.m. Righter K. *
Redox Variations in Early Solar System Materials and Implications for Late Stage Planetary Accretion and Planet Formation **[#2029]**
This paper provides an overview of oxygen fugacity measurements made on primitive solar system materials and planetary materials, and how they may influence later stages of planet formation.

9:40 a.m. Armytage R. M. G. * Debaille V.
Neodymium Isotopes in Enstatite and Ordinary Chondrites: Nebular Variation? **[#2036]**
Enstatite chondrites have been proposed to be sourced from the same isotopic reservoir as Earth, pointing to accretion in a shared region of the disk. However, our Nd isotopic data for enstatite chondrites show that this is unlikely to be the case.

10:00 a.m. Haghighipour N. * Maindl T. I. Schaefer C. M. Wandel O.
Accurate Treatment of Collision and Water-Delivery in Models of Terrestrial Planet Formation **[#2030]**
We have developed a comprehensive approach in simulating collisions and growth of embryos to terrestrial planets where we use a combination of SPH and N-body codes to model collisions and the transfer of water and chemical compounds accurately.

10:15 a.m. Jackson A. P. * Gabriel T. S. J. Asphaug E.
Constraining the Pre-Impact Orbits of Solar System Giant Impactors **[#2033]**
We provide a fast method for computing constraints on impactor pre-impact orbits, applying this to the late giant impacts in the solar system, and suggest that high-velocity impact scenarios in the inner solar system should be disfavoured.

10:30 a.m. *Coffee Break*

10:45 a.m. Perera V. * Jackson A. P. Elkins-Tanton L. T. Asphaug E.
Effect of Re-Impacts on the Lunar Magma Ocean **[#2015]**
Debris that escaped the Earth-Moon system after the Moon-forming impact would have returned and affected the thermal evolution of the Moon. We model the effect of those re-impacting debris onto a lunar magma ocean and quantify solidification time.

11:00 a.m. Kiefer W. S. * Castillo-Rogez J. C. Chabot N. L. Elardo S. M. Goodrich C. A. Righter K.
How Does Accretion Influence Planetary Differentiation?: Feed Forward from the Accretion Conference to the Differentiation Conference **[#2024]**
Planetary accretion and differentiation overlapped in time. Thus, our understanding of accretion influences differentiation models. We will report the current status of accretion modeling to the upcoming LPI Planetary Differentiation conference.

11:20 a.m. GENERAL DISCUSSION

12:10 p.m. *Meeting Adjourns*

Notes

SOURCES OF TERRESTRIAL VOLATILES: PRIMORDIAL ATMOSPHERES AND PLANETESIMALS FROM THE OUTER SOLAR SYSTEM. C. M. O'D. Alexander[1], [1]DTM, Carnegie Institution of Washington, 5241 Broad Branch Road, Washington DC 20011, USA (calexander@carnegiescience.edu).

Introduction: Identifying the major sources of volatiles remains one of the most important unsolved problems of terrestrial planet formation. The general assumption has always been that most of the planetesimal building blocks of the terrestrial planets were volatile depleted, either because the ambient temperatures in the inner Solar System were too high and the environment too reducing, or because they formed early and differentiated thereby losing their volatiles. Some H may have been adsorbed onto the grain surfaces from which the planetesimals formed [1], but this mechanism is unable to explain the presence of other volatile elements (C, N, noble gases, Cl, I, Cd, etc.).

The volatiles may also have been acquired from primordial atmospheres accreted directly from the nebula by the planets or their embryo precursors. The nebula dissipated later than ~4 Ma after CAIs, the accretion age of the youngest chondrites the CRs [2], and probably no later than 10 Ma after CAIs based on astronomical observations of disk lifetimes. Earth almost certainly did not approach its present mass until long after the nebula had dissipated. Mars, on the other hand, probably did reach a large fraction of its final mass while the nebula was present [3]. Thus, acquisition of primordial atmospheres by embryos is a possibility. The other likely sources of volatiles are planetesimals that formed later and/or further from the Sun.

The bulk H and N isotopic compositions of Earth and Mars are quite similar to one another. The bulk H and N isotopic compositions of the nebula are much lighter than those of Earth and Mars, seemingly ruling out primordial atmospheric sources. Comets may have contributed significantly to the noble gas inventories of Earth and Venus [4], but not to H, C and N. This really only leaves asteroidal sources for H, C and N. Meteorites provide samples of the objects in the asteroid belt, and of these only the CI and CM chondrites are consistent with the elemental and isotopic constraints [5, 6]. If CI- and CM-like material were the dominant sources of H-C-N, their isotopic compositions do require that ~10 % of the H and N that was accreted had a solar-like isotopic composition [5]. Accretion of some material with a solar-like composition is required by the He and Ne isotopic compositions of components within the Earth's interior. This material was unlikely to have been accreted directly from the nebula [7], but may have been acquired as material that was rich in implanted solar wind [8].

While the bulk of Earth and Mars seem to have formed from material that isotopically resembled the O and E chondrites, the volatiles appear to have been delivered before the Moon-forming impact in CI-CM-like material that is isotopically distinct [9-11]. In fact, there is a dichotomy between CCs and all other Solar System objects that we have samples of. One attractive explanation is that this dichotomy is the result of the growth of Jupiter to a size of ~20 M_{Earth} about 1 Ma after CAIs, at which point it isolated the inner from the outer Solar System [12]. The CCs were then scattered into the inner Solar System sometime after 4 Ma.

This isolation cannot have been complete as the O and E chondrites, which formed ~2 Ma after CAIs, seem to have accreted CI-like matrix material [13]. Also, the HED Stannern and the angrite D'Orbigny, both of which crystallized at about the same as the CRs accreted, have very similar H and N isotopic compositions to the Earth and Mars. This implies that Vesta and the angrite parent body accreted similar CI-CM-like material to the two planets before the scattering of the CCs. This could be explained by the migration of fine dust that was coupled to the gas past Jupiter, but would require that by ~1 Ma most material in the outer Solar System was already in objects that were too big to be strongly coupled to the gas. Also potentially problematic are the apparently low initial water contents of the CO, CV and CK chondrites, particularly if Jupiter formed near the snowline. The O and R chondrites accreted some water, so the snowline must have been sunward of Jupiter's orbit by ~2 Ma, and formed at about the same time as the CO-CV-CK chondrites.

References: [1] Asaduzzaman A. et al. (2015), *Meteoritics & Planet. Sci., 50*, 578-589. [2] Schrader D.L. et al. (2017), *GCA, 201*, 275-302. [3] Tang H. and Dauphas N. (2014), *EPSL, 390*, 264-274. [4] Marty B. et al. (2016), *EPSL, 441*, 91-102. [5] Alexander C.M.O'D. et al. (2012), *Science, 337*, 721-723. [6] Marty B. (2012), *EPSL, 313-314*, 56-66. [7] Jaupart E. et al. (2017), *Icarus, 293*, 199-205. [8] Péron S. et al. (2017), *Geochem. Perspectives Lett., 3*, 151-159. [9] Warren P.H. (2011), *EPSL, 311*, 93-100. [10] Budde G. et al. (2016), *EPSL, 454*, 293-303. [11] Fischer-Gödde M. and Kleine T. (2017), *Nature, 541*, 525-527. [12] Kruijer T.S. et al. (2017), *LPS, 48*, #1386. [13] Alexander C.M.O'D. (2005), *Meteoritics & Planet. Sci., 40*, 943-965.

NEODYMIUM ISOTOPES IN ENSTATITE AND ORDINARY CHONDRITES: NEBULAR VARIATION?

R. M. G. Armytage[1] and V. Debaille[1], [1]Laboratoire G-Time, CP 160/02, Université Libre de Bruxelles, Ave Fr. Roosevelt 50, 1050 Bruxelles, Belgium. (*email: rosalindarmytage@gmail.com)

Introduction: One of the key problems in planetary science is the identification of the building blocks of Earth, and whether they exist within our current collection of meteorites. Constraints on the initial isotopic composition of planetary bodies are key in the application of radiogenic chronometers and understanding subsequent planetary differentiation processes. Stable mass independent isotopic anomalies are a key tool in fingerprinting material coming from different accretionary regions within the protoplanetary disk. For a number of isotopic systems such as O[1], Ni[2], Ti and Cr [3], enstatite chondrites (EC) appear to be the strongest candidates for Earth's building blocks, despite their low Mg/Si ratios relative to the bulk Earth. It has been proposed that Earth, the Moon-forming impactor and enstatite chondrites all were originally sourced from the same reservoir in the protoplanetary disk, but subsequently experienced divergent chemical evolution pathways [4]. However, [5] recently used the correlation between Mo and Nd isotopes in bulk meteorites to argue that such a reservoir does not exist as the isotopic composition of enstatite chondrites is resolvable from Earth, and both are resolvable from ordinary chondrites (OC). In detail, while the Mo data for EC are clearly resolvable from Earth and OC, the Nd ratios show more variability and significant overlap with the isotopic composition of both the bulk Earth and ordinary chondrites. The variability in $^{142}Nd/^{144}Nd$ in EC has been previously identified by [6] and they observed that it appeared to be related to whether the EC was equilibrated or unequilibrated. However, [6] only focused on collecting high precision $^{142}Nd/^{144}Nd$, which also has contributions from the decay of the short-lived ^{146}Sm nuclide ($t_{1/2}$ ~103 Myr), making identification of nucleosynthetic anomalies less clear. While the study of [5] reports high precision $^{145}Nd/^{144}Nd$, $^{148}Nd/^{144}Nd$, and $^{150}Nd/^{144}Nd$ in addition to $^{142}Nd/^{144}Nd$, only equilibrated EC were analysed. Therefore with the currently published data it is unclear to what extent petrologic grade in the EC is responsible for the variation observed in the stable Nd isotopic ratios.

In order to better understand the genetic relationship between enstatite chondrites and the Earth we are carrying out a more systematic study including both equilibrated and unequilibrated enstatite chondrites, focusing on high precision analysis of all the stable Nd isotopic ratios. We have also analysed ordinary chondrites of different petrologic grades, as OC were previously proposed to better represent the bulk planetary Nd isotopic composition [7].

Method: Antarctic meteorites are valuable resource for such studies as they are particularly well preserved from the effects of terrestrial alteration. Approximately 1.8 g of sample was dissolved using acid digestion with the Nd being separated using ion-exchange chromatography. A Triton-Plus TIMS was used for the isotopic analysis with Nd analysed as Nd^+ using a multi-static routine after [8]

Results and Discussion: Our initial data for enstatite chondrites are consistent with [5-6,9] in showing that equilibrated enstatite chondrites are resolvable from Earth in their $^{142}Nd/^{144}Nd$ ratios. However, unlike [6], the $^{142}Nd/^{144}Nd$ ratios of the unequilibrated enstatite chondrites are not similar to the terrestrial values, weakening the arguments for ascribing $^{142}Nd/^{144}Nd$ variations to petrologic grade and the associated processing. We also observe significant variability in the stable ratios such as $^{145}Nd/^{144}Nd$ and $^{148}Nd/^{144}Nd$, which does not appear to correlate with petrologic grade.

Taking the EC together as whole, at the 95% confidence interval, student t-tests show that the modern convecting mantle, EC, and OC form three distinct populations with respect to their $^{142}Nd/^{144}Nd$. To assess to what degree this variation is nucleosynthetic in origin, and hence linked to accretionary processes, the isotopic ratios of Nd without a radiogenic contribution are key. However, in comparing the average $^{145}Nd/^{144}Nd$, $^{148}Nd/^{144}Nd$, and $^{150}Nd/^{144}Nd$ compositions of EC with either OC or the modern convecting mantle no clear picture emerges. With respect to the $^{148}Nd/^{144}Nd$ ratio, OC are resolvable from Earth at the 95% confidence interval, but the EC data overlap with both, and it is the same for $^{145}Nd/^{144}Nd$ and $^{150}Nd/^{144}Nd$. While our initial data would argue against the model of [4], where the Earth and enstatite chondrites are sourced from the same isotopic reservoir, it is clear that precise Nd stable isotopic composition of the enstatite chondrite reservoir has yet to be properly understood and constrained.

References: [1] Clayton R. N. et al. (1984) *Journal of Geophysical Research* 89:C245-C249 [2] Regelous M. et al. (2008) *Earth and Planetary Science Letters*, 272:330-338. [3] Trinquier A. et al. (2009) *Science* 324:374-376. [4] Dauphas N. and Schauble E. A. (2016) *Annual Reviews in Earth and Planetary Sciences*, 44:709-783. [5] Render J. et al. (2017) *Geochemi-*

cal Perspective Letters 3:170-178 [6] Gannoun A. et al. (2011) *Proceedings of the National Academy of Sciences* 108:7693-7697 [7] Andresaen R. and Sharma M. 2006 *Science.* 314:806-809. [8] Caro G. et al. 2006 *Geochimica et Cosmochimica Acta* 70:164-191 [9] Burkhardt C. et al. (2016) *Nature* 537:394-398

Effects of stochastic charging on micron sized grains in protoplanetary disks. K. S. Ashrafi[1], S. Esparza[1], C. Xiang[1], L. Matthews[1], A. Carballido[1], T. Hyde[1] and B. Shotorban[2], [1]Center for Astrophysics, Space Physics and Engineering Research, One Bear Place #97310, Baylor University, Waco, TX, 76798-7310, USA, [2]Department of Mechanical and Aerospace Engineering, The University of Alabama in Huntsville, Huntsville, AL 35899.

Introduction: Small dust grains are a major constituent of the material making up protoplanetary disks. In the earliest stages of planet formation, these grains agglomerate to form larger bodies, which are the precursors to planetesimals. In the last several years, numerical and semi-analytical models have shown that micron-sized dust grains play a significant role in the magnetohydrodynamic (MHD) evolution of protoplanetary disks (PPDs) [1,2,3]. The dust grains collect electrons and ions from the gas and provide a surface for electron recombination, affecting the ionization balance, which is crucial for the development of turbulence due to the magnetorotational instability [4].

Many of the sophisticated MHD disk models have assumed relatively simple recipes for dust charging, using, for example, analytical expressions for collision rates between charged particles and dust grains, as well as for electron sticking coefficients [5]. Likewise, these and other models mostly assume spherical grain shapes [1,3]. However, stochastic charging of grains can drive significant development of dust aggregate structure when the grains have a small charge [6]. This, in turn, would affects the available surface area for recombination on dust grains, and hence affect the overall ionization balance.

In this work, we use a model of discrete stochastic charging to calculate time-dependent electric charging of dust aggregates, with the aim of using the results for future MHD simulations of PPDs. We compare the electron and ion currents to micron and submicron grains which consist of aggregates of spherical monomers to those incident on spherical grains of equivalent mass. We calculate the average charge and charge distribution for (i) aggregates composed of monomers of 10 nm, 20 nm and 50 nm radius with an effective aggregate radius of 0.1 μm, and (ii) aggregates consisting of up to 50 monomers with monomer radius of 0.1 μm. Figure 1, 2, and 3 show the agreagates of equivalent radius 0.1 µm made of monomers of 10 nm, 20nm and 50 nm radius respectively.

Method: An aggregate charging code that relies on Orbital Motion Limited theory with a Line Of Sight approximation (OML_LOS) is employed [7].

The surface of each spherical monomer within an aggregate is divided up into many small patches. The electron and ion current to each patch is calculated by determining whether the line of sight from the patch center along a given direction is open or blocked by other momnomers within the aggregate. Only electrons or ions impinging from an open line of sight contribute to the charging currents.

The random charge fluctuations on the aggregates due to the electron and ion currents can be described by a master equation [8,9]

$$\frac{dP(Z,t)}{dt} = \sum_{p=1}^{N} I_{i,p}(Z-e_p)P(Z-e_p,t) + I_{e,p}(Z+e_p)P(Z+e_p,t) - [I_{i,p}(Z) + I_{e,p}(Z)]P(Z,t).$$

where N is the total number of patches on the aggregate, $Z = \{Z_1, Z_2, \ldots\ldots, Z_N\} \in R^N$ is the vector of the elementary charges collected on patches, $P(Z,\ t)$ is the probability density function of a state at which the patch p_i has Z_i charges, $I_{i,p}$ and $I_{e,p}$ are the rates of attachment for ions and electrons to the patch p, respectively, and $e_j \in R^N$ is the unit vector, e.g. $e_3 = \{0,0,1,0, \ldots,0\}$. In accordance with the master equation, the discrete stochastic method (DSM) is based on the following algorithm

1. Initialize the system with $Z = Z_0$ at $t = t_0$

2. Evaluate $I_{i,p}(Z)$ and $I_{e,p}(Z)$ of all patches and calculate

$$\lambda(Z) = \sum_{p=1}^{M} I_{i,p}(Z) + I_{e,p}(Z).$$

3. Generate the time interval τ between the attachment of the plasma particles to the aggregate according to $\tau = \frac{1}{\lambda(Z)}\ln(\frac{1}{r_1})$, where r_1 is a random number.

4. Generate p , the patch which experiences the attachment, according to p =the smallest integer satisfying $\sum_{p=1}^{M} I_{i,n}Z) + I_{e,n}(Z) > r_2\lambda(Z)$ where r_2 is another random number.

5. Use a third random number r_3 to specify the kind of attaching plasma particle according to: if $\frac{I_{i,p}}{I_{i,p}(Z)+I_{e,p}(Z)} > r_3$, then $Z = Z + e_p$; otherwise, $Z = Z - e_p$ electron.

6. Change t to $t + \tau$, and iterate

This algorithm is a customized version of the stochastic simulation algorithm developed for chemical kinetics [10].

Results: Figure 4, 5, and 6 show the charge distribution function *f*(*Z*) for grains in plasma with $T_e = T_i = 280\ K$, $n_e = 0.1\ n_i$ and aggregate equivalent radius of 0.1 μm for different monomer radius.

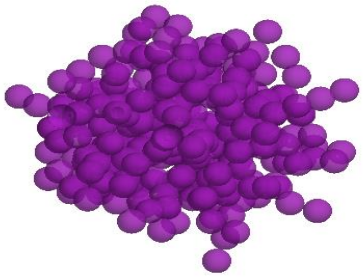

Figure 1: Aggregate radius of 0.1 μm made of monomers of radius 10 nm.

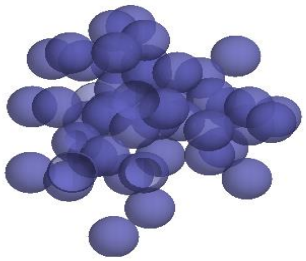

Figure 2: Aggregate radius of 0.1 μm made of monomers of radius 20 nm.

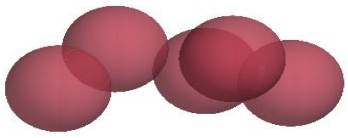

Figure 3: Aggregate radius of 0.1 μm made of monomers of radius 50 nm.

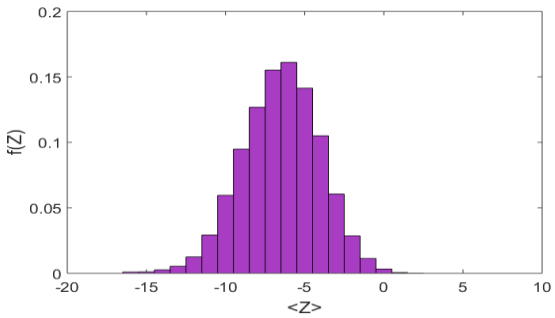

Figure 4: Charge distribution function *f*(*Z*) for 0.1 μm sized aggregates made of 10 nm sized monomers.

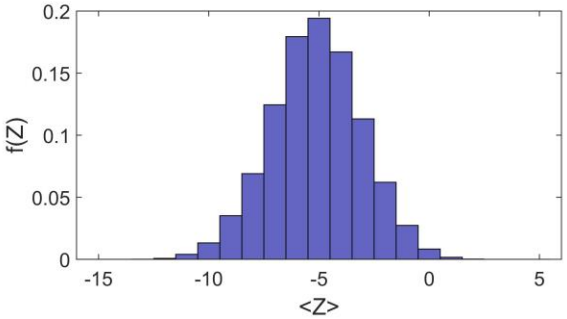

Figure 5: Charge distribution function *f*(*Z*) for 0.1 μm sized aggregates made of 20 nm sized monomers.

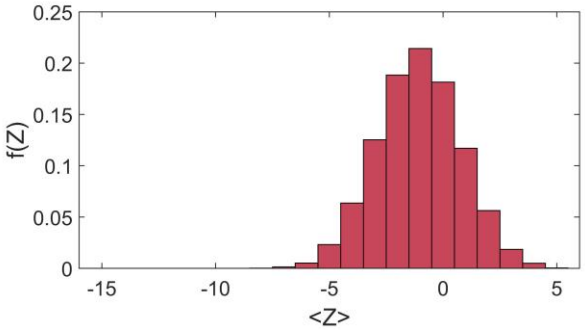

Figure 6: Charge distribution function *f*(*Z*) for 0.1 μm sized aggregates made of 50 nm sized monomers.

References: [1] Bai, X-N., Goodman, J. (2009), *ApJ, 701*, 737. [2] Turner, N. J., Carballido, A., Sano, T. (2010), *ApJ, 708*, 188. [3] Bai, X-N., (2011), *ApJ, 739*, 50. [4] Balbus, S. A., Hawley, J. F. (1998), *Rev. Mod. Phys., 70*, 1. [5] Draine, B. T., Sutin, B. (1987), *ApJ, 320*, 803. [6] Matthews, L. S., Shotorban, B., Hyde, T. W. (2013), *ApJ, 776*, 103. [7] Matthews, Land and Hyde (2012), *ApJ, 744*, 8. [8] Matsoukas and Russell (1995) *J. Appl. Phys., 77*: 4285-4292. [9] Shotorban, B. (2011), *Phys Rev E , 83*, 066403. [10] Gillespie (2007), *Annu. Rev. Phys. Chem, 58(1)*, 35-55.

REVEALING THE PHYSICAL AND THERMO-CHEMICAL EVOLUTION OF PLANET-FORMING DISK REGIONS. A. Banzatti[1], K. M. Pontoppidan[2], C. Salyk[3], E. F. van Dishoeck[4], G. J. Herczeg[5], G. A. Blake[6], A. Garufi[7], M. Kama[8], I. Pascucci[1], S. Edwards[9], [1]Lunar and Planetary Laboratory, The University of Arizona, Tucson, AZ 85721, USA (banzatti@lpl.arizona.edu); [2]Space Telescope Science Institute, 3700 San Martin Drive, Baltimore, MD 21218, USA; [3]Vassar College, 124 Raymond Avenue, Poughkeepsie, NY 12604, USA; [4]Leiden Observatory, Leiden University, P.O. Box 9513, 2300RA Leiden, The Netherlands; [5]Kavli Institute for Astronomy and Astrophysics, Peking University, Yi He Yuan Lu 5, Haidian Qu, 100871 Beijing, China; [6]Division of Geological & Planetary Sciences, MC 150-21, California Institute of Technology, Pasadena, CA 91125, USA; [7]Universidad Autonónoma de Madrid, Dpto. Física Teórica, E-28049 Madrid, Spain; [8]Institute of Astronomy, Madingley Rd, Cambridge, CB3 0HA, UK; [9]Five College Astronomy Department, Smith College, Northampton, MA 01063, USA.

Introduction: Radial velocity and transit surveys have discovered a plethora of exoplanets at orbital distances of < 10 au around other stars [e.g., 1,2]. Planet populations and their diversity are fundamentally linked to the structure, evolution, and dispersal of protoplanetary disks at these orbital radii. The water snow line at ~1-10 au plays a key role in shaping planetary system architectures and compositions, as suggested by models and by Solar System and exoplanet data [e.g., 3,4,5]. Moreover, inner disk dispersal is proposed to increase the efficiency of rocky planetesimal formation by decreasing the gas-to-dust ratio at < 10 au through gas removal, and to directly impact the orbital architecture of planetary systems [e.g., 6,7]. Understanding disk structure and evolution is key to building a comprehensive and predictive theory of planet formation.

Access to the structure and evolution of inner regions in protoplanetary disks, at the time when planets form, is now possible. While modern imaging techniques are limited to probing disks at ≥ 3-4 au at best [e.g., 8,9], a suite of other observational probes of inner disks has meanwhile been steadily improving. Here we report on recent results of a large ongoing campaign aiming at revealing the physical and thermo-chemical evolution of planet-forming disk regions, at ~0.05-20 au in protoplanetary disks.

A high-resolution, multi-tracer campaign: The first and main component of this campaign is high-resolution spectroscopy of molecular gas emission as observed at infrared wavelengths from protoplanetary disks. Infrared spectra of the main molecular tracers (CO, H_2O, OH, and some organic molecules) are rich in transitions that probe temperatures and densities found in planet-forming regions [10,11]. Their line profiles, broadened by Keplerian rotation around the central star, can be observed in full detail by high-resolution spectrographs on large telescopes with resolving powers of R~100,000 [12,13]. Detailed line shapes and fluxes, in turn, provide spatially-resolved information on temperatures, density, excitation, and dispersal of molecular gas in inner disks, including regions that are unreachable by direct imaging.

In addition to using high-resolution infrared spectroscopy to obtain spatially-resolved measurements in inner disks, the key elements of this campaign are: 1) the collection of an increasingly larger sample of protoplanetary disks (> 50 young disks around stars of masses between 0.3 and 3.5 solar masses), 2) the combined analysis of observed spectra of multiple molecules (first of all CO and H_2O, see Figure 1(a)), 3) the combination of multiple tracers, including molecular gas, dust, and atomic gas emission to probe both the gas and the dust, and both the disks and the winds that disperse them. By combining multiple datasets from a suite of telescopes from the ground and in space, we are working our way towards obtaining a global view of the evolution of planet-forming disk regions.

Disk cavities, and inner disk depletion: The analysis of high-resolution line profiles of rovibrational CO emission at 4.7 micron provided a groundbreaking discovery, and a fundamental framework for other datasets. CO lines excited in inner disks are observed to have line widths in the range of ~10-200 km/s, which correspond to Keplerian orbits of ~0.05-20 au (where *larger* velocity widths imply *smaller* orbits for the gas, and vice versa). A correlation has been discovered between the orbital radius of CO emission as derived from line widths (R_{co}), and the ratio of line fluxes between the second and first vibrational states, a sensitive "thermometer" of temperature and irradiation. Figures 1(b) and (c) show the sequence of inner disk depletion that this correlation has revealed: as CO emission moves to larger orbital radii (a consequence of removal of CO at smaller orbital radii), the observed emission probes colder and colder disk regions [14].

The dry-out of planet-forming disk regions: As a second step, we have combined the analysis of rovibrational CO emission and of H_2O vapor emission observed from inner disks [15]. The large sample of > 50 disks, coupled to the large coverage of water energy levels (~1000-9000 K), and to the orbital constraints provided by CO lines, clarified early findings of water-rich and water-poor disks in spectrally-*un*resolved observations [16]. Protoplanetary disks that show water-

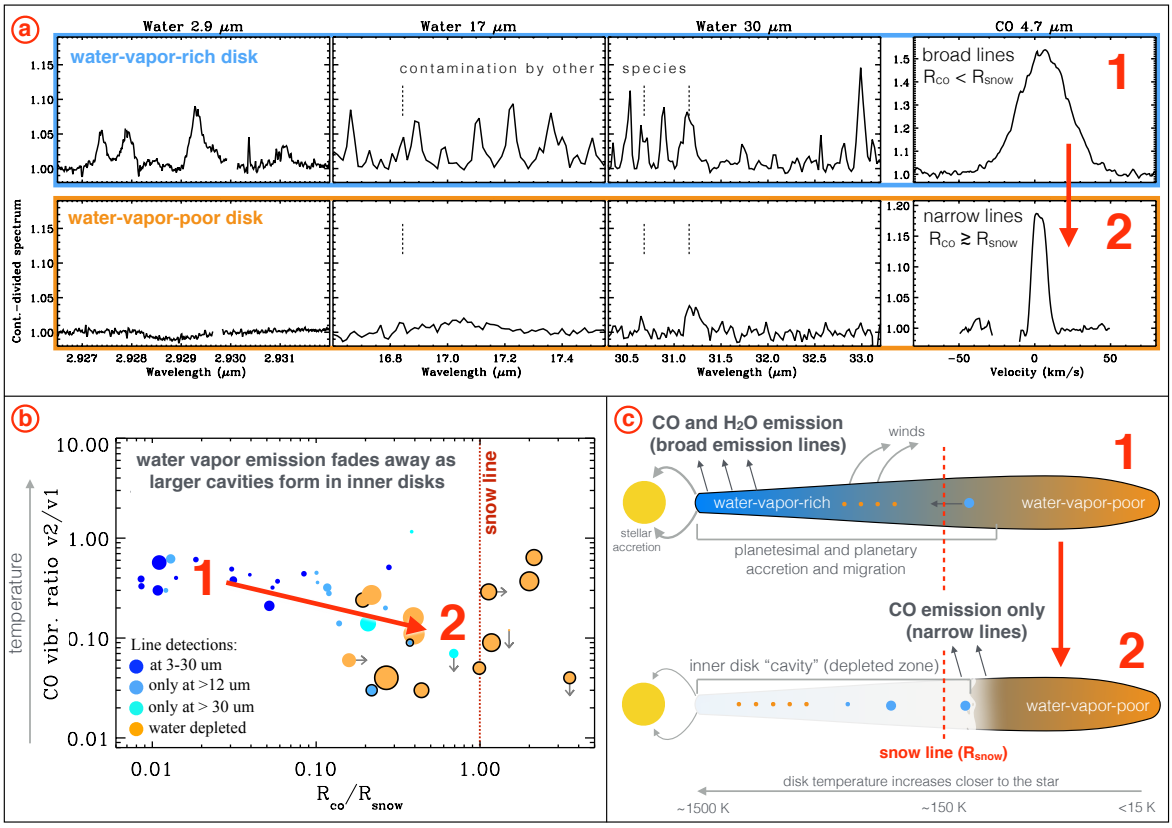

Figure 1 *– Results from this campaign to reveal the physical and thermo-chemical evolution of planet-forming disk regions. Panel (a) shows representative CO and H_2O infrared spectra of young protoplanetary disks, as obtained with VLT-CRIRES and Spitzer-IRS [15]. Panel (b) shows the decrease of water vapor emission as inner disk cavities form and expand to larger disk radii, as revealed by the orbital radius of CO emission (R_{co}). Panel (c) shows a cartoon to illustrate these findings in the context of the evolution of planet-forming regions in protoplanetary disks during planetary accretion.*

vapor-rich infrared spectra are found to have broad CO emission lines, demonstrating that their inner orbital regions are still rich in molecular gas. On the contrary, water emission fades away as CO lines become narrower, i.e. as the size of the inner disk cavity expands to larger disk radii. Water vapor emission disappears when the inner cavity reaches and exceeds the water snow line radius [15, Figure 1], beyond which water is frozen on icy bodies that, by migration and accretion, deliver water to the inner disk dry bodies [e.g. 17].

Dust and gas evolution, and dispersing winds: The next steps of this campaign include the combined analysis of molecular spectra and of tracers of inner disk dust and winds. In a series of papers in preparation, we are now exploring 1) the linked depletion of gas and dust in inner disks, pointing at the role of dust accretion into planetesimals and planets [18,19], and 2) the presence, nature, and effects of winds that disperse inner disks [6,20], which may contribute to the formation of the cavities observed in dust and in molecular gas. All together, these observations are providing and essential guidance towards a global understanding of the evolution of planet-forming regions, and of their links to the architecture and composition of planetary systems.

References:

[1] Mullally et al. (2015) *Astrophys. J. Suppl., 217,* 31. [2] Mayor et al. (2011) eprint arXiv:1109.2497. [3] Ida & Lin (2008) *Astrophys. J., 685,* 584. [4] Mordasini et al. (2012) *Astron. Astrophys. 541*, A97. [5] Morbidelli et al. (2016) *Icarus, 267,* 368. [6] Gorti et al. (2015) *Astrophys. J., 804,* 29. [7] Alexander & Pascucci (2012) *MNRAS, 422*, L82. [8] ALMA Partnership (2015) *Astrophys. J. Letters, 808,* L3. [9] Avenhaus et al. (2017) eprint arXiv:1705.09680. [10] Carr & Najita (2008) *Science, 319*, 1504. [11] Salyk et al. (2011) *Astrophys. J., 743*, 112. [12] Pontoppidan et al. (2011) *Msngr, 143*, 32. [13] Pontoppidan et al. (2011) *Astrophys. J., 733*, 84. [14] Banzatti & Pontoppidan (2015) *Astrophys. J., 809,* 167. [15] Banzatti et al. (2017) *Astrophys. J., 834,* 152. [16] Pontoppidan et al. (2010) *Astrophys. J., 720,* 887. [17] Ciesla et al. (2015) *Astrophys. J.,* 804, 9. [18] Bruderer S. (2013) *Astron. Astrophys.,* 559, A46. [19] Kama et al. (2015) *Astron. Astrophys.,* 582, L10. [20] Simon et al. (2016) *Astrophys. J., 831,* 169.

PLANETESIMAL FORMATION AND COLLISIONAL EVOLUTION. J. Blum[1], [1]Institut für Geophysik und extraterrestrische Physik, TU Braunschweig, Mendelssohnstr. 3, D-38106 Braunschweig, Germany (j.blum@tu-bs.de).

Introduction: The formation of planetesimals is still full of open questions. However, during the past decades, astronomical observations of protoplanetary disks (PPDs), PPD models and laboratory investigations have provided us with a much fuller picture about the processes that shape the planetary progenitors (see, e.g. [1,2]). As of today, we can distinguish three evolutionary phases:

- agglomeration of dust/ice particles,
- the formation of planetesimals, and
- the post-formation collisional evolution.

In the following, our current understanding of these phases will be outlined.

Agglomeration of dust and ice particles: In its initial stage, the PPDs are seeded with (sub-)micrometer-sized dust and ice particles, which partly condensed out of the cooling gas or were inherited from the parent molecular-cloud. Due to Brownian motion, differential drift motions, and gas turbulence, the dust and ice particles frequently collide among each other. As long as the collision speed does not exceed the threshold for sticking, all collisions result in the growth of agglomerates. Experiments have shown that sticking occurs for velocities below ~1 m/s for dust [3] and ~10 m/s for µm-sized water ice particles [4]. Numerical simulations suggest that direct collisional growth leads to dust aggregates up to ~1 cm in size in the inner parts of a minimum mass solar nebula (MMSN) [5]. In the outer reaches of a MMSN, the maximum aggregate sizes might not exceed ~1 mm [6].

Formation of planetesimals: There are two possible avenues from pebble- or sand-grain-sized dust or ice agglomerates to planetesimals:

- adhesion based growth or
- growth by gravitational instability.

Adhesion based growth models: Although the collision velocity exceeds the sticking threshold, dust/ice aggregates can still grow if (a) the size ratio between the (smaller) projectile and the (larger) target aggregate is below a certain threshold [7], (b) the absolute size of the projectile agglomerate is neither too large nor too small (in the former case, cratering will occur, in the latter erosion) [8], and (c) the impact velocities are within a given range [9]. The corresponding growth process relies on partial mass transfer from the fragmenting projectile to the non-fragmenting target. However, convolving the existing information about the collision velocities and collision outcomes into a planetesimal growth model shows that the required timescales for the formation of macroscopic planetary bodies are extremely long [10] and that the required size range for projectile agglomerates is extremely narrow [8], rendering this planetesimal formation scenario unlikely.

Models of planetesimal formation by gravitational instability: More promising are those models that predict the formation of planetesimals by the gentle gravitational collapse of a cloud of dust aggregates [see 2]. Under the conditions of (a) a sufficiently strong local pre-concentration of the dust aggregates, (b) dust aggregates sizes within a limited range such that their corresponding Stokes numbers are around St ~0.1, and (c) a metallicity of the nebula in excess of ~0.015 [11], the streaming instability [12] leads to local dust concentrations strong enough to cause the gravitational accretion of planetesimals with up to ~1000 km in size [see 2].

Observations of cometary nuclei and models of their activity suggest that these planetesimals were most likely formed through the gentle gravitational collapse of cm-sized dust/ice aggregates [13-15].

The post-accretional collisional evolution of planetesimals: Formation of planetesimals by the gravitational collapse of ~cm-sized dust aggregates leads to the formation of extremely porous bodies. For planetesimal radii $\lesssim$50 km, the pebbles stay intact so that their initial volume filling factor (the fraction of volume occupied by solid material) is ~0.25, in agreement with measurements for comet 67P [15]. For larger planetesimals, the pebbles are destroyed, resulting in somewhat higher volume filling factors of ~0.5.

Cometary nuclei: The obvious agreement between measured and predicted porosities for cometary nuclei as well as the presence of extremely fluffy of even fractal dust agglomerates suggest that these bodies never experienced a catastrophic collision after their formation by gravitational instability [16}. This finding is in stark contrast to earlier work in which cometary nuclei are (re-accreted) fragments of catastrophic collisions in the past [17-20]. Future investigations will have to show whether the high porosity of cometary nuclei and their mutual encounters at hyper-velocities can be brought into agreement or whether models of the early evolution of the outer reaches of the young Solar System require revision.

Asteroids: The extremely low porosities of meteorites suggest that their parent bodies underwent high-

speed collisions or impacts since their formation. Based on laboratory impacts into chondrule-matrix analog mixtures [21], simulations have shown that most of the required compaction occurred in the first ~1 Gyr after formation [22]. Such simulations and their comparison to meteoritic properties can yield important information on the collisional history of the Solar System.

References: [1] Testi L. et al. (2014) *Protostars and Planets VI*, 339-362. [2] Johansen A. et al. (2014) *Protostars and Planets VI*, 547-570. [3] Blum J. and Wurm G. (2008) *ARAA, 46*, 21-56. [4] Gundlach B. and Blum J. (2015) *ApJ, 798*, 34. [5] Zsom A. et al. (2010) *A&A, 513*, A57. [6] Lorek S. et al. *A&A (submitted)*. [7] Bukhari Syed M. et al. (2017) *ApJ, 834*, 145. [8] Kothe S. (2017) *PhD Thesis, TU Braunschweig*. [9] Teiser J. and Wurm G. (2009) *MNRAS, 393*, 1584-1594. [10] Windmark F. et al. (2012) *A&A, 540*, A73. [11] Yang, C.-C. et al. (2016) *arxiv:1611.07014*. [12] Youdin A. N. and Goodman J. (2005) *ApJ, 620*, 459-469. [13] Skorov, Y. and Blum J. (2012) *Icarus, 221*, 1-11. [14] Blum J. et al. (2014) *Icarus, 235*, 156-169. Blum J. et al. (2015) *Icarus, 248*, 135-136. [15] Blum J. *MNRAS (submitted)*. [16] Fulle M. and Blum J. (2017) *MNRAS (in press)*. [17] Morbidelli A. and Rickman H. (2015) *A&A, 583*, A43. [18] Rickman H et al. (2015) *A&A, 583*, A44. [19] Jutzi M. et al. (2017). *A&A, 597*, A61. [20] Jutzi M. and Benz W. (2017) *A&A, 597*, A62. [21] Beitz E. et al. (2013) *Icarus, 225*, 558-569. [22] Beitz E. et al. (2016) *ApJ, 824*, 12.

Additional Information: This work has been supported by various grants from the *Deutsche Forschungsgemeinschaft* (DFG) and the *Deutsches Zentrum für Luft- und Raumfahrt* (DLR).

WATER IN THE EARLY SOLAR SYSTEM AND MANTLE MELTING IN TERRESTRIAL PLANETS. A. D. Bravenec[1], G. D. Bromiley[1], and S. C. Kohn[2], [1]School of GeoSciences, University of Edinburgh, Edinburgh, UK (a.d.bravenec@sms.ed.ac.uk), [2]School of Earth Sciences, University of Bristol, Bristol, UK.

Introduction: Determining the origin and distribution of water in planetary interiors has important implications for understanding the formation and evolution of terrestrial planets and the emergence of life, both in the solar system and beyond. Despite the shared origin of the Earth and Moon, the Moon has remained comparatively unchanged over the past several billion years, while the Earth has experienced large scale geodynamics, resulting in the loss of evidence of Earth's original post-accretion composition. Therefore the Moon offers a unique opportunity to gain insight into the role volatile compounds play in planetary formation and early evolution in the Earth-Moon system. Since the discovery of water in lunar glass beads [1], melt inclusions [2], and minerals [3-4], constraining the exact water content in a range of lunar and Martian materials is an active area of interest [e.g. 5]. Because the Moon lacks plate tectonic processes to flux water into the deep interior, the presence of water in lunar magmas implies a hydrous interior in the Earth-Moon system inherited from initial accretionary processes and not completely lost during magma ocean formation or late accretion events.

However, our understanding of volatile incorporation in planetary interiors is largely based on experiments performed under the relatively oxidizing conditions of the modern terrestrial interior. Current estimates of lunar and Martian mantle water contents are based on partitioning data from experiments performed under terrestrial (more oxidized) conditions, as well as observed water contents of magmas, and models of mantle melting processes. Constraining interior water contents of these bodies from measured volatiles in surface materials is also highly questionable. The Martian mantle, lunar mantle, and early terrestrial magma ocean would have experienced reducing conditions [6-9]. Preliminary research suggests fO_2 has a significant influence on water partitioning and speciation in model lunar systems, implying that our understanding of how water is incorporated in the interiors of primitive terrestrial bodies is far from complete.

Experiments and Future Work: Experiments are being conducted in an end-loaded piston cylinder using a double-capsule technique to vary fO_2 with a simplified starting composition representative of the primitive terrestrial, lunar, and Martian mantle compositions respectively. Experiments with various fO_2 buffers (QIF, IW, FMQ, NNO, MH, graphite) will be conducted at varying P (1-4 GPa) and T (~1000-1700 °C). These experiments will determine 1) how H_2O speciation (OH, H_2O, H_2) varies as a function of oxygen fugacity and 2) the determination and quantitation of the effect of varying fO_2 on hydrogen species partitioning between mantle minerals and silicate melt. SIMS (secondary ion mass spectrometry), FTIR (Fourier transform infrared spectroscopy), and Raman spectroscopy will be used to analyze $H_2O/H_2/OH$ contents of minerals and melts. Data from these varied fO_2 experiments will be used to investigate the incorporation mechanisms of different water species in various mineral phases as a proxy for planetary interiors. Results will inform modelling the water content of lunar and Martian interiors, compare the modelled water content of the Earth, Moon, and Mars, and investigate the timing and sources of water in the early solar system.

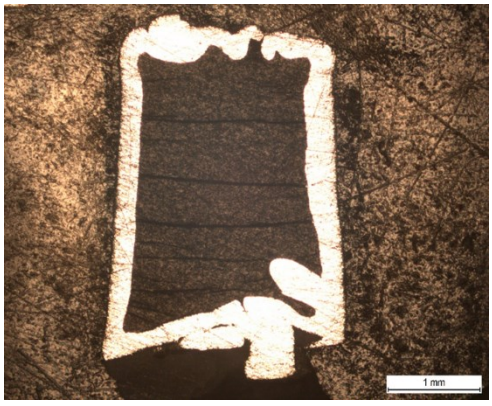

Figure 1. Backscattered electron image of experiment E6 (2 GPa, 1000 ˚C, 5 hours. Scale bar is 1 mm).

References: [1] Saal A.E. et al. (2008) *Nature,* 454, 192-196. [2] Hauri E.H. et al. (2011), *Science*, 333, 213-215. [3] McCubbin F. M. et al. (2010), *Proc. Natl. Acad. Sci. U.S.A*., 107, 11223. [4] Boyce J.W. et al. (2010), *Nature*, 466, 466. [5] McCubbin F.M. et al. (2016) *Meteor. Planet. Sci*., 51, 2036-2060. [6] Herd C.D.K. (2003) *Meteor. Planet. Sci*., 38, 1793-1805. [7] Shearer C. K. et al. (2006) *Am. Mineral*., 91, 1657-1663. [8] Karner J. M. et al. (2007) *Am. Mineral*., 92, 1238-1241. [9] Wadwha M. (2008) *Review Mineral. Geochem*., 68, 493-510.

USING ORBITAL PLATFORMS TO STUDY PLANET FORMATION.

J. Brisset[1], J. Colwell[1], A. Dove[1], and D. Maukonen[1]
[1]Planetary Sciences Group, Department of Physics, University of Central Florida, 4000 Central Florida Blvd, Orlando FL 32816-2385, julie.brisset@ucf.edu

Introduction:

The standard model of planet formation proceeds from the gravitational collapse of an interstellar cloud of gas and dust through collisional accretion of solids into planetesimals and eventual runaway growth to form the terrestrial and giant planets [1]. A critical stage of that process is the growth of solid bodies from mm-sized chondrules and aggregates to km-sized planetesimals where gravity becomes an important force for further growth. Theories on this dust growth phase include gravitational instability [2,3] and direct binary accretion of particles [4]. To characterize the collision behavior of dust in protoplanetary conditions, experimental data is required, working hand in hand with models and numerical simulations. In particular in the range of mm- to cm-sized particles, the collection of a statistical data set on collision behavior will allow to better characterize the growth of dust to planetesimal sizes.

In order to replicate the very low collision velocities that the dust grains experience in the protoplanetary disk (PPD), this experimental data has to be collected under microgravity conditions. Classical platforms include parabolic aircrafts or suborbital rockets, both limited in the microgravity time available. With the rise of miniaturized payloads, we are now able for the first time to access long-duration microgravity using orbital platforms, such as the International Space Station (ISS) or stand-alone CubeSats, thus revolutionizing the experimental possibilities.

Microgravity Experiments on Dust Aggregate Growth:

Dust growth experiments date back to the late 90s where the hit-and-stick behavior of µm-sized grains demonstrated a possible mechanism for grain growth inside the PPD [5,6]. Later experiments on larger grains have shown that, at the relative velocities expected in the PPD [7], sticking upon collisions yields to bouncing and fragmentation [8]. Figure 1 shows a dust collision model integrating the results of a decade of experimental data [9].

The transition between grain sticking and bouncing remains relatively unexplored experimentally as very slow collisions of mm- and cm-sized particles can only be performed under microgravity conditions. Microgravity platforms used to perform these experiments include drop towers (up to 9 s of free-fall time in Bremen, Germany), parabolic aircrafts (~ 20 s) , and suborbital rockets (~ 180 s). depending on the platform used, each experiment campaign can deliver from a few to 100 data points which makes a better characterization of the sticking to bouncing transition a slow and arduous process.

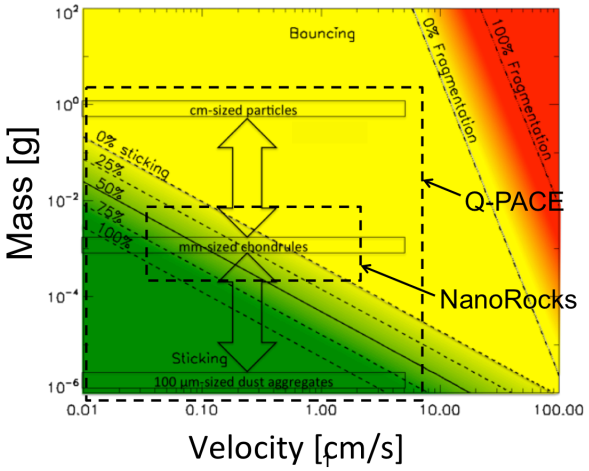

Figure 1: Dust collision model [9] showing the outcome of a collision as a function of the grains' mass and relative velocity (green for sticking, yellow for bouncing, and red for fragmentation). The regions of the parameter field that are addressed by the NanoRocks and Q-PACE experiments are marked with dashed boxes.

Miniaturized Payloads and Orbital Platforms:

In this context, the rise of miniaturized orbital payloads such as CubeSats make it possible to collect the required amount of data. Indeed, the small and cost-effective hardware does not require long development times and is adapted to the efficient collection of high amounts of grain collision data during years on orbit (usually Low Earth Orbit).

The Center for Microgravity Research (CMR) of the University of Central Florida (UCF) has flown a first miniaturized payload (1.5U in CubeSat units), NanoRocks, on the International Space Station (ISS) from September 2014 to March 2016 [10]. This payload recorded collisions between mm-sized particles in microgravity (Figure 2). The data analysis has demonstrated that the unprecedented amount of grain collision data collectedby NanoRocks allowed for a statistical approach to the data analysis rather than the classical measurement of individual collisions.

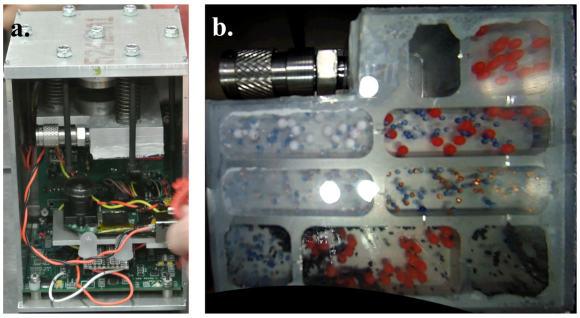

Figure 2: The NanoRocks experiment: a. Experiment hardware before closing: the camera and electronics can be seen at the bottom of the picture, while the tray and its springs and magnet are at the top. b. Recorded image of the experiment tray containing the eight particle samples during an experiment run on ISS.

Building on the success of the NanoRocks payload, the CMR is currently developing a 3U CubeSat to study collisions between cm-, mm-, and submm-sized particles. The CubeSat Particle Aggregation and Collision Experiment (Q-PACE) is a 3U satellite hosting an Experiment Test Cell (ETC) containing the particles, a camera to record the particle collisions, and all the avionics necessary to guarantee for the satellite's autonomy during its time on orbit (Figure 3). the collected data will be transferred to the Q-PACE ground stations at UCF and the University of Arkansas. Q-PACE is currently in manufacturing and is scheduled to launch with Virgin Galactic's ELaNa XX on December 1st, 2017.

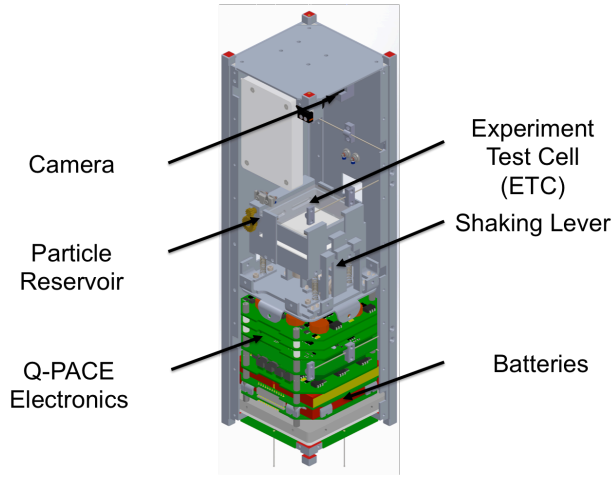

Figure 3: CubeSat Particle Aggregation and Collision Experiment (Q-PACE) design. The particles will be kept in the Experiment Test Cell (ETC) and their collision behavior recorded with the camera.

We will present results from the NanoRocks experiment as well as the mission design of Q-PACE to demonstrate how orbital miniaturized payloads can be used to collect unprecedented amounts of data on the collision behavior of PPD dust grains

Acknowledgements:

This work is based in part upon research supported by NASA through the Origins of Solar Systems Program grant NNX09AB85G and by NSF through grant 1413332. The NanoRocks experiment was supported by Space Florida, NanoRacks LLC, and the University of Central Florida.

References:

[1] Klahr, Hubert, and Wolfgang Brandner. "Planet Formation." Edited by Hubert Klahr and Wolfgang Brandner. (Cambridge University Press) 05 2006.

[2] Goldreich, Peter, and William R. Ward. *The Astrophysical Journal* 183 (1973): 1051-1062

[3] Youdin, Andrew N., and Eugene I. Chiang. *The Astrophysical Journal* 601, no. 2 (02 2004): 1109-1119.

[4] Windmark, F., Birnstiel, T., Güttler, C., Blum,, J., Dullemond, C. P., and Henning, Th. *Astronomy & Astrophysics* 540, (04 2012): 17.

[5] Poppe, T., Blum, J., Henning, T., The Astrophysical Journal 533, no. 1 (04 2000): 454-471

[6] Blum J, Wurm G, Kempf S, Poppe T, Klahr H, Kozasa T, Rott M, Henning T, Dorschner J, Schräpler R, Keller HU., *Physical Review Letters* 85.12 (2000): 2426.

[7] Weidenschilling, S. J., *Astrophysics and Space Science* 51.1 (1977): 153-158.

[8] Zsom, A., Ormel, C.W., Güttler, C., Blum, J. and Dullemond, C.P., *Astronomy & Astrophysics*, 513 (2010) p.A57.

[9] Güttler, C., Blum, J., Zsom, A., Ormel, C.W. and Dullemond, C.P., *Astronomy & Astrophysics* 513 (2010): A56.

[10] Brisset, J., Colwell, J.E., Dove, A., Maukonen, D., Brown, N., Lai, K. and Hoover, B., 2015, December. NanoRocks: A Long-Term Microgravity Experiment to Stydy Planet Formation and Planetary Ring Particles. In *AGU Fall Meeting Abstracts*.

WHAT MATERIAL ACCRETED TO FORM THE EARTH? T. H. Burbine[1], R. C. Greenwood[2] and I. A. Franchi[2], [1]Department of Astronomy, Mount Holyoke College, South Hadley, MA 01075, USA (tburbine@mtholyoke.edu), [2]Planetary and Space Sciences, School of Physical Sciences, The Open University, Walton Hall, Milton Keynes MK7 6AA, UK.

Introduction: One unsolved question in planetary science is what was the dominant material that accreted to form the Earth. Enstatite chondrites and aubrites all fall close to the terrestrial fractionation line on the three-isotope oxygen isotopic plot (**Figure 1**) [1]. (Aubrites are achondrites that are believed to be the product of the melting and differentiation of enstatite chondrite-like material [2].) Dauphas [3] noted that enstatite chondrites and aubrites are isotopically similar to the Earth over a wide variety of isotopic systems. However, enstatite chondrites and aubrites have much lower bulk FeO-contents (< 1 wt%) than the primitive upper mantle (PUM) (~8 wt%) [4]. Javoy et al. [5] argued that the increasing temperature during the Earth's formation would have caused iron in the mantle to oxidize.

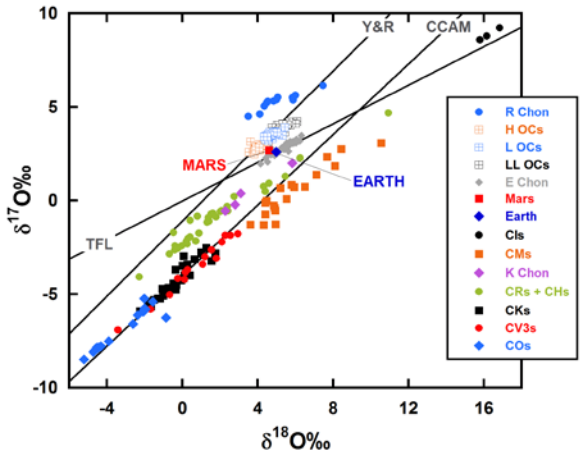

Figure 1. Oxygen isotope plot for the chondritic meteorite groups, the K chondrite grouplet, the Earth, and Mars. The terrestrial fractionation line (TFL), the Carbonaceous Chondrite Anhydrous Mineral (CCAM) line, and the Y&R (Young and Russell) [6] line are also plotted.

The estimated Mg/Si weight ratio for the PUM is much higher than the Mg/Si ratio for known chondrites [7] (**Figure 2**). Of known chondritic material, carbonaceous chondrites have Mg/Si ratios closest to that of the PUM. However, Warren [8] noted that the Earth is not isotopically similar to carbonaceous chondrites over a wide variety of isotopic systems. Enstatite chondrites have the lowest Mg/Si ratios of known chondrites. Incorporating Si into the core could resolve this apparent compositional difference between the chondrites and the PUM [7]. Additionally, this apparent compositional difference might be resolved if the PUM estimates are not representative of the bulk silicate Earth [7]. Another possible explanation is that the Earth is primarily composed of chondritic material not currently in our meteorite collections [9]. Dauphas [3] proposed that the Earth formed out of material isotopically similar to enstatite chondrites, but enriched in forsterite. Burbine and O'Brien [10] (**Figure 2**) found that no known mixture of chondritic material could match the chemical and isotopic composition of the bulk Earth. So what is the Earth made from? Could the Earth be composed primarily of chondritic material not currently found in our meteorite collections?

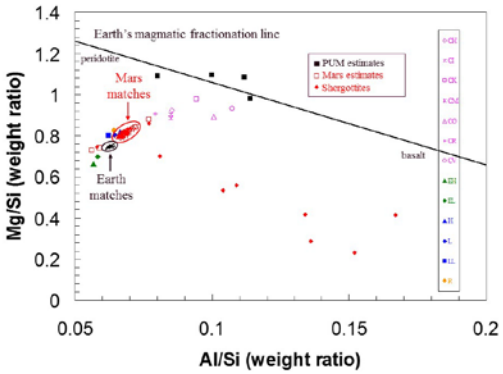

Figure 2. Plot of Al/Si versus Mg/Si weight ratios for chondritic meteorite groups (average values), estimated values for the PUM (black squares), estimated values for Mars (open red squares), and values for shergottite meteorites (red diamonds). The black line is the trend for terrestrial rocks, which is taken from Dreibus et al. [11]. Ellipses are drawn around the estimates of the composition of the PUM and Mars. The black dots are the matches for the Earth, and the red dots are matches for Mars. Figure is from Burbine and O'Brien [10].

Building Blocks of Mercury, Venus, and Mars: Estimates of the building blocks of the other terrestrial planets have also been done. The best chondritic analogs for Mercury's building material appear to be the enstatite chondrites [12] due to the low-FeO nature of Mercury's surface [13]. The building blocks of Venus are usually assumed to be similar to those of the Earth [14]. The "best" models for forming Mars contain a

mixture of a number of different chondritic meteorite groups, but usually include a sizeable proportion of ordinary chondritic material (**Figure 2**) [10].

Condensation Sequence: Grossman [15] calculated a condensation sequence for minerals in the solar nebula. The highest temperature condensates (corundum, perovskite, melilite group, and spinel) are found in calcium-aluminum inclusions (CAIs), which are major components of CV and CO chondrites. CAIs are the oldest dated material found in our Solar System and appear to have been preferentially transported outward to the outer Solar System. Lower-temperature condensates (enstatite and FeNi metal) are major components of enstatite chondrites, while even lower-temperature condensates (ferrous olivines and ferrous pyroxenes) are major components of ordinary chondrites (H, L, and LL) with FeNi metal. (Enstatite chondrites have olivine compositions of $Fa_{<1}$. Equilibrated H chondrites have olivines with $Fa_{16\text{-}20}$, equilibrated L chondrites have olivines with $Fa_{23\text{-}26}$, and equilibrated LL chondrites have olivines with $Fa_{27\text{-}32}$ [16].) Water, which would have condensed at even lower temperatures, is found in the hydrated silicates in carbonaceous chondrites.

One chondritic grouplet (K chondrites) have fayalite contents (Fa_4) intermediate between enstatite and H chondrites [17]. (Grouplets have less than five members.) K chondrites are named after the first identified member, Kakangari. However, K chondrites have bulk oxygen isotopic values that plot near CR chondrites (**Figure 1**), Mg/Si ratios that are slightly higher than H chondrites, and high matrix abundances that is similar to carbonaceous chondrites [17]. Therefore, chondrites intermediate in bulk FeO between enstatite and H chondrites and oxygen isotopic values that fall near the terrestrial fractionation line could have potentially formed.

Asteroid Belt: The asteroid belt shows a distribution of taxonomic classes that is roughly consistent with the condensation sequence [18,19]. Taxonomic classes that are primarily composed of material that would have condensed at higher temperatures tend to be found closer to the Sun than classes that contain material that would have condensed at lower temperatures. The interior part of the belt is dominated by E-type asteroids, which are believed to include the parent bodies of the aubrites. The middle part of the belt is dominated by S-complex bodies, which are believed to include the parent bodies of the ordinary chondrites. The outer part of the belt is dominated by C-complex bodies, which are believed to include the parent bodies of the carbonaceous chondrites. However, there are over 700,000 asteroids currently known and only ~120-132 identified possible meteorite parent bodies using both oxygen isotopic and mineralogical studies [20]. Therefore, a large number of chondritic meteorite types that are not currently found in our meteorite collections could potentially be present in the asteroid belt

Conclusions: The difficulty in making the Earth (and Venus) out of known chondritic material could potentially be solved by the existence of chondritic material not currently found in our meteorite collections. These chondrites would be intermediate in bulk FeO between enstatite and H chondrites and isotopically similar to enstatite chondrites. Models for forming the terrestrial planets should use a much larger array of starting materials than just the known chondritic meteorite groups. This material could still exist in the asteroid belt. However, this is a very unsatisfying explanation in many respects since this material has not been currently identified. The discovery and analysis of Mercurian and Venusian meteorites would also help us gain insight on potential building blocks for the terrestrial planets.

References: [1] Newton J. et al. (2000) *Meteoritics & Planet. Sci., 35,* 689-698. [2] Keil K. (2010) *Chemie der Erde, 70,* 295-317. [3] Dauphas N. (2017) *Nature, 541,* 521-524. [4] Robinson M. S. and Taylor G. J. (2001) *Meteoritics & Planet. Sci., 36,* 841-847. [5] Javoy M. et al. (2010) *EPSL, 293,* 259-268. [6] Young E. D. and Russell S. S. (1998) *Science, 282,* 452-455. [7] Palme H. and O'Neill H. St. C. (2014) In *The Mantle and Core* (Vol. 3), *Treatise on Geochemistry 2nd Ed.,* 1-39. [8] Warren P. H. (2011) *EPSL, 311,* 93-100. [9] Drake M. J. and Righter K. (2002) *Nature, 416,* 39-44. [10] Burbine T. H. and O'Brien K. M. (2004) *Meteoritics & Planet. Sci., 39,* 667-681. [11] Dreibus G. et al. (1998) *LPS XXIX,* Abstract #1348. [12] Namur O. et al. (2016) *EPSL, 439,* 117-128. [13] Nittler L. R. et al. (2011) *Science, 333,* 1847-1850. [14] Righter K. et al. (2006) In *Meteorites and the Early Solar System II,* 803-828. [15] Grossman L. (1972) *GCA, 36,* 597-619. [16] Weisberg M. K. et al. (2006) In *Meteorites and the Early Solar System II,* 19-52. [17] Weisberg M. K. et al. (1996) *GCA, 60,* 4253-4263. [18] Gradie J. and Tedesco E. (1982) *Science, 216,* 1405-1407. [19] DeMeo F. E. and Carry B. (2014) *Nature, 505,* 629-634. [20] Greenwood R. C. et al. (2017) *LPS XLVIII,* Abstract #2515.

Acknowledgements: THB would like to thank the Remote, In Situ, and Synchrotron Studies for Science and Exploration (RIS^4E) Solar System Exploration Research Virtual Institute (SSERVI) for support. Oxygen isotope studies at the Open University are funded by a consolidated grant from the UK Science and Technology Facilities Council (STFC) (Grant Number: ST/L000776/1).

FORMATION OF PLANETESIMAL THROUGH THE STREAMING INSTABILITY. D. Carrera, CEHW, Pennsylvania State University, 525 Davey Laboratory, University Park, PA 16802, danielc@psu.edu.

Introduction: Planetesimals are bodies 1-500 km in diameter that are the building blocks of terrestrial planets and the cores of giant planets. Asteroids and comets are planetesimals that were never incorporated into a planet. The origin of planetesimals is one of the most important open questions in planet formation. Their formation faces significant obstacles in the form of the fragmentation barrier, and the radial drift barrier e.g., [1], [2], [3], [4]. Many current models call for the concentration of chondrules or other small particles into dense regions whose density can exceed the Roche density and undergo gravitational collapse to produce planetsimal-size bodies e.g. [5], [6].

Streaming Instability: A promising mechanism to achieve these densities is the radial convergence of radial drift known as the streaming instability [7][8]. In it, the combination of aerodynamic drag and the solid-to-gas back-reaction leads to the formation of dense particle filaments. Much of my own work has been to constrain the conditions needed for these filaments to form [9][10].

In this talk I will give a general overview of the streaming instability. I will discuss how the instability works, and I will discuss the conditions needed for the effective formation of dense particle filaments. I will focus on recent results on the small-particle limit [10]. If time allows, I will also present preliminary work on the role of turbulence and the extent at which it might impede the formation of dense filaments.

References: [1] Weidenschilling, S. J. 1977, MNRAS, 180, 57 [2] Güttler, C., Blum, J., Zsom, A., Ormel, C. W., & Dullemond, C. P. 2010, A&A, 513, A56 [3] Ormel, C. W., Cuzzi, J. N., & Tielens, A. G. G. M. 2008, ApJ, 679, 1588 [4] Birnstiel, T., Fang, M., & Johansen, A., 2016, Space Sci. Rev., 205, 41 [5] Cuzzi J. N., Hogan R. C., Shariff K., 2008, ApJ, 687, 1432 [6] Meheut, H., Meliani, Z., Varniere, P., & Benz, W. 2012, A&A, 545, A134 [7] Youdin, A. N., & Goodman, J. 2005, ApJ, 620, 459 [8] Johansen, A., & Youdin, A. 2007, ApJ, 662, 627 [9] Carrera, D., Johansen, A., & Davies, M. B. 2015, A&A, 579, A43 [10] Yang, C.-C., Johansen, A., & Carrera, D. 2016, ArXiv e-prints, arXiv:1611.07014

CONSTRAINTS ON VESTA'S AND CERES' ORIGINS FROM DAWN'S OBSERVATIONS. J. C. Castillo-Rogez[1], H. McSween[2], T. B. McCord[3], M. C. De Sanctis[4], C. A. Raymond[1], S. Marchi[5], C. T. Russell[6], [1]Jet Propulsion Laboratory, California Institute of Technology, Pasadena, CA, [2]Department of Earth and Planetary Sciences, The University of Tennessee in Knoxville, TN, [3]Bear Fight Institute, Winthrop, WA, [4]Istituto di Astrofisica e Planetologia Spaziali, INAF, Roma, Italy. [5]Southwest Research Institute, Boulder, CO, [6]Institute of Geophysics and Planetary Physics, University of California, Los Angeles, CA. Corresponding Author: Julie.C.Castillo@jpl.nasa.gov.

Introduction: Before the Dawn mission, it was known that Vesta and Ceres have had a very different history. The surface compositions were determined from telescopic spectral observations to be, for Vesta, basaltic and very similar to basaltic achondrite meteorites [1], and, for Ceres, close to primitive carbonaceous chondrites, i.e., aqueously altered silicates with a darkening agent [2, 3]. Ceres mass and size measurements provided a density of about 2.1 g/cm^3, indicating a significant water content (~25% by mass). Thermodynamic modeling showed [4, 5] heating, ice melting and silicate hydrothermal alteration with mass differentiation, depending on the remaining water content and the alteration product densities. Basaltic Vesta, on the other hand, was known to be much denser (~3.46 g/cm^3), suggesting a dry and hot history [6].

Until the introduction of the Nice model [7] and Grand Tack model [8], Ceres and Vesta were thought to have formed in the same part of the protoplanetary disk near their current location [9]. The difference in current state was ascribed to a delay in the formation of Ceres with respect to Vesta, explained by a time of formation of ~2.85 My after CAIs for the latter [4, 6].

Thanks to the Dawn mission [10], Vesta and Ceres have become the best studied leftover planetary building blocks. We now have advanced knowledge of their internal evolution and its geological expression. These in turn can help track the early history of these bodies and put additional constraint on early solar system processes. In the context of the *First Billion Years* conference series, these bodies offer remarkable examples where differentiation state can help constrain accretional environments.

Dawn Findings: The Dawn spacecraft, orbiting first Vesta (2011-2012) and then Ceres (2015-2017), provided the first look at these large planetary building blocks with spatial resolution sufficient to define and analyze surface features, confirm the earlier findings, and provide much more information about their evolution and current states. Dawn's redundant framing cameras (FC), Visible-Infrared mapping spectrometer (VIR) Gamma Ray and Neutron Detector (GRaND), and coherent Doppler tracking data provided detailed information about 1) geophysical properties: size, shape, gravity field, internal mass distribution; 2) geomorphology: topographical expressions of surface and interior processes; and 3) composition: mineral, organic, and elemental, resulting from thermochemical processes.

Dawn determined Vesta to be differentiated with a massive iron core. Its ancient surface [11] is heavily cratered, with two large, overlapping impact basins (one fairly young) in the southern polar region. The largest of these impacts probed into the mantle within the resulting Rheasilvia basin, produced equatorial graben rings, distributed material nearly globally, and resulted in the creation of a dynamical asteroid family. Surface elemental and mineral compositions [12] confirmed and extended the telescopic findings that the howardite-eucrite-diogenite (HED) meteorites likely came from Vesta [13], enhancing the ability to use these samples to interpret Dawn's chemical and mineralogical mapping of Vestan material. Howardite is present nearly everywhere, but with varying mixing ratios of eucrite and diogenite. GRaND's unexpected discovery of concentrations of hydrogen are explained by localized incorporation of carbonaceous chondrite impactor into the regolith. The HED studies, combined with Dawn data, suggest extensive melting [14]. However, pervasive olivine deposits, expected as a product of global (magma ocean) melting, were not observed, even associated with large impact features that should have exposed mantle olivine. Although olivine was observed in localized areas [15], it appears that olivine must be sequestered in the vestan deep mantle, suggesting a shallow magma ocean with incomplete melting. Gravity anomalies suggest diogenite plutons intruded the basaltic crust, rather than forming a uniform global layer, indicating a complex igneous history [16]

Dawn found Ceres to have a shape and gravity field consistent with partial differentiation and almost complete isostatic adjustment [17]. The surface is heavily cratered, suggesting a stiff upper crust [18], but crater relaxation suggests a decrease in viscosity at depths greater than 40 km [19, 20]. Ceres' surface composition is a mixture of Mg- and ammoniated–phyllosilicates (such as serpentines and clays), carbonates, and absorbing dark materials, such as carbon or magnetite [21], suggesting extensive, global aqueous alteration [22]. Salts (in particular sodium carbonates) are present in bright deposits associated with what appear to be cryomagmatic features [23, 24]. Elemental abundances suggest extensive alteration and chemical differentiation and hydrogen is present exten-

sively, especially at high latitudes, in the upper meter of the surface [25]. Flow features, domes, and other features exist that suggest water- and fluid- related activity. Ceres appears to be a highly aqueously altered body but the mantle low density suggests internal temperatures never got above a few 100 deg. C [26].

In summary, Dawn confirmed that Vesta experienced extensive silicate melting and differentiation, resulting from a hot, dry evolution. On the other hand, Ceres exhibits a much milder thermal history. This contrast can be primarily attributed to the abundance of water in Ceres that helped moderate internal temperature via latent heat and hydrothermal circulation [26].

What Vesta and Ceres tell us about the Early Solar System: It has been suggested that Vesta and Ceres accreted from similar chondritic feedstocks but at different times, i.e., with different short-lived radioisotope budgets [4, 9]. Abundance of aluminum-26 could lead to rapid devolatilization of volatile components in Vesta, accreted earlier, while Ceres could preserve the bulk of its volatiles. However, in the context of recent developments in early Solar system dynamical evolution it seems likely that Vesta and Ceres' starting composition was very different, especially in terms of ice abundance. The remarkable discovery of ammoniated clays at the surface of Ceres [21] is a crucial clue. Multiple models have been suggested to explain the origin of volatiles in the asteroid belt. A model in which the ammonia snowline overlapped with the water ice snowline in Ceres' location [27] includes a number of caveats. On the other hand, several distinct episodes of volatile migration have been suggested. The first one is that planetesimals in the 100-meter size range migrated from the outer Solar system via gas drag and could gently accrete with growing asteroids in the main belt [28]. However, migration of supervolatiles across the gap opened by Jupiter in the solar nebula likely lead to devolatilization and loss of most of the ammonia [29]. An alternative is that larger planetesimals (1-10s km) migrated following destabilization of feeding zones by the growing giant planets [30]. While this scenario is more propitious to the preservation of volatiles, the accretion of that material reaching the main belt at velocities of 10s km/sec with growing asteroids is not well understood and remains to be modeled. Another model assumes that Ceres migrated from the Kuiper Belt [31] but dynamical and geophysical considerations [32] tend to discard this possibility. The Grand tack model introduced a few years ago might provide a compromise where Ceres came from the region between the giant planets [8]. Recent accretion models support the idea that planetesimals that large could form between Jupiter and Neptune [33].

These two intact protoplanetary bodies reveal that planetary accretion likely involved already chemical evolved and (partly) differentiated bodies. Accretion of Vesta-like bodies with large cores would have simplified core separation in planets. Accretion of Ceres-like bodies would provide volatiles in the form of both hydrous minerals and ices, as well as organics.

References: [1] McCord T. B. et al. (1970) *Science* 268, 1445-1447. [2] Johnson T. V. and Fanale F. (1973) *J. Geophys. Res.* 78, 8507-8518. [3] McCord T. B. and Gaffey M. (1974) *Science*, 186, 352-355. [4] McCord T. B. and Sotin C. (2005) *J. Geophys. Res.* 110:EO5009-5014. [5] Castillo-Rogez J. and McCord T. B. (2010) *Icarus* 205, 3443-459. [6] Ghosh A and McSween H. Y. (1998) *Icarus* 134, 187-206. [7] Morbidelli et al. (2005) *Nature* 435, 462-465. [8] Walsh et al. (2011) *Nature* 475, 206-209. [9] Russell et al. (2004) *Planet. Space Sci.* 52, 465-489. [10] Russell C. T. and Raymond C. A. (2011) *Space Sci. Rev.* 163, 3-23. [11] See *Icarus* special issue of Vesta geology 244, 2014. [12] See *Icarus* special issue on Vesta surface composition 259, 2015. [13] McSween et al., 2013, *MAPS* 48, 2090-2104. [14] De Sanctis et al. (2012) *Science* 336, 697-700. [15] Ammannito et al., 2013 *Nature* 504, 122-125. [16] Raymond et al. (2017) In: L. Elkins-Tanton and B. Weiss eds. *Planetesimals*, Cambridge University Press, 321-339. [17] Park R. S. et al. (2016) *Nature* 537, 515-517. [18] Bland et al. [19] Ermakov et al., submitted to *J. Geophys. Res.* [20] Fu et al., submitted to *EPSL*. [21] De Sanctis et al. (2015) *Nature* 528, 241-244. [22] McSween et al. (2017) submitted to *MAPS*. [23] De Sanctis et al. (2016) *Nature* 536, 54-57. [24] Ruesch et al. (2016) *Science* 353, aaf4286-1. [25] Prettyman et al. (2017) *Science* 355, 55-59. [26] Travis et al., submitted to *Icarus* [27] Dodson-Robinson et al. (2009) *Icarus* 200, 672-693. [28] Mousis and Alibert (2005) MNRAS 358, 188-192. [29] Turner et al. (2012) *Astroph. J.* 748:92. [30] Grazier et al. (2014) *Icarus* 232, 13-21. [31] McKinnon (2012) *DPS* 44, id.111.14. [32] Castillo-Rogez et al., *this Conference*. [33] Johansen et al. (2015*) Science Advances* 2015;1:e1500109.

Acknowledgements: *Part of this work is being carried out at the Jet Propulsion Laboratory, California Institute of Technology, under contract to NASA. The Dawn mission is led by the University of California, Los Angeles, and is managed by JPL under the auspices of the NASA Discovery Program Office.*

CONSTRAINTS ON THE TIME OF FORMATION OF CERES AND CERES-LIKE ASTEROIDS – A JOINT RESERVOIR WITH C-TYPE IRREGULAR SATELLITES? J. C. Castillo-Rogez[1], K. J. Walsh[2], P. Vernazza[3], D. Takir[4], [1]Jet Propulsion Laboratory, California Institute of Technology, Pasadena, CA, United States, (Julie.C.Castillo@jpl.nasa.gov), [2]Southwest Research Institute, Boulder, CO, United States, [3]Aix Marseilles Universite, CNRS, LAM, UMR 7326, Marseille, France, [4]SETI Institute, Mountain View, CA, United States.

Introduction: Per their large number, midsize asteroids in the 100-300 km diameter range represent the bulk of the mass of the asteroid belt after Ceres, Vesta, and Pallas are removed. This has been interpreted as a primordial feature [1], i.e., this generation of planetesimals accreted fast and then contributed to the growth of larger bodies. Smaller asteroids are fragments/debris from collisions between these midsize planetesimals, many of which are progenitors of asteroid families. Midsize planetesimals are also found in all small body reservoirs, such as the Kuiper Belt, the Trojan asteroids, and the irregular satellites. Phoebe stands out in the outer solar system as a high density planetesimal when most other 100-300 km objects in that region have cometary-like densities. Conversely, many asteroids found in the asteroid belt also have densities ≤1 g/cm^3. These discrepancies show that midsize planetesimals across the solar system had very different heat budgets and those belonging to the same reservoirs may have come from different accretional environments.

Comparison between populations of objects in the same size range can help constrain those environments via a quantification of the heat budget of these bodies, by taking current porosity estimates as a gauge of internal evolution. Gravitational energy and accretional heating are minor contributors to that class of bodies, per their small sizes [2]. Heat from long-lived radioisotope decay cannot keep up with heat lost by diffusion from these small bodies. They might promote some creep-driven compaction depending on the volume fraction of volatiles, but otherwise these bodies are expected to remain globally porous. Only short-lived radioisotopes, and especially ^{26}Al, can incur dramatic internal changes, e.g., extensive compaction, ice melting, and then aqueous alteration. We know this to be the case for C*h* and C*gh* asteroids, the classes of C-type asteroids that display a water of hydration signature over their surfaces [3] and are believed to be parent bodies of the CI/CM chondrites [e.g., 4]. Hence the density and spectral properties of <300 km planetesimals provide first order constraint on the time of formation of these bodies.

Approach and Results

We track the evolution of porosity in these bodies in order to explain the disparities in porosity between main belt asteroids and irregular satellites, on the one hand, and Kuiper Belt objects and Trojan asteroids, on the other hand. We model the thermal and porosity evolution of midsize planetesimals following previous work for Phoebe and Trojans [5, 6]. Representative results are presented in Figure 1.

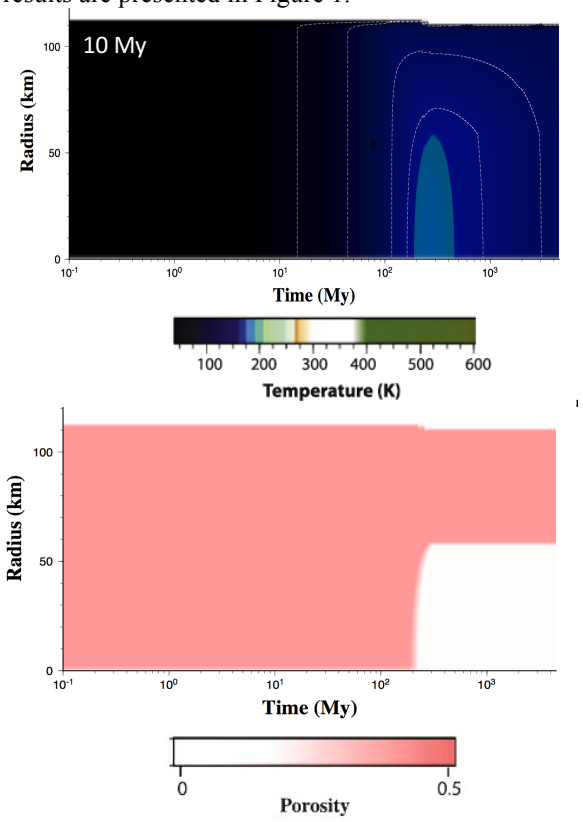

Figure 1. Thermal (top) and porosity (bottom) evolution models for a ~200 km planetesimal accreted 10 My after Calcium Aluminum Inclusions, a grain density of 1500 kg/m^3, and an accretion temperature of 50 K. The final average porosity in this model is ~35%.

In that example, long-lived radioisotopes drive a late and limited evolution of the interior and final bulk density of about 1 g/cm^3.

Genetic Relationships Between Reservoirs of Small Bodies: Similar evolution between Trojan asteroids, P- and D-type asteroids found in the main belt, Centaurs, and KBOs support a genetic relationship between these classes of bodies, as simulated by many studies [7, 8]. Limited internal evolution is consistent with accretion models; for example, Kenyon et al. [9] estimated that objects forming in the 20–25 AU region

would take at least 5 My to start accreting and reach a 100 km radius in ~1 My.

Many irregular satellites display spectral properties akin to C-asteroids, such as Phoebe and Himalia. Saturn's satellite Phoebe was suggested to come from the Kuiper Belt based on the observation that its density matches the grain density inferred from cosmochemical models of bodies formed in the Solar nebula [10]. Thermal modeling showed that most of Phoebe's original porosity could be removed provided that it accreted in less than 4 My after calcium-aluminum inclusions taken as a time reference [5]. The density discrepancy between Phoebe and KBO questions that relationship and cannot be uniquely explained by a difference in volatile content. Many previous studies noted the similarities between the spectra of Phoebe, Himalia, and hydrated asteroids and suggested that the two irregular satellites actually migrated from the inner Solar system [e.g., 11, 12]. The Grand Tack model [13] could provide an alternate scenario for a common origin for hydrated C-type asteroids and irregular satellites. In that context, the primary reservoir for C-types is between and beyond the orbits of the giant planets. So that material could have been available for capture by the giant planets early on. This model implies accretion was fast and early in that region, consistent with recent accretion scenarios [14].

Implications for Ceres: Late times of formation potentially carries implications for Ceres. Ammoniated material on its surface [15] suggests that Ceres formed from material originating beyond Jupiter. However, it is not confirmed yet whether Ceres as a whole originated far in the outer Solar system or if it grew from outer solar system planetesimals migrated to the main belt. Ceres could still evolve chemically and physically on long-lived radioisotope decay heat alone [16]. However, it might be possible to constrain Ceres' time of formation assuming it formed in the same region of the solar system as 10 Hygiea, an asteroid that shares a similar surface composition involving carbonates and ammoniated clays [17, 18]. Hygiea is half the size of Ceres and thus is more sensitive to the heat budget available post-accretion. Our modeling of Hygiea's thermal evolution requires ^{26}Al decay heat for its interior to reach conditions amenable for hydrothermal processing on a global scale. Furthermore, the depth of altered material should be relatively shallow in order to be exposed either by subcatastrophic disruption (which produced Hygiea's family) or by overturn of an unaltered crust. This leads to a time of formation of less than 3.5 My after CAIs for that body. This early formation falls in the same window as the CM chondrite parent bodies [e.g., 19] and Phoebe [5] and may point to a common reservoir depending on the accretion rates expected in the early solar system.

Summary: The heat budget of midsize planetesimals varied across the Solar system. Jupiter Trojan asteroids, D/P asteroids in the main belt, and midsize KBOs appear to have preserved up to 40% bulk porosity, which we explain as accretion with few or no short-lived radioisotopes. This reinforces the genetic relationship between these classes of bodies proposed by dynamical models. On the other hand, C-type bodies distributed in the main belt and among the irregular satellite population show evidence for low-porosity and, in many cases, aqueously altered material on their surface. This suggests C-type bodies shared a common reservoir that possibly existed early on between the orbits of the giant planets in the context of the Grand Tack.

References:

[1] Cuzzi J. N. et al. (2010) *Icarus* 208, 518-538. [2] Leliwa-Kopystynski J. and Kossacki K. J. (2000) *Planetary and Space Science* 48, 727-745. [3] Rivkin, A. S. et al. (2015) *Astron. J.* 150, id 198. [4] Vernazza P. et al. (2016) *Astron. J.* 152, 54. [5] Castillo-Rogez J. et al. (2012) *Icarus* 219, 86-109. [6] Marchis F. et al. (2014) *Astroph. J. Lett.* 783, id. L37. [7] Morbidelli A. et al. (2005) *Nature* 435, 462-465. [8] Levison H. F. et al. (2009) *Nature* 460, 364-366. [9] Kenyon S. J. et al. (2008) *In:* The Solar System Beyond Neptune, 293-312. [10] Johnson T. B. and Lunine J. I. (2005) *Nature* 435, 69-71. [11] Hartmann W. K. (1987) Icarus 71, 57-68. [12] Brown M. E. and Rhoden, A. R. (2014) *Astroph. J. Lett.* 793, L44. [13] Walsh K. J. et al. (2011) *Nature* 475, 206-209. [14] Johansen A. et al. (2015) *Sci. Adv.* 2015;1:e1500109. [15] De Sanctis M. C. et al. (2015) *Nature* 528, 241-244. [16] Castillo-Rogez, J. C. and McCord, T. B. (2010) *Icarus* 205, 443-459,. [17] Takir D. and Emery J. P. (2012) *Icarus* 219, 641-654. [18] Vernazza P. et al. (2017) *Astron. J.* 153, id. 72. [19] Jogo K. et al. (2017) *Geochimica and Cosmochimica Acta* 199, 58-74.

Acknowledgements: Part of this work is being carried out at the Jet Propulsion Laboratory, California Institute of Technology, under contract to NASA.

ZOOMING IN ON THE PHYSICS AND CHEMISTRY OF PROTOPLANETARY DISKS WITH ALMA

Cleeves, L. I., CFA, Harvard University [ilse.cleeves@cfa.harvard.edu]

During the protoplanetary disk phase, the physical environment and spatial composition of the disk play a direct role in the outcome of planet formation, both in the types of planets formed and their composition. Until recently, much of our understanding of the bulk disk properties (>10 AU), including densities, temperatures, irradiation, kinematics, and composition, has been limited to constraints from low resolution observations of the brightest sources. Within the last few years, new observations with ALMA have revolutionized our understanding of nearly all aspects of disk science, including the coupled evolution of dust and gas and its role in volatile transport, the nature of gas kinematics/accretion, the impact of midplane condensation fronts, the role of the external environment, and disk energetic processes. In this talk I will present an overview of recent results and how these fit into a newly emerging picture of protoplanetary disk evolution in the first few Myr.

PLANETESIMALS BORN BIG BY CLUSTERING INSTABILITY? Jeffrey N. Cuzzi[1], Thomas Hartlep[2], Justin I. Simon[3], and Paul R. Estrada[4]; [1]Ames Research Center, NASA (Mail Stop 245-3, Moffett Field, CA 94035); jeffrey.cuzzi@nasa.gov, [2]thomas.hartlep@nasa.gov, [3]justin.i.simon@nasa.gov, [4]paul.r.estrada@nasa.gov.

Introduction: Roughly 100km diameter primitive bodies (today's asteroids and TNOs; [1]) are thought to be the end product of so-called "primary accretion". They dominated the initial mass function of planetesimals, and precipitated the onset of a subsequent stage, characterized by runaway gravitational effects, which proceeded onwards to planetary mass objects, some of which accreted massive gas envelopes. Asteroids are the parents of primitive meteorites; meteorite data suggest that asteroids initially formed directly from freely-floating nebula particles in the mm-size range.

Unfortunately, the process by which these primary 100km diameter planetesimals formed remains problematic. We review the most diagnostic primitive parent body observations, highlight critical aspects of the nebula context, and describe the issues facing various primary accretion models. We suggest a path forward that combines current scenarios of "turbulent concentration" (TC) and "streaming instabilities" (SI) into a triggered formation process we call *clustering instability* (CI). Under expected conditions of nebula turbulence, the success of all of these processes in forming terrestrial region (mostly silicate) planetesimals requires growth by sticking into aggregates in the several cm size range, *at least*, which is orders of magnitude more massive than allowed by current growth-by-sticking models using current experimental sticking parameters [2-4]. The situation is not as dire in the ice-rich outer solar system.

Observations: Amongst the most diagnostic meteoritic observations are the several-Myr spread in formation ages [5,6], the apparent rapid accretion of a given body when it did occur [7], several indications that, before their internal heating, primitive 100km bodies were homogeneous thoughout – physically, chemically, and isotopically [8], and evidence both for [9] and against [10,11] radial mixing of initial constituent particles. At least one aspect of outer solar system planetesimals (high binary fraction) supports some kind of clustering instability [12,13]. These observations (and properties of asteroid families [1]) suggest gentle and sporadic formation of internally homogeneous, 100km objects directly from small nebula particulates, some of which may have wandered for hundreds of millennia since their formation.

Nebula context: The intensity of nebula turbulence is perhaps the most important and least well understood property of the planetesimal formation environment. Consensus on the intensity (the infamous "α" parameter), not to mention its cause, has shifted often over the years, and recent work leads to a lower limit around $\alpha = 10^{-4}$ [14,15]. The most refined incremental-growth-by-sticking models in such turbulent nebulae stall out at mm, cm, and m-size "barriers" due to bouncing, fragmentation, and radial drift [16,3]. In the icy outer solar system, growing particles *may* sneak past at least the first set of barriers in the form of ultra-high-porosity "puffballs" [17,18]. However, even if these barriers could be avoided, new barriers loom everywhere at 1-10km size, due to destructive collisions resulting from gravitational scattering by large-scale gas density fluctuations in turbulence [19-21]. Meanwhile, ongoing radial drift in the thermally evolving nebula during this extended stage can lead to changes in composition and redistribution of mass, that can affect how, when, where, and of what planetesimals ultimately do form [4].

Leapfrog or instability models: TC and SI are two somewhat different mechanisms that have been proposed to bypass the barriers to incremental growth, both providing a one-stage collapse from a dense, localized clump of small nebula particles straight to 100km planetesimals [22-24,8]. TC has the advantage of triggering planetsimal formation infrequently, allowing it to continue for several Myr. Original TC scenarios which operated on single-chondrule-size particles [23] have been found to be based on incorrect assumptions [25,26]; new results show that the general idea still forms large planetesimals, but particle sizes must start in the cm-dm range [27,28]. SI is a true linear instability: unless the conditions are right, nothing happens - and if they are right, nearly all the local mass becomes planetesimals immediately. This is problematic for a several-Myr-long planetesimal formation duration. In moderate turbulence, typical growth-limited particles are too small to settle vertically into sufficiently dense layers for SI to occur, while "lucky", atypically large particles are far too rare to lead to SI. (see [29] for a more in-depth discussion of SI).

Thus both TC and SI are in a similar bind, requiring particles much larger than current growth models are able to produce (mm-size) under current sticking assumptions. The "Pebble Accretion" [30,31] scenario is not a solution to *forming* planetesimals because it requires fairly large "seeds" on which to accrete pebbles. If it is to apply at all to planetesimals, it must merely add thin shells on top of already large objects formed some entirely different way, and the observations argue against inhomogeneity with depth [8].

Clustering Instability: For SI to occur in a nebula with $\alpha = 10^{-4}$, and local cosmic abundance of solids,

particles must grow to meter-radius for settling to occur. Particles of such sizes collide at about 30m/sec – a speed unlikely to be survived by loose aggregates. However, even if particles can only reach cm-dm size, less settled particle layers still exist. In such a turbulent environment, we suggested that TC may cluster cm-dm size particles within these dense (but SI-resistant) layers into clumps that can, perhaps, make use of the "peloton" physics of the SI to go on to planetesimals [27]. We call this triggered, or nonlinear, instability a *Clustering Instability* or CI. It combines the advantage of a slow, rate-limited triggering by TC (only statistically rare volumes achieve sufficiently high concentration) with a second advantage that only moderate growth-by-sticking beyond current model limits is needed – perhaps only to several cm radius. This remains merely an idea, and a full, numerical study of the CI has not been done. TC models which lead to planetesimal Initial Mass Functions (IMFs), rely on simplified analytical thresholds for planetesimal formation [23], and lack the full feedback contained in 3D numerical models that display SI [24]; however, none of the SI models have included global nebula turbulence, except for [22] which assumed particles that may be too large to be realistic for reasons given above.

Can "particles" grow larger than the best current models say? In the terrestrial planet region, observations suggest that "particles" of cm-dm size must be *aggregates of chondrules*, since all the most primitive chondrites are composed almost entirely of chondrules (with similar size particles of different composition and associated dust). Detailed models of the growth of aggregates of dust-rimmed chondrules found that growth stalled in the mm-radius range due to bouncing [2]. However, one new and intriguing observation suggests that the models may be missing something. The primitive Unequilibrated Ordinary Chondrite NWA 5717 [32-35] shows dark and light "lithologies" or chondrule clusters, several cm across, with different chemical and isotopic properties that are very hard to attribute to alteration after formation. These lithologies suggest growth by sticking of chondrules, in two distinct regions, into aggregates, followed by turbulent mixing of these very different kinds of aggregates into a region where they accreted together. Highly localized parent body aqueous alteration may have occurred if the chondrules in the darker lithology carried water ice in or on their rims, that was absent on/in the lighter-colored aggregates [32-35].

What can explain this more robust growth by sticking than expected? A clue may be found in the properties of Chondritic Porous (CP) Interplanetary Dust Particles (IDPs). The mineral grain monomers in several IDPs have sizes consistent with aerodynamic sorting [36]. Such tiny grains are strongly tied to the gas flow, and it is hard to sort them by aerodynamics using traditional physics. One new piece of physics that might explain this observation is an enhanced collision rate (because of local density enhancement), combined with a lower collision speed (avoiding the bouncing barrier) *for particles with stopping times very close to the eddy time of the smallest (Kolmogorov) eddy in turbulence* [37,28], The same physics could apply to IDP monomers and chondrules, because of their very different nebula environments. If the physics is validated, then monomer sizes (including the long-puzzling chondrule size distributions) [35,38] can tell us about their nebula gas environment. In addition, it may be that realistic, irregular, size distributions of silicate grains coated with "sticky" refractory organics [39], or even thin icy rims, might contribute to growing larger aggregate particles than previously thought.

Growth of few-cm-size aggregates composed of aerodynamically selected particles, in weakly-to-moderately turbulent nebula where both TC and SI-like processes combine to lead to a triggered CI, might thus allow roughly 100km diameter planetesimals to be "born big" directly, and sporadically, from freely-floating nebula particles [28].

References:

[1] Thomas C. this meeting; [2] Ormel C. et al. 2008, ApJ 679, 1588; [3] Zsom A. et al 2010, A&A 513, id.A57; [4] Estrada P. et al 2016, ApJ 818, art. id. 200; [5] Wadhwa M., this meeting; [6] Kita, N., this meeting; [7] Vernazza P. et al 2014, ApJ 791, art. id. 120; [8] Johansen A.; et al. 2016, in Asteroids IV, U. Az. Press (arXiv:1505.02941); [9] Zolensky M.. et al 2006, Science 314, 1735; [10] Warren P. (2016) EPSL 311, 93; [11] Kruijer T. et al 2017, 48th LPSC #1386; [12] Nesvorny D. et al 2010, AJ 140, 785; [13] Fraser W. et al 2017, Nat. Astron. 1, id. 0088; [14] Turner N. et al 2014, in PPVI (U. Az. Press); [15] Umurhan O. this meeting; [16] Birnstiel T. et al. 2010 A&A 513, id.A79; [17] Okuzumi S. et al 2012, ApJ 752, art. id. 106; [18] Krijt S. et al 2015 A&A 574, id.A83; [19] Ida S. et al (2008) ApJ, 686, 1292; [20] Nelson R. P. et al 2013, MNRAS 435, 2610; [21] Ormel & Okuzumi 2013; ApJ 771, art. id. 44; [22] Johansen A. et al 2007 Nature 448, 102; [23] Cuzzi JN, et al 2010 Icarus, 208, 518; [24] Carrera D. et al 2015, A&A 579, id.A43; [25] Pan L. et al 2011 ApJ 740, art. id. 6; [26] Hartlep T. et al 2017 Phys. Rev. E 95, id.033115; [27] Cuzzi J & T Hartlep 2016, 47th LPSC; id. 1832; [28] Hartlep T. et al this meeting; [29] Carrera D. et al, this meeting; [30] Ormel C. & Klahr H. 2010 A&A 520, id.A43; [31] Lambrechts M. & A. Johansen 2014 A&A 572, id.A10; [32] Bunch T. E. et al. 2010, 41st LPSC, #1280; [33] Cato M. et al 2017 48th LPSC, #1687; [34] Cuzzi J. et al 2017 48th LPSC, #1964; [35] Simon J. et al this meeting; [36] Wozniakiewicz P. et al 2013; ApJ 779, art. id. 164; [37] Pan L. & P. Padoan 2014, ApJ 797, article id. 101; [38] Friedrich J.et al 2015 Ch. d. Erde - Geochem. 75, 419; [39] Flynn G. et al 2013 Ear. Plan. Sp. 65, 1159.

HUNTING THE PLANETESIMALS SIZE DISTRIBUTION HIDDEN IN THE MAIN ASTEROID BELT

M. Delbo[1], A. Morbidelli[1], K. J. Walsh[2]. G. Tsirvoulis[3], C. Avdellidou[4], B. Bolin[1], and K. Tsiganis[5]. [1]*Université Côte d'Azur, CNRS-Lagrange, Observatoire de la Côte d'Azur - Boulevard de l'Observatoire CS 34229 - F 06304 NICE Cedex 4 France* (delbo@oca.eu, morby@oca.eu), [2]*Southwest Research Institute, 1050 Walnut St. Suite 300, Boulder, CO 80302, United States* (kwalsh@boulder.swri.edu). [3]*Astronomical Observatory, Volgina 7, 11060 Belgrade 38, Serbia.* [4]*Scientific Support Office, Directorate of Science, European Space Agency, Keplerlaan 1, NL-2201 AZ Noordwijk ZH, The Netherlands.* [5]*Department of Physics, Aristotle University of Thessaloniki, 54124 Thessaloniki, Greece*

Introduction: Understanding the process of the formation of planets from a disk of solids and gas around our young Sun and other stars is one of the most imporant challenges of planetary sciences. A first step in this mechanism is understood as the accretion of planetesimals [1], the building blocks of planets, from the tiny solid grains initially present in protoplanetary disks. But what is the size distribution of planetesimals? Do these objects have a typical size or size range? These questions are difficult to approach from a theorethical point of view as the size distribution of the planetesimals typically depends on the resolution of the simulations used to model the dust accretion process in protoplanetary disks [1-3].

Another line of attack to the aforementioned problem is to search for those planetesimals that escaped accretion into the planets in our Solar System: some of these bodies are thought to be still present in the Main asteroid Belt [4-6]. However, billions of years of collisional evolution have obscured the original planetesimal size distribution [5], creating families of asteroid fragments by the breakup of some of the orginal parent bodies (these are the so-called asteroid collisional families) [7,8]. Traditioanllly the search for the planetesimals in the Main Belt has been hampered by the fact that asteroid family identification by the classical HCM methods is very conservative [7,9], leaving many asteroid fragments in the "background" population: i.e. asteroids not associated to families. This restrictive identification of family members is performed in order to avoid the inclusion of interlopers and to have clear distinction between different families [7,9]. On the other hand, this limits against the identification of the oldest asteroid families in the Main Belt.

Identification of the oldest asteroid familes: We have developed new techniques [9,10] to idenfiy asteroids that are fragments of previous-generation asteroids broken up by collisions. Our methods consist in searching a distinctive feature (the so-called V-shape) of groups of asteroids that are family members [10] i.e. fragments of a single parent body (Fig. 1).

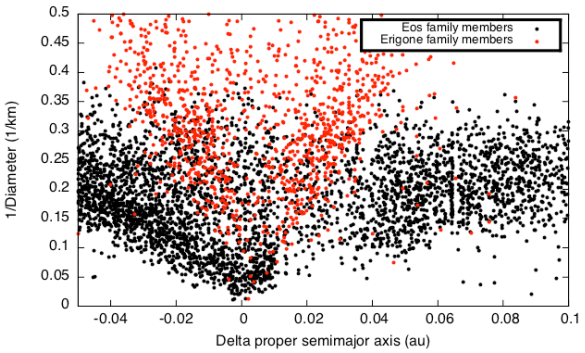

Figure 1: Example of V-shapes of known asteroid families. Because of the thermal Yarkovsky effect, asteroids drift in semimajor axis (a) at a rate da/dt proportional to the inverse of their diameter (D). Asteroids that are fragments created by a collision form a V-shape in the space (a,1/D) by drifting away from the impact point. There is one V-shape for each family. The slope of the sides of the V-shape is like a clock. Older familes have smaller slopes.

Results: Application of our new methods is undergoing [10,11]. Preliminary results in selected regions of the Main Belt are promising [11]. They confirm the paradigm that asteroids were born big [12], but with a very shallow size frequency distribution.

References: [1] Johansen, A. et al. 2016, *in Asteroids IV*, U. of Az.Press, arXiv:1505.02941; [2] Simon, J. B. et al. 2016. *The Astrophysical Journal* **822**, 55. [3] Klahr H., Schreiber A. 2016. *Asteroids: New Observations* **318**, 1. [4] Cuzzi, J. N. et al. 2010. *Icarus* **208**, 518. [5] Bottke, W. et al. 2016, *in Asteroids IV*, U. of Az.Press. [6] Russell, C. T. et al. 2012. *Science* **336**, 684. [7] Nesvorny, D. et al. 2016, *in Asteroids IV*, U. of Az.Press. [8] Carruba V. et al. 2016. *MNRAS* **458**, 3731. [9] Tsirvoulis G. et al. 2017. *Icarus* in press. [10] Bolin B. et al. 2017. *Icarus* **282** 290. [11] Delbo M. et al. 2017. *Science* submitted. [12]

HOW CHONDRULES AND CALCIUM-RICH, ALUMINUM-RICH INCLUSIONS CONSTRAIN DISK PROCESSES AND PLANET FORMATION. S. J. Desch[1] [1]School of Earth and Space Exploration, Arizona State University (PO Box 871404 Tempe AZ 85287-1404, steve.desch@asu.edu).

Introduction: Chondrules are found in abundance in chondrites, meteorites from unmelted asteroids that represent the most primitive planetary bodies for which samples exist. Chondrules comprise roughly half of the mass of almost all classes of chondrites. Chondrules are themselves igneous melt droplets, bits of rock melted while individually floating in the solar nebula. Radiometric dating shows that most chondrules in our collections formed 1.5 – 3 Myr into disk evolution [1] and other lines of evidence establish that chondrules formed during the lifetime of the protoplanetary disk and were witnesses to the processes in it. Whatever melted at least half of the mass of chondrites was a significant process in the evolution of the protoplanetary disk.

Likewise, calcium-rich, aluminum-rich inclusions (CAIs) are abundant in carbonaceous chondrites, although they are rare in ordinary and enstatite chondrites. CAIs contain minerals that are the first to condense from a solar-composition gas, and CAIs are the oldest solids formed in the solar system.

Because chondrites contain CAIs that are the oldest solids in the solar system, and because chondrites are the least processed planetary materials in our collection, chondrites are considered to be building blocks of planets. That paradigm is shifting because of new discoveries. The discovery of streaming instabilities [2] and pebble accretion [3] shows that growth of planetary bodies can be very rapid, providing a theoretical justification for the long-standing observation that iron meteorites formed in << 1 Myr [4]. Hf-W dating of Mars core formation shows that planetary embryos existed within the first 2 Myr of disk evolution [5]. These results show that planet formation in fact preceded the formation of chondrules, at least the chondrules in our collections in chondrites. The formation of chondrules must be seen in this context. Here I review a few models of chondrule formation and outline how chondrule formation can be used as a probe of disk processes.

Chondrule Formation:
As reviewed by Desch et al. [6], successful model of chondrule formation must meet multiple constraints. The thermal histories of chondrules inferred from their textures must be reproduced: peak temperatures above the liquidus for minutes, followed by cooling to the liquidus over hours. Other attributes like the frequency of compound chondrules and the suppression of evaporation of moderate volatiles constrain the density of chondrules. Chondrule formation must be repeoducible, as chondrules contain relict grains of other chondrule fragments. It must occur over a protracted but limited range of times in the nebula. Geochemical constraints also come into play: chondrules contain abundant iron, and are apparently complementary to matrix dust. It is incumbent on anyone suggesting a model for chondrule formation to build the model to the point that it makes quantitative predictions that can be compared against the chondrule record.

Bow shocks in front of planetary embryos on eccentric orbits satisfy all of these conditions [7-9]. For achievable eccentricities, shock speeds are ~ 8 km/s and lead to peak temperatures above the liquidus. Cooling rates are in the range 1000 – 5000 K/hr, which overlaps with the cooling rates needed to produce the predominant porphyritic texture of chondrules [6]. By processing material at the disk midplane, the needed densities of chondrules and the complementarity with matrix are achieved. Contact outgassed planetary atmospheres may help explain the inference of exceptionally high partial pressures of Na vapor in the chondrule formation region [10].

Outstanding issues of the model are whether the cooling rates ~ 1000 K/hr can be routinely achieved in the model and match porphyritic chondrules. It also remains to be seen whether the bow shock model can explain all chondrules. Multiple chondrule formation mechanisms are possible, especially impact melts by impacts between planetesimals. I will review these mechanisms in my presentation. But the fact that planetary bow shocks and impacts between planetary bodies are the leading models for chondrule formation illustrates that increasingly the paradigm is shifting from one of chondrules being the building blocks of planets, to being a side product of planet formation.

CAI Storage Problem:
I also discuss another long-standing problem in meteoritics, the CAI storage problem. CAIs formed early in disk evolution, and at high temperatures achieved only in the inner portions of the disk. In the 3 Myr it takes chondrites to form, CAIs should have spiraled in to the Sun. Although not widely discussed in the literature, a corollary is the further paradox that one would expect CAIs to be more abundant in those chondrites that

formed closer to the Sun, namely enstatite and ordinary chondrites. Instead, CAIs are most abundant in the carbonaceous chondrites, with the largest CAIs being found in CV chondrites like Allende. CAIs therefore have the potential to trace disk dynamics and planet formation, and I discuss a potential resolution of this paradox.

References:

[1] Villeneuve, J, Chaussidon, M and Libourel G (2009) *Science* 35, 985. [2] Johansen, A, Oishi, JS, Mac Low, M-M, Klahr, H., Henning, Th and Youdin, A (2007) *Nature* 448, 1022. [3] Lambrechts, M. & Johansen, A. (2012) Asron. & Astrophys. 544, A32. [4] Halliday, AN and Kleine, T (2006) in *Meteorites and the Early Solar System II* (eds. DS Lauretta & HY McSween, Jr.) Univ. Arizona Press: Tucson, 775. [5] Dauphas, N and Pourmand, A (2011) *Nature* 473, 489. [6] Desch, SJ, Morris, MA, Connolly, Jr., HC and Boss, AP (2012) *Meteoritics and Planet. Sci.* 47, 1139. [7] Morris, MA, Desch, SJ, Boley, AC and Athanassiadou, T (2012) *Ap.J.* 752, 27. [8] Boley, AC, Morris, MA and Desch, SJ (2013) *Ap.J.* 776, 101. [9] Mann, CR, Boley AC and Morris, MA (2016) *Ap.J.* 818, 103. [10] Alexander, CMO'D, Grossman, JN, Ebel, DS and Ciesla FJ (2008) *Science* 320, 1617.

A NEW MODEL FOR PLANETESIMAL FORMATION. H. Downes[1,2] and N. Rai [1,2,3], [1]Dept. of Earth and Planetary Sciences, and Centre for Planetary Sciences, Birkbeck University of London, Malet Street, London WC1E 7HX UK (h,downes@ucl.ac.uk), [2]Dept. of Earth Sciences, Natural History Museum, Cromwell Road, London SW7 5BD UK, [3]Dept. of Earth Sciences, Indian Institute of Technology, Roorkee, 247667, India (nrai.fes@iitr.ac.in)

Introduction: The HED parent body (asteroid 4 Vesta) is often thought to be the quintessential planetesimal left over from formation of the Solar System, and is commonly considered as a reference model for planetesimal formation [1]. However, ureilites, the second most abundant type of achondrite meteorites, give a different view of formation of asteroids and planetesimals [2,3].

Ureilites show correlations between their bulk chemistry and oxygen isotopes which are not seen (or are not so well developed) in other achondrite groups, including the HEDs. The bulk chemistry and oxygen isotope compositions of HED meteorites are well homogenized compared to ureilites, probably because Vesta experienced a high temperature magma ocean stage in which its silicate mantle was mostly or completely molten [4,5]. This would have obliterated any earlier compositional variations in Vesta's mantle.

In contrast, ureilites show a trend between Fe-rich compositions with high $\Delta^{17}O$ ratios and high-Mg compositions with lower $\Delta^{17}O$ values [6,7,8]. Figure 1 shows this correlation, using mg# in olivine as a proxy for bulk rock Mg#. This correlation must be explained in any model of formation of the original parent asteroid of ureilite meteorites.

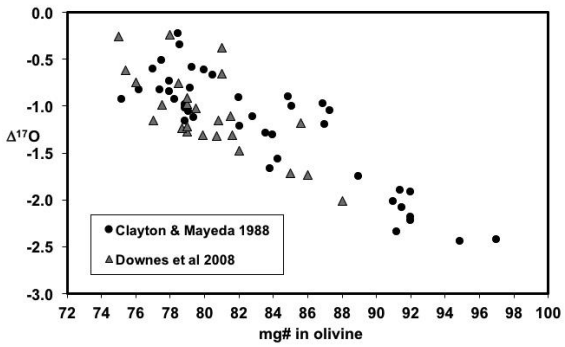

Figure 1. Correlation between mg# in olivines and $\Delta^{17}O$, in ureilite meteorites. Data from [6,8].

Methodology: We used Monte Carlo modelling to determine which combinations of primitive meteorites and meteoritic components could generate the observed trend of oxygen isotopes and bulk chemistry shown in Figure 1. Our modelling showed that all combinations of primitive C, O and E chondrites failed to generate the oxygen isotopes and bulk chemistry of ureilites. However, a model using a combination of Mg-rich and Fe-rich chondrules could perfectly generate the ureilite oxygen isotope trend. We then evaluated whether the range of compositions calculated from the combination of Mg-rich and Fe-rich chondrules could also account for the bulk compositional trends of the original parent urelite asteroid.

The "Proto-Ureilite Planetesimal": Unlike HED meteorites, which are mostly fragments of the crust of Vesta, ureilites are largely derived from the silicate mantle of their parent asteroid. Their significant LREE-depletion indicates that they represent the depleted mantle from which silicate melts have been extracted [9]. Thus, in order to reconstruct the composition of the undepleted mantle of the ureilite parent asteroid, it is essential to add back a silicate partial melt, basalt or trachyandesite [10], to the major element compositions of ureilites [7]. Furthermore, to achieve the bulk composition of the parent asteroid before core-mantle differentiation, we included a metallic core component. Using this approach, we propose a new compositional model for the ureilite parent asteroid which we call the "Proto-Ureilite Planetesimal". Our model based on a combination of Mg-rich and Fe-rich chondrules generates both the observed range of oxygen isotope signatures and the reconstructed bulk chemistry of the Proto-Ureilite Planetesimal. The model also reproduces the trends seen in Figure 1, which also suggests simple two component mixing. Mg-rich and Fe-rich chondrules are found together in the same meteorite [11], so mixing between them must have occurred in the early Solar System. However, the novel result of our modelling suggests a lack of matrix in the mixture, and also suggests a zoned or layered parent asteroid.

Accretion of the proto-Ureilite Planetesimal: During condensation and accretion in the solar nebula, the Mg-rich end-members of silicate minerals such as olivine and pyroxene would have condensed at slightly higher temperatures than those with more Fe-rich compositions. Thus a growing planetesimal would be formed of more Mg-rich minerals in its centre and more Fe-rich minerals in its outer layers (Fig. 2), i.e. having a layered bulk chemical structure. Differences in $\Delta^{17}O$ of the chondrules would also produce a radial gradient in oxygen isotopes (Fig. 2).

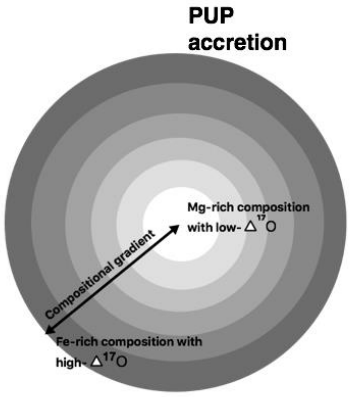

Figure 2. Initial concentric structure of the Proto-Ureilite Planetesimal (PUP) with Mg-rich silicate interior and more Fe-rich silicate outer shells, and a gradient in oxygen isotopes.

Geothermometry suggests that the Mg-rich centre of the Proto-Ureilite Planetesimal reached temperatures of ~1320 ºC, while the Fe-rich outer parts reached ~1190 ºC [7]. These temperatures are above the solidus of the Fe-FeS system, so that small amounts of metal-sulfide melt would have been formed. Being denser than the surrounding silicate minerals, this metallic melt would have percolated down to form a core. The temperaturews are also near the onset of melting of peridotite at low pressures, so that low-density silicate partial melts would have formed and moved upwards towards the surface of the body. Differences in degree of partial melting related to different P-T regimes within the planetesimal would have produced different silicate melt compositions. Formation and percolation of the metal and silicate partial melts did not destroy the original layered structure of the planetesimal.

Destruction of the planetesimal: Perhaps all differentiated planetesimals began with an initial compositionally layered structure as described above, but they continued to heat up (by decay of ^{26}Al or by kinetic energy of impact) to a point where the peridotite liquidus was approached and a magma ocean was formed. In this case, all evidence of the previous layered silicate structure would be destroyed. However, the Proto-Ureilite Planetesimal did not reach this point. Instead, while still hot and in a few regions still partially molten, it was disrupted and destroyed by an impact with another body.

A large proportion of the Proto-Ureilite Planetesimal was reaccreted as fragments, producing a daughter body from which our collection of ureilite meteorites has been derived (the present-day Ureilite Parent Body). This daughted asteroid has a distinctive compositional variation in which there is significantly more Fe-rich ureilite material than Mg-rich (Fig. 3), i.e. more of the outer layers of the Proto-Ureilite Planetesimal were preserved than the internal ones.

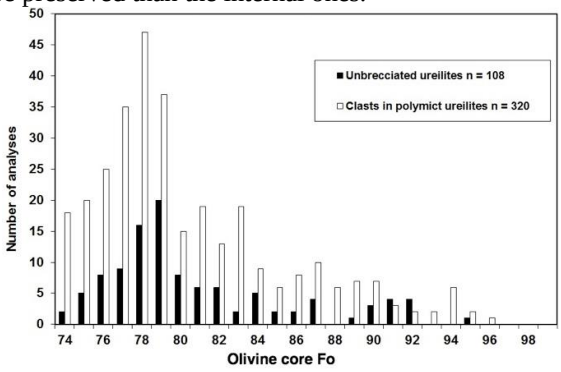

Figure 3. Histogram of distribution of Fe-rich and Mg-rich silicates in ureilites. Data from {2,8].

Conclusions: Ureilite meteorites are derived from the mantle of a differentiated planetesimal which did not experience a magma ocean stage and which therrefore did not become homogenized in terms of bulk composition and oxygen isotopes. Thus they give us a window into the early planetesimal accretion process, prior to magma ocean formation. We propose that a layered body formed from early condensed Mg-rich chondrules with low Δ^{17}O mixing with later condensed Fe-rich chondrules with higher Δ^{17}O. The body underwent heating to a temperature at which it formed a metallic liquid core and silicate melts, but the degree of partial melting was sufficiently low that the original layered structure of the silicate part of the planetesimal was preserved until the point when it was destroyed by impact. Reaccretion of a daughted asteroid (the present day UPB) preserved jumbled fragments of the compositionall layered structure.

References: [1] McSween H et al. (2014) *Elements* 10: 39-44. [2] Goodrich CA et al. (2004). *Chemie der Erde* 64, 283-327. [3] Sanders IS et al. (2017) *MAPS* 52, 690-708. [4] Greenwood RC et al. (2005) *Nature* 435: 916-917. [5] Steenstra ES et al. (2016) *GCA* 177, 48-61. [6] Clayton RN and Mayeda TH (1998) *GCA* 52: 1313-1318. [7] Warren PH (2012) *MAPS* 47: 209-227. [8] Downes H et al. (2008) *GCA* 72, 4825-4844. [9] Goodrich CA et al. (2009) *GCA* 73: 3055-3076. [10] Bischoff A et al. 92014) *PNAS* 111, 12689-12692. [11] Ruzicka A (2012) *MAPS* 47: 2218-2236.

Abundances of Short-lived Radionuclides and the Implications for the Formation of the Solar System Vikram V. Dwarkadas[1], Nicolas Dauphas[2], Bradley. S. Meyer[3], Peter H. Boyajian[1], Michael Bojazi[3], [1]Dept. of Astronomy and Astrophysics, University of Chicago, 5640 S Ellis Ave, ERC 569, Chicago, IL 60637 (vikram@oddjob.uchicago.edu), [2]Origins Lab, Department of the Geophysical Sciences and Enrico Fermi Institute, University of Chicago, [3]Dept. of Physics and Astronomy, Clemson University, Clemson, SC

Introduction: A critical constraint on solar system formation is the high abundance of ^{26}Al ($t_{1/2}$=0.7 Myr). The abundance of ^{26}Al as inferred in meteorites is ~17 times larger than the average ISM abundance at solar system birth from gamma-ray astronomy [1,2,3,6], which is too high [4,5,6] to be accounted for by long-term Galactic chemical evolution [7, 4, 8] or early solar system particle irradiation [9, 10].

This led to suggestions starting 40 years ago [11] that a nearby supernova (SN) explosion triggered the collapse of a molecular cloud and the formation of the solar system. ^{26}Al was created via stellar and SN nucleosynthesis, and injected into the protostellar cloud by the shock wave. This suggestion has been followed up by several authors [7,12, 13]. If correct, one would expect this to be accompanied by a high abundance of ^{60}Fe ($t_{1/2}$=2.6 Myr) which is produced in SN explosions. Recent work instead found that the ^{60}Fe/^{56}Fe ratio at solar system formation is about an order of magnitude lower that the average ISM value, inconsistent with direct injection from a nearby SN [6, 14].

Any potential model of solar system formation thus needs to explain both high ^{26}Al/^{27}Al and low ^{60}Fe/^{56}Fe ratios. The distribution of ^{26}Al in the Galaxy closely traces the distribution of very massive stars, making Wolf-Rayet (W-R) stars and core-collapse SNe the primary candidates for ^{26}Al production [20]. The former are stars with initial mass $\geq$ 25, which have lost their H and possibly He envelopes. In a study of the Carina region using INTEGRAL data, [21] found that the ^{26}Al signal could not be accounted for by supernovae alone, and the fraction of ^{26}Al ejected in W-R stars is high, indicating strong wind ejection of ^{26}Al. ^{26}Al has also been seen towards other star forming regions such as Cygnus [22], Orion [23], and Scorpius-Centaurus [24]. Many authors have suggested that stellar winds from massive stars, could be the source of ^{26}Al in the early solar system. [5, 14, 15, 16, 19, 45].

Using a combination of semi-analytic calculations, astronomical observations, and numerical modeling, in this presentation we advance the idea that ***our solar system was born inside a Wolf-Rayet wind bubble****. We show that this can simultaneously explain both the high ^{26}Al and low ^{60}Fe abundance.*

Wolf-Rayet Bubbles: W-R stars are post-main-sequence, hot massive stars which have strong winds with terminal velocities of 1000-2000 km s^{-1} [31]. The combined action of the supersonic winds and ionizing radiation results in the formation of photo-ionized wind-blown bubbles around the stars, consisting of a low-density interior surrounded by a high-density shell (Fig. 1). Most of the volume is occupied by a low-density high-temperature plasma.

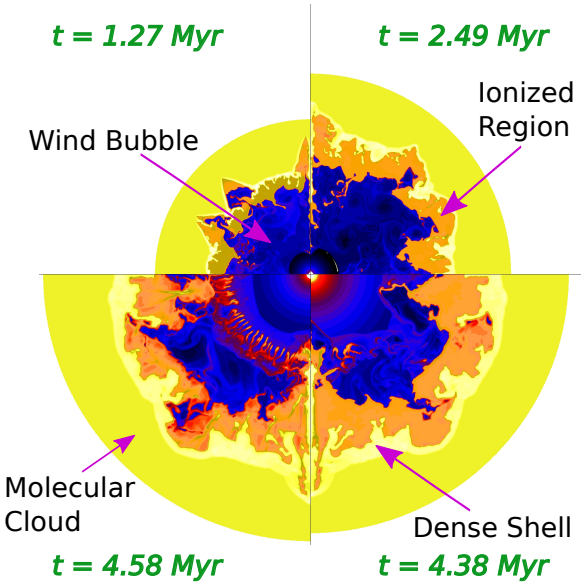

Figure 1: Density at 4 epochs in the evolution of a wind-blown bubble around a 40 $M_\odot$ star, at (clockwise from top left) 1.27, 2.49, 4.38 and 4.58 Myr. Note that the shell is unstable to several instabilities, related to both the hydrodynamics and the ionization front, which cause fragmentation and the formation of dense filaments and clumps [39, current work].

^{26}Al Yields from massive stars: In Figure 2 we show the ^{26}Al yields from stars with initial mass > 20 $M_\odot$ [25,26,27,28,29,30]. Newer yields take into account stellar rotation and improved mass-loss rates [25,26, 27]. The horizontal lines show the efficiency of mixing **η**, defined as the fraction of ^{26}Al required to mix with the dense shell of swept-up material to provide sufficient ^{26}Al to account for the early solar system budget of 3.3 parts per billion [19]. Stars above 50 $M_\odot$ generally provide sufficient ^{26}Al. The wind ^{60}Fe yield is negligible.

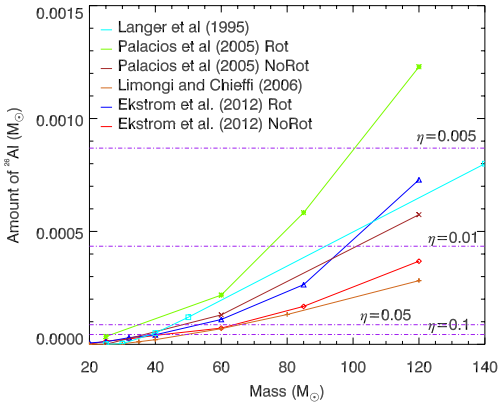

Figure 2

Wind Bubbles as Stellar Nurseries: Star formation at the boundaries of wind-bubbles around O and B stars has been revealed in astronomical observations [32,33,34,35]. Molecular cores undergoing gravitational collapse due to external pressure from the surrounding gas have been found around W-R star HD 211853 [36]. This stochastic star-formation is described in the context of two models, the `collect and collapse model' [37] and the `radiation-driven implosion' model [38].

Injection of ^{26}Al from the Wind to the Solar System: Injection of the ^{26}Al from the wind into the early solar nebula is an important ingredient. This topic has been studied mainly in the context of injection by a SN. [12,13] have shown that the injection efficiency due to hydrodynamic mixing between the SN shock wave and the collapsing cores is small, of order a few percent. This occurs late in the SN evolution, when it has reached the radiative stage and slowed down < 100 km s^{-1} (although see [40]). The W-R wind velocity substantially exceeds this value, while the density is much lower than in the SN ejecta. The efficiency of mixing will therefore be reduced. Winds sweeping past high-density cores will lead to shearing and the growth of Kelvin-Helmholtz instabilities at the interface, stripping material away. Hydrodynamic mixing does not appear a viable mechanism.

We suggest that ^{26}Al condenses onto, and is injected mainly via dust grains (see also [17,41]). Dust is seen around WC stars [42,43], although the formation mechanism at high temperatures is not well understood. Analysis of IR emission shows that dust forms close in to the star, with the grains estimated to be ~ 1μm in size [44]. The stopping distance of 1μm size grains in bubbles is several parsecs, exceeding the size of the bubble in the high density molecular cloud. The grains can survive passage through the reverse shock and the low density shocked wind, and reach the outer dense shell. The grains would then be injected into the high density cores, penetrating depths of 1 to several hundred AU depending on the density.

Finally, the massive star will explode as a SN of Type Ib/c. We have explored why the material ejected in the explosion, which contains both ^{26}Al and ^{60}Fe, may not be able to contaminate the early solar system.

References: [1] Lee T. et al (1976), *Geo. Res. Let., 3*, 109-112. [2] Jacobsen et al. (2008) *EPSL, 272*, 353-364. [3] McPherson et al. (1995) *Meteoritics, 30*, 365-386. [4] Huss et al. (2009) *Geo. Et Cosmo. Acta., 73*, 4922-4945. [5] Diehl R et al. (2006), *Nature, 439*, 45-47. [6] Tang H. and Dauphas N. (2012) *EPSL, 359*, 248. [7] Meyer B. and Clayton D. (2000) *From Dust to Terrestrial Planets*, 133–152. Springer. [8] Wasserburg et al. (2006) *Nuc. Phys. A, 777*, 5-69. [9] Marhas K. et al. (2002) *Sci., 298*, 2182-2185. [10] Duprat J. and Tatischeff V. (2007) *ApJL, 671*, 69-72. [11] Cameron A., and Truran J. (1977) *Icarus, 30*, 447-461. [12] Boss A. and Keiser S. (2013), *ApJ, 717*, 51. [13] Boss A. (2006) M&PS, 41, 1695-1703. [14] Tang H. and Dauphas N. (2015) *ApJ, 802*, 22. [15] Arnould M. et al. (1997), *A&A, 321*, 452-464. [16] Arnould M. et al. (2006), *A&A, 453, 653-659*. [17] Gaidos E. et al. (2009) *ApJ, 696*, 1854. [18] Tatischeff V. et al. (2010), *ApJL, 714*, L26-29. [19] Gounelle M. and Meynet G. (2012) *A&A, 545*, A4. [20] Knodlseder, J. et al. (1999), *ApL&C, 38, 379*. [21] Voss, R. et al. (2012), *A&A, 539, A66*. [22] Martin, P. et al. (2010), A&A, 511, A86. [23] Voss, R. et al. (2010), *A&A, 520, A51*. [24] Diehl, R. et al. (2010), *A&A, 522, A51*. [25] Ekstrom, S. et al. (2012), *A&A, 537, A146*. [26] Georgy, C., et al. (2012), *A&A, 542, A29*. [27] Georgy, C., et al. (2013), *A&A, 558, A103*. [28] Limongi, M. & Cieffi, A, (2006), *ApJ, 647, 483*. [29] Palacios, A. et al. (2004), *A&A, 429, 613*. [30] Langer, N. et al. (1995), *ApSS, 224, 275*. [31] Crowther, P. (2001), *ASSL, 264, 215* [32] Deharveng, L. et al. (2003), *A&A, 408, L25*. [33] Deharveng, L. et al. (2005), *A&A, 433, 565*. [34] Zavagno, A. et al. (2007), *A&A, 472, 835* [35] Brand, J. et al. (2011), *A&A, 527, 62*. [36] Liu, T. et al. (2012), *ApJ, 751, 68*. [37] Elmegreen, B., & Lada, C. (1977), *ApJ, 214, 725*. [38] Lefloch, B. & Lazareff, B. (1994), *A&A, 289, 559*. [39] Dwarkadas, V. V. & Rosenberg, D. (2013), HEDP, 9, 226. [40] Ouellette, N. et al. (2007), ApJ, 662, 1268 [41] Ouellette, N., et al. (2010), ApJ, 711, 597 [42] Rajagopal, J, et al. (2007), *ApJ, 671, 2017*. [43] Marchenko, S. & Moffat, T. (2007), *ASPC, 367, 213*. [44] Marchenko, S. et al. (2002), *ApJ, 565, L59*. [45] Young, E. et al. (2014), *E&PSL, 392, 16*

GROWTH AND DRIFT OF SOLIDS IN PROTOPLANETARY NEBULAE. P. R. Estrada[1,2] and J. N. Cuzzi[2], [1]Carl Sagan Center, SETI Institute, 189 N. Bernardo Ave. #200, Mountain View, CA 94043 (Paul.R.Estrada@nasa.gov), [2]NASA Ames Research Center, Mail Stop 245-3, Moffett Field, CA 94035.

Introduction: Planet formaton appears to be extremely robust and moreover lead to a very diverse set of outcomes [1]. However, our interpretation of how these planetary systems form and their resulting architectures and compostions is severely limited by our understanding of the complex physics that govern the earliest stages of growth - the very early evolution of solids, as they first decouple from the nebula gas and grow into planetesimals (e.g., asteroids and TNOs). We refer to this stage as "primary accretion".

The manner in which solids in protoplanetary disks (PPDs) can proceed from submicron dust to larger bodies remains problematic due to various barriers to growth that may be encountered. These include the bouncing and fragmentation barriers [e.g., 2] which, depending on nebula properties can nearly grind the process of incremental growth to a halt with particles not being able to grow much beyond "pebble" size [e.g., 3]. Another important effect of the slowed growth rate of solid particles, particularly in the outer portions of the disk, is that they drift radially faster than they can grow [3,4]. These barriers can be overcome if nebulae are not turbulent, but this is increasingly inconsistent with observations such as the formation ages of primitive meteorites and the duration of "dusty-gas" protoplanetary nebulae, as well as several new insights into purely hydrodynamical turbulence. Here we will examine the state of modeling of the PPD by various workers, and in particular examine moderately turbulent, global evolution under a variety of conditions taking into account the growth and radial drift of material of all sizes, diffusion and settling of small grains, and the importance of incorporating a self-consistent calculation of opacity and disk temperature as particles grow.

Indeed, the level of global nebula turbulence, which plays a key role in particle growth, remains very much a matter of debate. While predictions of MHD models have been trending towards low intensity near-midplane turbulence [5-6], purely hydrodynamical turbulence has re-emerged as a viable mechanism for driving disk evolution [7-8]. Moreover, a number of meteoritic and cometary properties point to an extended radial range of mixing of mineral constituents [e.g., 9], which are both difficult to reconcile with a globally non-turbulent nebula in the region of planetesimal formation. It seems appropriate to face the implications of at least moderate turbulence squarely, especially with respect to the various barriers it presents to incremental growth.

Being able to track various condensible species as they are transported throughout the disk, and at their respective evaporation fronts in particular turns out to be a very important aspect of disk evolution that has not been fully appreciated. By exploring a variety of conditions and dynamical properties, we can begin to assess the implications for planetesimal (and planet) formation and composition. One particular example is how fractal growth, porosity and compaction can help to overcome the radial drift problem. If radial drift is not overcome, one might expect to find planets much closer to their parent star as material from the outer disk inevitably ends up in the inner regions; on the other hand, in systems where radial drift is overcome one may find giant planets further out that become effective barriers to further inward drift of material. Also, the local chemistry can be affected by volatilized material of different composition that has been radially transported far from its original condensation site. We expect these kinds of models will be instrumental in helping to interpret current and future ALMA observations.

Summary: Herschel, Spitzer and now ALMA have demonstrated that PPDs are very diverse. Since the bulk of the mass is contained in the gas component, and since the growth from small dust particles into larger bodies depends on the evolving gas surface density profile, understanding the evolution of the gas is paramount in understanding planetesimal formation. Meanwhile understanding the chemistry and redistribution of the various species depends on the various evaporation fronts that exist in the nebula. In this talk we will review the state of modeling growth in the PPD, and especially be concerned with the H_2O, CO and CO_2 snowlines where for the latter stickiness, and thus efficiency of growth may be much less than for H_2O [10].

References:

[1] Wynn J. N. and Fabrycky D. C. (2015) *ARAA, 53,* 409. [2] Zsom A. et al. (2010) *A&A, 512,* id.A57. [3] Estrada P. R. et al. (2016) *ApJ,* 818, id.200. [4] Birnstiel, T. et al. (2010) *A&A,* 513, A79. [5] Bai X.-N and Stone J. M. (2013) *ApJ, 769* id.76. [6] Bai X.-N (2014), *ApJ, 791* id.137. [7] Turner N. et al. (2014), In *PPVI*, 666. [8] Umurhan O. M. et al. (2016), 47th LPSC, no. 1903, 2887. [9] Jozwiak et al. (2012), Meteor. Pla. Sci., 47, 471. [10] Musiolik G. et al. (2016), *ApJ 827,* id.63.

GROWING POROUS GRAINS IN 3D SPH SIMULATIONS. A.J.L. GARCIA[1] and J.-F. GONZALEZ[1], [1]Univ Lyon, Univ Lyon1, Ens de Lyon, CNRS, Centre de Recherche Astrophysique de Lyon UMR5574, F-69230, Saint-Genis-Laval, France (anthony.garcia@univ-lyon1.fr)

In protoplanetary discs, micron-sized grains should grow up to reach planetesimal sizes in order to ultimately form planets. However, dynamical studies show that once they reach a critical size, they drift rapidly into the accreting star. This is known as the radial-drift barrier.
In order to overcome this barrier, several methods have been proposed such as particles traps (e.g. vortices or planet gaps) which all involve large-scale dynamics. In this work, we choose to investigate the intrinsic properties of the grains during their growth, in particular their porosity. Grain fragmentation is not taken into account at this stage, it will be in a future work.

We thus consider the growth of grains with variable porosity as a function of their mass in several regimes of compression/expansion [1,2] and implement it in our 3D SPH (Smoothed Particle Hydrodynamics) two-fluid code [3].

We find that growth is accelerated for porous grains that can reach hundreds of meters in size in the inner disc while compact grain are meter-sized. We also find that drift is slowed down for porous grains that can grow up to larger sizes before drifting towards the star. As a result, grains in the outer regions of the disc reach larger sizes than when porosity is neglected. Those two mechanisms can help grains to overcome the radial-drift barrier and form planetesimals.

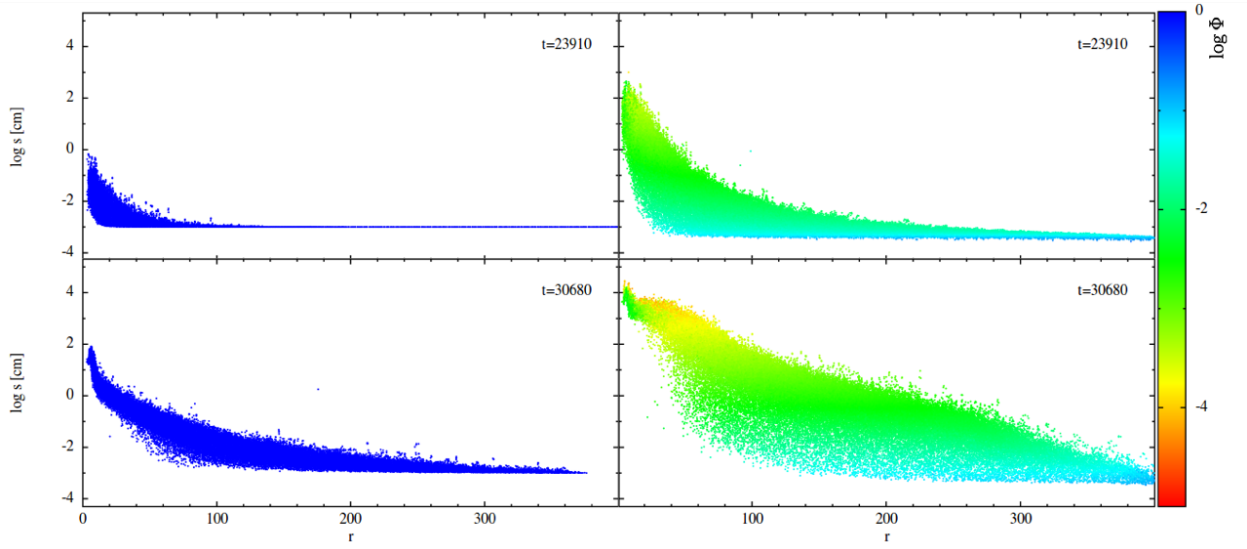

Figure 1. Radial grain size distribution for a disc where the gas' surface density Σ and temperature T profiles follow power laws of the distance from the star r with $\Sigma \propto r^{-3/2}$ and $T \propto r^{-3/4}$. Grains with 10 μm as initial size are injected in a gas disc at t = 23850 yrs. Left snapshots are for compact grains and right ones for porous grains. The color bar represents the grain filling factor ϕ: compact grains are in blue, porous ones are in green/yellow.

References:

[1] Kataoka, A. et al. (2013b) *A&A*, 554, A4
[2] Okuzumi, S. et al. (2012) *ApJ*, 752, 106
[3] Barriere-Fouchet L. et al. (2005) *A&A,* 443, 185

THE CARBONACEOUS – NON-CARBONACEOUS CHONDRITE RESERVOIR DICHOTOMY AND THE CHALLENGE OF UREILITES. C.A. Goodrich, Lunar and Planetary Institute, 3600 Bay Area Blvd., Houston, TX 77058 USA. cgoodrich@lpi.usra.edu.

Introduction: Oxygen isotope compositions are commonly used to distinguish or identify common source reserovirs among early solar system materials [1]. However, oxygen isotopes alone are not always definitive in this regard. A recent bloom of Cr- and Ti-isotope studies [2-14] has shown that combining ε^{54}Cr and ε^{50}Ti with Δ^{17}O provides a more powerful means of discerning cosmochemical relationships. Early solar system materials are divided into two main populations on diagrams of ε^{54}Cr or ε^{50}Ti vs. Δ^{17}O [3,4]. The carbonaceous chondrites, Eagle Station pallasites, and ungrouped achondrites inferred to be related to CC, form one (hereafter, CC) population, while Earth, Moon, ordinary chondrites, and most of the major groups of differentiated meteorites form the other (hereafter, NCC) population. Mo isotopes also show this dichotomy and can be used to associate iron meteorites with one or the other of the populations [15]. It has been suggested that the CC-NCC dichotomy reflects: 1) the difference between accretion in the inner (NCC) vs. the outer (CC) solar system [e.g., 3,4,]; and/or 2) a difference in time of accretion [16,17].

The Challenge of Ureilites: In the context of the CC-NCC dichotomy, the ureilites, a major group of achondrites, present a challenge [3,4]. ε^{54}Cr and ε^{50}Ti compositions of ureilites place them clearly in the NCC group. However, two essential properties of ureilites strongly distinguish them from other NCC materials: 1) they have high abundances of carbon, similar to the most C-rich carbonaceous chondrites (CI, CM, CR, Tagish Lake); and 2) their oxygen isotope compositions plot along the CCAM line on a 3-oxygen isotope diagram, with negative values of Δ^{17}O like most CC (and unlike most NCC), and δ^{18}O values similar to those of aqueously altered CC. These properties strongly suggest an affinity to CC-like materials. Furthermore, one interpretation of ureilite oxygen isotopes is that they result from aqueous alteration on the ureilite parent body (UPB) [17-20], which would imply that it accreted with water ice and therefore beyond the ice line (alternatively, ureilite oxygen isotopes were preserved from nebular precursors [21]). The carbon- and possibly water-rich nature of the UPB would suggest that it accreted in the volatile-enriched outer solar system. Thus, either the UPB accreted before ε^{54}Cr and ε^{50}Ti anomalies were introduced to the CC region [17], or volatile-rich materials were present and accreted into planetesimals in the inner solar system, at least at one time.

Long-Term Spatial Separation of the CC and-NCC Reservoirs and the Accretion Time of the UPB: From W and Mo isotopes, [22] argued that the CC and NCC reservoirs were spatially separated by ~1 Myr after CAI, and that their separation was preserved by the existence of Jupiter between them [23]. Thus, the argument that the UPB accreted in the outer solar system before nucleosynthetic anomalies were introduced to this region could only be correct if the UPB accreted <1 Myr after CAI. From thermal modeling, [24-26] obtained UPB accretion times of ~0.5-0.6 Myr after CAI, while [27,28] obtained 1.4-1.9 Myr. The difference between these results arises chiefly because [24-26] assumed efficient extraction of silicate melt from the mantle, while [27,28] did not. [29] showed that efficient silicate melt extraction on asteroids could be hindered by the presence of earlier-formed metallic melt. Whether this would be the case for the UPB depends on its initial metal and sulfide contents, which are not known [30]. Also, UPB melts may have contained significant carbon, which would be oxidized to CO_2 during ascent and increase melt buoyancy [21,24]. These and other factors will be evaluated.

Significance: It is uncertain whether ureilites accreted in the outer or the inner solar system. The latter could have important implications for the origin of carbon and water in Earth.

References: [1] Clayton R.N. (2004) *In* Treatise on Geochemistry, Vol. I., 129-142. [2] Yin Q.-Z. et al. (2009) LPS 40, #2006. [3] Warren P.H. (2011) GCA 75, 6912-6926. [4] Warren P.H. (2011) EPSL 311, 93-100. [5] Sanborn M.E. et al. (2013) MSM 76, #5220. [6] Sanborn M.E. et al. (2014) LPS 45, #2032. [7] Sanborn M.E. et al. (2014) Goldschmidt Conf., #2171. [8] Sanborn M.E. et al. (2014) MSM 77, #5169. [9] Sanborn M. E. and Yin Q.-Z. (2014) LPS 45, #2018. [10] Sanborn M.E. et al. (2015) LPS 46, #2259. [11] Williams C.D. et al. (2016) LPS 47, #1538. [12] Williams C.D. et al. (2016) Goldschmidt Conf., #3415. [13] Yin Q.-Z. et al. (2017) LPS 48, #1771. [14] Sanborn M. E. et al. (2017) MSM 80, #6277. [15] Budde G. et al. (2016) EPSL 454, 293-303. [16] Leya I. (2008) EPSL 266, 233-244. [17] Goodrich C.A. et al. (2017) GCA 203, 381-403. [18] Goodrich C.A. et al. (2002) LPS 33, #1379. [19] Kita N.T. et al. (2013) LPS 45, #1455. [20] Sanders I. et al. (2017) MAPS 52, 690-708. [21] Warren P.H. (2012) MAPS 47, 209-227. [22] Krujer T.S. et al. (2017) LPS 48, #1386. [23] Morbidelli A. (2016) Icarus 267, 368-376. [24] Wilson et al. (2008) GCA 72, 6154-6176. [25] Goodrich et al. (2015) MAPS 50, 782-809. [26] Wilson L. and Goodrich C.A. (2016) LPS 47, #1557. [27] Budde G. et al. (2015) EPSL *430*, 316. [28] Sanders I. and Scott E. (2012) MAPS 47, 2170. [29] Kiefer W.S. and Mittlefehldt D.W. (2017) LPS 48, 1798. [30] Goodrich C.A. (2013) GCA 112, 340-373.

ACCURATE TREATMENT OF COLLISIONS AND WATER-DELIVERY IN MODELS OF TERRESTRIAL PLANET FORMATION. N. Haghighipour[1], T. I. Maindl[2], C. M. Schaefer[2] and O. Wandel[2], [1]Institute for Astronomy, University of Hawaii (nader@ifa.hawaii.edu), [2]Dept. Astrophysics, Univ. Vienna, Austria. [3]Inst. Astron & Astrophys, Univ. Tübingen, Germany.

Introduction: It is widely accepted that collisions among solid bodies, ignited by their interactions with planetary embryos is the key process in the formation of terrestrial planets and transfer of volatiles and chemical compounds to their accretion zones [1]. Unfortunately, due to computational complexities, these collisions are often treated in a rudimentary way. Impacts are considered to be perfectly inelastic and volatiles are considered to be fully transferred from one object to the other. The employed perfect merging assumption also entirely neglects collisional-loss of volatile material (e.g., water) and draws an unrealistic connection between these properties and the chemical structure of the protoplanetary disk (i.e., the location of their original carriers).This zeroth-order approximation, although useful in proving the concept, has profound effects on the mass and composition of final planetary bodies as it grossly overestimates the masses of these objects and the amounts of volatiles and chemical elements transferred to them. We have developed a new and comprehensive approach in simulating collisions and the growth of embryos to planetary bodies where we use a combination of SPH and N-body codes to model collisions as well as the transport/transfer of chemical compounds accurately. Results of our simulations show clearly how accurate treatment of collisions avoids overestimation of the mass and water content of the final planets, and result in the formation of planets similar to Mars, Earth and Venus with water contents consistent with geological data.

Description of our codes: We simulate terrestrial planet formation using a combined N-body+SPH code. Unlike some of the publicly available N-body codes in which collisions between two objects are defined as when two points on their osculating orbits are closer than a critical distance (in which case the two bodies are merged), our N-body code has been developed to allow collisions to happen only when bodies are physically in contact with one another. At that stage, we model the collision using our full 3D SPH impact code [2,3].

Our SPH code includes material strength and self-gravity, and implements full elasto-plastic continuum mechanics extended by a model for simulating brittle failure [4, 5]. It also includes a fragmentation prescription and accounts for evaporation during the impact as well as the re-accretion of scattered materials. We apply a tensorial correction along the lines of [6] to achieve first-order consistency. The material model is based on the Tillotson equation of state [7]. As a result of this approach, i.e., SPH modeling of collisions within the N-body integration, our simulations are free of collisional artifacts and present more accurate values for the mass and volatile contents of the final planets.

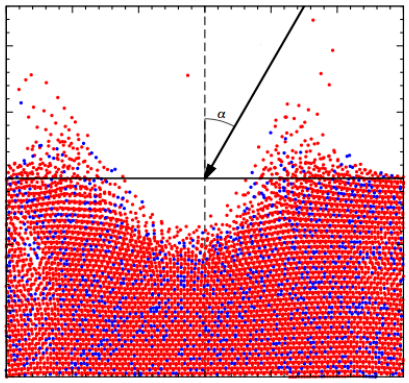

Fig1. SPH modeling of the collision of a planetesimal with an embryo. The embryo's water-mass fraction is 10%. As shown here, ice is exposed at the bottom and on the walls of the crater. Some of the scattered ice is also re-accreted on the surface of the embryo.

Simulations and Results: To accurately model the formation of terrestrial planets and the delivery of water, we carried out a large number of traditional N-body simulations. Each simulation included a few hundred Moon- to Mars-sized planetary embryos and several thousand km-sized planetesimals. To avoid un-necessary computations, we limited SPH simulations to only collisions with the seed embryos that resulted in the formation of final planetary bodies. For each seed embryo, we simulated its collision with other embryos as well as planetesimals. The latter is necessary to account for the loss of water due to ice sublimation from impact craters. Figure 1 shows a sample of these planetesimal-embryo impact simulations. We have included ice-sublimation in our N-body code using [8]

$$\dot{M} = P\left(\frac{\mu}{2\pi RT}\right)^{1/2} = 4.374\times10^{-5}\times P\left(\frac{\mu}{T}\right)^{1/2}$$

where

$$\ln\frac{P}{611\ (\mathrm{Pa})} = -\frac{51.058\ (\mathrm{MJ\ Kg^{-1}})}{R}\left(\frac{1}{T}-\frac{1}{273.16\ \mathrm{K}}\right)$$

and $\dot{M}, P, \mu, T$ and R are the rate of mass-loss, vapor pressure and molecular mass, temperature, and ideal gas constant. In each simulation, we determined the amount of ice exposed at the bottom and walls of the crater as well as those re-accreted on the surface of the embryo.

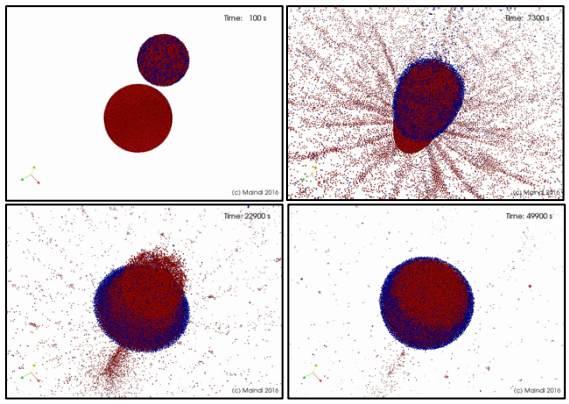

Fig 2. Snapshots of the SPH simulation of an impact between a 0.8 Moon-sized embryo with 10% water and a dry, 0.5 Mars-sized object (impact velocity = 6 km/s).

We then calculated the amount of sublimated ice until that embryo collided with another embryo or the exposed ice was fully sublimated.

Each collision of a seed embryo with other protoplanetary bodies was simulated using our SPH code. We considered embryos to be rocky and used the parameters for rock (basalt) and water ice as stated in [3]. Porosity was included using the *P*-α model [9-12]. At the lowest resolution, each embryo was resolved to at least 500,000 SPH particles. We determined the water content of the resulting body by keeping track of each SPH particle, and continued this process for subsequent collisions until the last impact event when the final planetary body formed. During this process, mass of the final planet and its water content were accurately determined. Figure 2 shows a snapshot of a sample of our embryo-embryo SPH simulations. Results of our simulations indicated that the amount of mass and water in planets formed in pure N-body simulations can be overestimated by up to 60%. Table 1 shows this for collisions between embryos for three different water-mass fractions (WMF) and two impact angles (in degrees).

Table 1: Overestimated water-mass fraction (WMF) of the final planet in embryo-embryo collisions in one of our typical N-body simulations

Impact Angle	Initial WMF (%)	Overestimated WMF (%)
0	5	39
0	10	42
0	29	45
30	5	61
30	10	61
30	20	63

To better understand the connection between the parameters of colliding bodies and the mass and water content of the final planets, we carried out a total of 60 SPH simulations of collisions between embryos of Ceres size and larger. Results indicated that even for collisions at moderate velocities, the amount of water lost during the impact is non-negligible. For instance, for embryos colliding at twice their mutual escape velocity, 10% to 60% of their water is lost in a collision. Figure 3 shows this in more detail. Noting that, in addition to collision, water is also lost due to evaporation and sublimation, and a seed embryo may be subject to a large number of collisions until a planetary body is formed, the above-mentioned water-loss percentages may be even larger.

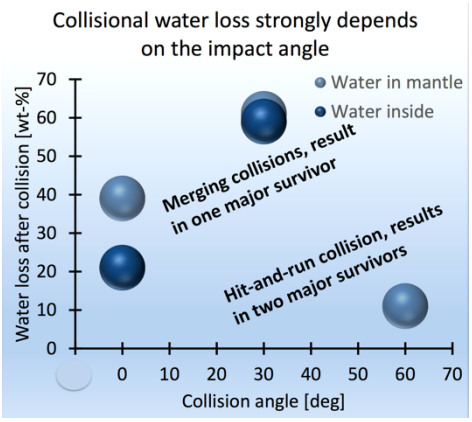

Fig 3. Water-loss after an embryo-embryo collision at 6 km/s for different collision angles and water distributions.

Concluding Remarks: Accurate simulations of collisions of protoplanetary bodies show that traditional N-body modeling of terrestrial planet formation overestimates the amount of the mass and water content of the final planets by over 60%. This implies that, as shown by [1], small planets such as Mars can also form in these simulations when collisions are treated properly. Another important implication of our study is that the distribution of water, volatiles, and chemical compounds cannot be post-formation and must be handled during a simulation, through proper treatment of collisions.

References: [1] Haghighipour, N. & Winter, O. C. (2016) CMDyA, **124**, 235. [2] Maindl, T. I., et al (2013) Astron. Nachr., **334**, 996. [3] Schäfer, C., et al (2016) A&A, **590**, A19. [4] Benz, W. & Asphaug, E. (1994) Icarus, **107**, 98. [5] Benz, W. & Asphaug, E. (1995) CPC, **87**, 253. [6] Schäfer, C. et al (2007) A&A, **470**, 733. [7] Tillotson, J. H. (1962) GA-3216, General Dynamics. [8] Schorghofer, N. (2008) ApJ, **682**, 697. [9] Hermann, W. (1969) J. Appl. Phys., **40**, 2490. [10] Carroll, M. M. & Holt, A. C. (1972) J. Appl. Phys., **43**, 1626. [11] Jutzi, M., et al (2008), Icarus, **198**, 242. [12] Jutzi, M., et al (2009) Icarus, **201**, 802.

EVIDENCE FOR ACCRETION OF FINE-GRAINED RIMS IN A TURBULENT NEBULA FOR CM MURCHISON. R. D. Hanna[1] and R.A. Ketcham[1]. [1]Jackson School of Geosciences, University of Texas, Austin, TX, 78712. E-mail: romy@jsg.utexas.edu.

Introduction: Fine-grained rims (FGRs) are dust-sized material that surrounds chondrules and refractory inclusions in chondritic meteorites. The origin of FGRs in CMs is still debated and formation in both nebular [1] and parent body [2-4] settings have been proposed. Nebular FGR formation involves accretion of unequilibrated nebular dust to chondrule surfaces [1]. Mechanisms of FGR formation in a parent body setting include: 1) formation in the parent body regolith through attachment and/or compaction of fine-grained material onto the chondrule surface [2-4] and 2) formation via aqueous alteration of the chondrule [2,4]. For the latter it is expected that as alteration proceeds and the volume of FGR increases, the shape of the chondrule core would increase in irregularity as embayments are formed along the chondrule exterior [4]. In this scenario it also may be expected that rim composition is influenced by the composition of the core particle.

One observation taken as evidence for nebular formation of FGRs in CMs is a positive correlation between rim thickness and the size of the interior chondrules [1,5], which is not expected for formation in a parent body regolith [3]. Although astrophysical arguments have been made for the positive linear correlation between rim thickness and interior chondrule radius [5] subsequent refinements hypothesize that dust accretion around chondrules results in a power law relationship between the FGR volume and interior chondrule radius that in turn provides information on nebular turbulence conditions [6-7].

Previous measurements of chondrules and their FGRs were made using 2D thin sections, which yield only apparent chondrule size and rim thicknesses. In addition, many CMs show evidence of deformation that would have altered the shape of the chondrule and rim [8-9]. We use X-ray CT to examine the 3D morphology and composition of FGRs in CM Murchison for which we have previously documented the deformational strain and resulting aqueous alteration [8]. The primary goal of our study is to determine whether a regular size relationship between the interior chondrule and exterior FGR exists and whether this relationship can shed light on FGR formation conditions.

Methods: We scanned six small orientated chips (0.143 – 3.6 g; some embedded in epoxy) of CM Murchison USNM 5487 at the University of Texas High-Resolution X-ray Computed Tomography Facility (UTCT). The final reconstructed voxel (3D pixel) size ranged from 5.5 to 9.9 µm. Chondrules within the X-ray CT datasets were manually segmented twice in Avizo: both with and without the FGR. Segmented data were exported into the Blob3D program [10-11] and chondrule size, shape, and orientation measured with and without the FGR. Chondrule FGR volume was determined by subtraction of the two measured volumes. To estimate FGR thickness for each chondrule prior to deformation the FGR volume was distributed evenly around a spherical chondrule of equivalent volume to that measured with Blob3D. To determine the current (post-deformation) 3D thickness of the FGR around the chondrule a new algorithm was implemented in Blob3D. For each rimmed chondrule, the algorithm "looks outward" from the chondrule center along a set of 3D traverses evenly covering a unit sphere and measures the thickness of the rim in each direction. Average rim thickness among all chondrules in each orientation is then calculated and plotted on a stereonet to determine if there is any spatial coherence to the varying rim thickness around the chondrules.

To determine the relationship between the FGR volume and interior core radius while including the uncertainty in FGR volume (4.1%) we used the Levenberg-Marquardt method to determine a non-linear least squares fit to the data [12]. To quantify shape irregularity we factor the previously used Convolution Index [13] (object surface area / surface area of volume-equivalent sphere) into Roughness (object surface area / surface area of best-fit ellipsoid) and Ellipticity (ellipsoid surface area / sphere surface area) indices. This separation makes the shape irregularity measurement independent of the degree of flattening the chondrules experienced during parent body deformation [8].

Results: A total of 61 chondrules were segmented. We find a moderate linear correlation between the average, pre-deformational thickness of the rim and equivalent spherical radius of enclosed chondrule core ($R^2 = 0.73$). However, we find a strong correlation ($R^2 = 0.98$) using a power law relationship between the rim volume and the equivalent spherical radius of the chondrule core as suggested by [6] for nebular FGR formation (Fig. 1). The power law exponent of this relationship indicates a weakly turbulent nebula environment and that the rimmed chondrules were slightly larger than Kolmogorov-stopping-time nebular particles [6]. In addition, the FGRs are consistently thicker (by ~2% of the chondrule core diameter) in the plane of foliation, indicating that the rims were deformed simultaneously with the cores.

We also find a chondrule-roughness dependence of the rim volume to interior chondrule radius relationship when the data are split into two groups based on the Roughness index (Fig. 2). This suggests that the irregular shape of the chondrules is a primary feature present at the time of nebular FGR accretion, and that it influenced the amount of dust accreted to them.

There is no correlation (R^2 = 0.00) between the roughness of the chondrule and relative rim volume, suggesting that the FGR is not a result of alteration of the chondrule core and is instead a primary feature. FGR composition as inferred from effective X-ray attenuation coefficient appears essentially uniform across interior chondrule types and compositions, also making formation by chondrule alteration unlikely.

Conclusions: We find strong morphological evidence that FGRs in CM Murchison were formed in a weakly turbulent nebula, as the relationship between FGR volume and interior chondrule interior radius is well fit by a power law relationship consistent with the presence of turbulence [6]. The fitted power law exponent suggests that the rimmed chondrules were slightly larger than Kolmogorov-stopping-time nebular particles. In addition, we rule out parent-body aqueous alteration as an origin for significant FGR formation based on several lines of evidence: the lack of correlation between interior chondrule shape irregularity (a proxy for degree of alteration) and FGR volume, the presence of a positive correlation between rim thickness and chondrule size, and evidence that FGRs are a similar composition despite their interior chondrule types (composition). Finally, we propose that the highly irregular shape of some chondrules in CM Murchison are a primary feature resulting from chondrule formation and that rougher particles accreted a relatively larger amount of nebular dust.

References: [1] Metzler K. et al. 1992. *Geochimica et Cosmochimica Acta* 56:2873-2897. [2] Sears et al. 1993. *Meteoritics* 28:5:669-675. [3] Trigo-Rodriguez J.M. et al. 2006. *Geochimica et Cosmochimica Acta* 70:1271-1290 [4] Takayama A. and Tomeoka K. 2012. *Geochimica et Cosmochimica Acta* 98:1-18. [5] Morfill G.E. et al. 1998. *Icarus* 134:180-184. [6] Cuzzi J.N. 2004. *Icarus* 168:484-497. [7] Cuzzi J.N. and Hogan R.C. 2003. *Icarus* 164:127-138. [8] Hanna R.D. et al. 2015. *Geochimica et Cosmochimica Acta* 171:256-282. [9] Rubin A.E. 2012. *Meteoritics & Planetary Science* 46:587-600. [10] Ketcham R. A. 2005. *Geosphere* 1:32-41 [11] Ketcham R. A 2005. *Journal of Structural Geology* 27:1217-1228. [12] Press et al. 2007. Cambridge University Press, 1256 p. [13] Zanda et al. 2002. LPSC 33, abtract #1852.

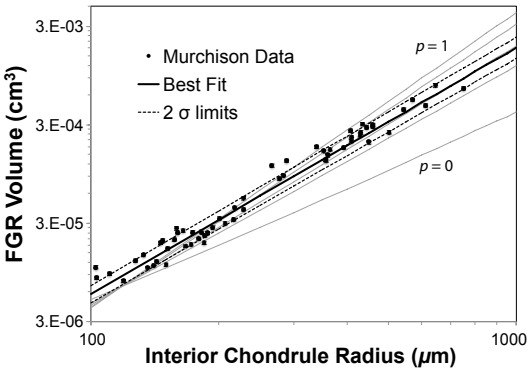

Fig. 1. Rim volume predictions for p = 0.0, 0.5, 0.7, 0.9, and 1.0 (different nebular conditions) using Eq. (11) from [6] (thin grey lines) and Murchison data (circles). The best fit (solid line) and with 2-sigma uncertainty (dotted lines) correspond to a p of 0.56 ± 0.02, indicating a turbulent nebula and that the rimmed particles were larger than Kolmogorov-stopping-time particles.

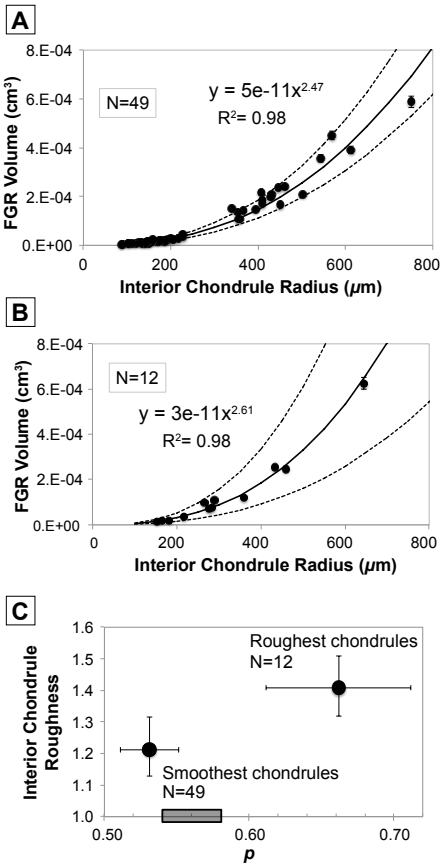

Fig. 2. Murchison data split into 2 groups based on interior chondrule roughness (A) Smoother chondrules (B) Rougher chondrules. (C) p values of each group with 2-sigma uncertainties. Groups are well separated in p space, indicating different nebular conditions or, more likely, differing amounts of accumulated dust due to chondrule shape. Gray bar shows p values using the full Murchison dataset (Fig. 1).

A PATH TO CHONDRULE AGGREGATES. Thomas Hartlep[1,2] and Jeffrey N. Cuzzi[2] (thomas.hartlep@nasa.gov, jeffrey.cuzzi@nasa.gov) [1]Bay Area Environmental Research (BAER) Institute, Petaluma, CA, [2]NASA Ames Research Center, Moffett Field, CA.

Introduction: The formation of the very first planetesimals remains an unsolved problem but their properties provides us some clues. In the inner protoplanetary disk, most of the mass of "fossil" planetesimals is in ~100km diameter objects that were (before melting) originally internally homogeneous, dominated by mm-sized chondrules and complementary mineral grains [1]. Traditional growth-by-sticking models in turbulent nebulae encounter various formidable barriers: a roughly meter-size fragmentation or drift barrier [2], and a 1-10km size erosion/fragmentation barrier [3,4]. Currently accepted limits of sticking (which are based on pure ice or silicates) also pose a mm-to-cm-size "bouncing" barrier [5]. To circumvent these barriers, an idea arose that planetesimals might have been "born big" in turbulence by collective effects, as explored in two main classes of "leapfrog" models [6,7]. However, both have been shown to be unable to produce 100km asteroids directly from mm-sized chondrules and require some growth beyond those sizes [8]. In this talk we will discuss recent advances in the understanding and modeling of gas-particle dynamics in turbulence which we hypothesize might be able to overcome the currently accepted mm-sized bouncing barrier to grow larger aggregates.

Turbulent Concentration (TC): The leapfrog scenario we have pursued [5,9] is based on the realization that in a turbulent flow, inertial particles are not distributed homogeneously but cluster in regions of high strain and low vorticity. It is envisioned that such dense zones can lead directly to planetesimal formation through gravitational collapse. This clustering or preferential concentration effect is particle-size dependent and specifically depends on the particles's aerodynamic stopping time t_s or Stokes number $St_\eta = t_s / t_\eta$ where t_η is the eddy time of the smallest (Kolmogorov) eddy in turbulence.

We have statistically modeled this process with a so-called "cascade" model [9,10] and, using crude but physics-based thresholds have derived production rates and planetesimal initial mass function (IMFs). The most refined models show that under reasonable assumptions for disk turbulence, we can only produce ~100km objects from particles in the cm-dm range, which we hypothesize could be aggregates of chondrules.

New Advances in Particle-Gas Dynamics: Current astrophysical coagulation models commonly consider a simplified collision kernel K^{COM} consisting only of the collision cross section πd^2 between two particles (d is the sum of the particle radii), and some characteristic relative velocity. For fluid turbulence, this velocity is generally taken to be the rms (root-mean-square) relative velocity between particles and is given by a Völk-type model [11,12,13]. However, new numerical simulations and more sophisticated modeling efforts in the general fluid dynamics community [e.g., 14, 15] have shown that such a collision model ignores several important effects that may significantly alter the results of coagulation models and may allow for aggregates to grow to larger scale. Strictly speaking, the mean collision kernel is given by $K = \pi d^2\, g(d)\, \bar{w}(d)$ [16] where g(d) is the so-called *radial distribution function* which describes the increased particle concentration due to turbulent clustering. Specifically, g(d) is the ratio of the number of particle pairs found having some separation d to the number one would expect if particles were homogeneously distributed. $\bar{w}(d)$ is the mean relative velocity between approaching particles, and not the rms relative velocity.

Clustering is completely ignored in the simple traditional kernel. For the coagulation problem, the scale of interest is the particle diameter d (or the sum of the radii for unequal particles) which is much smaller than η. For instance, $d/\eta \approx 2\times10^{-6}$ for mm-sized chondrules in a minimum mass solar nebula at 3AU. So, even though the same physical mechanisms operate as in the TC scenario for making "sandpile" planetesimals mentioned above, the detailed behavior is different in the dissipations range ($d \lesssim \eta$). Here, for particles with $St_\eta \lesssim 1$, numerical simulations have shown that g(d) in the dissipation range grows approximately as a power law with decreasing scale, at least to the scales current simulations can reach, with a St_η-dependent exponent that is largest for St = 1. In effect, it preferentially increases the collision probability between particles with $St_\eta \sim 1$.

Progress has also been made in understanding and modeling the statistics of the *relative velocity* between particles compared to Völk-type models. More sophisticated models [17,18] have made predictions for the rms relative velocity, w_{rms}, that compare well with simulations. In the dissipation range, w_{rms} decreases with decreasing scale, opposite to g(d). The mean rela-

tive velocity, $w_{-}(d)$, that appears in the mean collision kernel, has a simple relationship to w_{rms} if the velocity field is normally distributed (Gaussian): $w_{-}/w_{rms} \approx 0.4$. However, it has been shown that the relative velocity is *not* Gaussian at the small scales of interest ($d < \eta$) and in particular at $St_\eta \sim 1$. In fact, the ratio w_{-}/w_{rms} shows a dip for $St_\eta \sim 1$, and the deviation deepens with decreasing spatial scale and increasing Reynolds number. Overall, for $St_\eta \sim 1$ particles, the mean relative velocity is reduced, i.e. the probability of gentle, low-speed collisions is greatly increased. However, due to clustering, the total *mean collision kernel* for $St_\eta \sim 1$ is still larger than what the commonly used expression predicts, despite the reduced (mean) collision velocity (Figure 1). The deviation of the mean relative velocity can be traced to changes in the full probability distribution function (PDF) of the relative velocity, P(w,St); [19] and others have shown P(w,St) is non-Gaussian; that is, it has "fat" tails that not only increase the probability of low velocities which favors sticking, but also of high velocities. P(w,St) is also asymmetric, with very low collision velocities being more probable than high velocities.

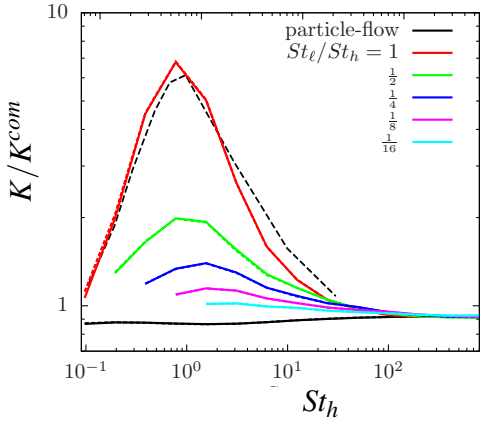

Figure 1: Ratio between the more realistic collision kernel $K = \pi d^2\, g(d)\, w_{-}(d)$ and the kernel K^{COM} commonly used in astrophysical models, from [14], at a scaled $d=0.25\eta$ for collisions between particles with equal Stokes numbers and different Stokes numbers. St_h (St_l) denote the Kolmogorov scale Stokes number St_η for the larger (smaller) particle. The dotted line shows the same kernel computed from the simulation results of [15] obtained at a larger Reynolds number.

Consequences for Coagulation Models: These new particle-gas dynamic effects for Stokes numbers of order unity (which chondrules arguably are [20]), have yet to be taken into account in a coagulation model. What the detailed effects will be remain to be seen, but it conceivable that the preferentially reduced velocities would lead to gentler collision increasing the likelihood of sticking as opposed to bouncing for chondrules. And, for as long as aggregates grow in the ``hit-and-stick" or fractal growth regime, they retain the monomer St_η because their radius-density product does not change [21], so we expect that the $St_\eta \sim 1$ signature will persist even as aggregates combine by sticking, until compaction becomes important, the bouncing barrier is reached, and growth stalls (but now at larger scale). Even though these aerodynamic effects are strongest for $St_\eta = 1$, a range of Stokes numbers/ particle scales participates in them (as seen in Figure 1). The hope would be that a refined coagulation model that take these effects into account would be able to explain the size distributions in chondrites [22] because of the specific $St_h \sim 1$ effects like this that are somewhat universal from the preferential sticking standpoint. Differences in the distribution between different chondrites could then likely be explained by different gas density and turbulence intensity.

References: [1] Johansen et al. 2015 [2] Brauer et al. 2008 A&A 480, 859 [3] Ida et al. 2008 ApJ 686, 1292 [4] Ormel and Okuzumi 2013 ApJ 771, 44 [5] Johansen, A. et al 2016,in Asteroids IV, U. of Az.Press, arXiv:1505.02941 [6] Johansen et al. 2007 Nature 448, 1022 [7] Cuzzi et al. 2008 ApJ 687, 1432 [8] Cuzzi et al. 2016 LPSC 47, 2661 [9] Cuzzi et al 2010 Icarus, 208, 518 [10] Hartlep et al. 2017 Phys.Rev.E, 95(3), 033115 [11] Völk et al. 1980 A&A 85, 316 [12] Markiewicz et al. 1991 A&A 242, 286 [13] Ormel and Cuzzi 2007 A&A 466, 413 [14] Pan and Padoan 2014 ApJ 797, 101 [15] Ireland et al. 2016 Journal of Fluid Mechanics 796, 617 [16] Sundaram and Collins 1997 Journal of Fluid Mechanics 335, 75 [17] Zaichik et al. 2003 Physics of Fluids 15, 2995 [18] Pan and Padoan 2013 ApJ 776, 12 [19] Pan et al. 2014 ApJ 792, 69 [20] Cuzzi et al. 2017 Accretion: Building New Worlds Conference [21] Okuzumi et al. 2012 ApJ 752, 106 [22] Simon et al. 2017 Accretion: Building New Worlds Conference

A TERRESTRIAL CONJECTURE ON CONVECTION, MAGNETIC FIELDS, AND WATER. W. Daniel Heinze[1], [1]GRAD, Intl., PO Box 2429, Fredericksburg, Texas, 78624; danheinze@gmail.com.

Introduction: Of the terrestrial planets, including the Moon, Earth is the only one to have retained a strong magnetic field and large quantities of water. Early Mars apparently had an erratic magnetic field that ranged from Earth's current field strength to about a tenth of that value [1]. Early Mars also had enough water to leave a persuasive set of apparently water deposited sediments but lost most of that water by 3.7 Ga (or possibly as late at 3.0 Ga) subsequent to the waning of its magnetic field which most likely occurred between 4.0 and 4.1 Ga [1] but may have occurred as late as 3.7 Ga [2]. Early Earth was apparently close to a water world and its magnetic field has persisted at least since 4 Ga [3]. Although not universally agreed, this suggests that a persistent, strong magnetic field and its associated magnetosphere protects a terrestrial planet's atmosphere and water from erosion by stellar winds [4, 5].

Conjecture: Terrestrial planets that accrete by a sufficiently large number of high energy impacts will have a liquid-iron core after initial cooling. Correspondingly those that accrete by sufficiently number of low energy impacts will have a largely solid-iron core after initial cooling. Magnetic dynamo modelling indicates that the former scenario in not likely to generate a strong or persistent magnetic field and the later will definitely not. Planets whose accretion falls along an intermediate scenario, will likely have solid/liquid core ratios that range from near zero to almost one. Venus, Earth, and Mars appear to nearly span these intermediate scenarios.

Given the likelihood that Venus received approximately twice the energetic impacts as did earth [6], I conjecture here that, after initial cooling, it had a fully liquid-iron core that had little or no capacity to support a long-term magnetic dynamo. Mars, on the other hand, possibly experienced a scenario near the other extreme. Initially, it had a core that was near the solidus, but had enough liquid to allow at least an occasionally strong, but fitful magnetic dynamo. Mars' mantle upon final accretion was very likely cooler than that of Earth or Venus [6] and its smaller size enhanced the planet's heat loss. Thus the Martian mantle, compared to that of Earth or Venus, had the potential to more rapidly cool the outer liquid core, thereby shrinking it until the magnetic dynamo permanently shut down.

Development: This conjecture suggests a broadly coherent story of terrestrial planet accretion/evolutionary trajectory. Assuming that results from Quintana and Barclay [6] are general, that terrestrial planets farther from their star tend to receive less total energy from accretion impacts, we hypothesize five classes of terrestrial planets from closest to farthest from their star. Given the wide range of the number and energy content of impacts in individual terrestrial planetary accretion simulations, these five "classes" may more appropriately be seen as signposts along a continuum. This discussion assumes that all terrestrial planets receive massive volatile delivery as part of accretion (which is consistent with some numerical modeling) and that radioactive heating is similar in all the planets (a substantial approximation).

1. Mercury-like Planets "very close" to their stars will: accrete very hot; have a very large core fraction; have a liquid core of mostly iron far above the solidus; have a mantle far above the solidus; outgas their volatiles early and completely; and lose most of any atmosphere that remains by stellar wind spallation. An early magnetic field could be strong but short lived in the rapid cooling environment of a planet without an atmosphere. It is unlikely to have a strong magnetic field that persists. Convection in the "thin" mantle may be sustainable.

2. Venus-like Planets "close" to their stars will: accrete hot; have a large core fraction; have a liquid core of mostly iron well above the solidus; have a mantle well above the solidus; outgas their volatiles early and nearly completely; and lose most of the lighter elements like hydrogen from their atmosphere by stellar wind spallation. An early magnetic field could be strong but very short lived as the planetary atmosphere soon becomes an effect thermal blanket and consequently a stagnant lid on the mantle will probably develop early, virtually eliminating the possibility of a persistent magnetic field. Sustained mantle convection unlikely.

3. Earth-like Planets at "intermediate distances" to their stars will: accrete somewhat hot; have an intermediate sized core fraction; have a liquid core of mostly iron above the solidus; have a mantle above the solidus; largely outgas their volatiles; and lose much of their atmosphere by stellar wind spallation before a strong, persistent magnetic dynamo starts within a few hundred million years of accretion and preserves most of the remaining atmosphere. The remaining atmosphere slows planetary cooling, but not dramatically. Sustained mantle convection likely.

4. Mars-like Planets "far" from their stars will: accrete warm; have a smaller core fraction; have a liquid

core of mostly iron just above the solidus; have a mantle just above the solidus; partially outgas their volatiles; and lose much of their atmosphere by stellar wind spallation before a strong, persistent magnetic dynamo starts within a few hundred million years of accretion and protects most of the remaining atmosphere for a time. This remaining atmosphere slows planetary cooling, but not dramatically. The magnetic dynamo fails as the planet cools and the mantle sucks enough heat out of the core to freeze most of it. Sustained mantle convection possible for the warmest accretion outcomes, but most likely too cool for substantial long-term mantle convection.

5. Asteroid Belt-range Planets "very far" from their stars (just inside or just outside the "snow line") will: accrete warm to cool; have a small core fraction; have a partially liquid core of mostly iron averaging about the solidus; have a mantle just below the solidus; very partially outgas their volatiles; and slowly lose their atmosphere by stellar wind spallation. A magnetic dynamo is unable to initiate or lasts for only a very brief period. No mantle convection.

A Proposal: Under simplified assumptions, sufficient knowledge of:

- the equations of state of the likely composition of terrestrial planets,
- advanced accretion modelling [6,7,8,9], and
- magnetic dynamo modelling [10]

are now available that enable the simulation of terrestrial planet accretion around a large range of star sizes (accretion disk size and surface density). This will allow an estimate of the parameter space in accretion disk size and surface density, planet size, and orbital radius where a strong, persistent magnetic dynamo is likely and the degree of overlap of this parameter space with the stellar habitable zone.

References: [1] Lillis, R. J., S. Robbins, M. Manga, J. S. Halekas, and H. V. Frey (2013), Time history of the Martian dynamo from crater magnetic field analysis, J. Geophys. Res. Planets, 118, doi:10.1002/jgre.20105. [2] Milbury, C., G. Schubert, C. A. Raymond, S. E. Smrekar, and B. Langlais (2012), The history of Mars' dynamo as revealed by modeling magnetic anomalies near Tyrrhenus Mons and Syrtis Major, J. Geophys. Res., 117, E10007, doi:10.1029/2012JE004099. [3] Tarduno, J. A., Cottrell, R. D., Davis, W. J., Nimmo, F. & Bono, R. K. Science 349, 521–524 (2015). [4] Scherf, Manuel et al. On the Earth's paleo-magnetosphere for the late Hadean eon. Abstract 420.02, Volume 48, Number 7, Division for Planetary Sciences Convention, American Astronomical Society, Pasadena, California, 16-21 October 2016. [5] Khodachenko, Maxim L. et al. The Martian paleo-magnetosphere during the early Naochian and its implication for the early Martian atmosphere. Abstract 420.03, Volume 48, Number 7, Division for Planetary Sciences Convention, American Astronomical Society, Pasadena, California, 16-21 October 2016. [6] Quintana, Elisa V. and Barclay, Thomas, Dynamical Models to Infer the Core Mass Fraction of Venus. Abstract 105.02, Volume 48, Number 7, Division for Planetary Sciences Convention, American Astronomical Society, Pasadena, California, 16-21 October 2016. [7] Barclay, Thomas and Quintana, Elisa V. Using Dynamical Models to Predict the Terrestrial-Mass Free-Floating Planet Population. Abstract 309.09, Volume 48, Number 7, Division for Planetary Sciences Convention, American Astronomical Society, Pasadena, California, 16-21 October 2016. [8] Jackson, Alan P., Travis SJ Gabriel, Erik Asphaug. Constraints on the pre-impact orbits of Theia, the Borealis impactor and the progenitor of Mercury. Abstract 318.06, Volume 48, Number 7, Division for Planetary Sciences Convention, American Astronomical Society, Pasadena, California, 16-21 October 2016. [9] Gabriel, Travis SJ et al. Mantle Debris in Giant Impacts: Parameter-Space Study and Scaling Laws. Abstract 518.04, Volume 48, Number 7, Division for Planetary Sciences Convention, American Astronomical Society, Pasadena, California, 16-21 October 2016. [10] Soderlund, Krista M. et al. Numerical Simulations of Ice Giant Interiors with Radially Varying Electrical Conductivity. Abstract 408.09, Volume 48, Number 7, Division for Planetary Sciences Convention, American Astronomical Society, Pasadena, California, 16-21 October 2016.

INSIGHTS INTO AGGREGATION OF SUBMICRON GRAINS FROM 3-D STRUCTURE OF A PRIMITIVE FINE-GRAINED COSMIC DUST PARTICLE. Z. W. Hu[1] and R. P. Winarski[2], [1]XNano Sciences Inc., P. O. Box 12852, Huntsville, AL 35815, USA (zwhu@xnano.org). [2]Center for Nanoscale Materials, Argonne National Laboratory, Argonne, IL 60439, USA.

Introduction: A significant portion of cosmic dust particles collected in the stratosphere [1] is fluffy or porous aggregates of mostly submicron grains, known as chondritic porous (CP) IDPs. CP IDPs are the most primitive extraterrestrial materials currently available for laboratory study [2]. They provide samples of primitive or the least altered fine-grained materials from the early solar system, some of which were either not incorporated or not preserved in common meteorites [3-5]. We have learned a great deal about the early solar system through laboratory analyses of the composition, mineralogy and organics of IDPs and thin-sectioned samples in particular [e.g., 2-7]. The morphology and structures of fragile, porous fine-grained IDPs at the 3-D nanoscale, however, were relatively little explored until recently [8], which provide new avenues of investigation into the aggregation of dust and ices in the protoplanetary disk – the crucial first step towards the formation of planetesimals and planets [9-10]. By developing phase contrast X-ray nanotomography (PCXNT) to noninvasively map aggregate IDPs with extreme sensitivity and high resolution, we have unlocked the structures of the first few bulk IDPs in 3-D ~ 10 nm detail [8]. In this presentation, we present new findings of the pristine or the least altered morphologies and structures of a protoplanetary porous fine-grained aggregate from this initial study, which yield insights into grain accretion in the outer protoplanetary disk.

Samples and Methods: An intact, ~ 10-μm-long CP IDP (U2015-M-1) was used for this study. The particle initially coated with silicone oil (a collection medium) was rinsed with hexane to remove the oil. The particle was then mounted on the top of a tungsten tip with 3M repositionable double-coated tape for a PCXNT experiment that was carried out on the Center for Nanoscale Materials (CNM)/X-ray Science Division Hard X-ray Nanoprobe Beamline at the Advanced Photon Source (APS), Argonne National Laboratory. Given that CP IDPs are structurally heterogeneous at the submicron/nanoscale level, with high abundances of low-density carbonaceous material, we have utilized phase changes of the wavefront induced by refractive index differences across the interfaces that define the structures of interest (e.g., grains and pores), combined with wave interference, to generate such high contrast at the interfaces that may be unobtainable otherwise (see ref 8 for experimental details and principles).

Results and Discussion: PCXNT has enabled us to noninvasively visualize and analyze the intact CP IDP morphologically and structurally in 3-D ~ 10 nm detail. The somewhat flattened particle is an elongated, porous aggregate of mostly submicron, elongated grains or clusters of smaller grains (Fig. 1), morphologically similar to porous comet 67P dust particles [11]. This porous IDP is revealed to be an inherently fragile and intricately porous aggregate of irregularly-shaped, submicron grains that are delicately bound together frequently with little grain-to-grain contact in 3-D space. The revealed characteristics of the particle provide the most detailed and direct structural evidence yet for its pristine state and cometary origin, consistent with the previous inference about the cometary origin of CP IDPs drawn from TEM observation of void spaces in microtomed CP IDPs [12] and the measurement of thermally stepped He release profiles of CP IDPs [13]. That the particle is made up of irregular submicron building blocks provides clear evidence that this dust aggregate formed through cluster-cluster aggregation.

The pore structures of the CP IDP are surprisingly intricate, consisting of two types of original voids that are interconnected in 3-D space: one is morphologically primitive, submicron intergranular voids that are ubiquitous; the other is morphologically evolved, well-defined intragranular nanoholes running through the cores of morphologically distinct refractory dust grains. The mean size of the indigenous voids present in the CP IDP is comparable to the inferred size of water ice grains in comet Hartley 2 [14] and comet Tempel 1 [15]. While more measurements are needed to obtain statistical information, the finding provides most direct evidence yet that supports the earlier speculation that voids in CP IDPs were initially filled with ices during their residence in the parent comet [12]. Our latest analysis indicates that submicron icy grains or ices initially filled small voids most likely played a key role in preserving the original structures of dust aggregates during accretional collisions and residence in the parent comet. The presence and preservation of the fragile, porous aggregate of submicron grains (or clusters of nanoscale grains) frequently with little grain-to-grain contact in 3-D space may well reflect the high sticking efficiency of icy grains during accretional collisions in the outer protoplanetary disk. 3-D numerical simulations of collisions between 0.1-μm-

radius icy clusters have shown that icy aggregates with high sticking thresholds did not experience catastrophic disruption at high relative velocities up to 50 m s^{-1} (that is comparable to the maximum collision velocity expected in protoplanetary disks) [16], which is consistent with laboratory experiments that show a much higher sticking threshold for ice grains at low temperatures than that of silica grains [17]. The PCXNT study reveals never-before-seen 3-D ~ 10 nm details of the structure and morphology of a primitive fine-grained IDP, giving us a glimpse into how small grains coagulate in the outer protoplanetary disk and complementing simulations of dust accretion processes and astronomical observations of protoplanetary disks including the water-snow line [18].

References: [1] Brownlee D. E. (1985) *Annu. Rev. Earth Planet. Sci.*, 13, 147-173. [2] Ishii H. A. et al. (2008) *Science* 319, 447-450. [3] Brownlee D. E (2016) *Elements* 12, 165-170. [4] Flynn G. J. et al. (2016) *Elements* 12, 177-183. [5] Taylor S. et al. Elements 12, 171-176. [6] Sandford S. A. et al. *Elements* 12, 185-189. [7] Messanger S. *Nature* 404, 968-971. [8] Hu Z. W. and Winarski R. P. (2016) *Meteoritics & Planet. Sci.,* 51, 1632-1642. [9] Weidenschilling S. J. and Cuzzi J. N. 1993. In *Protostars and Planets* III, 1031-1060. [10] Dominik C. et al. 2007. In *Protostars and Planets* V, 783-800. [11] Bentley M. S. et al. 2016 *Nature* 537, 73-76. [12] Bradley J. P. and Brownlee D. E. 1986. *Science* 231, 1542-1544. [13] Brownlee D. E. et al. 1995. 26th LPSC, p. 183. [14] A'Hearn M. F. et al. 2011. *Science* 332, 1396-1400. [15] Sunshine J. M. et al. 2007. *Icarus* 190, 284-294. [16] Wada K. et al. (2009) ApJ 702, 1490-1501. [17] Gundlach B. and Blum J. 2015. ApJ 798: 34(12pp). [18] Cieza L. A. et al. (2016) Nature 535, 258-261.

Acknowledgements: ZWH would like to thank M. E. Zolensky and the JSC cosmic dust curatorial staff for providing IDPs for this research. Use of the APS and CNM was supported by DOE, Office of Science, Office of Basic Energy Sciences, under Contract No DE-AC02-06CH11357. This work was supported by NASA grant NNX12AP38G.

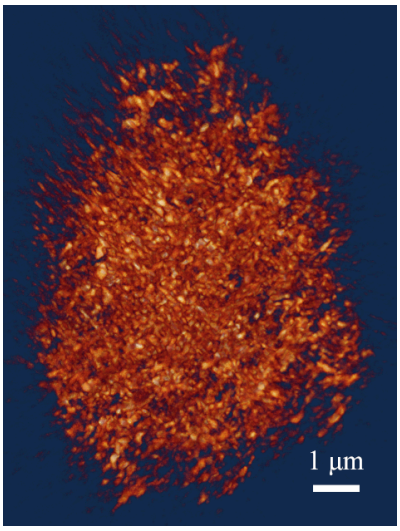

Fig. 1. 3-D rendered image of an entire CP IDP (U2015-M-1) with phase contrast X-ray nano-tomography.

CONSTRAINING THE PRE-IMPACT ORBITS OF SOLAR SYSTEM GIANT IMPACTORS

A.P. Jackson[1,2], T.S.J. Gabriel[2], E. Asphaug[2]. [1]Centre for Planetary Sciences, University of Toronto, Toronto, ON, Canada, [2]School of Earth and Space Exploration, Arizona State University, Tempe, AZ, USA.
Email: ajackson@cita.utoronto.ca

Introduction: Giant impacts are the final stage in the formation of terrestrial planets. In our own Solar system giant impacts have been proposed to explain features including the formation of the Moon [1], the Martian Borealis basin [2], the large core fraction of Mercury [3], and the formation of the Pluto-Charon system [4]. The ability to trace the origins of the impactors in these events greatly benefits our understanding of Solar system formation. For the Moon in particular there are concerns about matching the isotopic similarity with Earth. Meteorites display a diversity of isotopic signatures, which are widely believed to be the result of chemical gradients and inhomogeneities in the Solar nebula [5]. While there is evidence of a decrease in isotopic diversity for larger bodies [6] it is still expected that giant impactors and their targets will have different isotopic signatures [7]. Outlining the origin of giant impactors can thus provide testable geochemical constraints.

Relating impactor and target orbits: Our key to relating the impactor's orbit to that of the target is the relative velocity of the collision. Jackson et al. [8] presented a set of equations for the orbital change of a body after a velocity kick; we use these here with the 'kick' being the relative velocity. We assume the target orbit is similar to that of the final body, which is a good approximation in most cases since the target dominates the momentum budget. We can then take the relative velocity from giant impact models and predict the range of orbits allowed for the impactors.

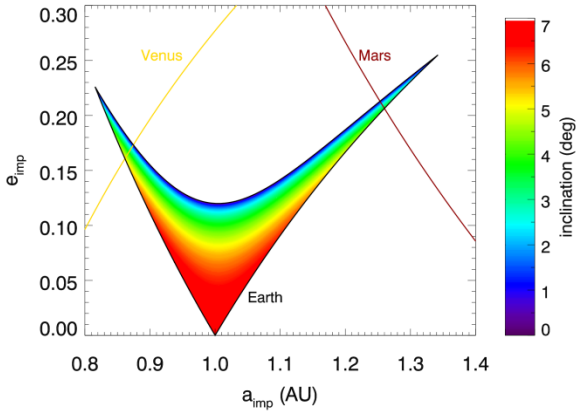

Figure 1: Allowed pre-impact orbits of Theia in the Canonical Moon formation scenario. Above the yellow and dark red lines orbits are Venus and Mars crossing respectively.

This is much faster than N-body approaches (e.g. [9]), albeit less nuanced, allowing us to rapidly explore large parameter spaces. Specific regions of pre-impact orbital parameters can then be identified for detailed follow-up.

Canonical Moon formation: The Canonical scenario for the formation of the Moon is a very low relative velocity impact [1]. The impactor, Theia, hits the proto-Earth at ~1.05v_{esc}, low compared with the 1v_{esc} of a pure free-fall impact, where v_{esc} is the mutual escape velocity of the colliding pair. In this scenario the pre-impact orbit of Theia must have been close to Earth, as also suggested by [9]. Few of our computed orbits lie in the Venus and Mars crossing regions. If there is a gradient in isotopic composition with distance from the Sun, we would expect the compositional difference between Earth and Theia to be smallest in this scenario. The model proposed by [10] of an impact between two nearly equal mass bodies uses a very similar impact velocity to the Canonical model, so the resulting range of allowed impactor orbits is very similar.

Reufer et al. Moon formation: An alternative scenario was proposed by [11] with a 'hit-and-run' type impact in which a substantial portion of Theia continues downrange after the impact and is not incorporated into the Earth-Moon system. This scenario uses a slightly higher impact velocity of 1.2v_{esc}. In comparison with the Canonical scenario the allowed range of orbital parameters is increased substantially. A significant proportion of the parameter space is now in regions that cross the orbits of Venus or Mars, and there is a tail that spans the main asteroid belt.

Ćuk & Stewart Moon formation: A very different Moon-forming scenario is proposed by [12], with a small Theia striking at high speed, ~2-2.5 v_{esc}. This allows a much broader range of impactor orbits, shown for 2.5v_{esc} in Figure 2. Scattering with terrestrial planets cannot easily produce such high relative velocities so we can further constrain the orbit to lie in the Jupiter crossing region above the magenta line. This is further emphasized by the high inclinations that dominate the non-Jupiter crossing region. In this scenario Theia must have been an outer Solar system object that would differ substantially from Earth in composition, likely being volatile-rich. Scattering with Jupiter is much more likely to result in

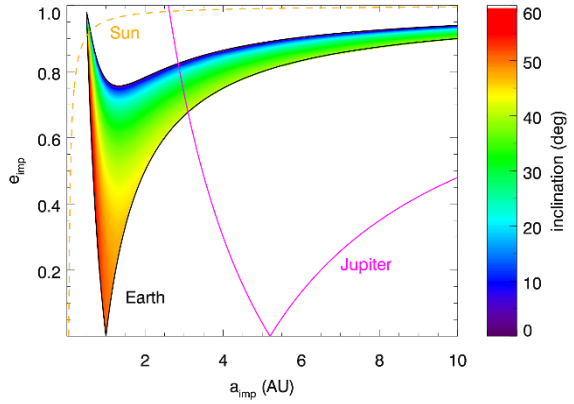

Figure 2: Allowed pre-impact orbits of Theia in the scenario of [12] for impact velocity of $2.5v_{esc}$. Above the gold and magenta lines orbits are Sun-grazing and Jupiter crossing respectively.

prompt ejection from the solar system than placement onto a collision trajectory with a terrestrial planet [13]. The dynamical pathway requiring scattering with a giant planet is thus intrinsically much less likely than the lower velocity scenarios.

Borealis basin impact: The northern hemisphere of Mars is dominated by the massive Borealis basin. In a scenario proposed by [2] this basin was formed by the impact of a roughly 2000 km body with Mars. Like the Canonical Moon formation scenario this is a low velocity impact at around $1.1v_{esc}$. As such we find that the impactor must have originated near Mars from within the range 1.2-2.2 AU. The parameter space of impactor orbits overlaps only minimally with the other terrestrial planets (Earth), but origins in the asteroid belt are readily allowed due its proximity to Mars.

Mercury formation: One method of achieving the very high present-day core-mantle ratio of Mercury is to begin with a body that has a core-mantle ratio similar to that of the other terrestrial planets and then remove a large fraction of the mantle through a giant impact. This is achieved in the scenario proposed by [3] in which a proto-Mercury 2.25 times its present mass is hit at high speed (~30 km/s) by an impactor 1/6 of its mass. As with the Moon-formation scenario of [12] this results in a very broad distribution of possible impactor orbits, but the most plausible way of achieving such a high velocity is scattering with one of the giant planets.

[14] propose instead removing the mantle of proto-Mercury through one or more hit-and-run impacts with Venus or Earth (such that proto-Mercury is the impactor in this case). For a single hit-and-run impact the required impact velocity is very similar to [12] at around 30 km/s. As such, as with [12], the impactor would then have likely been an outer solar system object for both single impact scenarios.

Alternatively, [14] suggest that 2-3 hit-and-run impacts at lower impact velocities of ~$1.5v_{esc}$ would be able to remove sufficient mantle material. This lower impact velocity trajectory can be achieved with scattering by the terrestrial planets, and individual such impacts are common [e.g. 15]. Thus we argue the multiple hit-and-run pathway for the formation of Mercury should be preferred.

Conclusions and implications: We provide a fast method for computing constraints on impactor pre-impact orbits, applying this to the late giant impacts in the Solar System. These constraints can be used to make quick, broad comparisons of different collision scenarios, identifying some immediately as low-probability events and narrowing the parameter space in which to target follow-up studies with expensive N-body simulations. We suggest that high-velocity impact scenarios in the inner Solar System, including all currently proposed single impact scenarios for the formation of Mercury, should be disfavoured. This leaves a multiple hit-and-run scenario as the most probable currently proposed for the formation of Mercury. We benchmark our parameter space predictions, finding good agreement with existing N-body studies for the Moon [9], and recommend that examinations of the origin of the impactor proposed for the Borealis basin on Mars should focus on the range from 1.2-2.2 AU.

Acknowledgements: The authors gratefully acknowledge support for from NASA through grant NNX16AI31G (Stop hitting yourself).

References:

[1] Canup R.M. (2004), *Annu. Rev. Astro. Astrophys.*, 42, 441
[2] Marinova M.M., et al. (2008), *Nature*, 453, 1216
[3] Benz W., et al. (2007) *Space Sci. Rev.*, 132, 189
[4] Canup R.M. (2011) *Astron. J.*, 141, 35
[5] Clayton R.N. (2003) *Space Sci. Rev.*, 106, 19
[6] Ozima M., et al. (2007) *Icarus*, 186, 562
[7] Kaib N.A, Cowan N.B (2015) *Icarus*, 252, 161
[8] Jackson A.P., et al. (2014) *MNRAS*, 440, 3757
[9] Quarles B.L., Lissauer J.J. (2015) *Icarus*, 248, 318
[10] Canup R.M. (2012) *Science*, 338, 1052
[11] Reufer A., et al. (2012) *Icarus*, 221, 296
[12] Ćuk M., Stewart S.T., 2012, Sci., 338, 1047
[13] Wyatt, et al. (2017), *MNRAS*, 464, 3385
[14] Asphaug E., Reufer A. (2014) *Nat. Geo.*, 7, 564
[15] Chambers J.E., (2013), *Icarus*, 224, 43

IMPACT GENERATION OF HOLES IN THE EARLY LUNAR CRUST A.P. Jackson[1,2], V. Perera[2], L.T. Elkins-Tanton[2], E. Asphaug[2]. [1]Centre for Planetary Sciences, University of Toronto, Toronto, ON, Canada, [2]School of Earth and Space Exploration, Arizona State University, Tempe, AZ, USA.
Email: ajackson@cita.utoronto.ca

Introduction: Magma oceans were common in the early solar system, whether produced by accretion energy [1,2], metal-silicate differentiation [3] or radiogenic heating [4,5]. As the number of small bodies, and so the frequency of impacts, was much higher than today, impacts onto bodies hosting a magma ocean would also have been common, but this has not been well studied previously.

How these impacts interact with the target body and influence its evolution depend on the nature of the target. A magma ocean with a free surface presents a very different scenario to one with an overlying lid. On large planets like Earth magma oceans freeze from a septum in the mantle outwards, maintaining a molten free surface until the magma ocean has fully solidified. On smaller planets like the Moon, and possibly Mercury, buoyant phases that rise to the surface can form a flotation crust [6]. Asteroids that undergo internal melting due to radiogenic heating may maintain a primitive crust that is never melted [7].

Magma oceans on the terrestrial planets formed as a result of giant impacts will be subject to especially intense bombardment since the giant impact will release large quantities of debris onto heliocentric orbits (~1.3 lunar masses for the, rather gentle, Canonical moon forming scenario [8]). This debris will have high probabilities for re-impacting the originating body. Such returning material will also have lower typical impact velocities than impactors originating from elsewhere in the solar system. This sets the stage for an immediate cataclysmic epoch that has been little studied, and that has important, testable, thermal and collisional consequences for the Moon and planets. Crusts as thin as a few tens of metres can serve as an insulating blanket over a cooling magma ocean. Re-impacting debris can therefore substantially influence the thermal evolution of the body by disrupting this blanket. In particular, we focus on the magma ocean that existed on the early Moon.

Methods: We use the well-established iSALE shock physics code [9,10,11] to simulate impacts into the flotation crust over the lunar magma ocean. We examine a range of impactor sizes, impact velocities and crustal thicknesses. Impacts by objects 10 km and smaller are simulated in a half-space setup, while those larger than 30 km use a 2D spherical setup. Impacts by objects between 10 and 30 km are simulated in both geometries to ensure continuity between regimes. Our Moon is constructed with a dunite mantle and a granite crust using the ANEOS equation of state [12]. These material choices satisfy our two primary criteria; the solid crust is less dense than the liquid mantle, and the crust has a higher melting temperature than the mantle. The depth of the liquid magma layer is determined by the crossing point of the mantle adiabat and melting temperature-pressure curve. This depth is matched to that in [13] for the appropriate crustal thickness by adjusting the temperature at the base of the crust.

Results: In fig. 1 we show an example of the state of the crust at the end of one of our simulations, here for a 10 km impactor at 5 km/s into crust 10 km deep (corresponding to a magma ocean depth of 90 km). There are two particular features of interest:

1) The central hot hole in which the crust has been substantially thinned and strongly raised in temperature, bringing the heat of the magma ocean in direct contact with the surface.
2) The extensive fracture zone throughout which the crust is heavily damaged.

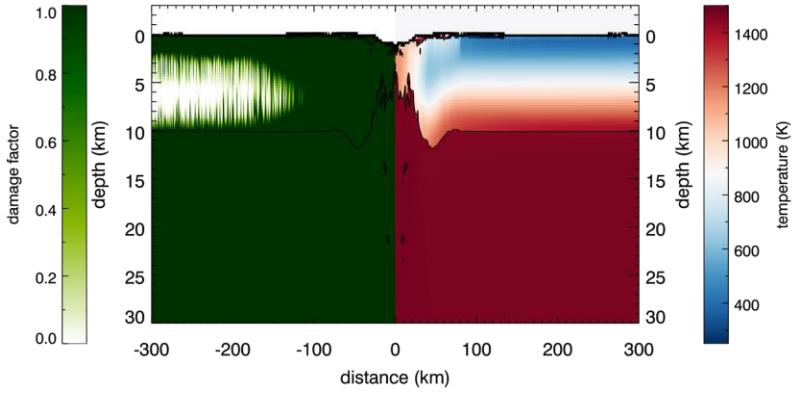

Figure 1: iSALE simulation of 10 km object impacting 10 km thick crust at 5 km/s, snapshot at 3500s. At this time the simulation volume is well settled into a post-impact equilibrium. The liquid magma ocean is 90 km deep. *Left-hand pane*: damage factor (liquid magma is strengthless and so completely damaged). *Right-hand pane:* temperature. Black contours indicate boundary between crust and mantle materials. The vertical scale is exaggerated. Thermal profiles in the punctured crust are plotted in figure 2.

Damage reaches unity once the tensile stress in the material exceeds a scalar threshold (we use the implementation of [14] for material damage). Previous studies of lithosphere rupture [15] show that damage can extend to several crater radii. Here the 10 km impactor results in significant damage to surface material over 100 km from the impact site in response to shock and large-scale flexure.

Fig. 2 shows the mean temperature between the surface and 10km depth against radial distance from the centre of the impact site. We define the hole as the region within which the mean temperature in the upper 10 km has been raised by at least 10%, however as shown taking a different threshold of 5% makes little difference. Here the hole is 29 km in radius. We can construct an estimate of the work required to excavate the hole as $\pi\rho g r_{\mathrm{hole}}^2 d_{\mathrm{cr}}^2$, where r_{hole} is the hole radius, d_{cr} is the crust thickness, ρ is the density and g is the acceleration due to gravity, and find a strong correlation with the impact kinetic energy, as shown in fig. 3. This allows us to estimate the efficiency with which impact energy is transformed into hole opening as 1-10%.

Implications: The combined effects of the creation of thermal holes and extensive fracturing of the crust have important consequences for the evolution of the lunar magma ocean and crust. The presence of hot holes will decrease the cooling time of the magma ocean by allowing more rapid escape of heat. The extensive fracturing will weaken the crust to subsequent impacts and may indicate that the lunar crust has always had a substantial mega-regolith component. Quench crust (the initial thin, rapidly cooled layer analogous to the surface of terrestrial lava lakes) formed in the holes could pollute the anorthosite of the lunar crust, while gradual closure of the holes through rising of new anorthosite from beneath could lead to variations in crust thickness. Re-impacting giant impact debris could also re-dilute the composition of the magma ocean towards its initial value.

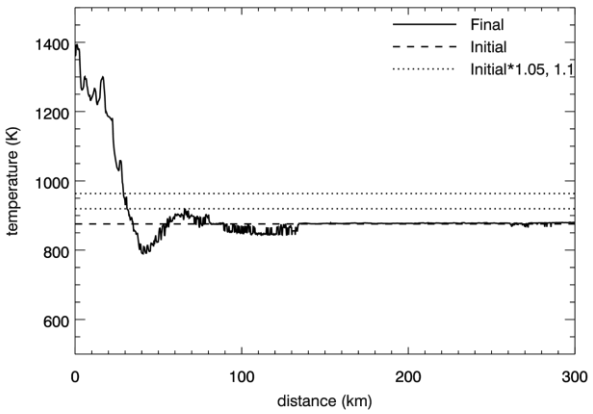

Figure 2: Mean temperature between 0 and 10 km depth at 3500s after impact (solid) and initially (dashed). Also shown are 5 and 10% thresholds above the initial value, used to define the hole boundary.

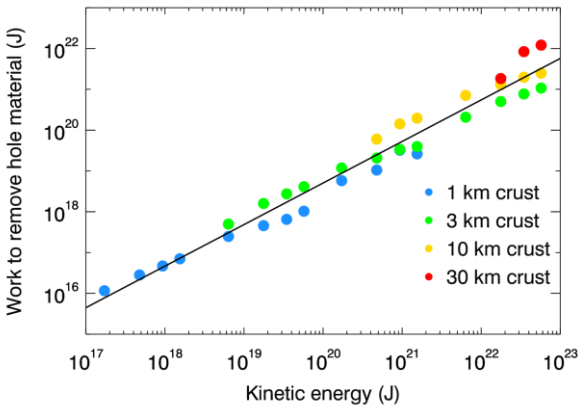

Figure 3: Work done to excavate the hole (J) against the impact kinetic energy (J). The colour of the points indicates the thickness of crust impacted. The black line represents the best fit, $y=10^{A}x^{B}$, where A=-1.66±0.70, and B=1.018±0.034.

Acknowledgements: The authors gratefully acknowledge support for this project through NASA grant NNX16AI31G (Stop hitting yourself). This work has made use of the iSALE shock physics code (Dellen release) [4,5,6] and we gratefully acknowledge the developers, including G. Collins, K. Wunnemann, D. Elbeshausen, B. Ivanov & H.J. Melosh.

References:

[1] Wetherill, G.W. (1980) *AREPS*, 18, 77
[2] Tonks, W.B., Melosh, H.J. (1993) *JGR*, 98, 5319
[3] Monteaux, J., Ricard, Y., Coltice, N., Dubuffet, F., Ulrova, M. (2009) *Earth Planet. Sci. Lett.*, 287, 353
[4] Miyamoto, M., Fujii, N., Takeda, H. (1981), *Proc. Lunar Planet. Sci. Conf.*, 12, 1145
[5] Merk, R., Breuer, D., Spohn, T. (2002) *Icarus*, 159, 183
[6] Elkins-Tanton, L.T. (2012) *AREPS*, 40, 113-139
[7] Elkins-Tanton, L.T., Weiss, B.P., Zuber, M.T. (2011) *Earth Planet. Sci. Lett.*, 305, 1
[8] Jackson, A.P., Wyatt, M.C, (2012) *MNRAS*, 425, 657
[9] Amsden, A., Ruppel, H., Hirt, C. (1980) *Los Alamos Nat. Lab. Rep.*, LA-8095:101p
[10] Collins, G.S., Melosh, H.J., Ivanov, B.A., *Meteoritics Planet Sci.*, 39, 217
[11] Wunnemann, K., Collins, G., Melosh, H. (2006) *Icarus*, 180, 514
[12] Melosh, H.J. (2007) *Meteoritics Planet. Sci.*, 42, 2079
[13] Elkins-Tanton, L.T. (2011) *Earth Planet. Sci. Lett.*, 304, 326
[14] Ivanov, B.A., Deniem, D., Neukum, G. (1997) *Int. J. Impact Eng.*, 20, 411
[15] Turtle, E.P., Pierazzo, E. (2001), *Science*, 294, 1326

CLUSTERING OF INNER SOLAR SYSTEM OXYGEN ISOTOPIC COMPOSITIONS: A RESULT OF GAP FORMATION IN THE PROTOPLANETARY DISK? L. P. Keller[1], C. Snead[2], and K. D. McKeegan[2], [1]ARES, Code XI3, NASA/JSC, Houston, TX 77058 (Lindsay.P.Keller@nasa.gov). [2]Dept. of Earth, Planetary, and Space Sciences, UCLA, Los Angeles, CA 90095.

Introduction: In plots of $\delta^{18}O$ versus $\delta^{17}O$, the oxygen isotopic compositions of the vast majority of meteoritic materials plot along a slope ~1 line which reflects mixing between two major O reservoirs, one that is ^{16}O-rich and the other that is ^{16}O-poor. Measurement of implanted solar wind oxygen returned by the Genesis mission [1] anchors the three-isotope diagram at $\delta^{18}O$, $\delta^{17}O$ ~(-60‰,-60‰, "solar"). Canonical self-shielding models predict the development of ^{16}O-poor water-rich reservoir from gas that was initially ^{16}O-rich. Primitive materials from water-rich bodies that interacted with a ^{16}O-poor reservoir either through oxidation or hydration should show evidence of mixing along the slope 1 line beyond (above) the terrestrial fractionation line (TFL). Indeed, several examples exist including cosmic symplectites (COS) and matrix analyses from Acfer 094 [2-3], the magnetite compositions reported from unequilibrated ordinary chondrites [4] and from interplanetary dust particles, cosmic spherules, and Stardust samples [5-12] with $\Delta^{17}O$ from 5‰ to ~120‰ (Figure 1). The oxygen isotopic compositions of these materials are direct evidence for the existence of a heavy, ^{16}O-poor reservoir in the outer solar system that developed via self-shielding. The compositions of most meteoritic materials however, plot between solar and ($\delta^{18}O$, $\delta^{17}O$; 0‰,0‰, "planetary"), with the Earth, Moon, Mars, and meteorites all having similar bulk oxygen isotopic compositions that are enriched in $\delta^{18}O$ and $\delta^{17}O$ relative to the Sun.

The intriguing aspect of the three isotope diagram is the concentration of compositions around and generally below the intersection of the slope 1 line and the TFL. Here, a model for the distribution of O isotope compositions in meteoritic materials is proposed, based on self-shielding [e.g. 13], but allowing for disk processes to control the mixing between reservoirs. In this model, the formation of proto-Jupiter opened a gap in the protoplanetary disk that prevented further mixing between ^{16}O-rich dust and a ^{16}O-poor ices. The lack of further mixing resulted in the concentration of O isotopic compositions of most inner solar system materials around planetary.

Results and Discussion: The initial assumption here is that the pre-molecular cloud dust and gas shared the same ^{16}O-rich composition, given that grain processing in the interstellar medium is believed to have resulted in efficient chemical and isotopic homogenization [14]. Thermal processing of this dust likely began during the collapse phase of the protosolar core and continued through the time the Sun was a Class I-III protostar until the transition to a debris disk. Refractory inclusions are among the earliest formed solids and are ^{16}O-rich, with the majority forming within ~0.2 My after T_0 (defined as 4567.3 My [15]). The major epoch of chondrule formation was largely complete by ~4 My, with the majority of chondrules forming ~2-3 My after T_0 [15] and have $\delta^{18}O$, $\delta^{17}O$ clustering close to planetary ($\Delta^{17}O$ of ~-5 to 0 ‰, [16]). Others have suggested that this distribution reflects mixing between "primordial" ^{16}O-poor dust and ^{16}O-rich gas [17], whereas we interpret the trend as an exchange between ^{16}O-rich inner solar system materials with a heavy ^{16}O-poor reservoir that was situated in the outer solar system [e.g. 18]. Inner solar system bodies are water-poor, while the outer solar system bodies are water-rich, suggesting that the water-condensation line in the disk (i.e. the snowline) separated these two distinct regions of the protoplanetary disk [19].

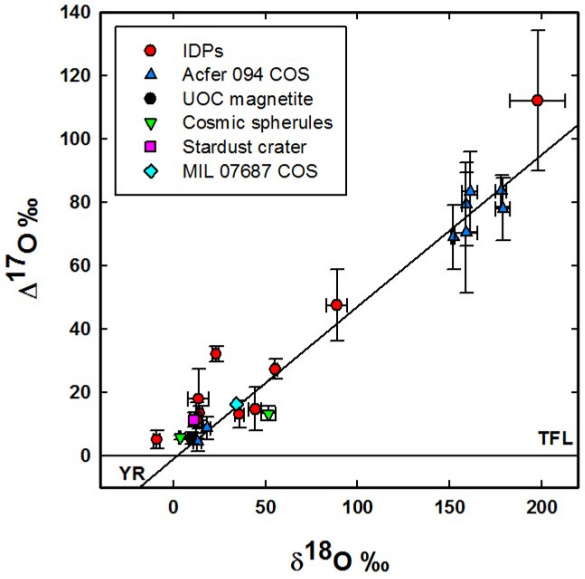

Figure 1. A plot of O isotopic compositions for meteoritic materials with $\Delta^{17}O$ >5‰. Data from [2-12].

While stellar accretion was active, ^{16}O-poor ices were brought into the inner solar system through mass transfer along the disk midplane as the proto-Sun was actively accreting disk material. These ices interacted with ^{16}O-rich materials producing intermediate O isotopic compositions along the slope 1 trend observed in the 3 isotope plot [18, 20]. However, the mixing be-

tween these two reservoirs effectively stopped at some point, and inner solar system bodies accreted (the terrestrial planets and main belt asteroids) within ~5 My of T_0 [21]. A possible mechanism for the disruption of the mixing between the ^{16}O-poor outer solar system volatile reservoir and inner solar system refractory materials was the formation of a gas giant planet (e.g. Jupiter). Once proto-Jupiter grew to a sufficient size (~20 Earth masses, [19]), it opened a gap in the protoplanetary disk. Dust and gas densities drop by orders of magnitude at gaps - a pressure maximum occurs at the outer edge of the gap that inhibits inward particle migration. The presence of this gap and its effects on particle movement in the disk prevented any further substantial transfer of outer solar system ices and silicates into the inner solar system [19]. Modeling efforts have constrained the time when Jupiter achieved sufficient mass to open a gap in the disk to ~3 My after T_0 [19], and that is consistent the the ages of the youngest (dated) nebular solids (chondrules).

In such a scenario, if Jupiter had not formed and opened a gap, the inner solar system would be more water-rich than at present, and the O isotopic compositions of solids would have continued to evolve beyond planetary up the slope 1 line. Dust models suggest that some fine-grained (<150 μm) particles can transit the gap as long as they are strongly coupled to the gas [22-23], however, these tiny particles are inefficiently captured by planetesimals and are rapidly swept up by the proto-Sun. It is noteworthy that the materials in Figure 1 that have Δ^{17}O >5‰ are all fine-grained (<50 μm) and are associated with mineralogically and chemically primitive bodies. These materials likely represent particulate samples of outer solar system bodies that successfully transited the gap opened by Jupiter.

Consequences: In our scenario, the carbonaceous chondrites formed in the inner solar system (~<5 AU), contrary to dynamical models that suggest that the C-complex asteroids (the presumed sources of the carbonaceous chondrites) formed well beyond Jupiter's orbit and were implanted later into the outer asteroid belt [e.g. 24]. Many of the carbonaceous chondrites are hydrated, and short-lived nuclides suggest their hydration occurred early in their history. If the carbonaceous chondrites accreted beyond Jupiter, they would have also accreted outer solar system ices that were ^{16}O-poor. Upon melting, the ^{16}O-poor water would have reacted with the anhydrous minerals, resulting in bulk O isotopic compositions that would not plot in the same region as other chondrites. More recent dynamical models [25] suggest that planetesimals from the Jupiter-formation zone could have been implanted in the outer main belt via interactions with scattered Jupiter-zone protoplanets, and this scenario would be consistent with our model.

Samples from outer solar system bodies should be among the best repositories of material to test our scenario, yet nearly all of the cometary solids that have been analyzed in the laboratory to date are dominated by anhydrous materials with inner solar system origins, many of which formed at high temperatures [e.g. 26-29]. The known materials from primitive, hydrated bodies that interacted with a ^{16}O-poor reservoir either through oxidation or hydration [2-12] are uncommon and fine-grained. This observation may be an indication that water:rock interactions in the outer solar system were limited. Alternatively, only fine-grained outer solar system materials were able to transit the gap and end up as xenoliths in accreting, primitive, inner solar system bodies.

References: [1] McKeegan, K. D. *et al.* (2011) *Science*, 332, 1528. [2] Sakamoto, N. *et al.* (2007) *Science*, 317, 231. [3] Nittler, L. *et al.* (2015) *LPSC* 46, #2097. [4] Choi, B-G. *et al.* (1998) *Nature*, 392, 577. [5] Starkey, N. A. *et al.* (2014) *GCA*, 142, 115. [6] Snead, C. J. *et al.* (2016) *LPSC* 47, #2850. [7] McKeegan, K. D. (1987) PhD Thesis, Wash. Univ. [8] Yada, T. *et al.* (2005) *GCA* 69, 5789. [9] Rudraswami, N. G. *et al.* (2016) *GCA* 194, 1. [10] Keller, L. P. *et al.* (2016) *MAPS*, #2525. [11] Snead, C. J. & McKeegan, K. D. (2015) *MAPS*, #5253. [12] Snead, C. *et al.* (2017) *LPSC* 48, #2623. [13] Clayton, R. N. (2002) *Nature*, 415, 860. [14] Zhukovska S. *et al.* (2008) *AA*, 479, 453. [15] Connelly, J. N. *et al.* (2012) *Science*, 338, 651. [16] Kita, N. *et al.* (2016) *MAPS*, #6378. [17] Krot, A. N. *et al.* (2010) *ApJ*, 713, 1159. [18] Young, E. D. (2007) *EPSL*, 262, 468. [19] Morbidelli, A. *et al.* (2015) *Icarus* 267, 368. [20] Ciesla, F. & Cuzzi, J. (2006) *Icarus* 181, 178. [21] Johansen, A. *et al.* (2015) *Sci. Adv.* 1:e1500109. [22] Paardekooper, S-J & Mellema, G. (2006) *AA* 453, 1159. [23] Zhu, Z. *et al* (2012) *ApJ* 755, 6. [24] Walsh, K. *et al.* (2011) *Nature* 475, 206. [25] Kretke, K. *et al.* (2016) *DPS* #48, id.518.03. [26] Brownlee, D. E. (2014) *AREPS* 42, 197. [27] Keller, L. P. and Messenger, S. (2005) *ASP Conf. Series*, 341, 657. [28] Keller, L. P. and Messenger, S. (2011) *GCA*, 75, 5336. [29] McKeegan, K. D. *et al.* (2006) *Science* 314, 1724.

How Does Accretion Influence Planetary Differentiation?: Feed Forward from the Accretion Conference to the Differentiation Conference

Walter S. Kiefer[1], Julie C. Castillo-Rogez[2], Nancy L. Chabot[3], Stephen M. Elardo[4], Cyrena A. Goodrich[1], and Kevin Righter[5], [1]Lunar and Planetary Institute, 3600 Bay Area Blvd., Houston TX 77058, kiefer@lpi.usra.edu, [2]Jet Propulsion Laboratory, California Institute of Technology, 4800 Oak Grove Drive, Pasadena CA 91109, [3]Johns Hopkins Applied Physics Laboratory, Laurel MD, [4]Geophysical Laboratory, Carnegie Institution of Washington, 5251 Broad Branch Road NW, Washington DC 20015, [5]NASA/Johnson Space Center, Mail Code XI2, 2101 NASA Parkway, Houston TX 77058.

The Lunar and Planetary Institute's *First Billion Years* topical initiative [1] focuses on the major processes that shaped the early history of the Solar System's planetary bodies, including accretion, differentiation, bombardment, and the development of habitable environments. An important aspect of the *First Billion Years* initiative is to understand the interplay between these processes. Because accretion and differentiation at least partially overlapped in time during early Solar System history, the style and rate of accretion must have influenced early planetary differentiation.

The authors of this abstract are members of the Science Organizing Committee for the forthcoming LPI Planetary Differentiation topical conference (planned for spring 2018). The goal of this abstract is to illustrate some of the ways in which accretion sets the stage for planetary differentiation, as well as how the existence of differentiated bodies constrains accretion rates. In addition to the ideas described here, we are interested in the varying perspectives of the participants in the Accretion topical conference about the dominant mechanisms and rates of accretion in various parts of the Solar System. Our objective is to carry a report of the major conclusions (and their associated uncertainties) from the Accretion conference forward as input to the Differentiation conference.

Timescales of Accretion and Differentiation

A broad range of accretion models exist in the literature ([2] provides a recent review). These range from models in which planetesimals gradually accrete to form planetary embryos [3-5] to more recent "pebble accretion" models in which meter-scale planetesimals very rapidly aggregate into planetary embryos [6]. In addition, some models incorporate varying amounts and rates of radial migration of Jupiter and Saturn through the solar nebula (the Nice model [7] and the Grand Tack model [8, 9]). Because small objects cool more rapidly than large objects, and because planetary differentiation requires reaching internal temperatures exceeding 1000 °C, the rate of accretion in the various classes of accretion models may have important implications for the ability of planetesimals and planetary embryos to differentiate. Thus, constraints on how rapidly planetesimals grow from kilometer scale to 100-1000 km scale in the various accretion scenarios and how the growth rate varies with distance from the Sun are important inputs to differentiation modelers.

For small (asteroid-size) objects, the primary energy source for melting and differentiation is radioactive decay of ^{26}Al (half-life 0.73 million years) and ^{60}Fe (half-life 2.6 million years). Melting and differentiation of dry objects requires accretion in less than 2 million years [10]. Thus, the very existence of differentiated silicate bodies such as the eucrite parent body (the asteroid Vesta, radius 263 km) and the angrite and urelite parent bodies [11-13] constrains the rate of accretion for at least some objects. Short lived radiometric chronometers, such as ^{182}Hf-^{182}W (which measures the separation of metal from silicate), also requires rapid accretion. Core formation on the angrite parent body occurred within 2 million years of CAI formation [14] and within 3.3 million years of CAI formation on the urelite parent body [15]. Melting in the parent bodies of five different classes of iron meteorites occurred with 0.6 million years of CAI formation [16]. Rapid accretion may also have been required further from the Sun, as models for the despinning of Saturn's satellite Iapetus have been interpreted as requiring formation within 5 million years of CAI formation [17]. Similarly, results from the Dawn mission indicate that Ceres had to accrete in less than 5 million years [18].

Mixing in the Solar Nebula and the Existence and Preservation of Distinct Chemical Reservoirs

It is generally accepted that the decrease in temperature with distance from the Sun resulted in a chemical composition gradient in the solar nebula, with volatile-depleted materials in the innermost Solar System (similar to enstatite chondrites) and increasingly volatile-rich materials (ordinary chondrites and carbonaceous chondrites) at greater distances. Superimposed on this gradient, a sharp division into inner versus outer Solar System materials [19, 20]

may have been maintained by the early presence of Jupiter [21]. In spite of this initial composition gradient, radial mixing during accretion likely caused all four of the terrestrial planets to incorporate some material from each of these compositional zones [22], partially erasing the original composition gradient. However, numerical modeling does not predict that the resulting planets will all be compositionally identical, and the existence of distinct isotopic compositions (particularly oxygen, chromium, and titanium [9, 19, 23]) in the Earth and various meteorite classes clearly demonstrates that radial mixing in the nebula was incomplete.

One effect of these compositional differences is on core differentiation. There is a gradient in oxygen fugacity (fO_2) between the various nebula chemical reservoirs, ranging from low fO_2 in the enstatite chondrite reservoir toward increasingly higher fO_2 in the ordinary chondrite and carbonaceous chondrite reservoirs [23, 24]. This is important for core size, because at low fO_2 most iron will be in the form of metallic Fe, resulting in larger cores, whereas increasing the fO_2 will result in more Fe as FeO in silicates, resulting in smaller cores and thicker mantles.

Accretion-related chemical composition differences among planets may also influence their long-term volcanic histories. Even subtle differences in composition between the various planets can have substantial effects on the differentiation and long-term volcanic histories. For example, the best models for the chemical compositions of the bulk silicate Earth [25] and Mars [26] indicate differences in the magnesium number and the alkali contents of the two planets (Earth: Mg# 89, Na_2O 0.35 wt. %, K 260 ppm; Mars: Mg# 80, Na_2O 0.50 wt. %, K 305 ppm). These differences are important, because the Mg# and the alkali abundance are the two strongest controls of the silicate solidus in the mantle (lower Mg# and higher Na reduce the solidus) and because ^{40}K is an important radioactive heat source, particularly early in Solar System history. The differences between Earth and Mars result in a lower mantle solidus and greater radioactive heating on Mars and thus in greater crustal production on Mars. With all other factors held constant, just making these small changes in composition can change the long-term crustal production on Mars by 20% [27].

References: [1] www.lpi.usra.edu/first-billion-years/ [2] Morbidelli and Raymond, *J. Geophys. Res.: Planets* 121, 1962-1980, 2016. [3] O'Brien et al., *Icarus* 184, 39-58, 2006. [4] Raymond et al., *Icarus* 203, 644-662, 2009. [5] Bond et al., *Icarus* 205, 321-337, 2010. [6] Levison et al., *Nature* 524, 322-324, 2015. [7] Tsiganis et al., *Nature* 435, 459-461, 2005. [8] Walsh et al., *Nature* 475, 206-209, 2011. [9] Brasser et al., *Earth Planet. Sci. Lett.* 468, 85-93, 2017. [10] Neumann et al., *Earth Planet. Sci. Lett.* 395, 267-280, 2014. [11] McSween et al., *Meteoritics Planet. Sci.* 48, 2090-2104, 2013. [12] Keil, *Chemie der Erde* 72, 191-218, 2012. [13] Wilson et al., *Geochim. Cosmochim. Acta* 72, 6154-6176, 2008. [14] Kleine et al., *Geochim. Cosmochim. Acta* 84, 186-203, 2012. [15] Budde et al., *Earth Planet. Sci. Lett.* 430, 316-325, 2015. [16] Kruijer et al., *Science* 344, 1150-1154, 2014. [17] Castillo-Rogez et al., *Icarus* 190, 179-202, 2007. [18] Castillo-Rogez et al., this conference, 2017. [19] Warren, *Earth Planet. Sci. Lett.* 311, 93-100, 2011. [20] Goodrich, this conference, 2017. [21] Morbidelli et al., *Icarus* 267, 368-376, 2016. [22] Chambers, *Icarus* 152, 205-224, 2001. [23] Mittlefehldt et al., *Rev. Mineralogy Geochem.* 68, 399-428, 2008. [24] Righter, this conference, 2017. [25] Palme and O'Neill, *Treatise on Geochemistry*, vol. 2 (ed. R. W. Carlson), pp. 1-38, 2004. [26] Taylor, *Chemie der Erde* 73, 401-420, 2013. [27] Kiefer et al., *Geochim. Cosmochim. Acta* 162, 247-258, 2015.

OXYGEN ISOTOPE SYSTEMATICS IN CHONDRULES FROM MULTIPLE CHONDRITE GROUPS: IMPLICATION TO THE ISOTOPE RESERVOIRS IN THE PROTOPLANETARY DISK. N. T. Kita[1], T. J. Tenner[2], T. Ushikubo[3], D. Nakashima[4], C. Defouilloy[1], A. T. Hertwig[1], N. Chaumard[1], N. G. Rudraswami[5], M. K. Weisberg[6,7], M. Kimura[8], H. Nagahara[9], and A. Bischoff[10]. [1]WiscSIMS, University of Wisconsin-Madison, Madison, WI 53706. (noriko@geology. wisc.edu). [2]Los Alamos National Laboratory, Los Alamos, NM 87545. [3]Kochi Institute for Core Sample Research, JAMSTEC, Kochi 783-8502, Japan. [4]Tohoku University, Miyagi 980-8578, Japan. [5]National Institute of Oceanography, Dona Paula, Goa 403004, India. [6]Kingsborough College and Graduate Center, CUNY, Brooklyn, NY 11235. [7]American Museum Natural History, New York, NY 10024. [8]National Institute of Polar Research, Tachikawa 190-8518, Japan. [9]ELSI, Tokyo Institute of Technology, Tokyo 152-8550, Japan, [10]Institut für Planetologie, WWU Münster, 48149 Münster, Germany.

Introduction: The Solar System appears to have started with exteremely heterogeneous ^{16}O abundances represented by the Sun ($\delta^{17}O$, $\delta^{18}O$: –60‰ [1]), Ca,Al-rich inclusions (CAIs; –50‰ [2]) and cosmic symplectites (COS; +200‰ [3]). Chondrules in primitive chondrites show a smaller and intermediate range of $\delta^{17,18}O$, from –15‰ to +5‰ [e.g., 4]. According to ^{26}Al-^{26}Mg chronology, most chondrules formed 2-3 Myr after CAIs [5] in a dust-rich environment [6]. It is suggested that chondrule formation occurred in an open system with respect to oxygen by evaporation and re-condensation processes [7] and oxygen in the ambient gas during chondrule formation would have been dominated by that from solid precursors [8-9]. If true, the O-isotope ratios of chondrules may reflect temporal and/or spatial varieties of such reservoirs in the protoplanetary disk.

We have conducted O 3-isotope analyses of ~600 chondrules from multiple chondrite groups (O, R, EH, CO, CV, CM, CR, CH, ungrouped C) using a secondary ion mass spectrometer (WiscSIMS) at sub-‰ precision [8-24]. For most chondrules, multiple spot analyses (n=4-10; 10-15 µm in diameter) were performed to test internal homogeneity of O-isotopes.

O-Isotope Homogeneity: Most chondrules have internally homogeneous O-isotopes within analytical uncertainty [25]. In Acfer 094 (ungrouped C3.00; the least metamorphosed chondrite), multiple mineral phases and glass show indistinguishable O-isotope ratios on a per-chondrule basis (Fig. 1, [9]). The exception is a minor occurrence of relict olivine grains with distinct O-isotope ratios, which likely remained solid during the final chondrule melting event [9-10]. Excluding relict olivine data, host O-isotope ratios of the final chondrule melt are calculated from the mean of multiple analyses in each chondrule (Fig. 1). The variability of host O-isotope ratios among chondrules is commonly reported as $\Delta^{17}O$ (= $\delta^{17}O$ –0.52×$\delta^{18}O$), which is the $\delta^{17}O$ deviation from the terrestrial fractionation line (TFL; Fig. 1).

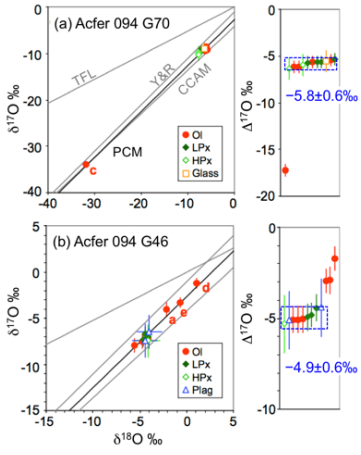

Fig. 1. O-isotope ratios of chondrules in Acfer 094 [11]. Homo-geneous data (dashed box) represent those of final melt. Three slope ~1 reference lines (CCAM, Y&R, and PCM) are shown [1,9,26].

General Trend in the O 3-Isotope Diagram: Chondrules show two distinct trends in O 3-isotope space (Fig. 2). Chondrule data from carbonaceous (C) chondrites plot mainly on the slope ~1.0 primitive chondrule mineral (PCM) line [9], which passes through data from the terrestrial mantle, CAIs and COS. Therefore, the PCM line may represent primary mass independent fractionation of O-isotopes in the protoplanetary disk. Chondrule data from ordinary (O) and Rumuruti (R) chondrites plot above the TF and PCM lines with a slope of ~0.5, suggesting they experienced mass-dependent isotope fractionation effects [8, 17-18]. Chondrule data from enstatite (E) chondrites show similar trends to chondrules from O and R chondrite [14]. However, a few chondrules from O, R, and E chondrites also plot below the TF line and on the PCM line, similar to those of C chondrite chondrules.

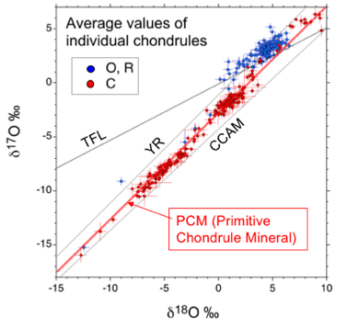

Fig. 2. O-isotope ratios of individual chondrules in O, R, CO, CV, CR, CH, Acfer 094, and Y-82094 ungrouped C chondrites [8-13, 17-19].

Mg#-$\Delta^{17}O$ Relationship: FeO contents of chondrule olivine and pyroxene, expressed as Mg# ([MgO]/

[FeO+MgO] in mol.%), depend on oxygen fugacity during chondrule formation [e.g., 11] and bulk Fe. The Mg# and $\Delta^{17}O$ values show characteristic distributions in each chondrite group (e.g., Fig. 3).

Most chondrules in O and R chondrites show positive $\Delta^{17}O$ values (~1‰) regardless of Mg# (70-100) [8, 17-18]. The $\Delta^{17}O$ values of chondrules in EH and metal-rich ungrouped chondrites (NWA 5492 and GRO 9551) are 0-1‰, similar to O and R, but with very high Mg# (>98) [14-16].

The distribution of $\Delta^{17}O$ values of chondrules in CO and Acfer 094 are bimodal and correlate with Mg#; (1) Mg# ≥98 and $\Delta^{17}O$~ –5‰ and (2) $\Delta^{17}O$~ –2.5‰ with a wide range of Mg# (99-30) [9-10]. In CR chondrites, the $\Delta^{17}O$ values of chondrules show a monotonic increase from –6‰ to 0‰ with decreasing Mg# (Fig. 3b). [11] interpreted this trend as mixing between ^{16}O-rich anhydrous dust ($\Delta^{17}O$: –6‰) and ^{16}O-poor water ice ($\Delta^{17}O$: +5‰) with dust-enrichments of ×100-2500. [27] found a correlation between $\Delta^{17}O$ values and Al-Mg ages of CR chondrules, ranging from 2.5 Ma to >3-4 Ma after CAI.

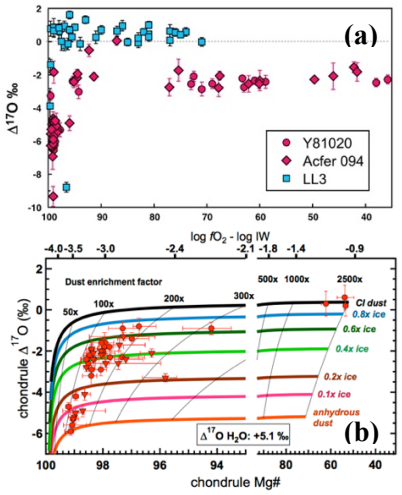

Fig. 3. Mg#- $\Delta^{17}O$ relationships among chondrules (a) CO (Y-81020), Acfer 094 and O (LL3) [10-12]. (b) CR data with O-isotope mixing model [11].

In CV, CM, and Y-82094 (ungrouped), the majority of chondrules are those with highest Mg# (≥98) and $\Delta^{17}O$~ –5‰ [12-13, 20-23]. They also contain chondrules with lower Mg#'s and $\Delta^{17}O$ values of ~ –2.5‰, but are less abundant compared to those in CO and Acfer 094. In addition, a few chondrules in Y-82094, CV, and Acfer 094 with intermediate Mg# (90-85) show $\Delta^{17}O$ ~0‰, which are similar to chondrules in O chondrites [12, 21]. Negative $\varepsilon^{54}Cr$ values are observed for FeO-rich BO chondrules with $\Delta^{17}O$ ~0‰ in Allende (CV3), strongly suggesting the mixing of OC-like isotope reservoirs to CV chondrite forming regions [24].

The majority of chondrules in CH have high Mg# (90-100) with a $\Delta^{17}O$ of –2.2‰ [19], similar to those reported for chondrules in CB by [28]. They also contain less abundant chondrules with highest Mg# (≥98) and lower $\Delta^{17}O$ ~ –6‰, as well as those with lower Mg# (90-60) and higher $\Delta^{17}O$ ~ +1.5‰ [19].

Implication for O Isotope Reservoirs: The Mg# - $\Delta^{17}O$ systematics among chondrules in C chondrites suggest that they formed near the H_2O ice condensation front (snow line) where precursor solids contained anhydrous dust and water ice with distinct $\Delta^{17}O$ values. Anhydrous dusts with $\Delta^{17}O$~ –5‰ would have been widely distributed in the protoplanetary disk near the snow line. In contrast, nearly constant and slightly positive $\Delta^{17}O$ values are observed from a wide range of Mg# among chondrules in O, E, R chondrites. They might have formed at the inner disk regions where O-isotope ratios were significantly homogenized among chondrule precursors, possibly by high temperature heating of the disk that predated chondrule formation.

Each chondrite group shows specific ranges of Mg# and $\Delta^{17}O$ often with multimodal distributions, suggesting each parent asteroid contains multiple populations of chondrules. If they represent chondrules from different regions of the disk, they provide important constraints for radial transport of solids in the disk [29].

References: [1] McKeegan K. D. et al. (2011) Science, 332, 1528-1532. [2] Clayton R. N. et al. (1977) EPSL, 34, 209-224. [3] Sakamoto N. et al. (2007) Science, 317, 231-233. [4] Krot A. N. et al. (2006) Chemie der Erde, 66, 249-276. [5] Kita N. T. and Ushikubo T. (2012) MaPS, 47, 1108-1119. [6] Ebel D. S. and Grossman L. (2000) GCA, 64, 339-366. [7] Nagahara H. et al. (2008) GCA, 72, 1442-1465. [8] Kita N. T. et al. (2010) GCA, 74, 6610-6635. [9] Ushikubo T. et al. (2012) GCA, 90, 242-264. [10] Tenner T. J. et al. (2013) GCA, 102, 226-245. [11] Tenner T. J. et al. (2015) GCA, 148, 228-250. [12] Tenner T. J. et al. (2017) MaPS, 52, 268-294. [13] Rudraswami N. G. et al. (2011) GCA, 75, 7596-7611. [14] Weisberg M. K. et al. (2011) GCA, 75, 6556-6569. [15] Weisberg M. K. et al. (2015) GCA, 167, 269-285. [16] Weisberg M. K. et al. (2010) LPSC 41, #1756. [17] Kita N. T. et al. (2008) LPSC 39, #2059. [18] Kita N. T. et al. (2015) LPSC 46, #2053. [19] Nakashima D. et al. (2010) MaPS, 47, A148. [20] Hertwig A. et al. (2016) MaPS, 51, #6472. [21] Hertwig A. et al. (2017) LPSC 48, #1227. [22] Chaumard N. et al. (2016) MaPS, 51, #6408. [23] Chaumard N. et al. (2017) LPSC 48, #1610. [24] Defouilloy C. et al. (2016) Goldschmidt Conf. #629. [25] Kita N. T. et al. (2016) LPSC 47, #2375. [26] Young E. D. and Russell S. S. (1998) Science, 282, 452-455. [27] Tenner T. J. et al. (2015) MaPS 50, #5325. [28] Krot A. N. et al. (2010) GCA, 74, 2190-2211. [29] Cuzzi J. N. et al. (2010) Icarus, 208, 518-538.

SOME EXAMPLES OF COSMIC BODIES ACCRETION FROM SOLID PARTICLES PRELIMINARY DENSITY SORTED IN ROTATING GAS-DUST CLOUD: SULFUR BEHAVIOR, G. G. Kochemasov, IGEM of the Russian Academy of Sciences, 35 Staromonetny, 119017 Moscow, RF, kochem.36@mail.ru

It is suggested that primary accretion minerals in some meteorites and probably also in the larger bodies of the Solar system are united by nearness of their densities rather than by temperatures of their condensation out of the protoplanet gas (for examples, common association of iron and troilite, association of carbonaceous matter and light Ca-Al rich inclusions in carbonaceous chondrites) [1, 2]. It is shown that the planetary bodies can be composed of mixtures of the main minerals from which, as it is thought judging by composition of meteorites, accumulated the planets and the parent bodies of meteorites [1, 2, 4]. Indeed, the specific gravities of the main minerals vary from >8 to <1 g/cm3: Ni-Fe 7.3-3.2, troilite 4.6-4.8, chromespinels 3.6-5.1, olivine 3.2-4.35, pyroxene 3.2-3.6, spinel 3.55, melilite 2.9-3.1, anorthite 2.76, chlorite 2.6-3.4, serpentine 2.5-2.65, graphite 2.2, carbonaceous matter 1.4, water ice 0.92. The densities of planets vary from 5.5 to <1 g/cm3 and decrease on the whole with their heliocentric distances (in brackets densities without pressure); Mercury 5.5 (5.2), Venus 5.2 (4.0), Earth 5.52 (4.0), Moon 3.34 (3.3), Mars 3.9 (3.7), asteroids ~ 3.5, Jupiter 1.4, Saturn 0.71, Uranus 1.32, Neptune 1.63, Pluto. Somewhat increased densities of the three outer planets can be explained by increased loss of volatiles at the periphery of the Solar system. The mean density of the Earth-Moon system is almost equal or even somewhat less (under zero pressure) than the Venus' density.

It is suggested that the main cause of forming in the Solar system of cosmic bodies (planets, moons, asteroids) of various compositions is preliminary mechanical (gravitational and aerodynamical) sorting of solid particles in the protoplanet cloud. A mixture of solid particles formed in the cooling cloud and transported from outside (Supernovae explosion) is sorted by an action of rotating and expanding gas medium source of which is the Sun. As a result of this imperfect sorting the narrow inner part of the cloud (the zone of the terrestrial planets) is enriched with relatively dense minerals and the wide outer part (the zone of giant planets)-with relatively less dense (light) minerals. Similar mechanical mineral differentiation further continues in limits of zones of accretion of individual planets which gradually appear in the cloud. As a result the inner parts of the zones became also enriched with relatively dense minerals. An accretion begins in the inner parts of the zones – thus relatively heavy (dense) planetary cores appear first. Subsequently, the lighter (less dense) material of the adjacent parts of the zones accretes on the cores and so on. Thus primarily layered heterogeneous planets are formed. This mechanism does not require very earlier intensive heating and melting for creating layered structures of cosmic bodies. If the Saturn's ring system could, in a measure, be an example of dust rings around a central body then the Voyager's 1 & 2 and Cassini data do not refute the proposed hypothesis. As follows from the above, the main issue of the hypothesis is in many steps layering of the disk cloud with a production of ring zones, subzones, and the finer divisions of various compositions and particle sizes.

An experimental support of the proposed mechanism of solid particles differentiation in the primordial cloud could be found in a device called "spiral separator". It is constructed for effective obtaining of "heavy fraction" (schlich) from alluvial sands during geological prospecting by sampling stream sediments. By means of descending down and rotating water-sand mixture "schlich" concentrates in the inner part of a chute.

The separation of the inner heavy faction zone in the primordial cloud is not perfect because mineral intergrowths (dense and less dense minerals) and various sizes particles take part in the process. Nevertheless, some examples of the primordial sorting of solid particles can be observed.

First of all, planetary system itself is remarkably not homogeneous. In the inner narrow zone small terrestrial planets formed. They are built of relatively dense silicates and metal iron. The extremely wide outer zone is domain of giant planets mainly built of various not dense ices. Between the inner and outer zones relatively wide Main asteroid belt occurs. It itself is heterogeneous. In its inner zone prevail dense metal rich (M) and stone (S) asteroids. In its wide outer belt prevail less dense carbonaceous asteroids (C).

The innermost planet Mercury has remarkably high sulfur content in its basalts [3]. Along with very massive iron metal core sulfur in form of dense troilite also presents. Gaseous sulfur compounds should be removed further from the Sun. The innermost Galilean satellite Io is relatively dense and remarkably sulfur rich as witness its numerous volcanoes.

The above examples from various systems (Solar system, planets, satellites, asteroids) indicate that sorting mineral particles by density occured before the bodies accretion.

References:

[1]. Kochemasov G.G.(1982) Sorting of dust particles in the protoplanet cloud as the cause of forming primary zoned cosmic bodies of various compositions in the Solar system // 13th LPSC (1982), Abstract 1206.

[2]. Kochemasov G.G. (1984) The latest data concerning the hypothesis of accretion of primary layered planets of different compositions in the Solar system // 15th LPSC (1984), Abstract 1222.

. **[3]**. Nittler L.R. et al.(2011) The major-element composition of Mercury's surface from MESSENGER X-ray spectrometry // Science. 2011. Vol. 333. P. 1847-1850.

[4]. Wark D.A. (1983) LPS XIV, p. 820-821.

ACCRETION AND PROCESSING OF PRESOLAR COMPONENTS AS RECORDED BY NEBULAR MATERIALS. L. Kööp[1,2] and A. M. Davis[1,2,3], [1]Department of the Geophysical Sciences, [2]Chicago Center for Cosmochemistry, [3]Enrico Fermi Institute, University of Chicago, Chicago, IL, USA (E-mail: koeoep@uchicago.edu).

Introduction: Isotopic studies of meteorites show that the early Solar System incorporated short-lived radionuclides (SLRs, e.g., ^{26}Al, ^{182}Hf) produced in previous generations of stars [e.g., 1,2]. In addition, nucleosynthetic isotope anomalies preserved in meteorites indicate that stellar materials were not completely destroyed and homogenized by heating and mixing in the solar nebula [e.g., 3–5]. In general, older nebular materials (i.e., Ca,Al-rich inclusions in meteorites, known as CAIs) show a larger range of nucleosynthetic anomalies than younger materials (e.g., chondrules) and bulk meteorites, suggesting that the isotopic heterogeneity of the solar nebula decreased with time [e.g., 4,6],

To trace the arrival, processing, and origin of different stellar components in the solar nebula, we review the ^{26}Al-^{26}Mg, Ca, and Ti isotopic systematics in different generations of nebular materials.

Review: *1. CAIs.* CAIs show large textural and mineralogical variation and range from <100 μm to cm-size. [7]. Unaltered CAIs consist of minerals that are predicted to be among the first to condense from a gas of solar composition (e.g., hibonite, spinel, melilite [7]).

The isotopic compositions of the large CAIs in CV chondrites have been studied with high precision. For Ti, anomalies were found in ^{50}Ti (excesses on the order of ~1‰ or less), which correlate well with anomalies in ^{46}Ti [e.g., 4]. Many CAIs have ^{26}Al/^{27}Al ratios of ~5×10^{-5}, which is known as the canonical ratio and generally considered to be the initial ratio of the Solar System [e.g., 8].

2. FUN CAIs. Most FUN (fractionated and unidentified nuclear effects) CAIs have large mass-dependent heavy isotope enrichments in one or more elements (e.g., Mg, O, Ca, Ti [9,10]). These are usually attributed to partial evaporative loss of the fractionated element, e.g., due to melt evaporation [9,10]. Classical FUN CAIs have refractory mineralogies similar to non-FUN CAIs [9], other FUN objects are more similar to PLACs [10] (see below).

The range of nucleosynthetic anomalies in FUN CAIs is about one order of magnitude larger than in non-FUN CAIs (e.g., δ^{48}Ca ranges from ~ –14‰ to +13‰ in classical FUN CAIs, up to ~ +43‰ in FUN hibonites [e.g., 9,10]). Anomalies in ^{48}Ca and ^{50}Ti in FUN CAIs are positive and negative and usually correlate in sign [e.g., 10], but exceptions exist (e.g., FUN CAI HAL, which has a resolved positive δ^{50}Ti and a negative δ^{48}Ca [11]).

Many FUN CAIs with resolved anomalies in ^{48}Ca and/or ^{50}Ti appear to have incorporated little or no ^{26}Al (^{26}Al/^{27}Al unresolved from 0 or as low as $(5\pm2)\times10^{-8}$ [10,12]). However, some FUN CAIs, particularly those with smaller anomalies (δ^{48}Ca <10‰), incorporated live ^{26}Al at an enhanced, but subcanonical level (^{26}Al/^{27}Al ~$(1–5)\times10^{-6}$ [e.g., 9, 10]).

3. PLACs. Most PLACs (platy hibonite crystals*)* are single crystals or aggregates of uniform, MgO- and TiO_2-poor hibonite [e.g., 3,6,13]. Most described PLACs are 30–100 μm in size and some have inclusions of perovskite [e.g., 3,6,13].

The range of nucleosynthetic anomalies in PLACs is another order of magnitude larger than in FUN CAIs (e.g., δ^{50}Ti range from ~ –70‰ to +270‰ [e.g., 3,13,14]). So far, anomalies of such high magnitudes have only been found in the two most neutron-rich isotopes of Ca and Ti, i.e., ^{48}Ca and ^{50}Ti. Similar to FUN CAIs, anomalies in ^{48}Ca and ^{50}Ti in PLACs typically correlate in sign and PLACs do not show evidence for incorporation of large amounts of ^{26}Al [e.g., 3,6,13].

Even though the magnitudes of their anomalies fall within the range found in presolar grains, PLACs are considered to have formed inside the Solar System based on their sizes (most presolar grains are <1 μm; [15]) and their O isotopic compositions, which fall within the range defined by other Solar System materials [6,13].

Interpretation: *Chronology.* The only CAIs that have been precisely dated with the absolute U-Pb chronometer are the large CAIs from CV chondrites. Their ages are the oldest of all Solar System materials [e.g., 16]. No absolute ages exist for FUN CAIs or PLACs.

If the SLR ^{26}Al was homogeneously distributed in the early Solar System, the ^{26}Al-^{26}Mg system has the potential to yield highly precise relative ages for early Solar System materials. A chronologic interpretation of the wide range of ^{26}Al/^{27}Al ratios inferred for CAIs, FUN CAIs, and PLACs would suggest that the ^{26}Al-poor FUN CAIs and PLACs formed up to 7 Ma after ^{26}Al-rich non-FUN CAIs. If this chronology was accurate, it would have important implications for our understanding of the lifetime of the protoplanetary disk. However, there are three lines of evidence that raise considerable doubt that the relative chronology inferred from the ^{26}Al-^{26}Mg system accurately describes the formation sequence of CAIs and PLACs. 1) Large nucleosynthetic anomalies are limited to the ^{26}Al-poor FUN CAIs and PLACs, suggesting that they formed in poorly mixed reservoirs. Such reservoirs are easier to reconcile with an early formation, before disk processes (e.g., mixing, heating) resulted in homogenization of stellar components [17,18]. 2) A minimum disk lifetime of ~7 Ma is long compared to astronomical observations of protoplanetary disks [19]. 3) A

recent relative Hf-W age for a FUN CAI does not allow for a formation as late as required by its ^{26}Al-^{26}Mg age [2]. Instead, it allows for a formation contemporaneous with or earlier than ^{26}Al-rich non-FUN CAIs. Therefore, it is often concluded that the ^{26}Al-poor, isotopically anomalous FUN CAIs and PLACs formed earlier than the ^{26}Al-rich CAIs [17,18]. Their formation region must have been initially ^{26}Al-poor and a late admixture of live ^{26}Al is required. The origin of live ^{26}Al could have been an injection from a nearby dying star (e.g., an asymptotic giant branch star or a massive star) or large-scale spatial heterogeneity in the distribution of ^{26}Al within the molecular cloud [17,18].

In summary, the ^{26}Al-poor character of isotopically anomalous PLACs and FUN CAIs is attributed to an early rather than a late formation. The inferred formation sequence is as follows: 1) PLACs and FUN CAIs; 2) ^{26}Al-rich CAIs; and 3) most chondrules and chondrite parent bodies.

Tracing the accretion of stellar components. If ^{26}Al arrived late in the solar nebula, other stellar components may have arrived late as well. To shed light on this issue, we compare the isotopic patterns between ^{26}Al-poor primitive and ^{26}Al-rich evolved Solar System objects.

1. Neutron-rich isotopes (^{48}Ca & ^{50}Ti): As summarized above, anomalies in ^{48}Ca and ^{50}Ti have been found in the ^{26}Al-poor PLACs and FUN CAIs (large magnitude, often correlated in sign) as well as in more evolved objects (in Ti for ^{26}Al-rich CAIs, and in Ca and Ti for bulk meteorites). In bulk meteorites, anomalies in ^{48}Ca and ^{50}Ti are small (<1‰) and highly correlated [5]. The anomalies in PLACs and FUN CAIs are not only larger but also more scattered [5,10]. But as these anomalies typically correlate in sign, their carriers were likely contributed by the same source(s) (e.g., a type Ia supernova [14]). Given that the different generations of Solar System materials largely show correlated variations in both isotopes, it seems plausible that the same stellar component(s) could be responsible for the anomalies in PLACs, FUN CAIs, bulk meteorites, and ^{26}Al-rich CAIs (with different degrees processing and mixing). If true, this interpretation suggests that the anomalous ^{48}Ca and ^{50}Ti components were present in the Solar System from the very beginning and that the solar nebula received no significant late input of materials with ^{48}Ca and ^{50}Ti anomalies. However, the relationship between ^{46}Ti and ^{50}Ti sheds some doubt on this interpretation (see below).

2. Ti isotopes (^{46}Ti and ^{50}Ti): Bulk meteorites and CV CAIs show a linear correlation between anomalies in ^{46}Ti and ^{50}Ti. In contrast, ^{26}Al-poor PLACs do not show this relationship as most PLACs lack large ^{46}Ti effects in spite of large variations in ^{50}Ti [6]. This observation could suggest that a ^{46,50}Ti-rich stellar component present in ^{26}Al-rich CAIs and bulk meteorites was not present in the ^{26}Al-poor nebula. Similar to ^{26}Al, the reason could be a late arrival of the ^{46,50}Ti-rich component, due to a late injection into the nebula or heterogeneity in the molecular cloud. Alternatively, it has been suggested that disk processes such as size sorting or selective thermal destruction of presolar grains could have produced correlated isotope anomalies even if their carriers originated from different sources, which could explain the good correlation between ^{46}Ti and ^{50}Ti [4]. However, if the same ^{46}Ti component already existed in the ^{26}Al-poor nebula, it is not clear why the range of ^{46}Ti anomalies is limited in PLACs compared to the effects ^{50}Ti.

Summary and conclusions: Nebular materials appear to record the accretion of stellar components and their processing in the solar nebula. The data suggests that live ^{26}Al arrived in the nebula after the first generations of refractory objects had formed. The ^{26}Al-poor, early nebula was characterized by a high degree of heterogeneity in the distribution of neutron-rich presolar component(s) [14]. A comparison of the isotopic patterns of materials that formed before and after arrival of live ^{26}Al suggests that other components may have arrived late as well, e.g., a component rich in ^{46}Ti and ^{50}Ti. If true, the data suggests that this late addition did not lead to a degree of heterogeneity comparable to the ^{26}Al-poor nebula. This could be explained if the late components were mixed well with solar materials before CAIs formed, perhaps during passage through the disk. This scenario seems to be supported by the available record for ^{26}Al: although some controversy exists whether a few CAIs have supracanonical ratios [e.g., 8,13,20], the overwhelming majority of CAIs has ^{26}Al/^{27}Al ratios between 0 and canonical, suggesting that ^{26}Al arrived in the CAI formation region gradually alongside ^{26}Al-poor material [20], preventing the formation of CAIs with highly supracanonical ratios.

References: [1] Lee T. et al. (1976) *Geophys. Res. Lett.,* 3, 109–112. [2] Holst J. C. et al. (2013) *PNAS*, 110, 8819–8823. [3] Ireland T. (1990) *GCA, 54*, 3219-3237. [4] Trinquier A. et al. (2009) *Science,* 324, 374–376. [5] Dauphas N. et al. (2014) EPSL, 407, 96–108. [6] Kööp L. et al. (2016) GCA, 189, 70–95. [7] MacPherson G. J. (2014) Treatise on Geochemistry, 2nd Ed. [8] Jacobsen B. et al. (2008). EPSL, 272, 353–364. [9] Krot A. N. et al. (2014) GCA 145, 206–247. [10] Kööp L. et al. (in press) *GCA*. [11] Ireland T. et al. (1992) *GCA*, 56, 2503–2520. [12] Fahey A. J. et al. (1987) *GCA*, 51, 329–350. [13] Liu M.-C. et al. (2009) *GCA,* 73, 5051–5079. [14] Hinton R. W. et al. (1987) *ApJ, 312*, 420–428. [15] Zinner E. (2014) Treatise on Geochemistry, 2nd Ed. [16] Connelly J. N. et al. (2012) *Science, 338,* 651-655. [17] Wood J. A. (1998) *ApJ*, 503, L101–L104. [18] Sahijpal S. & Goswami J. N. (1998) *ApJ*, 509, L137–L140. [19] Haisch K. E. et al. (2001) *ApJ*, 553, L153–L156. [20] Liu M.-C. et al. (2012) *EPSL*, 327–328, 75–83.

MIXING OF THE ASTEROID BELT DUE TO THE FORMATION OF THE GIANT PLANETS. K. A. Kretke[1], W. F. Bottke[2,3], H. F. Levison[2,3], and D. A. Kring[4,5], [1]SSERVI NPP Fellow (kretke@boulder.swri.edu), [2]Southwest Research Institute, 1050 Walnut St, Suite 300, Boulder, CO 80302, USA, [3]ISET, NASA-SSERVI, [4]LPI, 3600 Bay Area Blvd, Houston, TX 77058, USA [5]CLSE, NASA-SSERVI.

Introduction: The asteroid belt is observed to be a mixture of objects with different compositions, with volatile-poor asteroids (mostly S-complex) dominant in the inner asteroid belt while volatile-rich (mostly C-complex) asteroids dominate the outer asteroid belt. While this general compositional stratification was originally thought to be an indicator of the primordial temperature gradient in the protoplanetary disk, there is growing evidence that that meteorites believed to originate from those different types of asteroids appear to come from very distinct reservoirs, with distinct isotopic and elemental signatures [1,2,3]. This is suggestive, but by no means guaranteed, that the ordinary and carbonaceous chondrites originated in well separated locations in the Solar System.

A few years ago, it was suggested that a dramatic migration of Jupiter into the inner Solar System may provide a way to implant outer Solar System material into the asteroid belt [4,5]. However, this model was missing an important earlier piece of physics, how the giant planets actually formed. This is because, at the time, there was no dynamically self-consistent model for forming the giant planets.

In recent years, theories surrounding the formation of small-bodies and planets have been undergoing a radical shift. Particles with stopping times comparable to their orbital times, often called "pebbles" (although may they range from sub-centimeter to decimeter sizes), interact with gaseous protoplanetary disks in very special ways. Gas drag can first concentrate the pebbles, allowing them to gravitationally collapse and directly produce the planetesimal building blocks [6], and then drag will cause them to be efficiently accreted on to these planetesimals, rapidly producing larger planetary embryos and even gas giant cores [7]. Full dynamically self-consistent models can now show that giant planet can form in two stages, first pebble accretion can rapidly form 10-20 Earth mass rocky-icy cores large enough that they can efficiently accrete disk gas, and form the final gaseous planets [8].

Armed with this dynamically self-consistent model of planet formation we can investigate, how the process of giant planet formation will impact the surrounding planetesimal population, without requiring a dramatic migration of the giant planets.

Methods: We use the planet formation code LIPAD (the Lagrangian Integrator for Planetary Accretion and Dynamics) [9] to model to collisional and dynamical evolution of a solar system forming under these conditions. LIPAD is based upon the N-Body integrator SWIFT [10] but uses novel algorithms to statistically follow bodies that are too small and numerous to be handled in a traditional N-body integrator. This allows us to model how our system may have evolved starting from pebbles and planetesimals all the way to a mature planetary system.

To test the effect of giant planet formation in the asteroid belt we placed a population planetesimals in outer Solar System and allow them to accrete pebbles. To speed up runs and increase the number of runs we could carry out we began with 4 larger near Mars-sized planetesimal seeds to serve as the initial location of the giant planet cores. We place these seeds in positions expected to approximate the location of the giant planets before the late instability, i.e. either in their pre-Nice 2 initial conditions [11] or a bit more widely spaced. These compact initial conditions are consistent with where planets form in our comprehensive planet formation models [8]. We note that even if we begin the planetesimals in the pre-Nice initial conditions they tend to move due to their interactions with the other planetesimals and even with the pebbles, therefore the planets do not end up in the same positions.

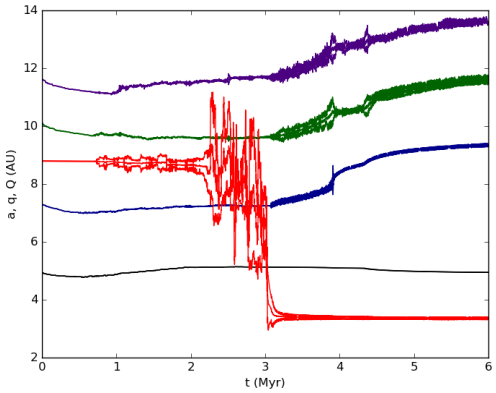

Figure 1: The semi-major axis, perihelion and aphelion of an outer Solar System body scattered into the asteroid belt (red) the planets (dark blue, dark green, indigo).

Results: As the giant planets cores grow via by pebbles accretion, they scatter surrounding planetesimals both inwards and outwards. In figure 1 we show the orbital evolution of an example asteroid. As the

planetary embryos accrete pebbles (and later gas) then begin to dynamically excite and scatter nearby planetesimals. Once the giant planets grow large enough, the planetesimals chaotically diffuse, scattering from one planetary core to another.

Additionally, the giant planet cores move modestly because of interactions with the surrounding planetesimals as well as with interaction with the other growing cores. This can cause additional outer-Solar Systems asteroid to be scattered inwards. This is a very stochastic process with large variations between then runs. The planetesimals detach from Jupiter either due to small movements of Jupiter or due to gas drag or, more rarely, due to chaotic interactions with the asteroids already present within the asteroid belt. In figure 2 we show the distribution of remaining planetesimals scattered inwards, scaling the runs to the final location of Jupiter.

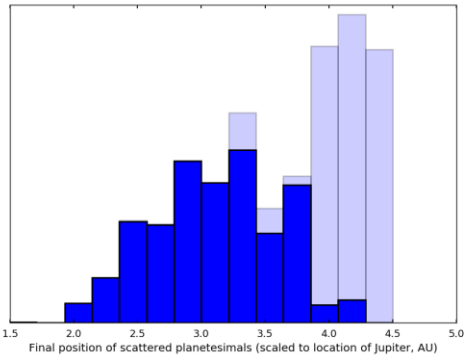

Additionally, we ran the resulting distribution in the presence of the current Juipter/Saturn locations to observe what would be stable in the current Solar System.

Figure 2: The distribution of planetesimals, scaled to the final location of Jupiter. In light blue show the original distribution of implanted planetesimals, dark blue shows those objects that are stable for 1 Myr for Jupiter/Saturn in their present day configuration.

Notes on the formation of Ceres. Of particular interest in this system is Ceres. Ceres is observed to have ammonia on its surface, a material believed to be from the very distant outer Solar System [12]. In our model, we have two possible explanations for Cere's observed composition. First, as we observe particles transported into the inner Solar System from the entire giant planet forming area (although it is less likely to occur from the more distant regions), it is possible that Ceres is simply a member of that population. In this case, we should find many other small bodies in the asteroid belt with similar compositions. An alternative, and we believe more likely option, is that as Ceres, as the largest body in the asteroid belt, underwent a small amount of pebble accretion before being scattered inwards. The efficiency of pebble accretion strongly depends upon the planetesimal's size; therefore a Ceres sized body could accrete these pebbles that formed in the very distant parts of the Solar Nebula much more efficiently that the smaller counterparts [13,7]. Under this scenario, Ceres (and possibly the other large asteroids) would have compositional differences from the bulk of the asteroids.

Conclusions: We find that the pebble accretion model can successfully explain many attributes of the Solar System: an outer Solar System with a few giant planets and ice giants and a Kuiper belt [8], an inner Solar System with terrestrial planets, a small Mars, and a low mass asteroid belt [13] which, as described in this abstract consists of material mixed from the inner and outer Solar System. Furthermore, the asteroid belt can be excited after formation by excitation from embryos scattered from the terrestrial planet system, or by excitation by chaotic interactions between the giant planets [14]. This could potentially provide an alternative non-Grand Tack [3] solution to the origin of many C-complex bodies, including Ceres.

References: [1] Warren (2011) E&PSL, 311, p.93-100. [2] Budde et al. (2016) E&PSL, 454, p.293-303. [3] Keller et al. (2017) LPSC, no. 1964. id 2457. [4] Walsh et al. (2011) Nature, vol 475, issue 7355, pp. 206-209. [5] Walsh et al. (2012) M&PS. Vol 47, issue 12 pp. 1941-1947. [6] Johansen et al (2014) PPVI, Univ. of Arizona Press, Tuscon, 914 pp, p. 547-570.

[7] Lambrechts & Johansen. (2012) A&A, 544, id.A32. [8] Levison, Kretke & Duncan (2015) Nature, 524, 322-324. [9] Levison, Thommes, & Duncan (2010) A&A, 139, 1297-1314. [10] Duncan, Levison, & Lee (1998) ApJ, 115, 2067-2077. [11] Levison et al. (2011) AJ, 142 (5) 152. [12] De Sanctis et al. 2015. Nature 528, 241-244. [13] Ormel & Klahr (2010) A&A, 520, id A43, 15pp. [14] Levison et al. (2015) PNAS, 112, 14180-14185. [15] Izidoro et al (2016) ApJ, 833 (1) id. 40. 18pp.

CONNECTING CO ABUNDANCES BEFORE, DURING, AND AFTER PEBBLE MIGRATION

S. Krijt[1], K. Schwarz[2], F. J. Ciesla[1], and E. A. Bergin[2], [1]Department of the Geophysical Sciences, The University of Chicago, 5734 South Ellis Avenue, Chicago IL 60637 (skrijt@uchicago.edu), [2]Department of Astronomy, University of Michigan, 311 West Hall, 1085 South University Avenue, Ann Arbor, MI 48109

Introduction: Pebbles (~mm to cm-size dust particles) are believed to play an important role during the early stages of planet formation [1]. The idea is that these pebbles form throughout the protoplanetary disk (via the coagulation of smaller solids) and drift inward because of the gas drag they experience [2,3]. The resulting radial flux of pebbles can kickstart planetesimal formation by triggering streaming instabilities [4,5], or speed up growth of existing protoplanets through efficient pebble accretion [6,7].

The creation of pebbles and their tendency to settle vertically & drift radially are expected to significantly alter volatile abundances (both gas-phase and in the form of ice) in different regions of the protoplanetary disk. In the outer disk, the presence of a population of pebbles close to the midplane can act as a sink for ices, leading to the gradual removal of gas-phase volatiles from the warmer upper parts of the nebula [8–10]. As icy pebbles drift towards the warmer inner disk, gas-phase carbon and oxygen abundances in the inner regions can be enhanced [11] while ices potentially pile-up behind different radial snowlines [12,13].

Observational studies of nearby disks appear to support this narrative, finding that: (i) volatiles are depleted from the gas-phase in the outer disk [9,14,15], and (ii) the radial extent of the pebble population is usually much smaller than that of the gas disk itself [e.g., 16]. Interpreting such observations is difficult however, because we lack a detailed understanding of how dust evolution and astrochemistry interact, and because key quantities like the dust-to-gas ratio and total disk mass are often poorly constrained.

Towards a 2D Hybrid Model: We present new modeling efforts designed specifically to study how the formation and subsequent dynamical evolution of pebbles impacts volatile abundances spatially and temporally on a disk-wide scale. The model considers three distinct physical components: gas-phase volatiles (in this case, CO), small well-coupled dust grains, and large decoupled pebbles (see Fig. 1). The CO vapor and small dust components are treated as concentrations on a 2-dimensional (r and z) grid, while the pebbles are represented by Lagrangian tracer particles [10,17]. Calculating forward in time, we solve for a variety of interactions between these three components (the arrows in Fig. 1), including dust coagulation (the formation of pebbles out of microscopic dust) and condensation, sublimation, and photo-desorption of CO molecules. While these processes are taking place, we follow the dynamics and transport of vapor, solids, and ices using a combination of grid-based and Monte Carlo methods that consider turbulent mixing as well as gravitational settling and radial drift.

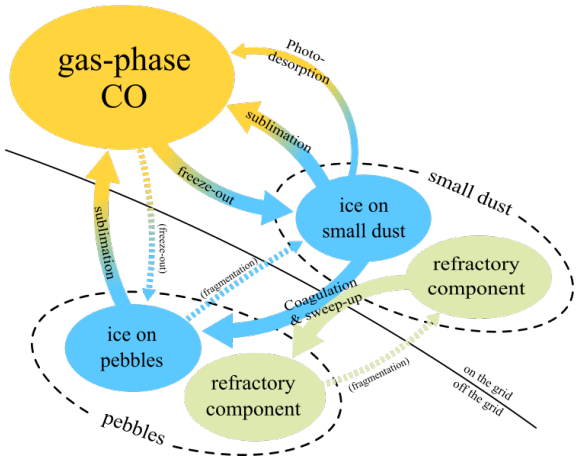

Figure 1: Schematic of the hybrid approach. Vapor and small dust concentrations exist on a 2D grid and larger pebbles are described using Lagrangian tracer particles.

A major advantage of this approach is that we can describe the pebbles as particles with unique histories (every pebble's current size and chemical make-up is a function of its journey through the disk) but still resolve interactions in regions of the disk where the dust density is low.

Results: Figure 2 shows an example of a model run for a disk around a Sun-like star. The upper panels show gas-phase CO abundance and the lower panels indicate locations of the pebble tracer particles (individual symbols) and contours representing magnitude of small dust depletion. The colors in the bottom panel indicate CO-ice mass fraction of the various solids. This particular simulation assumes a turbulent $\alpha = 10^{-3}$ and the region above 3 pressure scale-heights is excluded from the calculation.

At the start of the simulation (Fig. 2a), the dust-to-gas ratio is 0.005 everywhere and no pebbles are present; CO is frozen out in the midplane of the outer disk while being present in the vapor phase in the warmer inner region and upper parts of the disk. After 30,000 years (Fig. 2b), pebbles have formed abundantly in the inner disk (where coagulation timescales are shortest) and are starting to form outside the CO snow-

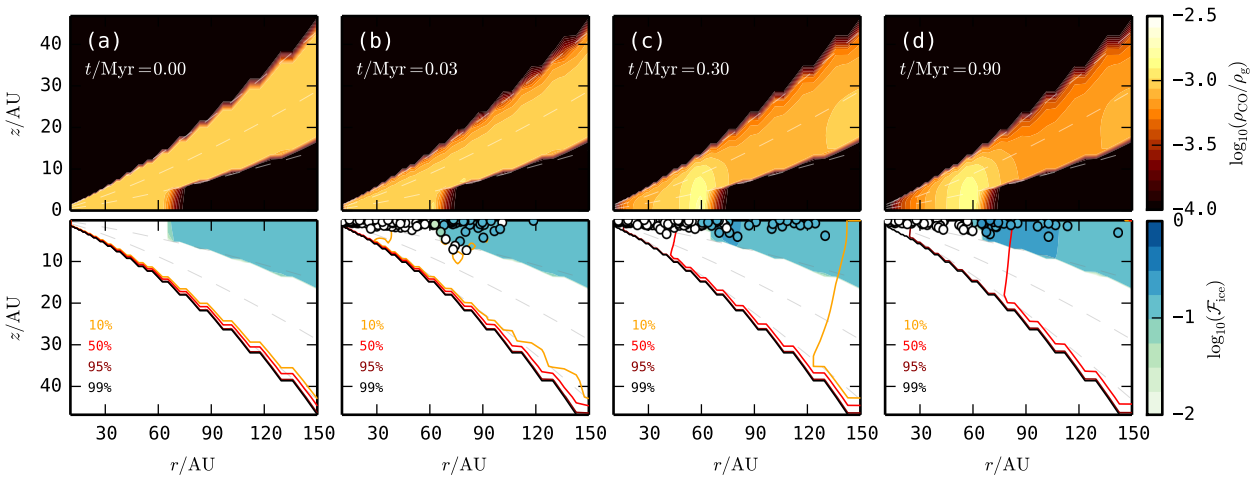

Fig. 2: Snapshots of calculation for a disk around a Solar-type star (see text). Upper panels show gas-phase CO abundance (mass density relative to H_2). In the bottom panels, the colors refer to CO-ice mass fractions of the small dust (background color) and pebbles (individual circles). The contours denote depletion of small dust relative to the initial dust-to-gas ratio of 0.005. Faint dashed lines correspond to $z/H=\{1,2,3\}$, with H the gas pressure scale-height.

line as well. After forming, pebbles quickly settle to the midplane. After 300,000 years (Figs 2c), sufficient time has passed for pebbles to be present throughout the midplane of most of the disk. With a increasing fraction of the CO being sequestered in the midplane in the form of ice, the gas-phase abundance in the upper parts of the disk decreasing. Interior to the midplane CO snowline (around r = 60 AU), the inward radial flux of icy pebbles has led to an increase in CO vapor. This freshly-released vapor is in turn diffusing vertically and radially. As such, the magnitude and shape of this CO peak is set by a balance between the influx of icy pebbles and the details of the diffusive process. The situation after 900,000 years (Fig. 2d) looks fairly similar, but the reservoir of pebbles in the outer disk is beginning to be exhausted. Once the supply of icy pebbles has ceased, the spike of CO interior to the snowline will slowly disappear. Note how the outward diffusion of CO vapor has increased the ice content of small grains exterior to the (midplane) snowline.

Summary: We have developed a new framework for simulating the evolution of volatiles and solids in protoplanetary disks. The method is designed to physically link several key observables: (1) gas-phase volatile abundances as a function of height in the inner and outer disk; (2) the mass and radial extent of the pebble disk; and (3) the abundance of well-coupled (sub)micron grains. Solving the gas-phase CO abundance in two dimensions is particularly valuable for comparing the models to observations, as different tracers/wavelengths probe different parts of the protoplanetary nebula [e.g., 18,19].

Understanding how the underlying processes (dust coagulation, transport, and volatile condensation/sublimation) interact and how their behavior depends on key parameters such as (initial) dust-to-gas ratio and disk mass are important steps towards connecting astrochemical and planetesimal formation models, and will allow us to identify and interpret observational signatures of the early stages of planet formation in nearby young disks.

References: [1] Ormel C. W. (2017), *in "Formation, Evolution, and Dynamics of Young Solar Systems" (ed. M. Pessah & O. Gressel)*. [2] Birnstiel T. et al. (2010), *Astron. Astroph.*, 513, A79. [3] Krijt S. et al. (2016), *Astron. Astrophys.,* 586, A20. [4] Carrera D. et al. (2015), *Astron. Astrophys.*,579, A43. [5] Drążkowska, J. et al. (2016), *Astron. Astroph.*, 594, A105. [6] Ormel C. W. and Klahr H. H. (2010), *Astron. Astrophys.*, 520, A43. [7] Lambrechts M. and Johansen A. (2012) *Astron. Astrophys.*, 544, A32. [8] Meijerink R. et al. (2009), *Astrophys. J., 704,* 1471. [9] Kama M. et al. (2016) *Astron. Astrophys., 592,* A83. [10] Krijt S. et al. (2016) *Astrophys. J., 833,* 285. [11] Öberg K. I. and Bergin E. A. (2016) *Astrophys. J. Lett., 831,* L19. [12] Stammler S. et al. (2017), *Astron. Astroph.*, 600, A140. [13] Schoonenberg D. and Ormel C. W. (2017), *Astron. Astrophys.*, 602, A21. [14] Du F. et al. (2015) *Astrophys. J. Lett., 807,* L32. [15] Du F. et al. (2017), *Accepted for publication in Astrophys. J.* [16] Andrews S. et al. (2012), *Astrophys. J.*, 744, 162. [17] Krijt et al. (2017), *LPSC XLVIII, 2291.* [18] Schwarz K. et al. (2016) *Astrophys. J., 823,* 91. [19] Zhang K. et al. (2017), *Nat. Astron.*, 1, 130.

Acknowledgments: This material is based upon work supported by NASA under Agreement No. NNX15AD94G for the program "Earths in Other Solar Systems".

PLANETARY ACCRETION AS INFORMED BY METEORITIC SAMPLES OF EARLY SOLAR SYSTEM PLANETESIMALS. David A. Kring, Lunar and Planetary Institute, Universities Space Research Association, 3600 Bay Area Blvd., Houston, TX 77058 (kring@lpi.usra.edu).

In the Beginning: Impact events are a key part of the formation of planets, both during the initial accretional phase and late in the growth of a planet when giant impact events may dramatically alter the final outcome. Large collisions, for example, have been implicated in the formation of the Moon from the Earth [1-3], the stripping of Mercury's mantle [4], the northern-southern hemisphere dichotomy of Mars [5-8], and the formation of Charon from Pluto [9]. Periods of enhanced impact bombardment of post-accretion planetary surfaces have also been deduced from Solar System exploration studies. Apollo, for example, demonstrated that the Moon was heavily cratered sometime during the first ~600 million years of its existence in what has been termed by some to be the period of Late Heavy Bombardment (LHB). The cadence of that event is still uncertain, but it is clear there were a large number of basin-forming impact events in that first half-billion years.

Dusty circumstellar disks around young stars outside our Solar System indicate the collisional evolution of young planetary systems can be violent. Spitzer Space Telescope data indicate that some systems have dust signatures well above the average at ages from 100-600 Myr [10]. Observations by Su et al. [11] and Beichman et al. [12], for example, support the idea that the ~350 Myr-old A star Vega and the ~2 Gyr-old G star HD 69830 recently experienced collisions between large planetesimals that generated these elevated dust signatures. Both Vega and Fomalhaut may have planetesimal rings akin to the precursor of our main asteroid belt [13].

The Accretional Epoch Among Chondritic Planetesimals: Our record of collisional processes among planetesimals is extraordinarily ancient. We have, for example, a fragment of rock from a collision among planetesimals that occurred during the accretion of Earth and prior to the formation of the Moon. The MIL 05029 meteorite is an impact melt breccia that was produced in a collision ~4.54 Ga that created a 25-60 km diameter crater and shattered the interior of the 100-200 km diameter L-chondrite parent body [14]. A similar study showed that the Portales Valley meteorite may have been produced beneath the floor of a >20 km diameter crater on the 150-200 km diameter H-chondrite parent body [15] in an event that occurred >4.46 Ga [16]. On the R-chondrite parent body, impacts appear to have occurred 4.34-4.38, 4.4, and 4.47 Ga ([17] and references therein]. Other collisions during the accretional epoch have been detected on the E-chondrite (~4.53 Ga), IAB (>4.47 and perhaps >4.52 Ga), HED (~4.48 Ga), and L-chondrite (4.46 and 4.43) parent bodies ([18] and references therein).

On at least two planetesimals, the impact events produced significant volumes of melt that differentiated to form the IAB-MG and IAB-sLM groups of iron meteorites (e.g., [19]). Cooling rates of those meteorites [20] suggest craters ~150 to 300 km in diameter on planetesimals ~300 km diameter or larger.

Collectively, these data indicate sizeable impact events were occurring among planetesimals as the accretional phase wound down and the largest planetary collisions (e.g., the Moon-forming giant impact) were occurring. They also suggest, but do not prove, that collisional velocities and dynamic stirring of the nascent planetary disk were relatively high.

The Accretional Epoch Among Differentiated Planetesimals: Variable planetesimal accretion rates and, thus, abundances of short-lived isotopes for interior heating, produced equally variable outcomes. While some planetesimals remained chondritic, as described above, and largely preserve a nebular record, other planeteismals became hot enough to differentiate. It is difficult to discern impact-reset radiometric systems in meteoritic samples of these objects, because simple cooling of a planetesimal may not reach radiometric closure temperatures until 4.47-4.49 Ga, as seen in silicates among IIE iron meteorites (e.g., [18] and references therein). That is, if an impact occurred, the planetesimal may be too warm to quench a radiometric age of that impact. At some point, the objects were involved in collisions sufficiently energetic to strip away the mantle and expose the differentiated cores. As most of the planetesimals represented by meteoritic relicts are among iron meteorites, that type of collisional erosion may have been common. That, too, implies relatively high collisional velocities and, thus, an excited dynamical system.

The Puzzle of Sources. As this is a workshop designed for discussion, let me wade into the curious problem of the sources of the accreting material and impactors. Isotopic signatures of volatile elements suggest the Earth, Moon, and Mars were accreting carbonceous chrondritic material (e.g,. [21-23]), sometime between the main accretional phase of Earth [24] and the solidification of the lunar crust from a magma ocean [23]. As noted in the introduction, planetesimals continued to hit the Earth and Moon (and other inner

solar system planets) for several hundred million years. Analyses of lunar impact melts point to sources of those impactors that remain contested: some suggest the objects evolved, over time, from carbonaceous impactors to ordinary chondrite impactors, with one or more iron projectiles stochastically hitting during that evolution, while others suggest end member mixing among carbonaceous and iron impactors (see, for example, the discussion of [25] and references therein). Curiously, the first mineralogical relicts of impactors found in ancient regolith breccia samples [26], produced near the end of the LHB, are entirely carbonaceous. A diverse array of other impactors, more reflective of the current population of meteorite falls, is not found until much later in lunar history.

If carbonaceous impactors were entering the inner solar system, and if they were accreting at vastly different times (e.g., during primary accretion and later during the LHB), does that mean they were scattered by a single process or more than one process?

Also, if carbonaceous chondritic objects were entering the inner solar system and, presumably, passing through the inner asteroid belt, why do we not see abundant clasts of them among regolith samples of ordinary chondrite planetesimals?

This is where dynamical modeling is providing a complementary perspective. At least one other paper submitted to this workshop [27] will present one of those models.

Although the sources of the accreting material over time currently remain a puzzle, renewed attention on impactor signatures (geochemical, isotopic) in Earth, on impactor signatures (geochemical, isotopic, mineralogical, and geologic) in lunar samples, on meteoritic samples of planetesimals that either co-accreted with planets or later pummeled them, and in dynamical models that complement those data, the community may be in a position to soon accelerate our understanding of this earliest epoch of solar system history.

References: [1] Hartmann W.K. and Davis D.R. (1975) *Icarus, 24*, 504–515. [2] Cameron A.G.W. and Ward W.R. (1976) *Lunar Science VII*, 120–122. [3] Canup R.M. and Righter K. (eds.) (2000) *Origin of the Earth and Moon*, 555 p., Univ. Arizona Press. [4] Benz W. et al. (1988) *Icarus, 74*, 516–528. [5] Wilhelms D.E. and Squyres S.W. (1984) *Nature, 309*, 138–140. [6] Andrews-Hanna J.C. et al. (2008) *Nature, 453*, 1212–1215. [7] Marinova M.M. et al. (2008) *Nature, 453*, 1216–1219. [8] Nimmo F. et al (2008) *Nature, 453*, 1220–1223. [9] Canup R.M. (2005) *Science, 307*, 546–550. [10] Rieke G. et al. (2005) *ApJ, 620*, 1010–1026. [11] Su K. et al. (2005) *ApJ, 628*, 487–500. [12] Beichman C. et al. (2005) *ApJ, 626*, 1061–1069. [13] Su K. et al. (2013) *ApJ*, *763*, 118, 14p. [14] Weirich J. R. et al. (2011) *Meteoritics & Planet. Sci., 45,* 1868–1888. [15] Kring D. A. et al. (1999) *Meteoritics & Planet. Sci., 34,* 663–669. [16] Bogard D. D. and Garrison D. H. (2009) *GCA, 73*, 6965–6983. [17] Righter K. et al. (2016) *Meteoritics & Planet. Sci., 51,* 1678–1684. [18] Bogard D. D. (2011) *Chemie der Erde, 71*, 207–226. [19] Worsham E. A. et al. (in press) *Earth Planet. Sci. Letters*. [20] Goldstein J. I. et al. *(2014) Geochim. Cosmochim. Acta*, *140*, 297–320. [21] Alexander C. M. O. D. et al. (2012) *Science, 337*, 721–723. [22] Marty B (2012) *Earth Planet. Sci. Letters, 313–314*, 56–66. [23] Barnes J. J. et al. (2016) *Nature Comm., 7*:11684, doi: 10.1038/ncomms11684. [24] Fischer-Gödde M. and Kleine T. (2017) *Nature, 541*, 525–528. [25] Liu J. et al. (2016) *Geochim. Cosmochim. Acta, 155*, 122–153. [26] Joy K. H. et al. (2012) *Science, 336*, 1426–1429. [27] Kretke, K. A. et al. (2017) this conference.

ACTIVE PROCESSES IN ASTEROIDS AND PLANETS DEVELOPED TO WATER PLANET AND LIFE.

Y. Miura, Yamaguchi University (Chuou 4-1-23, Yamaguchi, Japan, 753-0074; yasmiura50@gmaiul.com)

Introduction: Primordial to present stars and planets are studied from remained solids of Asteroids, the Moon and planets (with life fossil), where global data of older atmosphere and ocean are estimated in remained rocks. Purpose of the paper is to propose active model of water-planet and life system of the Earth-type planets to be applied to exoplanets [1-3].

Active process: Active process includes dynamic and static reactions, where dynamic reaction at extreme conditions of high temperature and pressure in short time forms widely amorphous mixed solids found beyond the Solar System. Static reaction with slow time in Earth is chemical and physical changes with formation of large crystalline minerals [1-7].

Extreme conditions: The extreme condition existed in the Space and the Solar system produces ion states of all elements by shock-wave explosions of the Big-Bang, nuclear fusions in the Stars, the Supernova and active planets of volcano and asteroid impacts. Molecules formed from light elements by reaction with evaporation is produced everywhere in the Space by any heated processes locally and shortly. Global ocean water of planet Earth is formed widely to be changed between gas and solid as quenched intermediate steps by the giant impacts including planetary collision process [2-7]

Experiment of water formation by heating: Author has produced water droplets in laboratory from heated the Allende carbonaceous chondrite, which is certificated by molecular formation from ion elements by heating reaction in this study. This suggests that all molecular fluids in the Space including celestial bodies of any Asteroids and Mars are formed by impact heating locally and shortly, which are observed remained surface topographic features by image observation of space exploration [5-7].

Chondrule formation: Dynamic process with short and local melting and evaporation in the Space and Asteroids produces quenched solids with stopped at the primordial ages mainly, which are found in Asteroids and Earth-type planets. Chondrules of Asteroids are quenched solids with primordial mixture and some tiny crystalline mineral locally as closed system without any developed further [7] .

Life in Earth: Planet Earth shows two characteristics of primordial stage and present water-related active planet, where the water-planet shows mixture of static and dynamic systems to be kept global air-ocean water-rock system. Rock crystals of water-Earth are formed by continuous shallow-interior heating developed by active plate tectonics movements. Dynamic process of the planet Earth is observed largely at local volcano, quake and meteoritic impacts globally. Life activity on the water-planet which is called as mini-Earth system of three material changes in any life and human (Home sapiens) body system with short existence developed by continuous generation process on water-Earth [2-7]

Six material steps on the Solar System: On the Solar System of the Sun star, six steps of formations from ion, molecules, solid rocks, air-fluid-rock processes, global activity of water planet Earth and life of mini-Earth system are shown as active process diagram [4-7].

Telescopic image investigation: The present result indicates application by remote-sensing analyses of local fluid formation and remained surface triggered by shock-wave explosion of volcano, quake and Asteroid impact on Earth-type planets, Asteroids and the Moon. Life existence should be discusses on global ocean existence formed by carbon-bearing ocean deposits by remote-image analyses including exoplanet case in near-future [4-7].

Summary: The results are summarized as follows.

1) Active process includes dynamic and static reactions are formed by amorphous and crystalline solids by extreme high temperature and pressure conditions.

2) Water droplets formed from meteorite heating are obtained in the laboratory study to be evidences of volatiles ions in the meteorite interior.

3) Chondrules of asteroids are formed by dynamic quenching and local short crystallization with mixed aggregates stopped at primordial periods.

4) Life of mini-Earth system has to be produced at large water-planet system relatively as copied system of larger water-planet system.

5) Life evidence on other planets should be observed indirect evidence of ocean sea-floor sedimentary deposits with carbon elements.

References: [1] Miura Y. and Kato T. (1993): *Amer. Inst. of Physics Conf. Proc.*, 283, 488-492. [2] Miura Y. (1994) *Astronomical Society of the Pacific Conference Series*, 63, 259-264..[3] Miura Y. and Fukuyama S.(1999), J. Materials Proc. Tech. (Elsevier), 85, 192-193.[4] Miura Y. (2010) LPI Contribution (AbSciCon), abstract #5037.#5398. [5] Miura Y. (2017): LPSC2017 (USRA, LPI, USA), abstract #3028. [6] Miura Y. (2017): JpGU-AGU 2017 (Makuhari, Japan), abstracts #C5357, #C2249, # C2158. [7] Miura Y. and T. Kato (2010) Chondrules as Astrophysical Objects (UBC, USRA), abstract #2028.

COMETARY DUST AND THE YOUNG SOLAR SYSTEM R. C. Ogliore. Department of Physics, Washington University in St. Louis, St. Louis, MO 63130, USA.

Introduction: Comets are small Solar-System bodies that accreted in cryogenic conditions in the outer solar nebula. By definition, comets show "cometary activity" as they near the Sun (Figure 1): the ejection of gas and dust due to ice sublimation which forms a coma and dust tail. Comets contain a substantial fraction of ice but are still mostly made of rocky material ("frosty rocks" instead of "dirty snowballs"). Cometary dust, mostly unaltered by the aqueous alteration and thermal metamorphism that affected asteroids, should be among the most primitive surviving rocky material in the Solar System.

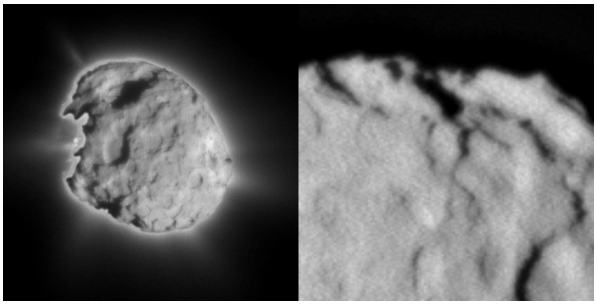

Figure 1: Left: Composite image of a long-exposure and short-exposure image of the nucleus of comet Wild 2, showing surface features and jet activity. Right: Close-up view from a different image showing pinnacles, craters, and ridges on Wild 2.

Cometary dust was returned from comet Wild 2 by NASA's Stardust mission. A sub-sample of interplanetary dust collected by high-altitude aircraft, as well as fine-grained micrometeorites collected from snow in Antarctica, is likely of cometary origin [1, 2]. Chemical, structural, and isotopic analyses of this material yields insight into the first few million years of Solar System evolution. Below I discuss four questions about cometary dust and the implications to the early evolution of the Solar System.

1) What is the origin of coarse-grained cometary dust? Both giant cluster IDPs and comet Wild 2 samples in Stardust aerogel tracks are composed of both fine-grained (<1 μm) and coarse-grained (>1 μm) particles. The coarse-grained particles in the Stardust sample survive as terminal particles at the ends of larger Stardust cometary tracks. The majority of these particles are high-temperature igneous rocks, like CAI and chondrule fragments, similar to those seen in meteorites [3] (Figure 2). The majority of these objects have ^{16}O-poor compositions [4], also similar to chondrules in meteorites. Analyses of Mn and Fe contents in olivine grains from Wild 2 and a giant cluster IDP show a very broad distribution compared with olivines from UOC, CC, and CR chondrules [5].

Coarse-grained cometary dust likely formed in the inner Solar System by the same high-temperature processing that formed high-temperature rocks found in primitive meteorites, and was subsequently transported to the outer Solar System. Comets, which then formed beyond the orbit of Neptune, accreted a mixture of high-temperature dust from various reservoirs of inner Solar System materials.

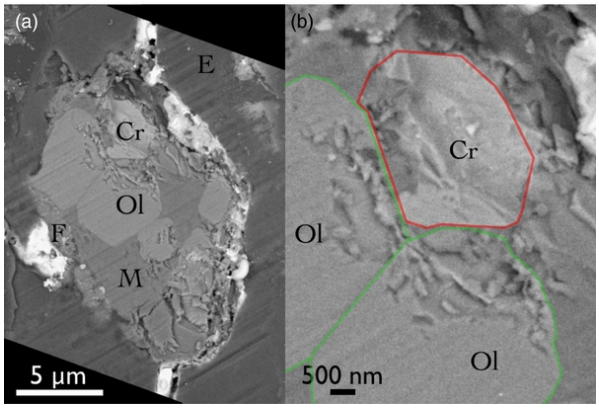

Figure 2: (a) BSE image of the Wild 2 particle Iris (Ol: olivine; Cr: chromite; M: mesostasis; F: fusion crust; E: epoxy+aerogel). (b) A closer view of the triple junction between two olivine grains and chromite with the olivines outlined in green and the chromite outlined in red. From [6].

2) Did cometary rocks form without ^{26}Al? The short-lived radionuclide ^{26}Al ($t_{1/2}$=0.72 Myr) was incorporated into most most CAIs from CV chondrites at the "canonical" level of ^{26}Al/^{27}Al $\approx 5.2\times10^{-5}$ [7]. Chondrules from various chondrite groups incorporated less ^{26}Al (^{26}Al/^{27}Al $\approx 10^{-6}$–10^{-5}), implying most of these objects formed 1–3 Myr after CV CAIs. To date, the initial ^{26}Al/^{27}Al ratio has been measured in eight objects from comets: Iris (Wild 2 chondrule fragment, $<3\times10^{-6}$ (2σ one-sided), Figure 2), Inti (Wild 2 CAI fragment, $<5\times10^{-5}$ [8]), Coki (Wild 2 CAI fragment, $<1\times10^{-5}$ [9]), Pyxie (Wild 2 FeO-poor ferromagnesian grain, $<4\times10^{-6}$ [10]), Manchanito (Al-rich amorphous grain from a giant cluster IDP, $<7\times10^{-6}$, [11]), and two corundum-bearing IDPs ($<10^{-6}$ and $<7\times10^{-6}$, [12].

The lack of ^{26}Al can be explained if these particles formed prior to the injection and subsequent homogenization of ^{26}Al in the solar nebula (as is hypothesized to explain FUN CAIs [13]). However, the FeO-rich and ^{16}O-poor compositions of Iris and Pyxie indicate that they formed in an oxidizing environment with

a high dust/gas ratio, which is unlikely to exist in the very young Solar System. It is much more probable that these objects formed, or were chemically altered, after ^{26}Al had decayed.

Though the data set is still small, these analyses hint that comets preferentially accreted coarse-grained material that formed relatively late (>3 Myr after CAIs) in the inner Solar System and was subsequently transported outward to the comet-forming region. The necessity of large-scale, late-stage mixing of dust between the inner and outer Solar System may constrain the formation of Jupiter [6], which opens a gap in the disk and effectively cuts off outward migration of dust.

3) When and where did secondary minerals in comets form? Secondary minerals are rare but present in the Wild 2 samples (e.g. cubanite [14]), interplanetary dust [15], and UCAMMs (Figure 3). Perihelion passage, impacts, or cometary activity may create the right conditions to form secondary minerals on a cometary nucleus [16, 17]. Alternatively, secondary minerals may be formed in the inner Solar System on asteroidal parent bodies and transported outward to the cometary region following disruption of those bodies. High-precision Mn-Cr and O isotope systematics may elucidate the timing of formation and source reservoirs of these phases and allow for comparison to secondary phases in asteroids [18, 19].

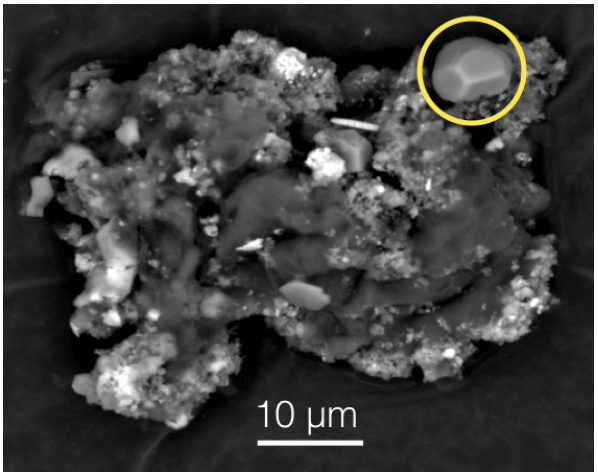

Figure 3: BSE image of an ultra-carbonaceous Antarctic micrometeorite, with carbonate grain circled in yellow. Image courtesy of Elena Dobrică (University of New Mexico).

4) What is the origin of fine-grained cometary dust? Fine-grained Wild 2 material in aerogel tracks has proven difficult to analyze due to hypervelocity capture effects (Figure 4). Nonetheless, TEM analyses have showed that Wild 2 fines are consistent with CI chondrites in their Fe-Mg-S composition [20] but are heterogeneous on a particle-by-particle basis. This is consistent with analyses of fine-grained chondritic porous interplanetary dust particles: they are heterogeneous aggregates of sub-μm grains with bulk composition close to CI [1]. Oxygen isotope measurements of individual small grains in the bulb of a Stardust track shows a very wide range of compositions [4]. This suggests that comet Wild 2 fines are either primitive, unequilibrated dust inherited from the Solar System's parent molecular cloud, or a very diverse sampling of inner Solar System compositional reservoirs that accreted along with a large number of inner-Solar-System rocks to form comet Wild 2. More precise analyses of the volatile content and presolar grain abundances of Wild 2 fines will help distinguish between these two scenarios.

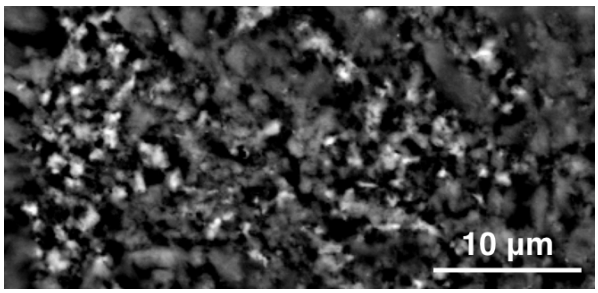

Figure 4: BSE image of fine-grained Wild 2 dust intermixed with aerogel.

References: [1] J. Bradley (2003) *Treatise on geochemistry* 1:711. [2] E. Dobrică, et al. (2009) *Meteoritics & Planetary Science* 44(10):1643. [3] D. Brownlee, et al. (2012) *Meteoritics & Planetary Science* 47(4):453. [4] R. C. Ogliore, et al. (2015) *Geochimica et Cosmochimica Acta* 166:74. [5] D. Brownlee, et al. (2016) *Meteoritics & Planetary Science*. [6] R. C. Ogliore, et al. (2012) *The Astrophysical Journal Letters* 745(2):L19. [7] B. Jacobsen, et al. (2008) *Earth and Planetary Science Letters* 272(1):353. [8] H. Ishii, et al. (2010) in *Lunar and Planetary Science Conference* vol. 41 2317. [9] J. Matzel, et al. (2010) *Science* 328(5977):483. [10] D. Nakashima, et al. (2015) *Earth and Planetary Science Letters* 410:54. [11] J. Stodolna, et al. (2012) *Meteoritics and Planetary Science Supplement* 75:5392. [12] K. D. McKeegan (1987) *Science* 237:1468. [13] A. Krot, et al. (2012) *Meteoritics & Planetary Science* 47(12):1948. [14] E. L. Berger, et al. (2011) *Geochimica et Cosmochimica Acta* 75(12):3501. [15] J. Aléon, et al. (2009) *Geochimica et Cosmochimica Acta* 73(15):4558. [16] F. Reitmeijer, et al. (1987) in *Diversity and Similarity of Comets* vol. 278. [17] K. Nakamura-Messenger, et al. (2011) *Meteoritics & Planetary Science* 46(6):843. [18] J. Matzel, et al. (2014) in *Lunar and Planetary Science Conference* vol. 45 1645. [19] R. C. Ogliore, et al. (2014) in *77th Annual Meeting of the Meteoritical Society* vol. 1800. [20] J. Stodolna, et al. (2012) *Geochimica et Cosmochimica Acta* 87:35.

EFFECT OF RE-IMPACTS ON THE LUNAR MAGMA OCEAN. V. Perera[1], A.P. Jackson[1,2], L.T. Elkins-Tanton[1], and E. Asphaug[1], [1]School of Earth and Space Exploration, Arizona State University (PO Box 876004, Tempe, AZ 85287-6004. Email: viranga@asu.edu), [2]Centre for Planetary Sciences, University of Toronto, Toronto, ON, Canada.

Introduction: A giant impact likely initiated the Moon formation process [1, 2]. After a number of refinements, the Canonical giant impact model is a low-velocity, glancing impact by a Mars-sized body [e.g. 3]. However, recent work on isotopic compositions of the Earth and the Moon have called the Canonical model into question [e.g. 4, 5]. This has led to other proposals for re-equilibrating isotopic compositions between the Earth and the proto-lunar disk [e.g. 6] and new giant impact scenarios [e.g. 7, 8]. Nevertheless, the basic premise that the Moon formed from a giant impact event does not seem to be in doubt [9].

A consequence of a giant impact origin is that the Moon would have formed partially or completely molten. Anorthosite fragments found in lunar samples support the past existence of a lunar magma ocean (LMO) [10]. Previous work found that it would have taken at least 10^7 years for the LMO to crystallize [11].

Previous LMO works have mostly ignored the effect of impacts. In this study, we investigate how impacts could have affected the crystallization of the LMO. While a fairly high background flux of impactors is expected in the early solar system, earliest bombardment of the Moon is dominated by re-impacting debris material that escaped the Earth-Moon system after the Moon-forming impact. In the Canonical model [3] about 10^{23} kg (1.3 lunar masses) of material have sufficient velocity to escape [12, 13]. That debris would subsequently return to the Earth-Moon system [13] and they should affect the thermal evolution of the Moon. New scenarios proposed for the Moon forming impact [e.g. 7, 8] are more violent events which would release more debris, thus the Canonical impact serves as a basis case.

Methods: For this work, we consider a one-dimensional thermal model for a spherically symmetric LMO. Initial LMO depth is set to 1000 km following [11] and, for simplicity, LMO density is set to a constant 3 g/cm^3. Small volume fractions of the LMO are crystalized iteratively at the boundary between the base of the LMO and the solid interior. Heat of fusion and secular cooling are accounted for with the rate of energy release determined self-consistently with surface conditions. Unlike [11], in this work, we consider a layer of quench crust (i.e. a thin rapidly crystallized surface layer, similar to the surface of lava lakes on Earth). Thus, there is always at least a thin conductive layer at the surface of the LMO. For each iteration, we also consider the mass of impactors that struck the surface (from [13]). The size of a punctured hole would depend on parameters such as impactor size, impactor velocity and on crustal thickness. However, estimating impactor size is difficult due to the lack of constraints. Therefore, at each iteration, we use a simple conversion factor to convert total impactor mass to a surface area of holes produced. This allows us to easily explore a wider range of parameter space. Early in the cooling process, energy released by crystallizing and cooling the LMO was released conductively through quench crust and through holes produced by impacts. The punctured crust would recover by recrystallization (quantified using the Stefan problem), with a hole considered closed once quench crust in the hole has re-attained the thickness of the surrounding crust. [11] found that plagioclase should become stable when the LMO depth is 100 km, thus at that point the model partitions the crystallizing material between the interior, the flotation crust, and closing of impact generated holes. Unlike the early phase of cooling, where holes were closed by forming new quench crust, in the later

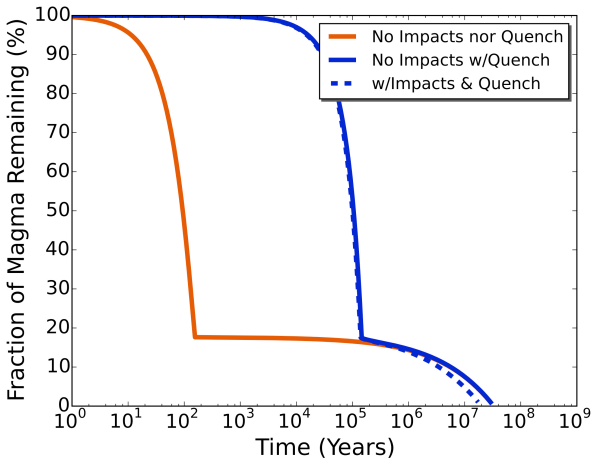

Figure 1: Fraction of magma ocean remaining over time for different scenarios. The orange line shows a scenario similar to [11] with the early thermal evolution governed by radiation (Flux $\propto$ Temp.^{4}), thus no quench crust, and the later evolution governed by conduction (due to flotation crust). Like [11], that scenario does not consider impacts. The blue lines show scenarios that have quench crust; therefore, the LMO cools only through thermal conduction. The broken blue line includes re-impacts.

stage holes are plugged from the bottom due to plagioclase buildup. Again, energy is released conductively through the crust while considering the crustal thickness. Note that we do not consider energy added to the LMO due to impacts since that is a minor effect. The iteration is terminated once only 1% of the initial LMO remains. This is similar to [11] and done to stop the evolution at the point when the remaining LMO is equated with the ur-KREEP layer (i.e. layer of incompatible elements composed of potassium, rare earth elements, and phosphorous) [14].

Results: In Figure 1, we show results for the cooling time of the LMO by plotting the fraction of LMO remaining over time. The orange line is a similar scenario to [11]; however, in this model, we do not consider the geochemistry of the crystallizing process (i.e. tracking variations in chemical composition due to fractional crystallization). Similar to [11], the LMO crystallizes rapidly in 10^2 years due to the surface flux being proportional to the forth power of the magma ocean surface temperature. In that scenario, though the initial cooling is rapid, the remaining 20% of the LMO takes about 10^7 years to crystallize. This is due to the conductive plagioclase lid that forms. When quench crust is considered (blue lines), the first 80% of the LMO takes considerably longer to cool (i.e. 10^4 years). Though quench crust delays the initial cooling process, without impacts, the overall cooling time is again about 10^7 years (solid blue line). Addition of re-impacts (broken blue line) reduces the cooling time by around a factor of 2, depending on the scaling of impactor mass to hole area. When comparing quench cases with and without impacts, the early stages are nearly identical since impact generated holes fill in with quench crust and recover quickly. Additionally, the latter cooling stage is sped up only by a small fraction since again holes do not stay open and release energy radiatively but rather are plugged by quench crust and newly formed plagioclase. Each scenario produced a global crustal thickness of about 40 km, which is consistent with the modeled average lunar crustal thickness using GRAIL gravity data [15].

Discussion: As compared to previous work [11], this work considered two effects that alter the total cooling time of the LMO in different directions. Quench crust serves to delay the initial cooling of the LMO, while re-impacts serve to quicken the cooling process by puncturing holes that allow more energy to escape from the LMO. The more intense the bombardment, the quicker the cooling should be. We used a conversion factor of $5 \cdot 10^6$ kg/m^2. It should be noted that this conversion factor is constant through time and groups complexities of impactor size and velocity, as well as crustal thickness and crust strength over time. The conversion factor should be taken as an average that allows us to convert incoming impactor mass to a surface area of holes without having to work out, for instance, the impactor mass distribution. Thus, the conversion factor should not be interpreted as predicting the size of hole generated by any individual impactor. Re-impacts puncturing holes into the nascent lunar crust possibly could have left detectable variations in crustal thickness, since it takes time for holes to be plugged by plagioclase buildup. Furthermore, the approximately 10^7-year cooling time of the LMO may imply that the $2 \cdot 10^8$-year range in lunar crustal ages is not solely a temporal record of the LMO crystallization. Rather, one way of interpreting the large range of crustal ages may be to classify the oldest ages as a record of the LMO crystallization and the younger ages as a record of recrystallization events after the initial LMO crystallization. We note that even after the LMO has fully crystallized the Moon will still be subject to intense bombardment by returning debris, which might re-melt portions of the surface.

Conclusions: (1) Quench crust has a significant effect on the LMO cooling process. (2) Re-impacting debris expedite the LMO cooling time by factor of 2 or more. (3) Crustal ages may span the re-impact timescale. Details of the LMO crystallization are important to the wider lunar science community. For example, if the LMO stayed fully molten for longer, it could have implications for the Moon's orbital elements and possibly its global shape [16].

Acknowledgements: We thank Mark S. Robinson and Travis S.J. Gabriel for helpful discussions. This work is supported by a NASA grant (NNX16AI31G).

References: [1] Hartmann, W.K. and Davis, D.R. (1975) *Icarus*, 24(4):504–515. [2] Cameron, A.G.W. and Ward, W.R. (1976) *LPSC*, 7:120–122. [3] Canup, R.M. (2004) *Annu. Rev. Astron. Astrophys.,* 42(1):441–475. [4] Zhang, J., et al. (2012) *Nat. Geosci.*, 5:251–255. [5] Touboul, M., et al. (2007) *Nature*, 450:1206–1209. [6] Pahlevan, K. and Stevenson, D.J. (2007) *Earth Planet. Sci. Lett.*, 262(3–4):438–449. [7] Cuk, M. and Stewart, S.T. (2012) *Science*, 338(6110):1047–1052. [8] Canup, R.M. (2012) *Science*, 338(6110):1052–1055. [9] Asphaug E. (2014) *Annu. Rev. Earth Planet. Sci.*, 42:551–578. [10] Wood, J.A., et al. (1970) *Geochim. Cosmochim. Acta*, 1:965. [11] Elkins-Tanton, L.T., et al. (2011) *Earth Planet. Sci. Lett.*, 304(3-4):326–336. [12] Marcus, R.A., et al. (2009) *Astrophys. J.*, 700(2): L118–L122. [13] Jackson, A.P. and Wyatt, M.C. (2012) *Mon. Not. R. Astron. Soc.*, 425 (1):657–679. [14] Borg, L.E., et al. (2014) *Meteorit. Planet. Sci.*, 50(4):715–732. [15] Wieczorek, M.A., et al. (2013) *Science*, 339(6120):671–675. [16] Garrick-Bethell, I., et al. (2014) *Nature*, 512:181–184.

DETERMINING THE RELATIVE TIMING OF FORMATION OF CHONDRULES VS PLANETARY EMBRYOS THROUGH EXPERIMENTS. A. M. Perez[1], S. J. Desch[1], D. L. Schrader[1], and C. B. Till[1], [1]School of Earth and Space Exploration, Arizona State University, P.O. Box 871404, Tempe, AZ 85287-1404, alexandra.m.perez@asu.edu

Introduction: Chondrules are major constituents in the most primitive meteorites called chondrites, and they provide valuable clues to understand the origins of the Solar System including the formation of planets. Specifically, they are key to understanding the energetic processes going on during the initial stages of the Solar System. Despite their importance, the formation mechanism(s) of chondrules has yet to be identified conclusively [1]. Deciphering such a mechanism can provide further clues pertaining to the timescale for accretion.

Chondrules display an array of textures that tell a story and these chondritic textures are the result of melting and crystallization, and refer to the overall appearance (size, shape, orientation, etc.) of larger grains within a matrix. The most common type of these igneous textures are porphyritic and can make up approximately 82 to 99% of all chondrules in a given chondrite group [2]. Porphyritic textures are defined as euhedral to subhedral phenocrysts set within a fine grain matrix. Important parameters that control chondrule textures include grain size, peak temperature, heating duration, and cooling rate. Specifically, the retention of nucleation sites is a very important parameter in the formation of porphyritic textures. Due to the complete dominance of porphyritic textures in the chondrule population, astrophysical models must be able to predict these textures.

The nebular shock models are currently the most favored as a chondrule formation mechanism, which include large-scale (spiral density wave) shocks and by bow shocks around planetary embryos. We are investigating the planetary embryo bow shock model and cooling rates associated with this model are predicted to be > 1000 K/hr and often are > 3000 K/hr [1]. These fast cooling rates are due to radiation escaping to cooler regions along with chondrules cooling as the traverse pass the gas-cushioned planetary embryo. Previous investigations of cooling rates are shown in Figure 1 and it is unclear on whether or not porphyritic textures can be reproduced at such higher end cooling rates.

The planetary embryo bow shock model meets all the thermal constraints required for an ideal chondrule formation mechanism. Some of these constraints include ambient temperature, heating duration, and peak temperature [5]. First, the ambient temperature is less than 650 K based on the presence of sulfur in the melt. Next, the model predicts a heating duration of less than

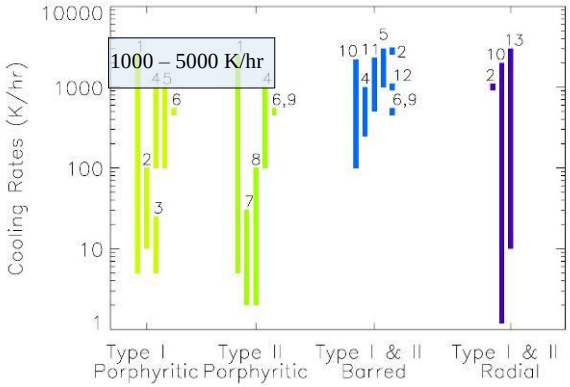

Figure 1. Cooling rates previously investigated to produce chondritic textures [5]. The shaded region shows the cooling rates being investigated here.

10 minutes which is determined by the evaporation of volatiles such as Na and K as well as the lack of isotopic fractionation. Lastly, the model agrees with a peak temperature above the liquidus. This is an attractive model, but porphyritic textures have only been reproduced at cooling rates upwards to 2500 K/hr [6]. This supports that accretion was very rapid. If porphyritic textures can be reproduced at cooling rates consistent with the planetary embryo bow shock model, the model can be validated as a chondrule formation mechanism. However, it is presumed that chondrules are the building blocks of planets, but validating this model as a formation mechanism would suggest that the accretion of planetary embryos must have taken place before the formation of chondrules. To address this, we have conducted vertical furnace experiments to investigate cooling rates consistent with the planetary embryo bow shock model in an effort to reproduce porphyritic textures and determine the relative timing of formation of chondrules versus planetary embryos.

Approach: To experimentally investigate the planetary embryo bow shock model, we have created experimental chondrule analogs by mixing natural mineral separates of olivine, diopside, and albite to produce bulk compositions similar to chondrules as well as those used in previous experiments [6, 7] as shown in Table 1. The liquidus for our bulk composition is calculated to be 1608°C [8]. We have investigated experimental starting mixes with grains sizes of 63-90 μm and 212-250 μm, as well as peak experimental temperatures at the liquidus and liquidus ±50° C. We chose heating durations of 1,5, and 10 minutes, durations

consistent with the thermal constraints of chondrule formation.

Table 1. EPMA analysis of precursor material. Precision is 1% for major elements.

Oxide	San Carlos Olivine (wt %)	Amelia Albite (wt %)	Dog Lake Diopside (wt %)	Analog (wt%)
SiO_2	40.89	68.55	55.52	49.99
TiO_2	n.a.	n.a.	0.04	0.01
Al_2O_3	n.a.	20.09	0.03	5.03
FeO	9.07	n.a.	0.75	5.55
Cr_2O_3	0.02	n.a.	n.a.	0.01
MnO	0.12	n.a.	0.07	0.01
MgO	50.26	n.a.	18.50	32.93
CaO	0.07	0.46	26.04	4.06
Na_2O	n.a.	11.69	0.06	2.93
K_2O	0.01	0.12	n.a.	0.04
TOTAL	*100.44*	*100.91*	*101.01*	*100.65*

Cooling rates investigated include 1000, 3000, and 5000 K/hr. The analogs are placed in Pt baskets suspended from a thermocouple inside a 1 atmosphere vertical gas mixing furnace located at the Experimental Petrology and Igneous process Center (EPIC) at ASU, and undergo various parameter combinations. After melting and cooling, the analogs are mounted in epoxy, polished, and carbon coated for electron probe microalysis.

Results: To begin the investigation, we have used known parameters to reproduce porphyritic textures consistent with the results of previous studies [6,9,10] (Figure 2).

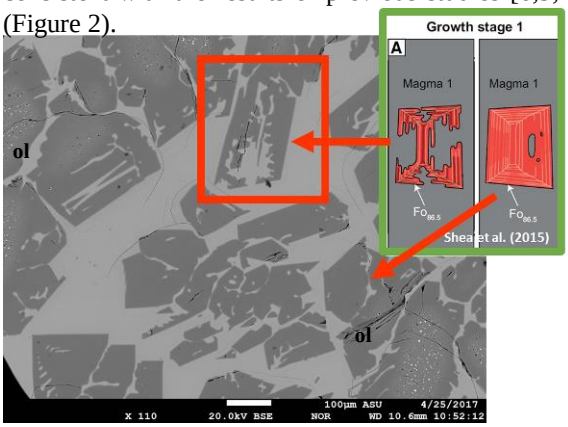

Figure 2. BSE image of an experimental run with a cooling rate of 1000 K/hr. The secondary image shows the rapid growth of olivine in terrestrial rocks [11]. This result shows several skeletal grains as well as more matured grains that had essentially "filled" in. The overall texture shown is porphyritic.

Results show a continuum of textures at cooling rates around 5000 K/hr (Figure 3). Despite using identical parameters, we observe different textures emphasizing the importance of grain size. So far, we have not seen porphyritic textures at cooling rates above 1000 K/hr with the given set of parameter combinations. However, the planetary embryo bow shock model can be associated with lower cooling rates than expected if dust evaporation is present and models have shown a similar cooling rate at approximately 2000 K/hr through the crystallization range [1].

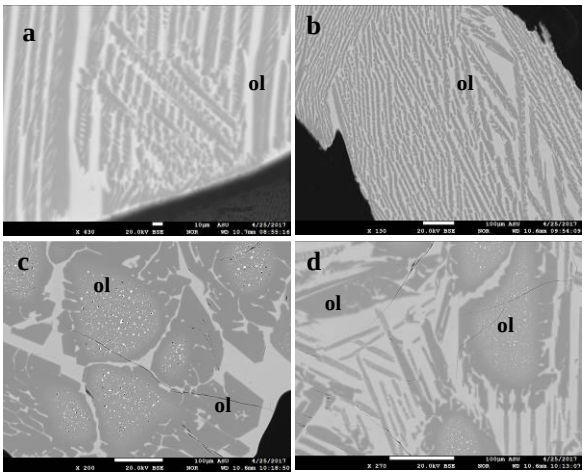

Figure 3. BSE images using a cooling rate of 5000 K/hr with a,b,c having identical parameter combinations. a) b) Spinifex-like texture, a term used to describe quench crystals. c) Possibly larger relict grains with former skeletal grains that have matured d) Combination of possible relict grains and spinifex texture

Ongoing Work: We are continuing to investigate our current set of parameters. In addition, we are further investigating the role of seed nuclei by incorporating spinel into our starting bulk composition. By successfully reproducing porphyritic textures consistent with the planetary embryo bow shock model, we can further understand the timescales for accretion.

References: [1] Mann C. R. et al. (2016) *Astrophysical Journal, 818(2).* [2] Jones R. H. (2012) *Meteoritics & Planet. Sci., 47(7),* 1176-1190. [3] Hood L. L. and Weidenschilling S. J. (2012) *Science, 279,* 681-684. [4] Boley et al. (2013) *Astrophysical Journal, 776(2).* [5] Desch S. J. et al. (2012) *Meteoritics & Planet. Sci., 47(7),* 1139-1156. [6] Lofgren G. and Russell W. J. (1986) *Geochimica Et Cosmochimica Acta, 50(8),* 1715-1726. [7] Hewins R.H. and Fox G.E. (2004) *Geochimica Et Cosmochimica Acta, 68(4),* 917-926. [8] Herzberg C. T. (1979) *Geochimica Et Cosmochimica Acta, 43,* 1241-1251. [9] Hewins R. H. et al. (2005) *Chondrites and the Protoplanetary Disk, 341,* 286-219. [10] Radomsky P. M. and Hewins R. H. (1990) *Geochimica Et Cosmochimica Acta, 54(12),* 3475-3490. [11] Shea T. et al. (2015) *Geology, 43(10),* G37082.

A ROLE OF JUPITER IN THE PROCESS OF THE TERRESTRIAL TYPE PLANETS BOMBARDING BY THE SOLAR SYSTEM PERIPHERAL SMALL BODIES. N. I. Perov[1]. [1]State Autonomous Organization of Cultural and Education named after V.V. Tereshkova. 150000, Russia, Yaroslavl', Chaikovskogo str., 3. E-mail: perov@yarplaneta.ru

Introduction: In the work [1] the migration of comets from Oort's and Hill's clouds to the terrestrial type planets has been considered. The mass of the perturbed bodies has been in dozens times less then the mass of the Moon The perihelion distance of the perturbed bodies has been equal to 10^4. Here we also determine the conditions of collisions of small bodies and the terrestrial type planets. Jupiter with the circle orbit is the perturbed body. The initial perihelion distance of the small bodies with initial unperturbed parabolic orbit equals 10^1 AU. The region of the initial positions of Jupiter in which the parabolic orbits of the small bodies transform into the elliptical orbits of the terrestrial type planets crossers is investigated.

Fundamental Equations: In the frame of the planar circular restricted 3 body problem (the Sun – Jupiter – the small body) the vector differential equation of the small body motion is

$$d^2\mathbf{r}/dt^2=-Gm_S\mathbf{r}/r^3-Gm_J(\mathbf{r}-\mathbf{r}_J)/|\mathbf{r}-\mathbf{r}_J| \quad (1)$$

Here, $\mathbf{r}$ and $\mathbf{r}_J$ are the heliocentric radii - vectors of the small body and Jupiter, G is gravitational constant, m_S and m_J are mass of the Sun and Jupiter correspondingly. t is the Newtonian time. r_J=5.2 AU.

Using the system of the units in which the semi major axis of the Earth's orbit a_E=1 AU, m_S=1, G=1 and independent variable is the true anomaly of the Earth (v_E), which is measured from axis of abscissas. The equation of (1) may be presented in the form

$$d^2\mathbf{r}/dt^2=-\mathbf{r}/r^3-m'_J(\mathbf{r}-\mathbf{r}_J)/|\mathbf{r}-\mathbf{r}_J|^3. \quad (2)$$

where m'_J is m_J/m_S.

Let's denote by letter φ an angle between the x-axis and the initial position of Jupiter. At this angle the small body must cross the orbit of a terrestrial type planet. Let $r_{(J\text{-}c)min}$ is a minimal distance between Jupiter and the small body, $r_{(S\text{-}c)min}$ is a minimal distance between the Sun and the small body.

Numerical Experiments: The initial conditions of the small body moving along the heliocentric parabolic orbit (that is unperturbed only in initial moment of time) are following x_0= 34.000000000000000000000 (units of length), y_0=21.0713075057054776968028 (units of length), $(dx/dv)_0$ = -0.21505813167606566929323 (units of length/units of time), $(dy/dv)_0$ =-0.061237243569579452454932 0 (units of length / units of time). In the table 1 and in the figures (1–5) the results of integrating of the equation (2) are presented.

Table 1.

The minimal distances between the small bodies and the massive bodies for parameter φ'

φ'=-8.72323 rad

$r_{(S\text{-}c)min}$ =0.9639AU; v_E=191.04 rad.

$r_{(J\text{-}c)min}$=0.00014 AU < R_J, v_E=123.9538005 rad.

φ'=-8.7247523821 rad

$r_{(S\text{-}c)min}$ =0.98545AU; v_E=132.825 rad.

$r_{(J\text{-}c)min}$=0.01631 AU >R_J, v_E=123.9695 rad.

φ'=-8.7271 rad

$r_{(S\text{-}c)min}$ =0.98545AU; v_E=132.825 rad.

$r_{(J\text{-}c)min}$=0.01631 AU >R_J, v_E=123.9695 rad.

It should be noted that angular diameter of Jupiter equals 0.0018 rad for the Earth's observer, and so, any of small and fall down Jupiter bodies, moving along straight lines trajectories do not cross orbits of the terrestrial type planets.

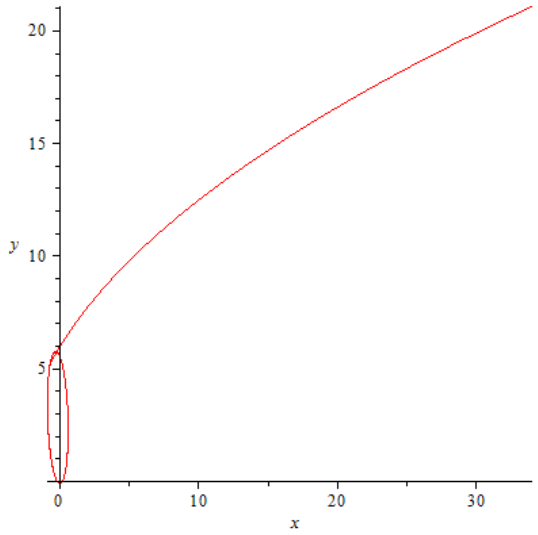

Fig. 1. Transitions of the small bodies from the heliocentric parabolic orbits into a jovocentric trajectory and in a heliocentric elliptical orbit (after approaching Jupiter). φ' = -8.7247523821 rad. i=0°. $r_{(J\text{-}c)min}$ = 0.004999 AU, 0<v_E<200 rad. Radius of Jupiter equals R_J = 0.00047789444440 AU. $r_{(Sun\text{-}c)min}$ = 0.095 AU, v_E=133.45 rad.

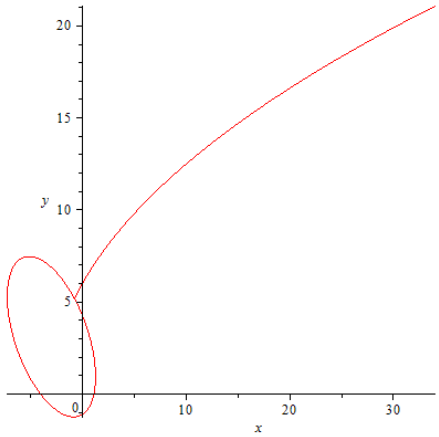

Fig. 2. A heliocentric trajectory of the small body. $0<v_E<200$ rad. $\varphi'=-8.72323$ rad. $r_{(Sun\text{-}c)\ min}=0.9639$ AU, $v_E=191.04$ rad. Minimal distance between Jupiter and the small body equals 0.00014 AU < R_J, $v_E=123.9538005$ rad.

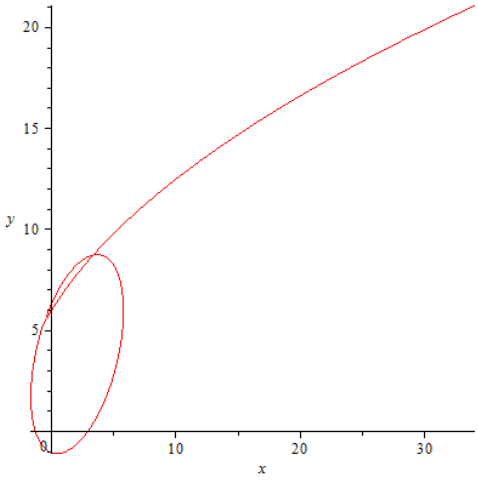

Fig. 3. A heliocentric trajectory of the small body. $0<v_E<200$ rad. $\varphi'=-8.7271$ rad. $r_{(Sun\text{-}c)\ min}=0.98545$ AU, $v_E=132.825$ rad. Minimal distance between Jupiter and the small body equals 0.01631 AU > R_J, $v_E=123.9538005$ rad.

Conclusion: 1. The corresponding "key holes" for the considered small bodies which must cross the orbits of the terrestrial type planets, after approaching Jupiter, are equal approximately 0.004 rad (-8.7271 рад < φ'< -8.72323 рад), that is in comparison with the angular diameter of Jupiter (0.0018 rad for the Earth's observer). 2. For the extremal cases, the elliptical orbits of the bodies (initially moving along the parabolic orbit) are symmetrical in respect of the axis of ordinates (Fig.2 and Fig. 3). 3. The perturbed bodies with mass that in dozens time less than mass of the Moon are also transfer of the small bodies to the region of terrestrial type planets, but the corresponding "key holes" are less in thousands times [1].

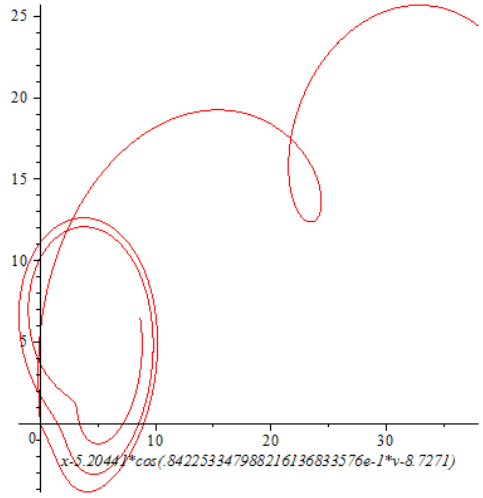

Fig. 4. Jovocentric trajectory of the small body. φ'=-8.7271 rad. $0<v_E<300$ rad. Minimal distance between the Sun and the small body equals 0.98545 AU, $v_E=132.825$ rad. Minimal distance between Jupiter and the small body equals 0.01631 AU > R_J, $v_E=123.9538005$ rad.

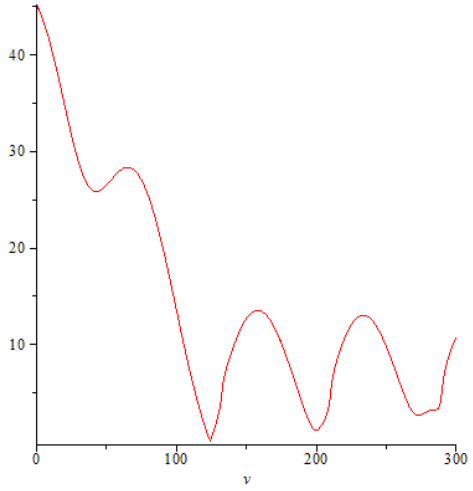

Fig. 5. A distance between the Sun and the small body. $0<v_E<300$ rad. $\varphi'=-8.7271$ rad. $r_{(Sun\text{-}c)\ min}=0.98545$ AU, $v_E=132.825$ rad. Minimal distance between Jupiter and the small body equals 0.01631 AU > R_J, $v_E=123.9538005$ rad.

References: [1] Perov N. I. (2016) *LPS. IIIL*, Abstract #1010.

ON THE NEED OF CONSTRAINING THE ^{244}PU CONTENT OF THE EARLY SOLAR SYSTEM.

M. K. Pető[1] and M. A. Lugaro[1], [1]Konkoly Observatory, Hungarian Academy of Sciences (maria.k.peto@mta.cskf.hu)

The increasing knowledge of both stable and short-lived radioactive isotope systems allows us to study the origin and early evolution of matter in the Solar System (SS) [1-3]. Technological advances over the last decade have led to a highly improved characterization of nucleosynthetic components (carrier phases) and their variability in meteorites [4], and the results have been used to model nucleosynthesis in different stellar environments [e.g. 5]. Using the short-lived radionuclides we can now investigate temporal constraints on the last astrophysical events that added freshly synthesized material to the matter in the interstellar medium that ended up in the SS and constrain the isolation time of the star-forming cloud where the Sun was born [6]. We can trace processes (e.g., production of ^{26}Al) in massive stars within this stellar nursery and constrain the pre-solar history of the SS matter. Importantly, short-lived isotope sytems may constrain the timing of element fractionation during the first few hundred million years following the formation of the first condensed mineral assemblages from the hot solar nebula, the material processing in the proto-planetary disk, as well as early planetary differentiation events such as core formation, large scale silicate melting, and major volatile depletion events [7].

However, in order to obtain a consistent picture of the earliest processes shaping our SS, the initial abundance of each short-lived radionuclide at the time of the formation of the Sun has to be inferred with very high accuracy. Specifically, we plan to improve the current estimates of the initial ^{244}Pu abundance of the SS and to apply the Pu-Xe system to both pre-solar and terrestrial chronometry.

^{244}Pu is an extinct actinide with a half-life of 81 Ma produced exclusively by the rapid neutron-capture (r) process, and whose presence is recorded in the xenon isotope spectrum of early-formed solids [7]. Due to the atmophile nature of noble gases, the ^{244}Pu-Xe chronometer has a great potential to date early volatile depletion events, however, the initial ^{244}Pu abundances estimated from equilibrated ordinary chondrites and angrites vary by almost a factor of two [8,9]. Further, the two estimates have complementary caveats: i) The direct approach [8] involved analysis of neutron irradiated samples of the St Severin equilibrated ordinary chondrite (LL6). The induced fission of ^{235}U produces fissiogenic Xe isotopes in different proportions to Pu. With this method an initial $(^{244}Pu/^{238}U)_{o.SS}$ ratio of 0.007±0.001 (2σ) at 4567 Ma was obtained directly from Xe measurements of stepwise heating experiments (and the $(^{235}U/^{238}U)_{o.SS}$ value). However, St Severine has a complicated and heterogeneous lithology, and may not be representative of the bulk SS composition ii) The indirect approach [9] involved analysis of pyroxene and whitlockite phases of the Angra dos Reis angrite using ^{150}Nd as a reference isotope. This resulted in a significantly lower value of the initial $(^{244}Pu/^{238}U)_{o.SS}$ ratio of 0.0044±0.001 (2σ) at 4567 Ma. This approach, however, measured the absolute abundances of Nd on aliquots separate from the Xe analysis.

We show that current noble gas, REE and absolute age data on different volatile depleted meteorites do not improve the current estimate of the initial $(^{244}Pu/^{238}U)_{o.SS}$ ratio, but calls for a new comprerhensive set of experiments. We outline our new approach that should establish reproducible differences, if any, between volatile depleted mineral separates, igneous differentiated meteorites, ordinary chondrites, and CAIs. We present simple volatile degassing models that consider recent findings in solid Earth noble gas geochemistry [10,11,12,13] and highlight the importance and the several implications of an updated estimate of the initial value: from constraints on the r-process site, to the birth of the Sun and the timing of the Moon Forming Giant Impact.

References: [1] Dauphas N. et al., (2015) *EPSL, 427*, p. 236-248. [2] Burkhardt, C. Schönbächler, M., (2015) *GCA, 165*, 361-375. [3] Dauphas N. and Chaussidon M., (2011) *AR EPS, 39*, 351-386. [4] Nitler L. R. and Ciesla F. (2016) *Annu. Rev. Astron. Astrophys. 54*, 53-93. [5] Lugaro M. et al. (2003), *ApJ, 593*, 486. [6] Lugaro M. et al. (2014), *Science, 345*, 650-652. [7] Carlson R. W and Boyet M., (2009) *EPSL, 279*, 147-156. [8] Hudson, G. B. et al. (1989) *LPSC, 19*, 547-554. [9] Lugmair G. W. and Marti K. (1977) *EPSL, 35*, 273-284. [10] Mukhopadhyay S. (2012) *Nature, 486*, 101-104. [11] Pető M. K. et al. (2013) *EPSL, 369*, 13-23. [12] Caracausi et al., (2016) *Nature, 533*, 82-85.[13] Marty B. et al., *Science, in press.*

REDOX VARIATIONS IN EARLY SOLAR SYSTEM MATERIALS AND IMPLICATIONS FOR LATE STAGE PLANETARY ACCRETION AND PLANET FORMATION. K. Righter[1], [1] Mailcode XI2, NASA Johnson Space Center, Houston, TX 77058; kevin.righter-1@nasa.gov.

Introduction: Oxygen fugacity plays an important role in determining the detailed physical and chemical aspects of planets and their building blocks. Basic chemical properties such as the amount of oxidized Fe in a mantle (as FeO), the nature of alloying elements in the core (S, C, H, O, Si), and the solubility of various volatile elements in the silicate and metallic portions of embryos and planets can influence physical properties such as the size of the core, the liquidus and solidus of the mantle and core, and the speciation of volatile compounds contributing to atmospheres. This paper will provide an overview of the range of fO_2 variation observed in primitive and differentiated materials that may have participated in accretion (cosmic dust, Stardust and meteorites), a comparison to observations of planetary fO_2 (Mercury, Mars and Earth), and a discussion of timing of variation of fO_2 within both early and later accreted materials. This overview is meant to promote discussion and interaction between students of these two stages of planet formation to identify areas where more work is needed.

The record in primitive materials: A wide range of fO_2 is recorded in primitive materials ranging from the most reduced enstatite chondrites and CAIs both recording fO_2 near IW-7, to the most oxidized IDPs and dust particles that record fO_2 near or just above the IW buffer [1]. Between these two end members are a nearly continuous range of fO_2 recorded in ordinary, R, and carbonaceous chondrites, Stardust particles, and chondrules (references in [1]; Figure 1).

The record in planets: All planets experienced reducing conditions that allowed a core to form, but do not necessarily retain that early reduced nature, as crustal and magmatic products on Mars and Earth are generally more oxidized than the conditions during core formation [2]. Mercury seems well defined between IW-7 and IW-4, the most reduced planet in our inner solar system [3]. Mars has a significant range of fO_2 from IW to FMQ+1 [4]. Earth shows the largest variation in fO_2 - nearly 10 log fO_2 units - from near IW buffer to as high as the HM buffer [5,6]. The causes of variation in planetary materials is discussed further below.

Processes that change fO_2: Nebular processes, such as chemical gradients or variation in volatile speciation may cause early variations in fO_2 in materials [7]. Physical transport of materials from one part of the nebula to another may also cause redox variation [8]. Such early records can be modified by heating (thermal metamorphism) or fluid alteration (aqueous alteration on parent bodies) [9,10].

Pressure variation does not produce fO_2 variation in most cases, but if graphite or diamond is present, the C phases and co-existing gas can cause large fO_2 variation with small pressure changes compared to standard metal-oxide equilibria (e.g., ureilites and R-chondrites; [11,12]). High pressure equilibria in planetary interiors have potential to change fO_2, whether the equilibria involve solids [13,14] or liquids [15,16], but much work remains to understand multi-component rather than simple two or three component systems (e.g., Fe-S or Fe-S-C) or reduced peridotitic melts rather than evolved oxidized MgO-poor melts.

Timing: Variations in elemental valence of V and Ti have been observed in chondritic materials, and attributed to both oxidation and reduction processes. Transient behavior has been proposed for many of these, and such observations have been made in carbonaceous, ordinary, and enstatite chondrites indicating a widespread phenomenon [17-19]. A connection between oxygen isotopes, oxygen fugacity, and dust:gas ratios in the solar nebula has been proposed and argued based on measurements in CR chondrites, and constrained within the first several Ma of solar system [7].

Variations in fO_2 have also been proposed for the later planet formation stage, but there is not consensus. Some argue for early reducing and later oxidized, as championed by early accretion models for Earth [20] and utilized more recently [21,22]. Early oxidized followed by later reduction was proposed by [23], and shown to be a possible consequence of deep metal-silicate equilibria [15,24]. However, the latter study also highlighted uncertainties in high pressure properties of silicate melts that allow for little to no change in fO_2 resulting from deep metal-silicate equilibria [15,24].

Outstanding questions: There are plenty of outstanding questions and avenues for future research to help understand the chemical and physical environments and the causes of fO_2 variation.

First, how oxidized was the early nebula – some matrix material has high Fe^{3+} [25], but it is unclear what environment or how high fO_2 was to generate this

material. Second, the role of pressure in Fe redox equilibria – both Fe-FeO in embryos and planets, and later FeO-Fe_2O_3 equilibria in planets – is poorly constrained, as is the controlling role of volatiles and volatile speciation at pressure. To what extent do dust and sub-meter sized materials become completely transformed by higher temperature and pressure processes, thus erasing any nebular or primitive redox signature? Third, during oligarchic growth, the role of relative mass and volatiles in controlling redox equilibria needs to be better defined. For example, if there is an impact between two bodies with a target:impactor mass ratio of 7:3, involving a reduced target and oxidized impactor, what is the fO_2 of the resulting body? Does the more massive body "win", or is the resulting body simply a mix of the two? This is currently unknown. And fourth, what is the role of heliocentric distance? Was the inner solar system uniform from Mars inwards, or was there nonetheless variation? [26].

References: [1] Righter, K. et al. (2016) *American Mineralogist* 101, 1928-1942. [2] Righter, K. et al. (2008) *Met. Planet. Sci.* 43, 1709-1723. [3] McCubbin, F. et al. (2012) *Geophysical Research Letters* 39. [4] Righter, K. et al. (2014) *American Mineralogist* 99, 2313-2319. [5] Righter, K. et al. (2006) MESS II (ed. D. Lauretta and H.Y. McSween, Jr.), Univ. of Arizona Press, Tucson, 803-828. [6] Carmichael, I.S.E (1991) *Contributions to Mineralogy and Petrology* 106, 129-141. [7] Tenner, T. et al. (2015) *Geochimica et Cosmochimica Acta* 148, 228-250. [8] Dyl, K. et al. (2011) *Geochimica et Cosmochimica Acta* 75, 937-949. [9] Kessel, R. et al. (2004) *Meteoritics & Planetary Science* 39, 1287-1305. [10] Zolotov, M. et al. (2006) *Meteoritics & Planetary Science* 41, 1775-1796. [11] Goodrich, C.A. et al. (1992) *Meteoritics & Planetary Science 27*, 327-352. [12] Righter, K and Neff, K. (2007) *Polar Science* 1, 25-44. [13] Frost et al. 2004 *Nature 428*, 409-412. [14] Boujibar, A. et al. (2016) *American Mineralogist* 101, 1560-1570. [15] Righter, K. and Ghiorso, M.S. (2012) *Proc. Nat. Acad. Sci.* 109, 11955-11960. [16] Zhang, H. et al. (2017) *Geochimica et Cosmochimica Acta* 204, 83-103. [17] Paque et al. (2013) *Meteoritics & Planetary Science* 48, 2015-2043. [18] Simon, S. et al. (2016) *Geochimica et Cosmochimica Acta* 189, 377-390. [19] Ihinger, P. and Stolper, E. (1986) *Earth and Planetary Science Letters* 78, 67-79. [20] Wänke, H. et al. (1984) In *Archaean Geochemistry* (pp. 1-24). Springer Berlin Heidelberg. [21] Rubie, D.C. et al. (2011) *Earth and Planetary Science Letters 301*, 31-42. [22] Wood, B.J. (2008) *Philosophical Transactions of the Royal Society of London A: Mathematical, Physical and Engineering Sciences, 366*, 4339-4355. [24] Siebert, J. et al. (2013) *Science 339*, 1194-1197. [24] Righter, K. and Ghiorso, M.S. (2012b) *Proc. Nat. Acad. Sci. 109*, 16749-16750. [25] Stodolna, J. et al. (2013) *Geochimica et Cosmochimica Acta, 122*, 1-16. [26] Burkhard, C. et al. (2017) *Meteoritics & Planetary Science* 52, 807-826.

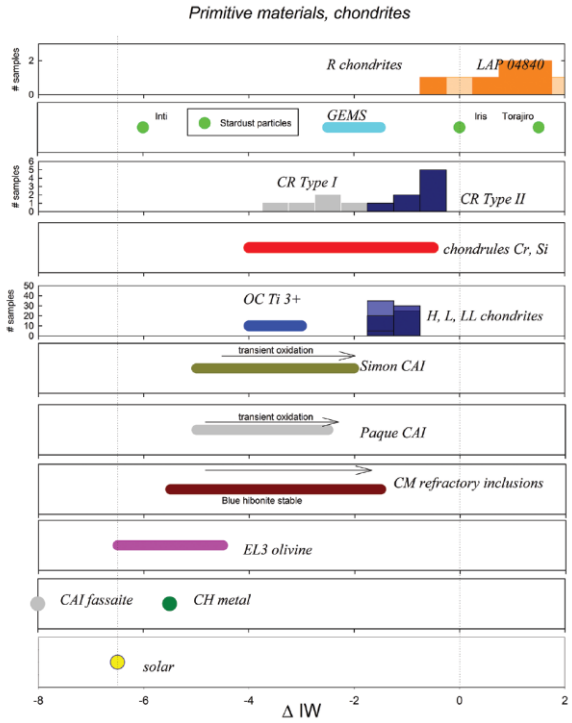

Figure 1: Range of oxygen fugacity (fO_2 relative to the IW buffer) recorded in various primitive materials and chondrites. Total range of all materials is nearly 10 orders of magnitude, which makes fO_2 an important intensive parameter for understanding the early solar system. Figure from [1].

Forming the Cold Classical Kuiper belt by Collisional Pebble accretion, Considering the Hot. Andrew Shannon[1,2], Yanqin Wu[3], Yoram Lithwick[4,5], and Rebekah Dawson[1,2], [1]Department of Astronomy & Astrophysics, The Pennsylvania State University, State College, PA, USA, [2]Center for Exoplanets and Habitable Worlds, The Pennsylvania State University, State College, PA, USA, [3]Department of Astronomy and Astrophysics, University of Toronto, Toronto, ON, Canada, [4]Department of Physics and Astronomy and Center for Interdisciplinary Exploration and Research in Astrophysics (CIERA), Northwestern University, Evanston, IL, USA.

Kuiper Belt objects are conventionally thought to have grown by the pairwise collision of planetesimals within a massive belt that contained tens of earth masses of material [1,2,3], a few thousand times its present-day mass. We show that this picture very generically results in a low efficiency of forming large bodies, making it incompatible with Neptune's migration history[4], and the survival of the long-period binaries[5]. It would also necessitate debris disks parent bodies growing in a different fashion from Kuiper Belt objects[6], which seems a dubious preposition. We present a new model for the growth of Cold Classical Kuiper Belt objects, where most of the primordial mass begins in grains of centimeter size or smaller. These grains collide frequently and maintain a dynamically cold belt out of which large bodies grow efficiently. While pairwise growth of large planetestimals is only ~0.1% efficient in making big bodies in the Kuiper belt, this collisional 'pebble-accretion' model can result in order-unity of the solid mass being converted into large bodies. This high efficiency can address all the problems posed for in-situ formation of the Cold Classical Kuiper belt. This scenario may also account for the high binary fraction of Cold Classical Kuiper belt objects [7], and their flattened mix of prograde and retrograde orbits [8]. While considering the Hot populations is complicated by the fact that much of the information on where they formed and under what conditions was lost when they were scattered outwards [9], we develop dynamical constraints on the high mass end of the primordial Hot population as a precursor to evaluating whether its growth is compatible with collisional pebble accretion.

References: [1] Kenyon S. J. and Luu J. X. (1998) *AJ*, *115*, 2136–2160. [2] Ormel C. W. et al. (2010) *Icarus*, *210*, 507-538. [3] Schlichting H. E. and Sari R. (2011) *ApJ* , *728*, 63. [4] Gomes R. S. et al. (2004) *Icarus*,*170*, 492. [5] Parker A. H. and Kavelaars J. J. (2012) *ApJ*, *744*, 139 [6] Shannon A. and Wu Y.(2011) *ApJ*, *728*,68 [7] Fraser W. C. (2017) *Nature Astronomy*, *1E*, 88F [8] Parker A. H. et al. (2011) *ApJ*, *743*, 1 [9] Levison H. F. et al. (2008) *Icarus*, *196*, 258-273

PLANETESIMAL FORMATION IN PROTOPLANETARY DISKS. J. B. Simon[1,2], P. J. Armitage[1,3], A. N. Youdin[4], R. Li[4], [1]JILA, University of Colorado and NIST, 440 UCB, Boulder, CO 80309-0440, [2]Department of Space Studies, Southwest Research Institute, Boulder, CO 80302, [3]Department of Astrophysical and Planetary Sciences, University of Colorado, Boulder, [4]Department of Astronomy and Steward Observatory, University of Arizona, 933 North Cherry Avenue, Tucson, AZ 85721

Introduction: Planetesimals are the precursors to planets, and understanding their formation is an essential step towards developing a complete theory of planet formation, whether it be that of our own solar system or of the many extrasolar planetary systems discovered in recent years. Furthermore, a detailed understanding of planetesimal formation is necessary for explaining the observed properties of asteroids and Kuiper Belt objects.

Traditional theories attempt to explain planetesimal formation from a "bottom-up" approach; small particles (e.g., dust grains) continually grow upward in mass and scale, finally reaching gravitationally bound objects. For these small solid particles to coagulate into planetesimals, however, requires that these particles grow beyond centimeter sizes; with traditional coagulation physics, this is very difficult [1,2]. The streaming instability [3,5], however, generates sufficiently dense clumps of these smaller constituents that the mutual gravity between the particles eventually causes their collapse towards planetesimal mass and size scales.

Results: Here, we present a series of high resolution, first principles numerical simulations of protoplanetary disk gas and dust to examine in detail, the formation of planetesimals and their resulting size frequency distribution. We find that their differential size distribution can be well-modeled as a power law with power law index -2.8. This equates to a top-heavy distribution, with most of the mass in the largest objects (see Figure 1). This power law index is robust to resolution, initial particle size and concentration, relative strength of gravity to tidal shear, and conditions prior to collapse. We present tentative evidence that this universality can be tied to the power spectrum of particle mass density prior to collapse.

References: [1] T. Birnstiel et al. (2010) *A&A,* 513, A79. [2] J. Blum & G. Wurm (2008), *ARA&A*, 46, 21. [3] A. Johansen et al. (2007), *Natur*, 448, 1022. J. B. Simon et al. (2016), *ApJ*, 822, 55 [5] A. N. Youdin, & J. Goodman, (2005), *ApJ*, 620, 459.

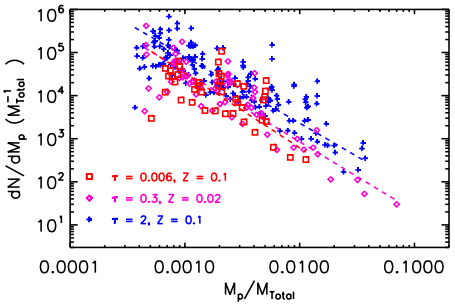

Figure 1 - The initial differential planetesimal mass function derived from simulations with different particle Stokes numbers, τ, and concentrations, Z. The simulation with the smallest particles (τ = 0.006, red) forms a significantly smaller total mass of planetesimals during the duration of the run, but no significant differences in the slope of the derived mass function are observed. The best fit power law is overplotted as dashed lines. (This figure is a modified version of Fig. 2 in [4]).

Utilizing Stable Isotopes and Isotopic Anomalies to Study Early Solar System Formation Processes. J. I. Simon, Center for Isotope Cosmochemistry and Geochronology, Astromaterials Research and Exploration Science Division, EISD-XI3, NASA Johnson Space Center, Houston, TX 77058, USA (justin.i.simon@NASA.gov).

Introduction: Chondritic meteorites contain a diversity of particle components, i.e., chondrules and calcium-, aluminum-rich refractory inclusions (CAIs), that have survived since the formation of the Solar System. The chemical and isotopic compositions of these materials provide a record of the conditions present in the protoplanetary disk where they formed and can aid our understanding of the processes and reservoirs in which solids formed in the solar nebula, an important step leading to the accretion of planetesimals.

Isotopic anomalies associated with nucleosynthetic processes are observed in these discrete materials, and can be compared to astronomical observations and astrophysical formation models of stars and more recently proplyds, e.g., [1]. The existence and size of these isotopic anomalies (e.g., [2]) are typically thought to reflect a significant state of isotopic heterogeneity in the earliest Solar System, likely left over from molecular cloud heterogeneities on the grain scale [3], but some could also be due to late stellar injection (e.g., [4]). The homogenization of these isotopic anomalies towards planetary values can be used to track the efficiency and timescales of disk wide mixing, e.g., [5-7].

Mass-dependent fractionation recorded by the isotopic compositions of early formed solids is primarily controlled by chemical volatility. Evaporation/sublimation are well understood through both theory and experimental work, but until recently we've only had a qualitative understanding about the fractionation effects of condensation (see [8, 9]).

I will present several "case studies" that emphasize the useful insights that can be had, and the complexity of the stable isotope records contained in early formed astromaterials. These isotopic records reflect the temperatures, pressures, and gas compositions in which early formed solids originated, as well as, the timing in which these particles exchanged with different nebular gas reservoirs. In combination with theoretical models of isotopic fractionation, these results can be used to critically test assumptions and input parameters (i.e., temperature, pressure, nebular gas composition, and timescale) of contrasting astrophysical models of protoplanetary disk evolution.

Analytical Background: Many current isotopic discoveries are possible because of improvements in analytical methods. These either reflect advancements in precision (e.g., calcium, [9]), spatial resolution (e.g., oxygen [10]), or a bit of both (e.g., magnesium [11]). It is common for these measurements to be made in conjunction with radiogenic dating methods (see Wadhwa, this workshop) and we strive to integrate all of these isotopic measurements into their petrological context.

Theoretical Background: The anomalous distribution of oxygen isotopes among planetary materials is a fundamental chemical feature of the Solar System [12]. Mass independent variations in ^{16}O relative to ^{17}O and ^{18}O (expressed as deviations from the terrestrial mass-fractionation line, $\Delta^{17}O$) is commonly ascribed to photochemical self shielding by CO, which produces ^{16}O-depleted H_2O, and because this H_2O gas readily exchanges with silicate minerals. The isotopic signature of CO self shielding is likely a function of position and time in the protoSolar disk [13]. It can be argued that heterogeneities in early formed solids reflect their evolutionary history in the nebula, although later parent body alteration can certainly obscure this history.

Theoretical and experimental studies imply that evaporative residues must have been heated at low pressures for appreciable mass dependent isotopic fractionation to be preserved [14-22], e.g., the heavy Mg isotope enrichments of many CAIs imply that they experienced evaporation at low pressures ($<10^{-4}$ bar), conditions that are thought to be typical near the protoSun.

The isotopic consequences of condensation from a nebular gas can be considered in terms of the kinetics of condensation, the degree of undercooling, and potential reservoir effects [8, 9]. The magnitude of fractionation is controlled mainly by the transformation from vapor to solid with the exact identity of the solid phase(s) being of less importance. Ultimately, the relative importance of equilibrium versus the potentially much larger kinetic effects in the isotope fractionation depends on the degree of "overstepping" thermodynamic equilibrium, which can be equated with a temperature difference (i.e., undercooling).

Oxygen isotopes: In general, CAIs are understood to start ^{16}O-rich relative to chondrules and other "more" planetary materials and to record the isotope composition of solar nebular gas from which they grew. Recent high spatial resolution oxygen isotope measurements afforded by ion microprobe analysis across the margins and rims of CAIs reveal systematic variations in $\Delta^{17}O$, which suggests formation from a diversity of nebular environments [10, 23]. The variability implies that CAIs probably formed from several oxygen isotopic reservoirs. The observations support early and short-lived fluctuations of the environment in which CAIs formed,

either because of transport of the CAIs themselves to different regions of the solar nebula or because of varying gas composition near the protoSun.

Recently, NanoSIMS oxygen isotopic imaging of a primitive spinel-rich CAI spherule (27-2) from the MIL 090019 CO3 chondrite has confirmed the existence of outward enrichment of ^{16}O [24], indicating that at least some CAIs exchanged with ^{16}O-poor nebular gas followed by a more ^{16}O-rich gaseous reservoir. Likewise, the observed radial oxygen isotopic heterogeneity among multiple occurrences of the same mineral in this inclusion strongly supports interpretations of interactions with distinct nebular oxygen reservoirs.

Magnesium (and Silicon) isotopes: Significant advances in measuring moderately volatile Mg (and Si) have been made by coupling a short-pulsed laser with a MC-ICPMS. In particular, this *in situ* approach affords the measurement of detailed intra-particle isotope zoning profiles across the margins of inclusions and rims that make up the outer portion of most CAIs [11]. Because Mg isotope zoning across melilite at the margins of CAIs can be decoupled from the chemical zoning of the melilite (typically dropping from the relatively heavy Mg isotopic enrichments indicative of the cores to normal Mg isotopes at the margins), the Mg isotope zoning profiles are interpreted to reflect solid-state diffusive exchange with the gas attending growth of their rims [25]. Furthermore, the near normal Mg isotopic compositions observed in the rims indicate that these mineral layers are in part condensates that formed at relatively high gas pressures (P_{H2} and/or P_{Mg}) while the heavy Mg isotopic enrichments of the interiors of igneous CAIs (once molten in space) show that they are evaporative residues formed at lower gas pressures (P_{H2}) [11].

Fractionation of Mg isotopic compositions in rims, e.g. [11], has not been quantified. These rims can have lower Mg isotopic compositions than typical of planetary materials and are not convincingly explained by parent body processes. Using a new fractionation theory for condensation [9] it can be shown that these rims likely formed by small (0.5-1.0 ^{o}C) degrees of non-equilibrium condensation (i.e., undercooling) from a gas with a "normal" planetary Mg isotopic composition.

Because silicon is also a moderately volatile element, the comparison of Mg with Si isotope measurements to models for the chemical and isotopic effects of evaporation of molten CAIs can be used to produce a univariant relationship between pressure (P_{H2}) and time during melting [20]. These results show that igneous CAIs were molten for short periods of time (hours to days). In some cases, subsolidus heating sufficient to produce diffusion-limited heavy isotope enrichment at the margin is required [20, 25]. The cumulative timescale for the sublimation history is longer, years to 100's years, but not as long as the 10^3 to 10^4 years required for the inward diffusive exchange computed by modeling the "normal" Mg isotopic zoning and O isotopic zoning commonly seen in other CAIs [23, 25].

Calcium and Titanium isotopes: Using isotopic compositions of the refractory elements Ca and Ti to understand the isotopic effect of condensation allow us to more accurately assess the initial isotopic ratios of the more volatile Mg and Si potentially overprinted by later evaporation events. Furthermore, these results allow us to assess whether a given CAI is a primary condensate from a homogeneous solar gas or instead represents a mixture of materials from a variety of early reservoirs.

Although substantial work remains, it is clear that many "normal" CAIs, and/or their precursor materials, record a multi-step/source condensation history [2, 9]. The extreme depletions of Ca isotopes and slight enrichments of Ti isotope effects measured in a fine-grained CAI exemplify the complicated condensation history of early formed solids. Such fine-grained textures are often assumed to signify a primitive nature for nebular materials, but they may in fact reflect condensation from relatively evolved (fractionated) nebular gas. An origin as primordial condensates might be incorrect. Additionally, the discovery of Ca isotopic zoning [9] in a Type B1 igneous CAI likely involves condensation from an evolving gaseous reservoir, presumably after now extinct ^{26}Al was added to the Solar System, but before its moderately volatile element isotopic signatures were set. Thus, the existence of Ca isotopic zoning in this inclusion implies that a majority of its Mg isotope record pertains to a later, likely subsolidus, nebular history.

References: [1] Smith, R.L., et al. (2015) *The Astrophys. Journal* 813, 16p., [2] Niederer, F.R. and D.A. Papanastassiou (1984) *GCA* 48, 1279-1293, [3] Young, E.D. (2016) *The Astrophys. Journal* 826, 6p., [4] Dauphas, N., et al. (2010) *The Astrophys. Journal* 720, 1577-1591, [5] Simon, J.I., et al. (2009) *The Astrophys. Journal* 702, 707-715, [6] Moynier, F., et al. (2010) *The Astrophys. Journal* 718, L7-L13, [7] Jordan, M.K., et al. (2017) in *48th LPSC,* Abs. #3032, [8] Simon, J.I. and D.J. DePaolo (2010) *EPSL* 289, 457-466, [9] Simon, J.I., et al. (in press) *EPSL*, [10] Simon, J.I., et al. (2011) *Science* 331, 1175-1178, [11] Simon, J.I., et al. (2005) *EPSL* 238, 272-283, [12] Clayton, R.N., et al (1973) *Science* 182, 485-488, [13] Young, E.D. (2007) *EPSL* 262, 468-483, [14] Davis, A.M., et al. (1990) *Nature* 347, 655-658, [15] Esat, T.M., et al. (1986) *Nature* 319, 576-578, [16] Grossman, L., et al. (2000) *GCA* 64, 2879-2894, [17] Nagahara, H. and K. Ozawa (2000) *Chemical Geology* 169, 45-68, [18] Yamada, M., et al. (2006) *Planet. and Space Sc.* 54, 1096-1106, [19] Young, E.D. and S.S. Russell (1998) *Science* 282, 452-455, [20] Shahar, A. and E.D. Young (2007) *EPSL* 257, 497-510, [21] Knight, K.B., et al. (2009) *GCA* 73, 6390-6401, [22] Zhang, J., et al. (2014) *GCA* 140, 365-380, [23] Simon, J.I., et al. (2016) *GCA* 186, 242-276, [24] Simon, J.I., et al. (2017) in *80th MetSoc,* Abs. #6123, [25] Simon, J.I. and E.D. Young, *EPSL* 304, 468-482.

Broad size-dependent particle populations in chondritic meteorites: implications for planetary accretion. J. I. Simon[1], K. A. McCain[2], M. J. Cato[3], P. A. Christoffersen[4], K. R. Fisher[1], P. Srinivasan[3], A. W. Tait[5], J. N. Cuzzi[6]. [1]NASA Johnson Space Center, Houston, TX 77058, USA (justin.i.simon@NASA.gov), [2]University of California, Los Angeles, Los Angeles, CA, 90095, USA, [3]University of New Mexico, Albuquerque, NM, 87131, USA, [4]The University of Western Ontario, London, Ontario, N6A 3K7, Canada, [5]Monash University, Clayton, 3168, VIC, Australia, [6]NASA Ames, Moffett Field, CA 94035, USA.

Introduction: Magnesium-rich silicate chondrules and calcium-, aluminum-rich refractory inclusions (CAIs) are fundamental components of chondritic meteorites. Concentration of these early-formed particles is conventionally understood to reflect nebular sorting processes leading to accretion of planetesimals, planetary bodies that represent the building blocks of the terrestrial planets. In principle, studies of chondrule [1] and CAI [2] size-frequency distributions in chondritic meteorites can be used to test astrophysical sorting processes, but with a few exceptions (e.g., [3]) the data sets are rather small and differences within and between these distinct particle groups, both of which are made up of diverse subgroups with different minerals and thermal histories, remain poorly quantified.

Here we present particle size-frequency data for Northwest Africa 5717, a primitive ordinary chondrite (ungrouped 3.05) and the well-known carbonaceous chondrite Allende (CV3). Instead of the relatively narrow size-distributions often used in astrophysical models to simulate the dynamics of protoplanetary disks, we observe broad size-frequency distributions across all particle types in both meteorites. Detailed microscopic image analysis of Allende provides evidence that initial differences in the size-frequency distributions of chondrule subtypes existed, but that collectively these subpopulations comprise a composite "chondule" size-frequency distribution that is similar to the broad size-frequency distribution found for CAIs. These data suggest that astrophysical disk models that predict a narrow particle size population and conventional particle analysis methods must be critically reevaluated.

Methods: Energy-dispersive X-ray chemical maps were obtained by scanning electron microscope (SEM) analysis of six Allende fragment samples (0.86 cm^2, 1.52, cm^2, 1.82 cm^2, 1.86 cm^2, 1.91 cm^2, 2.11 cm^2 sized pieces) using the JEOL 7600 field emission SEM at NASA Johnson Space Center. Integration of characteristic X-ray emission from multiple elements was used to create chemical phase maps in which all of the particles greater than ~50 μm in diameter were characterized.

Results obtained from X-ray image analyses were compared to results derived from a mosaic of photographic images obtained from an adjacent slab of Allende that is ~20 cm x 25 cm (see [4]). A similar photo mosaic was made for a ~11 cm x 14 cm slab of NWA 5171. To evaluate the particles of the slabs, we photographed each using a camera attached to an optical microscope. Constituent particles (e.g., chondrules and CAIs) within the photo mosaics were outlined in Adobe Illustrator or Photoshop using a large digitizing art board. One side of each slab, comprised of ~300 and 400 images for NWA 5171 and Allende respectively, was chosen for detailed analysis. Although some particles as small as ~25 μm were identified, an accurate account of particles less than ~250 μm in the slabs was not feasible.

The characterization of all particles identified by SEM X-ray images (and in the slabs) were divided into subgroups (after [5]). Unless stated otherwise, the size measurements denote the geometric mean size of particle cores without the added thickness of their associated rims (Fig. 1).

Results and Discussion: From this analysis, 13 size-frequency data sets were selected for which enough data was collected to yield statistically meaningful results. These data sets are: (1) Maximum chondrule size (ChonMax, n=2339) that includes the added thickness of rim when present, (2) Chondrule core size (AllchonCore, n=2556) regardless of whether they have rims, (3) All inclusions types (n=195), (4) Chondrule cores (CoreNoRim, n=2161) that lack rims, (5) Chondrule cores (CoreWRim, n=387) of chondrules with rims, (6) Porphyritic Olivine (PO) chondrule cores (n=1306), (7) Porphyritic Olivine Pyroxene (POP) chondrule cores (n=1042), (8) Porphyritic Pyroxene (PP) chondrule cores (n=153), and (9) Type A CAIs (n=157) for Allende SEM data and (10) all particles for Allende slab (n=6530), (11) particles contained only in the light lithology of NWA 5717 slab (n=4121), (12) particles contained only in the dark lithology of NWA 5717 slab (n=8206), and (13) all particles for NWA 5717 slab (n=12,966).

The broad size-frequency distributions of chondrules and CAIs in Allende are depicted in Fig. 1A. The distributions of the most abundant particle subgroups detailed in the SEM images are shown in Figure 1B. The largest differences observed exist between POP chondrules (n=1042) that are relatively more abundant at larger sizes and PO chondrules (n=1306) that are relatively more abundant at smaller sizes. The third most

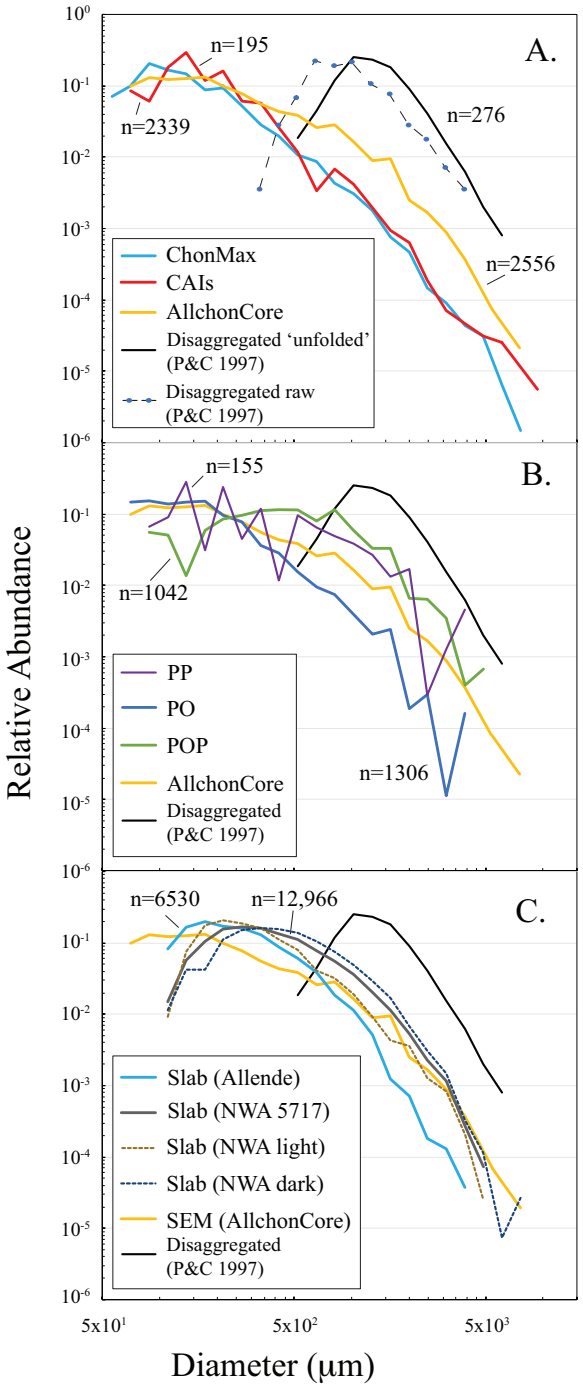

Figure 1. Size-frequency distributions of the particle components of Allende and NWA 5717 meteorites. (A) Distributions of chondrules and CAIs compared to the narrow range of particles disaggregated by [6]. (B) Distributions of most abundant petrographically distinct particle types. (C) Slab data of Allende and ordinary chondrite NWA 5717. Particles are binned geometrically. The effect of non-diametric particle sectioning is corrected for with unfolding calculations [7].

abundant chondrule subgroup (PP) defines a distribution that is nearly indistinguishable from the overall broad distributions of CAIs and chondrules ("ChonMax"), the latter of which is largely comprised of POP and PO chondrules. It is remarkable, but unlikely a coincidence that when the POP and PO chondrule populations are grouped together that they exhibit nearly the same size-frequency distribution as PP chondrules and CAIs.

The SEM results are generally consistent with component particles identified in the photo mosaic Allende slab sample. Although CAIs in the slab are generally visible against the dark matrix, the outlines of chondrules proved more difficult to delineate as compared to X-ray maps and their frequency appears to have been undercounted due to selection bias at sizes less than ~200 μm (Fig. 1C). A similar apparent drop in particle counts at the smaller sizes is seen in the NWA 5717 slab data (Fig. 1C). Likewise, based on the largest particle sizes that have been reported in the literature, the X-ray image data are not fully representative for the largest sizes. Despite these complications, in both types of Allende data and in NWA 5717, broad particle size-frequency distributions are measured. These observations contrast sharply with existing studies (see [1] and references therein) and suggests that there are systematic selection bias effects in previous investigations, likely undercounting both smaller and larger sized particles to a degree that is significantly greater than in this study.

Summary: The similar broad distribution of particle sizes measured among particles in primitive meteorites, in particular among subgroups in Allende (i.e., ChonMax, unrimmed core, and CAIs) suggests that one final event or process sorted CAIs, rimless chondrules, and already-rimmed chondrules collectively prior to their incorporation into the chondrite parent body. The accretion event would have over-printed previous differences (e.g., PO vs. POP) that existed between particle types, which are either due to differences in their initial formation or due to previous sorting events of the distinct particle types. The similarity between the size-frequency distributions of Fe-Mg-Si-O chondrules and the more refractory Ca-Al-rich inclusions indicate size played a dominant role in the sorting of early-formed particles. The universally observed broad size-frequency distributions reported in this study affords strict constraints on protoplanetary disk planetesimal models.

References: [1] Friedrich et al. (2015) *Chemie der Erde* 75, 419-443, [2] Hezel et al. (2008) *MAPS* 43, 1879-1894, [3] Rubin (1989) *MAPS* 24, 179-189, [4] Tait et al., (2016) *EPSL* 454, 213-224, [5] Gooding and Keil (1981) *EPSL* 16, 17-43, [6] Paque and Cuzzi (1997) 28th *LPSC*, Abstr. #071, [7] Cuzzi and Olson (2017) *MAPS* 52, 532-545.

THE CURRENT SOLAR SYSTEM AND CLUES TO ITS PAST. C. A. Thomas[1], [1]Planetary Science Institute (1700 East Fort Lowell, Suite 106, Tucson, AZ 85719, cthomas@psi.edu)

Introduction: The current physical characteristics of the small body populations enable investigations of the evolution of our Solar System. For instance, the range of observed compositions can tell us a lot about the starting conditions and early dynamical evolution of the primordial disk. Each measured physical property (e.g., size frequency distributions, rotation rates) sheds light on some past evolution. As we continue to characterize these populations, we further our understanding of the Solar System as a whole.

Small Body Populations: In this talk, I will discuss compositional and dynamical constraints revealed by observations of the various asteroid populations.

Main Belt Asteroids. The Main Asteroid Belt is important because it is what remains of the initial planetesimal population in the inner Solar System. Early observations of MBAs demonstrated that there was a heliocentric gradient in the Main Belt with the silicate-rich, volatile-poor S-type objects preferentially located in the inner Main Belt and the primitive, volatile-rich C-type objects more prevalent in the outer Main Belt [1]. This basic structure of the Main Belt is consistent with the idea that the protoplanetary disk had decreasing temperature with increasing distance from the Sun. However, the different taxonomic types are also partially mixed in semi-major axis, which suggests that the populations have dynamically evolved from their formation locations [2].

One way of studying the chemical evolution of the asteroids is to examine asteroid families. Families are dynamical groups produced by catastrophic collisions and large cratering events. Due to their formation processes, families provide us with the opportunity to probe the interiors of the former parent bodies.

Trojan Asteroids. Jupiter's Trojan asteroids are trapped in the stable L4 and L5 Lagrange regions and are estimated to be as numerous as the Main Belt asteroids. Dynamically, their orbits are stable over the age of the Solar System [3]. Their composition and inferred origin of the Trojan asteroids could provide evidence to distinguish between the different models of Trojan capture and Solar System dynamical evolution. Unfortunately, their compositions are still poorly constrained.

Near-Earth Asteroids. The majority of near-Earth objects originated in collisions between bodies in the Main Belt and subsequently found their way into near-Earth space through a series of dynamical interactions. The NEO population is dynamic and has changed over time as the material entering into the Main Belt source regions has changed. One of the big challenges in the study of NEOs is determining the relationships between the NEOs, their Main Belt source regions, and the meteorite populations. By solidifying these links, we can infer the compositions of various asteroids. We can also compare the compositions of the various populations. For instance, we expected the compositional diversity of the meteorite fall population to match the variety of compositions seen in the NEO population. However, as we learn more about the NEO population we see that the two populations are not as similar as expected.

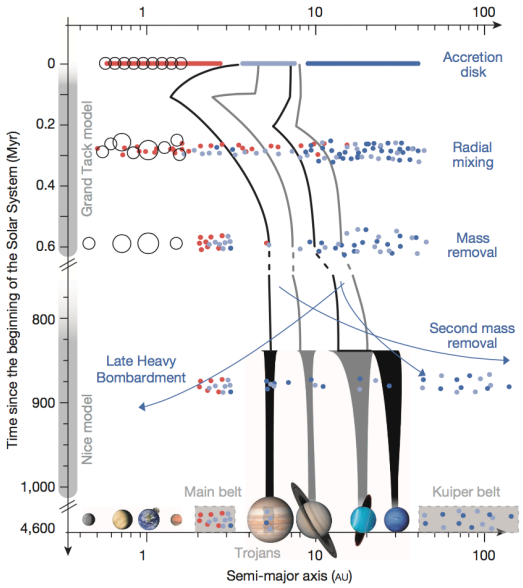

Figure 1: Cartoon of the effects of planetary migration on the Main Belt from DeMeo and Carry [4]. The figure shows some major components of current dynamical models.

References:

[1] Gradie J. and Tedesco E. (1982) *Science, 216,* 1405-1407. [2] Morbidelli A. et al. (2015) *Nature, 435,* 462. [3] Levison H. et al. (1997) *Nature, 385,* 42. [4] DeMeo F. E. and Carry B. (2014) *Nature, 505,* 629-634.

TURBULENCE IN PROTOPLANETARY DISK DEAD ZONES – RECENT ADVANCES., O. M. Umurhan[1,2], P. R. Estrada[1,2], J. N. Cuzzi[1], [1]NASA Ames Research Center, MS 245-3, Moffett Field, CA 94035-1000, SETI, Carl Sagan Institute, Mountain View, CA 94043, (orkan.m.umurhan@nasa.gov)

Introduction: Theoretical advances on the dynamical nature of protoplanetary disk (pp-disk, hereafter), especially inside their so-called Dead Zones (DZ), have several important implications for the accumulation and evolution of planetesimal dust. This presentation reviews the current state of understanding of fluid dynamical processes in pp-disks with a special emphasis on what appears to drive turbulence in DZ's including the Vertical Shear Instability (VSI), Convective Overstability (CO) and the Zombie Vortex Instability (ZVI). These processes have been theoretically identified to be relevant in DZ's only in the last 5 years. Each of the mechanisms discussed critically depend on the thermal distribution and cooling times of the disk and are fundamentally thermomechanical processes drawing on the radiant energy of the star.

Given recently developed and published global pp-disk models, we pin-point which mechanism operates in which part of the disk for a given evolutionary epoch of the pp-disk and what qualitative effect they will have upon the kineamatics of planetesimals. The opacity and the temperature distributions in many published global disk models depend upon the parametrization of the turbulent stresses thought to be present. Turbulent stresses are often represented in these model by a classic $\alpha-$ disk parametrization which assumes these stresses are released in the disk both steadily and uniformally. Realistic disks exhibiting any one (or a combination) of these dynamical processes will have turbulent stresses that are distributed in both space and time which, in turn, will affect the thermal and cooling-time properties of the disk as well as the concentration of dust. For typical pp-disk conditions, the above linear instability mechanisms appears to drive turbulence to the level of $\alpha \sim 10^{-4} - 10^{-3}$.

Instabilities and how they fit together in a pp-disk turbulence paradigm: The last ten years has seen a explosion of theoretical interest in the dynamical state of the pp-disk DZ's [1]. Their importance hinges on the expectation that bulk of planetesimal growth likely takes place within these relatively quiescent regions of disks. The degree to which the flow is disordered directly effects the quality of and degree to which planetesimal growth occurs -- and for how long. Over these past ten years DZ's have gone from being considered absolutely inactive to now possibly harboring a whole suite of dynamically active processes involving, to varying degrees, the influence and interaction between disk gas and dust particles. These processes include those that are classical linear instabilities of Keplerian and near-Keplerian flows as well as

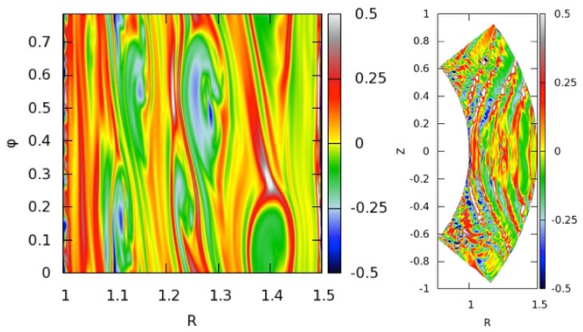

Fig. 1. Numerical simulation of the full turbulent development of the VSI [8]. Left panel: midplane view of vorticity while the Right panel shows radial-vertical height view of the azimuthal vorticity field.

non-modal growth mechanisms. The former category includes the dynamics of the subcritical baroclinic instability (SBI), the Rossby wave instability (RWI), the vertical shear instability (VSI, Fig. 1) [2,4-6] the Zombie vortex instability (ZVI) [7,8], Convective overstability (CO) [9-11], the elliptical instability (EI) [12], and the streaming instability (SI) – a summary is found in [2] and also see [3].

In this presentation we review these various mechanisms, under what conditions they operate and, ultimately, how they relate to one another within a proposed hierarchical turbulence framework (e.g., Fig. 2).

These relatively localized small-scale instabilities occur in stable vertically stratified disk sections. Their presence or absence depends upon the thermal relaxation timescales τ_r of the disk material, which are set by the optically thick/thin radiative processes, and are a function of both the radius and vertical location within the disk: (1) The VSI becomes active when $\tau_R < 0.1\tau_{orb}$ where τ_{orb} is the local disk orbit time [7,8], (2) ZVI is active in the opposite regime where $\tau_r > 10 - 20\tau_{orb}$ [4], while CO is expected to be active in a window centered on $\tau_r \approx \tau_{orb}$ [10]. For all linear instability mechanisms, the degree of emergent turbulent activity, as measured by the inverse of the turbulent Reynolds number, $\alpha \equiv 1/\mathrm{Re}_{turb}$, broadly falls in the range of $\alpha = 10^{-4} - 10^{-3}$.

Thermal/Opacity profiles: The thermal cooling/relaxation times, which are directly influential in the operation of the above mentioned linear instaiblities, depend critically on the disk opacities. Disk opacities, dominated by the growing dust particles, evolve on a short timescale and are sensitive to the

degree of turbulence in the disk. However, examining the long term evolution of global pp-disk models (including their dust constituent) while concommitently resolving the underlying dynamical turbulence mechanisms still remains a computationally expensive proposition. Dimensionally reduced models of pp-disk evolution that take into account growth and transport of dust necessarily requires parametrizing the momentum transport induced by the turbulence mechanisms (like the ones mentioned above) using familiar disk modeling techniques. Recent results of [13] (ECM-16) which describe vertically integrated axisymmetric disk evolution models predict the density, temperature, opacity and dust particle distribution as a function of disk location and epoch for input values of dust porosity and turbulent α in addition to other gross properties of the circumstellar system. The evolving nature of the thermal relaxation times are intimately connected to the development of the Rosseland/Planck mean opacities which is a sensitive function of the input values of α.

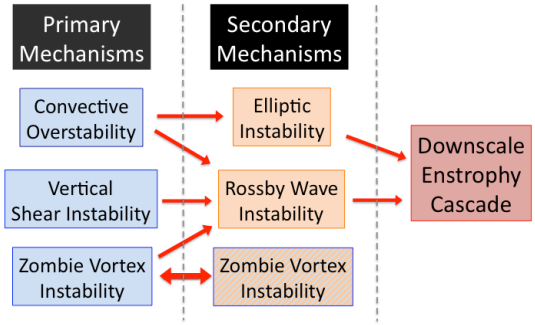

Fig. 2. Proposed scenario of turbulent cascade for pp-disk mechanisms.

(expressed in terms of local scale height H). Degree of turbulence is $\alpha \sim 4 \times 10^{-4}$.

As such, the thermal structure and opacity distribution of a disk depends upon the degree of underlying turbulent intensity. However, the very same turbulence and its intensity, as described above with regards to the operation of the aforementioned linear instability mechanisms, depends upon the opacities. I will present some preliminary results estabilishing the location of an evolving ECM-16 pp-disk model. Figure 3 offers a flavor of the results of where to expect which linear instability mechanism in the form of a pp-disk "butcher" diagram. Similar work along these lines have been published and these will be discussed as well [14].

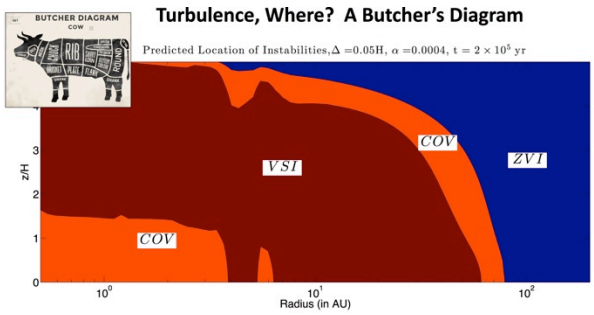

Fig. 3. As derived from 1D evolution models of ECM-16. The mutually exclusive cooling-time/opacity requirements of the 3 primary turbulence mechanisms means that any one part of a pp-dsk DZ has some turbulent activity. Time corresponds to 200,000 yr and Δ indicates radial scale of primary turbulent driving

References:. [1] Turner, N.J. et al. (2014) *Protostars and Planets VI,* 411. [2] Richard, S. et al. MNRAS 456, 3571. [3] Fromang, S. & Lesur, G.,(2017) (arXiv:1705.03319) [4] Nelson, R. P., et al. (2013), MNRAS 435, 2610. [5] Stoll, M. H. R., & Kley, W. 2014, A&A, 572, A77 [6] Umurhan, O. M. et al. (2016) A&A, 586, A33 [7] Marcus, P.S.; et al.. 2015; ApJ 808, id 87; [8] Lesur, G.R.J & Latter, H. (2016) A&A 462, 4549. [9] Klahr, H. & Hubbard A. (2014) ApJ 788, 21. [10] Lyra, W. (2014) ApJ 789, 77. [11] Latter, H. N. (2015) MNRAS 455, 2608. [12] Lesur, G. & Papaloizou, J.C.B. (2010) A&A 513, 60. [13] Estrada, P. R. et al. (2016) ApJ, 818, 200. [14] Malygin, M.G. et al. (2017) (arXiv:1704.06786).

NORTHWEST AFRICA 11042: A PRIMITIVE ACHONDRITIC MELT FROM THE L CHONDRITE PARENT BODY. Z. Vaci[1], C. B. Agee[1], K. Ziegler[1], Y. Asmerom[2], V. J. Polyak[2], M. Humayun[3], [1]Institute of Meteoritics, [2]Department of Earth and Planetary Science, University of New Mexico, Albuquerque, NM; [3]Department of Earth, Ocean, and Atmospheric Science, Florida State University, Tallahassee, FL.

Introduction: Northwest Africa 11042 (NWA) is an ungrouped primitive achondrite with unique petrology and geochemistry that groups it with the L chondrites. A single 90.1 g stone was purchased from Abdelhadi Aithiba in Morocco in 2016. The stone is covered in black fusion crust with a broken surface that displays a low degree of weathering.

Petrography: NWA 11042 is ultramafic and displays a phaneritic cumulate texture of olivine (Fo=75, 46 vol%), pyroxene (En=74 Fs=20, 38 vol%), maskelynite (Ab=83 An=12, 15 vol%), and chromite (1 vol%). Trace phases are troilite which is usually paired with kamacite and minor taenite, and trace apatite (ClA=80). All plagioclase has been transformed to maskelynite.

Shock-melt pockets that range in size from a few hundred µm to a few mm are found throughout the groundmass, and some contain olivines which have been partially transformed to the high-pressure phase ringwoodite (Fig. 1). In backscattered electron (BSE) imagery, dark rims are observed around the melt pockets (Fig. 2). Metal nanoparticles are observed exsolving from surrounding mineral grains within these dark rims, indicating that areas surrounding the melt pockets are being reduced by the melt.

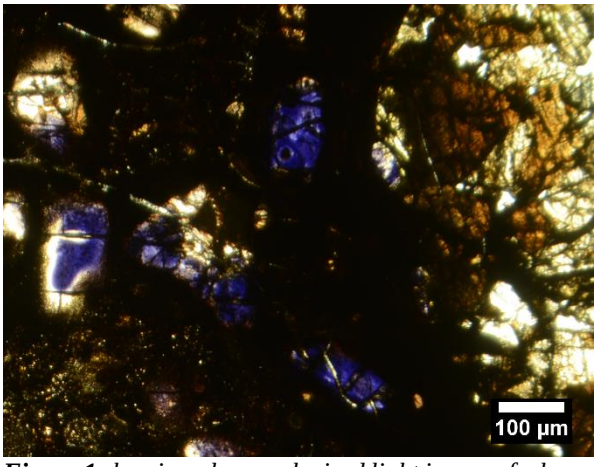

Figure 1 *showing plane-polarized light image of a large shock-melt pocket with blue ringwoodite visible.*

Geochemistry: The oxygen isotopic composition of NWA 11042 does not match that of any grouped achondrite. Instead, it plots within the range of the L chondrites ($\delta^{18}O$=4.46; $\delta^{17}O$=3.34; $\Delta^{17}O$=1.03) (Fig. 3). The whole-rock rare earth element (REE) composition is approximately 2X CI chondritic [1] and displays an almost entirely flat pattern (Fig. 4). Maskelynite shows a positive Eu anomaly, and pyroxenes display complementary negative Eu anomalies, both of which are characteristic of igneous differentiation.

The $^{143}Nd/^{144}Nd$ and $^{147}Sm/^{144}Nd$ values for a whole-rock sample and olivine, pyroxene, and melt pocket separates were measured in order to find a crystallization age. The olivine, pyroxene, and whole-rock samples plot a 3-point isochron with an age of 4100 ± 160 Ma (Fig. 5). The melt pocket separate plots off of this isochron at a much younger age.

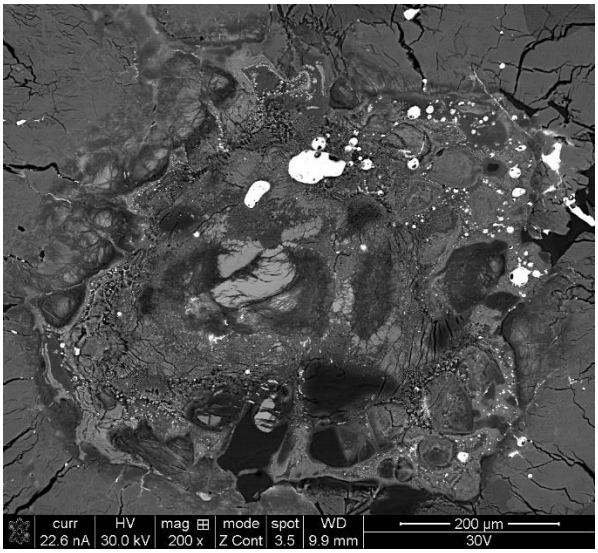

Figure 2 *showing BSE image of shock-melt pocket. Partially melted relict phases are surrounded by glassy melt, and a dark reduction rim surrounds the melt.*

Discussion: While the oxygen isotopic composition and REE pattern of NWA 11042 is L chondritic, its major element chemistry and petrology are distinctly achondritic. It does not contain any relict chondrules, and its igneous texture is overprinted by shock-melt features and thus is not produced by them. It is also depleted in siderophile elements relative to the L chondrites (Fig. 6), suggesting it is a product of differentiation. The oxygen isotope composition of NWA 11042 is similar to that of two other ungrouped achondrites, NWA 4284 ($\delta^{18}O$=4.22; $\delta^{17}O$=3.24; $\Delta^{17}O$=1.02) and NWA 6698 ($\delta^{18}O$=4.77; $\delta^{17}O$=3.74; $\Delta^{17}O$=1.23). NWA 4284 has a similar igneous texture and mineralogy, with higher modal pyroxene and plagioclase. Some of its

plagioclase has been transformed to maskelynite, but it does not feature shock-melt pockets or veins.

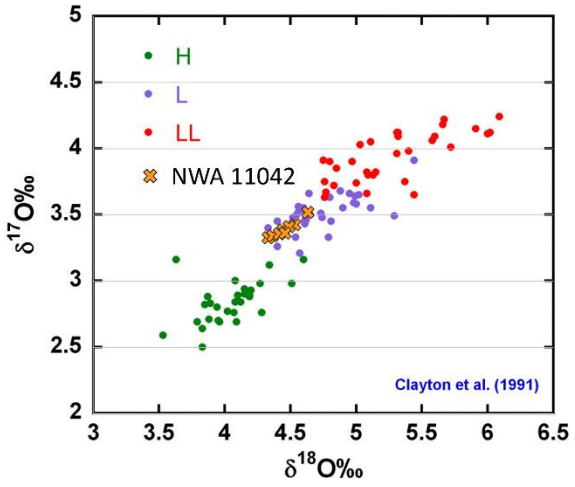

Figure 3 *showing triple-O diagram for ordinary chondrites and NWA 11042.*

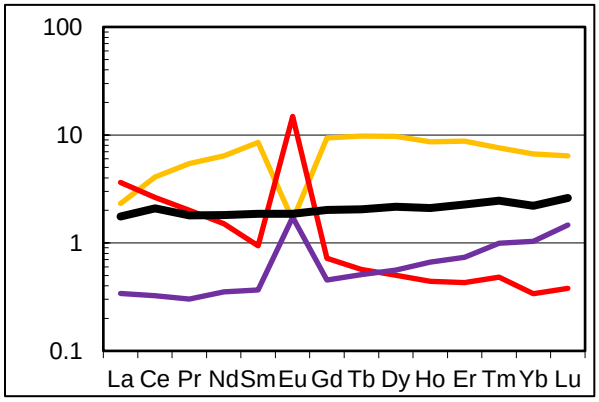

Figure 4 *showing NWA 11042 REE pattern for whole-rock (black), pyroxene (yellow), maskelynite (red), and melt pocket (purple).*

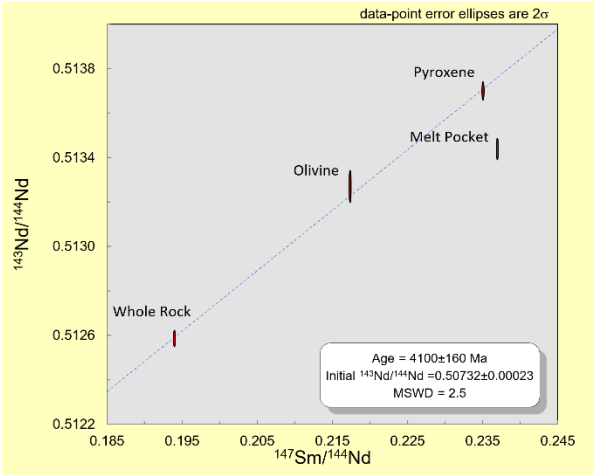

Figure 5 *showing Sm-Nd isochron for NWA 11042.*

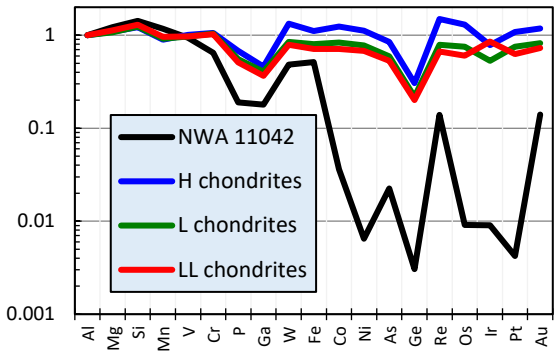

Figure 6 *showing CI chondrite and Al-normalized siderophile element abundances for NWA 11042 and ordinary chondrites [2]*

The flat REE pattern of NWA 11042 suggests that it was derived from L chondritic material. However, its depleted siderophile element content (Fig. 6) imply that its parent body underwent a core formation event. Its Sm-Nd crystallization age is also younger than any chondrite by several hundred Ma. This includes the highly metamorphosed L5 and L6 chondrites, which have younger ages than L3 and L4 because they were heated for longer by the decay of extinct radionuclides [3]. The young age of this meteorite could possibly be an artifact of contamination and incorporation of partially reset shock-melt material into the mineral separate isochron. Alternatively, if NWA 11042 is a product of melt and differentiation within the L chondrite parent body, it could have undergone an unusually long and intense heating event for chondritic material and thus its Sm-Nd isotopic composition took longer to reach closure temperature, resulting in a younger age.

The well-known "onion shell" model of the L chondrite parent body [4] displays increasing thermal metamorphic gradient with depth. The L3 chondrites form the outer shell, followed by the L4, L5, and L6 chondrites with increasing depth. The minimum time required for material to cool past its closure temperature increases with temperature and depth, and this is why the more metamorphosed chondrites are progressively younger. The existence of a melt within the L chondrite parent body further raises the necessary temperatures and minimum time before radioisotope closure. It would also increase the minimum size requirement for the L chondrite parent body, as a larger size is needed to heat chondritic material past its melting point.

References: [1] Lodders K. (2010) *Principles and Perspectives in Cosmochemistry* p. 379-417. [2] Wasson and Kallemeyn (1988) *Proc. Roy. Soc. London* A325 [3] Blackburn T. (2017) *Geochimica et Cosmochimica Acta* 200:201-217. [4] Bennett M. E. and McSween H. Y. (1996) *Meteoritics & Planetary Science* 31:783-792.

METEORITIC CONSTRAINTS ON TIMESCALES OF PLANETESIMAL ACCRETION IN THE EARLY SOLAR SYSTEM. M. Wadhwa[1], [1]Center for Meteorite Studies, School of Earth and Space Exploration, Arizona State University, Tempe, AZ 85287

Introduction: The details of the physical processes involved in the accretion of planetesimals in the early Solar System are not well understood, and have been the focus of several recent theoretical modeling investigations (e.g., [1] and references therein). The precise timescales of these processes are key inputs for such models. Most constraints on the timescales involved in the transition from dust-sized particles in the protoplanetary disk to planetesimals (diameters ~100-1000 km) come from chronologic investigations of meteorites and their components. The following provides a review of the current state of knowledge in this area, which has implications for timescales for accretion of planetesimals in the early Solar System.

Constraints from chondritic components: Chondritic meteorites are composed of variable proportions of four main components formed in the solar nebular environment, i.e., refractory inclusions, chondrules, fine-grained matrix and Fe-Ni metal [2]. Chronologic investigations of the refractory inclusions and chondrules in particular have provided important constraints on the accretion timescales of chondritic parent bodies and are discussed below.

Calcium-aluminum-rich inclusions: The refractory calcium-aluminum-rich inclusions (CAI) in primitive chondritic meteorites range in size from tens of micrometers to centimeters, and represent the earliest solids to form in the solar protoplanetary disk [2,3]. As such, these objects can be considered to be markers that define the beginning of the Solar System (T_0) and provide a record of the earliest epoch in the evolution of the solar protoplanetary disk. Since the confirmation of $^{238}U/^{235}U$ variation in CAIs [4], only a few studies have been conducted where Pb-Pb ages were reported for CAIs for which the U isotope compositions were also measured [5-7]. These ages range from 4567.2±0.5 Ma and 4567.3±0.2 Ma for CAIs from Allende [5] and Efremovka [7] CV3 chondrites, respectively, to 4567.9±0.3 Ma for a CAI from Northwest Africa (NWA) 6991 CV3 chondrite [6]. Previous studies have shown that both the Allende and Efremovka parent bodies experienced significant but variable alteration [8,9] and thus CAIs in these CV meteorites may be affected to varying degrees. This raises the possibility that the systematically younger ages of CAIs in these meteorites may be the result of isotopic disturbance, and CAIs in other, potentially less altered, primitive chondrites should be investigated for accurately determining the absolute chronology of Solar System formation.

Regardless of the absolute age of CAI formation, high-precision ^{26}Al-^{26}Mg systematics indicate that some CAIs that formed as condensates from the nebula, as well as the precursor solids of those that underwent subsequent melting, formed during a very short time interval of ≤20 Ka [10-13]. Furthermore, other CAIs appear to have undergone melting and re-melting episodes in the solar nebula over a somewhat more extended time period lasting a few hundred Ka (e.g., [13]). This requires CAIs to have remained as free-floating objects in the solar nebula for at least this duration. This time interval is consistent with the Al-Mg relative ages determined for Wark-Lovering (WL) rims from some CAIs [14,15]. However, a recent high spatial resolution ^{26}Al-^{26}Mg study of WL rims from two relatively pristine CAIs from the NWA 8323 CV3 chondrite suggested that these CAIs may have remained as free-floating objects (without accreting into larger parent bodies) for up to ~2-3 Ma in the solar nebula [16].

Chondrules: Chondrules are tens of micrometers to millimeter-sized igneous-textured ferromagnesian spherules that typically comprise a significant fraction of chondritic meteorites [2]. The Al-Mg systematics in chondrules from a variety of chondrite types have been extensively studied and suggest that most chondrules were formed ~2-3 Ma after CAIs ([17] and references therein). Absolute Pb-Pb ages for individual chondrules have so far only been reported by [7]. These authors reported ^{207}Pb-^{206}Pb ages ranging from 4567.3±0.4 Ma to 4564.7±0.3 Ma for five chondrules from the Allende CV3 and the NWA 5697 L3 chondrites (assuming a $^{238}U/^{235}U$ ratio of 137.786±0.013), suggesting that the chondrule formation process began essentially contemporaneously with CAI formation and lasted for at least 2–3 Ma thereafter.

Given the absolute and relative ages of chondritic components (i.e., CAIs and their WL rims, as well as chondrules) discussed above, it is evident that chondritic parent bodies accreted at least ~3-4 Ma after CAI formation.

Constraints from differentiated meteorites: High-precision chronologic studies of meteorites that formed on parent bodies that underwent wholesale melting and differentiation can provide additional constraints on accretionary timescales of planetesimals in

the early Solar System ([18] and references therein) and are discussed below.

Achondritic meteorites: Achondrites like the Howardite-Eucrite-Diogenite (HED) meteorites and the angrites represent crustal materials from differentiated planetesimals [19]. Internal isochron ages obtained from the absolute Pb-Pb and relative Al-Mg, Mn-Cr and Hf-W chronometers indicate that some basaltic achondrites (in particular, some noncumulate eucrites, quenched angrites and ungrouped basaltic achondrites such as Asuka 881394 and Northwest Africa 7325) crystallized as early as ~3-5 Ma after CAIs (e.g., [20-27]). This implies that their parent planetesimals had accreted and differentiated within this time interval. Whole-rock isochrons for the Mn-Cr and Hf-W systems defined by bulk samples of the eucrites and angrites additionally provide evidence of early planetesimal-scale (metal-silicate and silicate-silicate) differentiation at ~1-2 Ma after CAI formation [20,25,26,28].

Magmatic iron meteorites: Iron meteorites that define compositional trends consistent with fractional crystallization of a metallic core of a differentiated planetesimal are referred to as "magmatic" (e.g., IIAB and IIIAB irons) [29]. The Hf-W chronometer has been applied to magmatic irons to precisely date the time of metal segregation on planetesimals, and yields core formation ages that extend from ~0.7 Ma (for IIAB irons) to ~3 Ma (for IID and IVB irons) after CAI formation [30].

The temporal constraints discussed above are for events on differentiated planetesimals (such as basalt crystallization and metal segregation) that post-dated their accretion in the early Solar System. These constraints can be used with thermal modeling to estimate the accretion times for these planetesimals. For example, given the time interval for core formation on the parent bodies of the magmatic irons determined by [30], these authors made model calculations (assuming post-accretion heating with ^{26}Al in parent asteroids with ~40 km radii) that indicated that these parent bodies were accreted as early as ~0.1 to ~0.3 Ma after CAI formation.

Implications for the accretion timescales of planetesimals in the early Solar System: Within the last decade, high-precision chronologic investigations of a variety of meteoritic materials have provided unprecedented temporal resolution for processes occurring in the early Solar System. In particular, it is now evident that the solar protoplanetary disk was a dynamic environment where episodic heating events over the first ~2-3 Ma resulted in the formation and reprocessing of chondritic components. Accretion of the earliest planetesimals (ranging from ~100 km to ~1000 km in diameter) in this protoplanetary disk began well within a million years after the formation of the first solids. Soon thereafter, these early-accreted planetesimals melted and underwent metal-silicate and silicate-silicate differentiation (primarily from internal heating resulting from the decay of ^{26}Al). Specifically, this resulted in core formation (which extended from ~0.7 to ~3 Ma after CAI formation for these early formed planetesimals) and crust formation (~3-5 Ma after CAI formation) on these planetesimals. Chondritic parent bodies were accreted approximately 3-4 Ma after CAI formation, after most of the initial abundance of ^{26}Al had decayed away.

References: [1] Cuzzi J. N. et al. (2017) This meeting. [2] Scott E. R. D. and Krot A. N. (2014) Treatise on Geochemistry 2nd Edition, Vol. 1, 65-137 pp. [3] MacPherson G. J. (2014) Treatise on Geochemistry 2nd Edition, Vol. 1, 139-179 pp. [4] Brennecka G. A. et al. (2010) Science, 327, 449-451. [5] Amelin Y. et al. (2010) Earth & Planet. Sci. Lett., 300, 343-350. [6] Bouvier A. et al. (2011) Geochim. Cosmochim. Acta, 75, 5310-5323. [7] Connelly J. N. et al. (2012) Science, 338, 651-655. [8] Scott E. R. D. et al. (1992) Geochim. Cosmochim. Acta, 56, 4281-4293. [9] Krot A. N. et al. (1995), Meteoritics & Planet. Sci., 30, 748-775. [10] Thrane K. et al. (2006) Astrophys. J. Lett., 646, L159. [11] Jacobsen B. et al. (2008) Earth & Planet. Sci. Lett., 272, 353-364. [12] MacPherson G. J. (2010) Astrophys. J., 711, L117-121. [13] MacPherson G. J. (2012) Earth & Planet. Sci. Lett., 331-332, 43-54. [14] Simon J. I. et al. (2005) Earth & Planet. Sci. Lett., 238, 272-283. [15] Kawasaki N. et al. (2017) Geochim. Cosmochim. Acta, 201, 83-102. [16] Mane P. et al. (2015) LPS XXXVI, Abstract #2898. [17] Davis A. M. and McKeegan K. D. (2014) Treatise on Geochemistry 2nd Edition, Vol. 1, 361-395 pp. [18] Kleine T. and Wadhwa M. (2017) Planetesimals: Early Differentiation and Consequences for Planets, 224-245 pp. [19] Mittlefehldt D. W. (2014) Treatise on Geochemistry 2nd Edition, Vol. 1, 235-266 pp. [20] Lugmair G. W. and Shukolyukov A. (1998) Geochim. Cosmochim. Acta, 62, 2863-2886. [21] Srinivasan G. et al. (1999) Science, 284, 1348-1350. [22] Amelin Y. (2008) Geochim. Cosmochim. Acta, 72, 221-232. [23] Connelly J. N. et al. (2008) Geochim. Cosmochim. Acta, 72, 4813-4824. [24] Wadhwa M. et al. (2009) Geochim. Cosmochim. Acta, 73, 5189-5201. [25] Kleine et al. (2012) Geochim. Cosmochim. Acta, 84, 186-203. [26] Touboul M. et al. (2015) Geochim. Cosmochim. Acta, 156, 106-121. [27] Koefoed P. et al. (2016) Geochim. Cosmochim. Acta, 183, 31-45. [28] Trinquier A. et al. (2008) Geochim. Cosmochim. Acta, 72, 5146-5163. [29] Benedix G. K. et al. (2014) Treatise on Geochemistry 2nd Edition, Vol. 1, 267-285 pp. [30] Kruijer T. et al. (2014) Science, 344, 1150-1154.

PLANET FORMATION CONSTRAINED BY THE EARLY ASTEROID BELT K. J. Walsh[1] [1]Southwest Research Institute, 1050 Walnut St Suite 300, Boulder, CO 80302, USA (kwalsh@boulder.swri.edu)

Introduction: Models of inner Solar System formation and evolution have struggled for decades to adequately and consistently produce reasonable analogs of our Terrestrial Planets. Now, a handful of models utilizing a wide range of evolution scenarios – migrating planets or accretion directly from cm-sized pebbles – can regularly produce the planets, but diverge on their implications for the early evolution in the Asteroid Belt. Tracking down the collisional history of the asteroid belt can thus help constrain our understanding of the planet formation processes. Looking at today's asteroid belt, and meteorites derived from its population, constraints and can be built for evolution models.

Planetesimals and Planet Formation: Models of planet formation were once nearly independent of planetesimal formation – they all started from a population of ~100-ish km planetesimals regardless of how they formed. Now, dynamical models have shown that the cm-sized building blocks ("pebbles") of planetesimals can also serve to jump-start planet formation and build planetary embryos very rapidly [1]. While such speedy growth is *very* important for the Giant Planets, it is less clear what problems this can solve for the inner Solar System and all of the implications [2,3].

The Asteroid Belt: Simply looking at the physical and orbital properties of today's asteroid belt can provide severe constraints for the evolution of the inner Solar System. With a total mass orders of magnitude below that expected from smooth distributions of solids, dynamically excited orbits filling nearly all stable phase space and overlapping distributions of taxonomic types of bodies, the current asteroid belt is a total mess of information.

Previous works analyzing the integrated effects on the size frequency distribution and total mass loss find that the Asteroid Belt could have been substantially larger in the past [4]. However, there are numerous implications to grinding away different amounts of mass over the history of the Asteroid Belt.

Asteroid Families: Grinding away a huge primordial asteroid belt implies a huge amount of collisions – including lots of big ones. We see remnants of this process in large asteroid families and they can trace some of the collisional history of asteroid belt – but our ability to detect them decreases going further back in time, and is potentially completely frustrated by the Solar System dynamical re-shuffling associated with the Giant Planet instability (whenever it occurred).

Remnants of the collisions in the gas disk: Similarly a large primordial asteroid belt, depending on when it was dynamically excited, may have started experiencing collisions when the gas disk was still around [5]. These collisions have long been pointed too as possible ways to form some types of chondrules [6].

Tracing the Collisional History: Here we focus on the implications for the primordial asteroid belt mass and dynamical excitement for different flavors of terrestrial planet formation models. These implications are then confronted with the constraints from the Asteroid Belt. In particular two recent studies will utilized- the first focuses on the Asteroid Belt dynamical excitement required to form CB Chondrites [5]. Here, the need for a high-velocity collision between two large bodies (~100's km) in the presence of the gas disk pushes formation models to dynamically excite the Asteroid Belt *very* early, which is difficult to do in the absence of interference by the Giant Planets.

Second, the history of the Asteroid Belt seen through the population of Asteroid families shows relatively frequency large collisions in the last ~Gyr, but inability to detect very old families muddies the history back 3-4 Gya [7]. In a new work very old families are hunted using a new technique with a possibility to debias our catalog of families over time and constrain the Asteroid Belt mass over time [8].

References:

[1] Lambrechts M. and Johansen A. (2012) *Astronomy and Astrophysics, 544,* A32. [2] Levison H. F., Kretke K., Walsh K. J. and Bottke W. F., (2015) *PNAS*, *112*, 46. [3] Morbidelli A., Lambrechts M., Jacobson S. A. and Bitsch B., (2015) *Icarus, 258,* 418. [4] Bottke W. F., Durda D. D., Nesvorny D., Jedicke R., Morbidelli A., Vokrouhlicky D. and Levison H. F. (2005) *Icarus, 179,* 63. [5] Johnson B. C., Walsh K. J., Minton D. A., Krot A. N. and Levison H. (2017) *Science Advances, 2,* e1601658. [6] Krot A. N., Amelin Y., Cassen P. and Meibom A. (2005), *Nature, 436,* 989-992. [7] Broz M., Morbidelli A., Bottke W. F., Rozenhal J., Vokrouhlicky D. and Nesvorny D. (2013) *Astronomy and Astrophysics*, *551,* 117. [8] Delbo M., Walsh K. J., Bolin B., Morbidelli A. and Avdellidou, C. (2017) *submitted.*

HISTORY OF THE SOLAR NEBULA FROM METEORITE PALEOMAGNETISM. B. P. Weiss[1], R. R. Fu[2], H. Wang[3], X.-N. Bai[4], J. Gattacceca[5], R. J. Harrison[6], D. L. Schrader[7], [1]Department of Earth, Atmospheric, and Planetary Sciences, Massachusetts Institute of Technology, Cambridge, MA, USA, [2]Department of Earth and Planetary Sciences, Harvard University, Cambridge, MA, USA, [3]Planetary Science Institute, School of Earth Sciences, China University of Geosciences, Wuhan, China, [4]Institute for Theory and Computation, Harvard-Smithsonian Center for Astrophysics, Cambridge, MA, USA, [5]CNRS, Aix-Marseille Université, Institut de Recherche pour le Développement, College de France, CEREGE, Aix-en-Provence, France, [6]Department of Earth Sciences, University of Cambridge, Cambridge, UK, [6]Center for Meteorite Studies, School of Earth and Space Exploration, Arizona State University, Tempe, AZ, USA.

Introduction: A key stage in the origin of planetary systems is the formation of a gas-rich protoplanetary disk. Theoretical studies suggest that magnetic fields mediated the global evolution and structure of protoplanetary disks by transporting angular momentum and driving disk accretion [1]. However, the nature and history of nebular magnetic fields have been poorly constrained. Here we review recent advances in our understanding of the magnetism of the solar nebula as inferred from meteorites. We discuss their implications for the mechanism and rate of accretion, the dispersal time of the nebula, the formation of chondrules and the gas giants, and planetary migration.

The solar nebula and nebular magnetism: Until recently, evidence for magnetic fields in the terrestrial planet-forming regions of disks around young stellar objects (YSOs) and in the early solar system had been absent. Two recent classes of measurements are filling this gap: astronomical and meteoritic studies.

Astronomical observations: Although there are presently no techniques available for resolving magnetic fields in the midplane region at stellar distances of ~0.1-50 AU, Zeeman spectroscopy and spectropolarimetry have mapped magnetic field intensities and directions on the surface of T Tauri stars and their innermost disks (<0.05 AU)[2]. The orientations of magnetic fields at scales of >50-100 AU could be mapped via their alignment of the spin axes of aspherical dust grains spun-up by radiation torques, which leads to emission polarized perpendicularly to the field direction [3]. Recent millimeter and mid-infrared observations have observed polarized emission of embedded objects and those with visible disks with masses ranging from ~0.2-2.5 solar masses ($M_\odot$) [3]. However, it is unclear whether the observed polarization is a signature of magnetic fields or is due to dust self-scattering [4, 5].

Meteorite measurements: Recent paleomagnetic measurements of chondrules from the Semarkona meteorite [6] indicate the that solar nebula magnetic field was 5-50 μT in the midplane at ~2-3 AU at the time of chondrule formation at ~1-3 My after the formation of calcium aluminum-rich inclusions (CAIs) (assumed here to be 4567.30 ± 0.16 My ago [7], just after the collapse of the molecular cloud). Furthermore, paleomagnetic studies of seven CM chondrites indicate they were magnetized by a field of >4 ± 3 μT sometime between 2.4-4 My after CAI formation (from I-Xe dating) although it is unclear whether this field was nebular or generated by the CM parent body [8] (note these paleointensities are twice those reported by [8] to take into account rotation of the CM body). Collectively, these data indicate a minimum duration of between ~2 ± 1 My after CAI formation for the nebular field and a minimum duration of ~3.7 ± 0.3 My after CAI formation for the nebular gas. The CM chondrite data constrain the field averaged over the timescale of aqueous alteration of the meteorites (~1-10^4 years) while the Semarkona data are near-instantaneous field records.

Lifetime of the nebula: There have been few direct, accurately-dated meteoritic constraints on the lifetime of the nebula and nebular magnetic fields [9]. We review recent advances in astronomical and meteorite studies.

Astronomical observations: Measurements of infrared excesses have inferred that 50% of all protoplanetary disks around Sun-like YSOs disperse somewhere between ~2-6 My after collapse of their parent molecular clouds [10, 11], with this large age uncertainty due to the poorly-known ages of YSOs [10]. In addition to this uncertainty in the median disk lifetime, it is also unknown where our solar system lies in the distribution of disk lifetimes.

Meteorite measurements: Because the sustenance of magnetic fields requires a conducting medium, the dispersal of the solar nebula can be timed by determining when nebular fields disappeared as inferred from the absence of paleomagnetism in meteorites younger than a certain age (see [13] for details). Our recent studies of four different meteorite groups have provided consistent constraints on the timing of the dispersal of the nebular magnetic field.

First, the absence of stable magnetization with unblocking temperatures above 250ºC in the Kaba CV chondrite indicates that the field during magnetite formation was less than ~0.3-3 μT [12] at ~4-6 My after CAI formation as dated by I-Xe and Mn-Cr chronometry [12]. Secondly, it was found that volcanic angrites cooled in a null field environment (<0.6 μT), precisely timed by Pb-Pb chronometry to have occurred at ~3.8 My after CAI formation [13]. Thirdly, the absence of primary magnetization in the ungrouped achondrite NWA 7325 indicates that it also cooled in the absence of a field (<1.6 μT) at ~4.2 ± 0.3 My after CAI formation as indicated by Al-Mg ages [14]. Finally, ongoing analyses of chondrules from the CR chondrite LAP 02342 [15] find that they carry no internally-coherent components of magnetization, suggesting that the magnetic field strength in the CR chondrule formation environment was <15 μT at ~3.7 ± 0.3 My after CAI formation (from Pb-Pb and Al-Mg chronometry [16]).

Independently from meteorite paleomagnetism, it has been observed that the elemental (Si/Mg and Fe/Mg) [17] and isotopic (for W and Mo) [18] compositions of chon-

drules differ from those of the accompanying matrices in several chondrite groups even though the bulk composition of the chondrites is solar. Assuming this complementarity formed prior to accretion [19], it suggests that both chondrules and matrix formed out of a single reservoir of solar composition. If the reservoir was the nebula, this would imply the nebula persisted until at least the formation of CR chondrules at ~3.7 ± 0.3 My after CAI formation [16]. However, because chondrule-matrix complementarity only requires that the parent reservoir was chondritic in composition and was not necessarily the gaseous nebula itself, it does not strictly constrain the nebula's lifetime.

Implications:

Accretion and nebular lifetime: The 5-50 μT paleofield intensities inferred from Semarkona chondrules are consistent with typically observed protostellar accretion rates of ~10^{-8} solar masses ($M_\odot$) year^{-1} [20]. This supports the hypothesis that nebular magnetism played a central role in mass and momentum transport in the protoplanetary disk.

The most precisely dated zero-field constraint (<0.6 μT inferred from angrites) suggests that accretion rates dropped to <10^{-9} $M_\odot$ year^{-1} by 3.8 My after CAI formation [21]. Astronomical observations and theory have found that such a decline in accretion rates is associated with near-total dissipation of the nebula in just 10^5 years [21]. Therefore, our near-zero paleointensities suggest that by ~3.8 My after CAI formation, the nebular gas itself in our solar system had similarly dispersed. This timing is compatible with the observed ~2-6 My half-lifetimes for extrasolar protoplanetary disks [10, 11].

Giant planet formation and migration: This nebula lifetime is not so short as to require the giant planets to have formed by very rapid mechanisms such as collapse due to gravitational instabilities (which can occur in <0.1 My) [22]. Combined with recent isotopic evidence that Jupiter reached 50 Earth masses ($M_\oplus$) following the formation of CR chondrites [23], it indicates that Jupiter then grew from <50 $M_\oplus$ to its final size of 318 $M_\oplus$ within ≲0.5 My by ~3.8 My after CAI formation. This rapid rate strains some variants of the core accretion model, particularly for the ice giants [22]. The nebula lifetime also sets a 3.8-My limit for planetary orbital migration via planet-disk interactions.

Chondrule formation: The Semarkona paleointensities also can be used to distinguish between hypothesized chondrule formation mechanisms. The paleointensities are significantly lower than the >80 to 400 μT values predicted for chondrules formed by the x-wind model [24]. Furthermore, mechanisms invoking intense currents such as magnetic reconnection flares and current sheets predict fields >500 μT during chondrule heating [25]. Instead, they appear to be more consistent with chondrule formation by nebular shocks [26] (for which fields are expected to be <100 μT) and/or planetesimal collisions (which are compatible with a wide range of field values) [6].

Additionally, the existence of magnetization in Semarkona chondrules requires that they did not collide during cooling in order to maintain a steady orientation with the background field. For relative chondrule velocities of 0.001-1 m s^{-1}, this constrains chondrule number densities to between 40-4×10^4 m^{-3}, consistent with chondrule forming in regions with in the nebula with enhanced dust-gas ratios relative to solar composition (e.g., [26]).

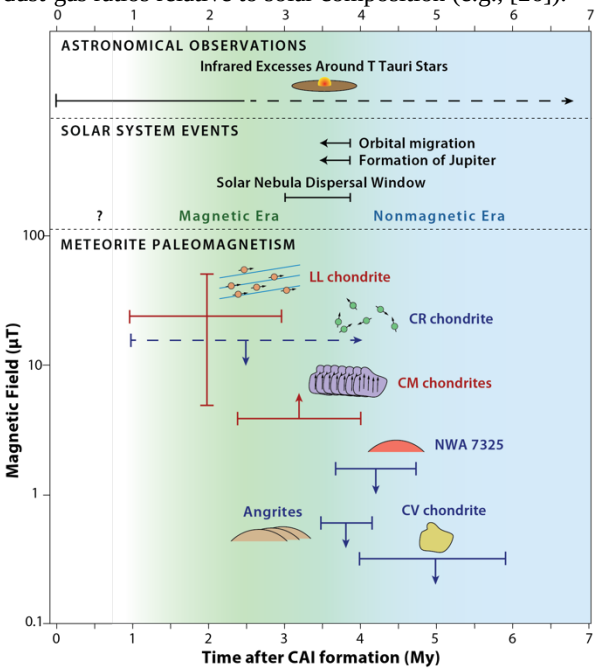

Fig. 1. Meteorite paleomagnetism and astronomical constraints on the intensity and lifetime of the solar nebula field and inferred associated solar system events. Each point in the bottom panel represents the paleointensity of the ambient field from a given meteorite or meteorite group. Downward- (upward-) pointing arrows indicate upper (lower) limits. CV chondrite value is from blocking temperatures >250ºC. See text for references.

References: [1] Turner, N.J. et al. (2014) in *Protostars and Planets VI*, pp. 411-432. [2] Linsky, J.L. & M. Schöller (2015) *SSR 191*, 27-76. [3] Tazaki et al. (2017) *ApJ 839*, doi:10.3847/1538-4357/839/1/56. [4] Yang, H. et al. (2016) *MNRAS 456*, 2794-2805. [5] Kataoka, A. et al. (2015), *ApJ 809*, doi:10.3847/1538-4357/839/1/56. [6] Fu, R.R. et al. (2014) *Science 346*, 1089-1092. [7] Connelly, J.N. et al. (2012) *Science 338*, 651-655. [8] Cournède, C. et al. (2015) *EPSL 410*, 62-74. [9] Chaussidon, M. & M.-C. Liu (2015) *AGU Geophys. Mon. 212*, 1-26. [10] Bell, C.P.M. et al. (2013) *MNRAS 434*, 806-831. [11] Mamajek, E.E. (2009) *AIP Conf. Proc. 1158*, doi:10.1063/1.3215910. [12] Gattacceca, J. et al. (2016) *455*, 166-175. [13] Wang, H. et al. (2017) *Science 355*, 623-627. [14] Weiss, B.P. et al., *EPSL 468*, 119-132. [15] Fu, R.R. et al. (2015) LPSC *XLVI*, 1587. [16] Schrader, D.L. et al. (2017) *GCA 201*, 275-302. [17] Palme, H. et al. (2015) *EPSL 411*, 11-19. [18] Budde, G. et al. (2016) *EPSL 454*, 293-303. [19] Zanda, B. et al. (2012) *LPSC* XLIII, 2413. [20] Hartmann, L. et al. (1998) *ApJ 495*, 385-400. [21] Alexander, R. et al. (2014) in *Protostars and Planets VI*, pp. 475-496. [22] Helled, R. et al. (2014) in *Protostars and Planets VI*, pp. 643-666. [23] Kruijer, T.S. et al. (2017) *PNAS*, doi/10.1073/pnas.1704461114. [24] Shu, F.H., et al. (1996) *Science*, 1996. *271*, 1545-1552. [25] Levy, E.H. & S. Araki (1989) *Icarus 81*,74-91. [26] Desch S.J. & H.C. Connolly (2002) *MAPS* 37, 183-207.

Experimental and Theoretical Considerations for Proton Processing of Early Solar System Solids C.J. Wetteland[1], M. Crespillo[1], D. J. Keffer[1], K.E. Sickafus[1], H.Y. McSween Jr.[2], and L.A. Taylor[2]; <cjw @utk.edu>: [1]Materials Science and Engineering, University of Tennessee, Knoxville, TN 37996; [2]Earth and Planetary Sciences, University of Tennessee, Knoxville, TN 37996

Introduction: In the first billion years of solar system development, the energetic particle environment was vastly different from that of the present day. Seminal literature from ground-based telescopes describes episodic events from developing stars, which include increased luminosity (FU Orioni) and massive discharges of gas and charged particles (T Tauri) [1, 2]. As stars develop, massive eruptions are replaced by solar energetic particle events (SEP). These events are analogous to present day solar flares, but are considerably more powerful and frequent [3, 4].

The enhanced SEP are defined by the types of particles, energy, flux (particles/area-time), and duration. The events predominately consist of ionized hydrogen (protons) and have an energy spectrum generally described over the keV-MeV range. The flux (generally in protons/cm^2-s) distribution as a function of energy favors low energy particles and falls off rapidly in the MeV range [5]. Flares may last between several minutes to hours.

While an enhanced flux of energetic particles in the MeV range has been invoked as a mechanism for the formation of short-lived radionuclides (SLRs) [6], collateral effects may be present from the much-larger flux of lower-energy particles. Of interest, could be thermal processing, which is the result of particles depositing energy as they come to rest over nm-mm length scales in solids.

In this work, we report novel results from experimental work and theoretical considerations that suggest an enhanced SEP may play a significant role in processing early solar material.

Experimental: A variety of silicate, sulfide, metallic and pure elemental targets were irradiated using particle accelerators to explore irradiation conditions likely present in the early solar nebula. Previous work [7] determined that single crystal fragments irradiated by high-flux protons catastrophically explode, so polycrystalline pellets were additionally examined in this study. Pellets were fabricated from ball milling: synthetic forsterite, San Carlos olivine (Sc), Nain anorthosite (N), Stillwater anorthosite (Sw), and synthetic corundum (Crn). Powders were pressed and sintered into 13 mm diameter pellets and sliced into mm thick slabs; followed by grinding to thicknesses of approximately 0.5 mm. The slabs were irradiated with low (50 and 80 keV) and medium energy (2 MeV) protons (p) using fluxes between ~10^{13}-10^{14} p/cm^2-s; overall fluences were between $5x10^{15}$-$1x10^{17}$ p/cm^2. During irradiation, a Stanford Research Systems Residual Gas Analyzer (RGA) was used to monitor volatile products that could be evolved over the course of the experiment. Pellets were examined post irradiation using a scanning electron microscope (SEM) and energy dispersive spectroscopy (EDS) to examine microstructural and chemical changes.

Results: When subjected to specific combinations of flux and fluence, both low and medium energy protons are capable of modifying the microstructure of silicates. Figure 1 shows the microstructure for (a) un-irradiated synthetic forsterite, (b) 50 keV irradiated synthetic forsterite, and (c) 2 MeV irradiation of a mixture of 80/20 SC/N by weight. The synthetic forsterite was irradiated with a $6.3x10^{14}$ p/cm^2-s flux to a fluence of $1.1x10^{17}$ p/cm^2, while the San Carlos/Nain mixture was irradiated with a flux of $2x10^{14}$ p/cm^2-s to $2x10^{16}$ p/cm^2. The unirradiated microstructure shows abundant porosity with minimal sintering. After the respective proton irradiations, the porosity is absent, with the overall texture resembling isolated grains embedded in a glassy matrix.

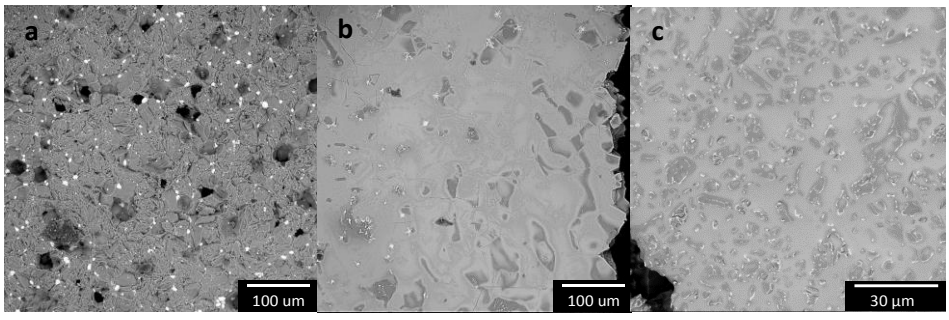

Figure 1. Backscattered electron images showing a) un-irradiated porous microstructure, b) 50 keV irradiated synthetic forsterite, and c) 2 MeV Sc/N mixture. The irradiated microstructure resembles a melt texture. The bright phase is zirconia from the ball milling process.

Further SEM interrogation of the San Carlos-containing pellets indicates the formation of metallic micro-droplets on the surfaces of olivine grains, as observed in figure 2. The droplet micro-structure can be observed in both 80 keV and 2 MeV irradiations. In the 80 keV irradiations, the droplets are sparsely located and oftentimes associated with areas of increased surface carbon. In the case of figure 2, the subsurface of a 2 MeV irradiated pellet was exposed during post experimental handling. The droplets were located in the epicenter of the beam spot and have an approximate 4/1 ratio of Fe/Ni as measured with EDS.

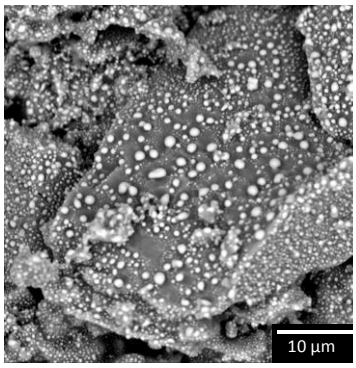

Figure 2. Droplet morphology from the 2 MeV proton irradiation. The droplets have an approximate Fe/Ni ratio of 4/1 as measured by EDS.

Search for volatile products generated during the polycrystalline silicate irradiations yielded limited results. However, an irradiated slab of FeS_2 showed a dramatic response to proton irradiation. Figure 3 shows an RGA scan of mass 64, S_2, from an irradiated polished slab of FeS_2. At an elapsed time of 360 seconds, a flux of $6.2x10^{13}$ p/cm^2-s was applied to the target; no change in the spectrum was observed. However, at 720 seconds the flux was increased to $9.5x10^{13}$ p/cm^2-s, and a significant change in the S_2 signal was measured. The scan shows a steady increase for approximately 720 seconds before it begins to level out. At approximately 1500 seconds, the signal has a drastic increase again; in this case there was no change in the beam current. Post experiment SEM and EDS analyses of the target indicate the irradiated area was sulfur deficient. The sharp increase in S_2 was likely the exposure of fresh FeS_2 material to the beam due to a small portion of the surface spalling off. Significant discoloration in the vicinity of the beam can be seen as a black coating on the surface of the sulfide. This is consistent with most other irradiations; however the degree of discoloration was significantly less on the silicates.

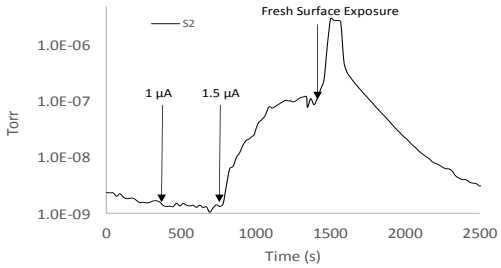

Figure 3. Partial pressure of S_2 generated during a 2 MeV proton irradiation. The generation of S_2 was highly dependent of the flux of the beam.

Discussion

The results indicate that when irradiated with protons at threshold flux and fluence values, early solar system materials can be physically and chemically altered. Theoretical considerations have examined whether the flux conditions examined in these investigations are relevant to the particle environment of the early solar system.

The total integrated flux for SEP events for an energy range between 1 keV and 10 MeV was calculated using equations from [5] and applying the 10^5 enhancement as predicted in [3]. These calculations indicate an enhanced integrated proton flux of $10^{12\text{-}16}$ p/cm^2-s between 1 keV and 10 MeV at 1 AU can be present in SEP during stellar evolution. This range of flux is similar to those performed in the above experiments, which resulted in temperatures exceeding the melting temperatures in some silicates. Furthermore, the energy deposited in SEP exceeds that required to melt chondrule precursors as determined by [8], and should be considered as a chondrule formation mechanism. Additional observed consequences of experiments include rapid thermal expansion followed by surface spallation, and hydrocarbon deposition.

Conclusions: We present some of the first experimental results and theoretical considerations for irradiation processing of early solar system material. Our ion beam irradiation experiments have determined that keV and MeV protons can deposit significant amounts of energy into early solar system solids; this energy can provide enough heat to melt and vaporize early solar materials. Furthermore, the conditions examined during the experiments align well with predictions of enhanced solar flares, which would have been prominent during stellar evolution. The energy deposited may result in physical and chemical modification of early solar material prior to and during the accretion process and should be considered as an active mechanism during the first billion years.

References [1] Herbig, G.H., *Vistas in Astron.* (1966) 8, 109-125. [2] Kuhi, L.V., *The Astroph, J.* (1964) 140, 1409-1437. [3] Feigelson, E.D., et al., *The Astrophys. J.* (2002) 572, 335-349. [4] Feigelson, E.D. and T. Montmerle, *Ann. Rev. of Astron. and Astrophys*., (1999) 37, 363-408. [5] Caffee, M., et al., *In Meteorites in the Early Solar System*, (1988) 205-245. [6] Goswami, J., et al. *In Chondrites and the Protoplanetary Disk*. (2005) 485-513 [7] Wetteland, C. J., et al. *LPSCXL VIII* (2016) abst. # 2490. [8] Wasson J.T. *In Chondrules and the Pro-toplanetary Disk* (1996) 45-54.

Modeling the growth of chondrule dust rims with molecular dynamics. C. Xiang[1], L. S. Matthews[1], A. Carballido[1], M. A. Morris[2,3] and T. W. Hyde[1], [1]Center for Astrophysics, Space Physics and Engineering Research, One Bear Place #97310, Baylor University, Waco, TX, 76798-7310, USA, [2]School of Earth and Space Exploration, Arizona State University, PO Box 876004, Tempe, AZ, 85287-6004, USA, [3]Physics Department, State University of New York, PO Box 2000, Cortland, NY, 13045, USA.

Introduction: Dust mantles or rims around chondrules encode important information regarding processes in the solar nebula. Such rims are generally considered to have an accretionary origin, that is, they are thought to have been acquired by free-floating chondrules in the nebular gas (although there are arguments in favor of rim formation from the impact and compaction of matrix material around chondrules that were already incorporated into parent bodies). If the nebular hypothesis is correct, the structure of chondrule rims could ultimately be used to infer values of gas velocities, turbulent viscosity, and ionization state [1, 2].

Calculations derived from measurements of chondrule dust rims in the Allende CV carbonaceous chondrite [3], as well as experimental measurements of rims around chondrule analogs [4] indicate that rims are generally very porous. Porosities of ~60 to 80% have been reported, although lower values due to compaction or thermal/aqueous alteration are not ruled out. In this work, we use a molecular dynamics code to model rim growth through the collection of micron-sized dust particles. We investigate the impact of the chondrule size on the thickness and porosity of the rim in two regions of the solar nebula with different turbulent strengths ($\alpha = 10^{-2}$, 10^{-4}). We also compare the rims formed by the collection of single spherical monomers and collection of aggregates of spherical monomers in neutral and charged environments.

Method: The accretion of the chondrule rim was modeled using the conditions in a MMSN turbulent protoplanetary disk at a distance of 1 AU. The initial dust population is silicate spheres with radii $0.5 \leq a \leq 10$ μm with a power law size distribution $n(a)\mathrm{d}a \propto a^{-3.5}\mathrm{d}a$. The hydrogen plasma environment had equal electron and ion temperature, $T_e = T_i = 900$ K. In the case of low dust density, a negligible percentage of the electrons reside on the dust grains, and the number density of electrons and ions in the gas is set to be $n_e = n_i = 7.49 \times 10^{13}$ m^{-3} [5].

We use an N-body code, Aggregate_Builder (AB) to model the detailed collision processes between the chondrule, which is represented by a (sub) millimeter-sized spherical body, and the dust, taking into account the aggregate morphology, trajectory, and orientation [6,7]. The temporal evolution of the dust population is determined by a Monte Carlo algorithm used to select incoming dust particles [8, 9].

In each iteration, the chondrule is placed with its center of mass at the origin, and the dust particle is shot towards its COM plus an offset, with the relative velocity between the dust particle and the chondrule determined by coupling of the particles to the turbulent gas environment [10,11]. The possible collision outcomes are sticking at the point of contact, bouncing, or rolling on the surface, which results in compaction. These outcomes are determined by the critical bouncing velocity and the critical rolling energy [12]. Charged particles moving toward the chondrule experience a repelling electrostatic force; the deflection and deceleration can cause them to miss the chondrule. For computational expediency, we restrict dust aggregates to accumulate on a small patch of the chondrule surface, measuring ~120 μm by 120 μm.

Results: The dust rim is divided into a few horizontal layers (i.e., parallel to the chondrule's surface) to analyze its structure and composition. The porosity of each layer is the ratio of the volume of voids within the layer to the total volume of the layer. The innermost layer has the lowest porosity, with the rim becoming more porous with distance from the chondrule center. The size distribution of monomers in each layer shows that the outer layers tend to have a higher ratio of large monomers to small monomers. This is because small particles can pass through the gaps and travel closer to the bottom of the rim, while large particles are usually stopped by other monomers and stick at the point of contact if they don't have enough energy to cause restructuring.

Strong turbulence produces larger relative velocities between the chondrules and dust particles than weaker turbulence. Greater relative velocities increase the collision rate and enhance restructuring, causing the chondrule rims to be more compact (Figure 1) and grow more rapidly (Figure 2).

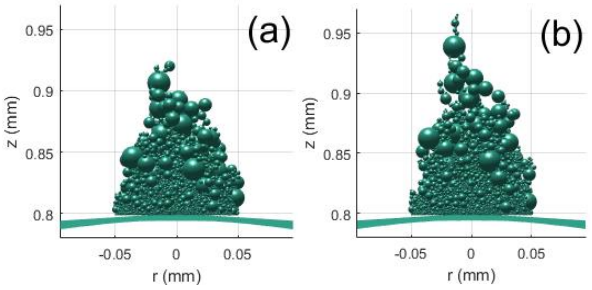

Figure 1: Rim growth on a 100 μm-diameter patch on the surface of a chondrule with a radius of 800 µm for two different turbulent strengths a) $\alpha=10^{-2}$, b) $\alpha=10^{-4}$, for the addition of single monomers.

The charge also plays an important role in both the structure and the growth rate of the dust rim. The decreased relative velocity between charged grains causes small grains to be repelled from the chondrule in regions of weak turbulence, while in regions with strong turbulence, the main effect is a reduction of the restructuring. Both of these effects result in a more porous dust rim (Figure 2), which in turn increases the effective cross-sectional area of the chondrule, enhancing collisions.

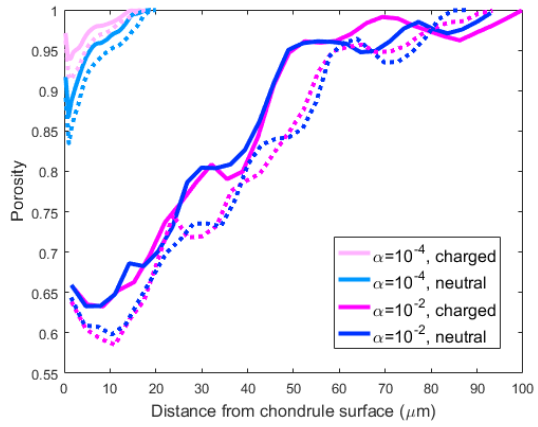

Figure 2: Porosity of the dust rim formed after 84 days as a function of the distance from the chondrule surface, for chondrule radii of 600 µm (solid lines) and 900 µm (dotted lines). With weak turbulence ($\alpha = 10^{-4}$), the rim formed with charged particles is more porous as small monomers are repelled and there is little restructuring.

Another important factor affecting the dust rim is the size of the chondrule. Larger chondrules have greater cross-sectional area, as well as larger relative velocity with respect to the dust particles, and therefore collide more frequently with the dust. At the same time, more dust is required to build a rim of a certain thickness than for smaller chondrules. As shown in Figure 3, the rim thickness scales linearly with the chondrule radius and as predicted by Paque & Cuzzi [13]. Figure 3 shows that the linear relationship becomes steeper over time, as the greater collision cross section and larger relative velocities of the larger chondrules increases the collision rate, causing the large chondrules to grow even faster.

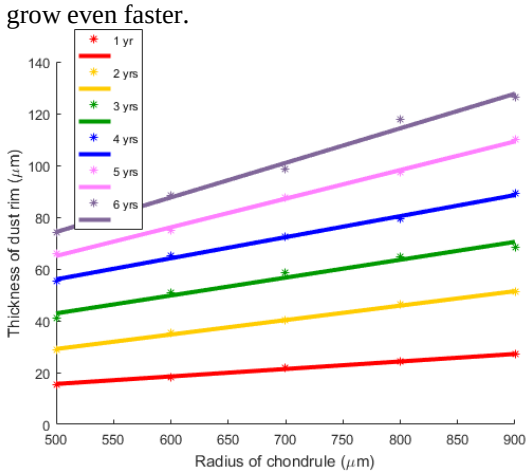

Figure 3: The thickness of the dust rim formed through the addition of single monomers after 1, 2, 3, 4, 5, 6 years, with turbulent strength $\alpha = 10^{-4}$ for different chondrule radii (the outer rim with porosity > 0.9 is removed). The thickness of the dust rim is nearly proportional to the chondrule radius.

Conclusion: The porosity of chondrule rims built up after 2 years is ~70% - 75%, comparable to laboratory measurements [3,4]. Formation of dust rims by cluster aggregation leads to higher porosity than rim formation through the addition of single monomers, consistent with results reported in [1]. Most collisions result in little restructuring, with restructuring collisions representing 0.2% of interactions for the turbulence strength $\alpha = 10^{-4}$ and 19% for $\alpha = 10^{-2}$. Thus hit-and-stick is the main process of dust rim growth for small particles and low turbulence strength ($\alpha < 10^{-4}$).

Other factors, such as thermal/aqueous and nebula shock waves, that may lead to a lower porosity are not considered in this model. Future work will take these factors into consideration, and investigate the effect of the dust rim on the collisions between chondrules.

References: [1] Ormel, C. W. et al. (2008) ApJ, 679:1588–1610. [2] Carballido, A. (2011) Icarus, 211, 876. [3] Bland, P. A. et al. (2011) NatGe, 4, 244. [4] Beitz, E. et al. (2013) Geochim. et Chosmochim. Acta, 116, 41.5.5. [5] Matthews, L. S. et al. (2012) ApJ, 744 (1): 8. [6] Ma, Q. et al. (2013) ApJ 763 (2): 77. [7] Matthews, L. S. et al. (2016) IEEE 44 (4): 519–24. [8] Ormel, C. W. et al. (2007), A&A 461, 215-232. [9] D. T. Gillespie (1975) AMS 32 (10): 1977-1989. [10] A. Carballido et al. (2010) MNRAS 405 (4): 2339–44. [11] A. Carballido et al. (2016) ApJ 823 (2): 80. [12] A. Chokshi et al. (1993) ApJ 407:806-819. [13] Paque J. And Cuzzi J. N. (1997) Lunar Planet. Sci. XXVIII, 1189 (abstract).